NUREG/CR–5757
ANL–91/25

Received by OSTI
SEP 30 1991

Verification of Piping Response Calculations of SMACS Code with Data from Seismic Testing of an In-Plant Piping System

Prepared by
M. G. Srinivasan, C. A. Kot, B. J. Hsieh

Argonne National Laboratory

Prepared for
U.S. Nuclear Regulatory Commission

DISTRIBUTION OF THIS DOCUMENT IS UNLIMITED

DISCLAIMER

This report was prepared as an account of work sponsored by an agency of the United States Government. Neither the United States Government nor any agency thereof, nor any of their employees, makes any warranty, express or implied, or assumes any legal liability or responsibility for the accuracy, completeness, or usefulness of any information, apparatus, product, or process disclosed, or represents that its use would not infringe privately owned rights. Reference herein to any specific commercial product, process, or service by trade name, trademark, manufacturer, or otherwise does not necessarily constitute or imply its endorsement, recommendation, or favoring by the United States Government or any agency thereof. The views and opinions of authors expressed herein do not necessarily state or reflect those of the United States Government or any agency thereof.

DISCLAIMER

Portions of this document may be illegible in electronic image products. Images are produced from the best available original document.

AVAILABILITY NOTICE

Availability of Reference Materials Cited in NRC Publications

Most documents cited in NRC publications will be available from one of the following sources:

1. The NRC Public Document Room, 2120 L Street, NW., Lower Level, Washington, DC 20555

2. The Superintendent of Documents, U.S. Government Printing Office, P.O. Box 37082, Washington, DC 20013-7082

3. The National Technical Information Service, Springfield, VA 22161

Although the listing that follows represents the majority of documents cited in NRC publications, it is not intended to be exhaustive.

Referenced documents available for inspection and copying for a fee from the NRC Public Document Room include NRC correspondence and internal NRC memoranda; NRC bulletins, circulars, information notices, inspection and investigation notices; licensee event reports; vendor reports and correspondence; Commission papers; and applicant and licensee documents and correspondence.

The following documents in the NUREG series are available for purchase from the GPO Sales Program: formal NRC staff and contractor reports, NRC-sponsored conference proceedings, and NRC booklets and brochures. Also available are regulatory guides, NRC regulations in the *Code of Federal Regulations*, and *Nuclear Regulatory Commission Issuances*.

Documents available from the National Technical Information Service include NUREG-series reports and technical reports prepared by other Federal agencies and reports prepared by the Atomic Energy Commission, forerunner agency to the Nuclear Regulatory Commission.

Documents available from public and special technical libraries include all open literature items, such as books, journal articles, and transactions. *Federal Register* notices, Federal and State legislation, and congressional reports can usually be obtained from these libraries.

Documents such as theses, dissertations, foreign reports and translations, and non-NRC conference proceedings are available for purchase from the organization sponsoring the publication cited.

Single copies of NRC draft reports are available free, to the extent of supply, upon written request to the Office of Administration, Distribution and Mail Services Section, U.S. Nuclear Regulatory Commission, Washington, DC 20555.

Copies of industry codes and standards used in a substantive manner in the NRC regulatory process are maintained at the NRC Library, 7920 Norfolk Avenue, Bethesda, Maryland, for use by the public. Codes and standards are usually copyrighted and may be purchased from the originating organization or, if they are American National Standards, from the American National Standards Institute, 1430 Broadway, New York, NY 10018.

DISCLAIMER NOTICE

This report was prepared as an account of work sponsored by an agency of the United States Government. Neither the United States Government nor any agency thereof, or any of their employees, makes any warranty, expressed or implied, or assumes any legal liability of responsibility for any third party's use, or the results of such use, of any information, apparatus, product or process disclosed in this report, or represents that its use by such third party would not infringe privately owned rights.

NUREG/CR--5757
TI91 018982

Verification of Piping Response Calculation of SMACS Code with Data from Seismic Testing of an In-Plant Piping System

Manuscript Completed: June 1991
Date Published: September 1991

Prepared by
M. G. Srinivasan, C. A. Kot, B. J. Hsieh

Argonne National Laboratory
9700 South Cass Avenue
Argonne, IL 60439

Prepared for
Division of Engineering
Office of Nuclear Regulatory Research
U.S. Nuclear Regulatory Commission
Washington, DC 20555
NRC FIN A2251

MASTER

DISTRIBUTION OF THIS DOCUMENT IS UNLIMITED

Verification of Piping Response Calculation of SMACS Code with Data from Seismic Testing of an In-plant Piping System

by

M. G. Srinivasan, C. A. Kot, and B. J. Hsieh

Abstract

The objective of this effort was to evaluate the piping analysis part of the SMACS code for estimating the response of realistic piping systems subjected to seismic excitation, given as multiple, independent support acceleration histories. The experimental data from the seismic testing of an in-plant piping system at the HDR Test Facility in Germany were used for this purpose. Of the six different support systems tested, two were selected for the evaluation: one a 'stiff' configuration containing both struts and snubbers, and the other, a more flexible configuration with no snubbers. Described are the analytical modeling, calculations, and results of the posttest simulation of two tests each for both support configurations, with excitations at 100% and 200/300% of safe-shutdown-earthquake loading.

Almost all the calculated peak response quantities were smaller (by different amounts) than the corresponding test measurements. However, pipe displacements and bending stresses were better estimated than the pipe accelerations and support forces. The discrepancies are mainly attributable to the inability of the linear analysis to model the nonlinear behavior of the VKL piping system, characterized by gaps in support connections and the friction at pipe clamps. A similar trend of underestimating test responses was observed in the linear analyses performed by other investigators.

Contents

Figures

Tables

Acknowledgments

The work reported here was supported by the U.S. Nuclear Regulatory Commission, Office of Nuclear Regulatory Research.

Executive Summary

The U. S. Nuclear Regulatory Commission, Office of Research (NRC/RES) has cooperated with the HDR Safety Project (PHDR) of the Kernforschungszentrum Karlsruhe (KfK) in the performance of seismic or dynamic testing of the containment and subsystems in the Heissdampfreaktor (HDR) Test Facility in Kahl/Main, Federal Republic of Germany. Simulated earthquake excitation tests, denoted SHAM, were performed in 1988 on the Versuchskreislauf (VKL) piping system in the HDR reactor building. Validation/verification of analytical methods with experimental data has been one of the important goals of the program. Data obtained from the tests have been used to validate analytical methods for piping response calculations. An effort to evaluate the subsystem analysis module of the SMACS (Seismic Methodology Analysis Chain with Statistics) code, using some of the SHAM test data is the subject of this report. The SMACS code links the calculations of seismic input, soil-structure interaction, major structure response, and subsystem response. The analysis of response of piping systems accounts for independent multisupport excitations and is the focus of the present verification effort.

Of the six different support configurations tested in the SHAM series of tests, two were selected for the current effort. The NRC configuration was a relatively stiff system, with struts and snubbers. The KWU configuration did not have any snubbers and was more flexible. The excitation in the SHAM tests, in the form of a displacement history, was applied at two points of the VKL system. The piping support systems were designed for a hypothetical safe-shutdown earthquake (SSE) with a peak acceleration of 0.6 g. The SHAM series included tests at high excitation levels, up to 800% of the SSE, that induced plasticity in the pipes. However, only the lower levels of excitation, viz., 100 to 300% SSE tests, of the NRC and KWU configurations were simulated in the present effort because the pipe was in the elastic regime in these tests.

The posttest simulations for evaluating the SMACS method were blind calculations in the sense that no test results were used for setting up or modifying the finite element model. The models consisted of pipe, truss, and beam elements. Truss elements represented the struts and snubbers. The beam elements were used only for modeling a pipe clamp in the KWU configuration. Actual test excitations were used as input to the calculations. However, to circumvent baseline drift problems, it was found necessary to use acceleration histories obtained by differentiating measured actuator displacement histories.

The modal frequencies determined by the code were found to be close to those determined from other calculations, and many of them were also close to

frequencies identified from test data. However, for the same frequency range, more modes were identified from test data than were estimated by calculations.

Most of the response quantities, i.e., pipe accelerations, displacements, and bending stresses, and forces in the snubbers and struts were underestimated by the calculations. As a class, the snubber forces were the most poorly estimated quantity. The spatial consistency of the response estimates was uneven, especially for accelerations and support forces. The peak values of displacements and bending stresses were better estimated than the accelerations and support forces and these estimates had more spatial consistency.

Estimates made by linear analysis with other codes by different investigators also showed similar discrepancies. The complex and nonlinear behavior of the snubbers and the clamp-to-pipe attachment of the supports in general could not be simulated in a linear analysis code. While the experimental data were low pass filtered to 60 Hz, spurious high-frequencies occur both in the input excitation and the response measurements. These may be responsible for the poorer estimation of acceleration and support forces. As integration reduces the effect of these higher frequency contents, displacements and stresses were better estimated.

The discrepancy between test results and calculated estimates cannot all be attributed to the calculational method. There are uncertainties in the experimental data and analytical model that may have contributed to the differences. Because of these it has not been possible to evaluate the SMACS piping calculation code in isolation. However, the effort should be considered as an attempt to verify the whole process that is typical of a design calculation with a linear code. The results have shown that the process could result in significant underestimation of responses in general and support forces in particular. Neglecting the nonlinear behavior of the connection between pipe and support members appears to be the primary deficiency of linear analysis method of the SMACS and other such programs.

1 Introduction

Various experiments related to the design and safety of nuclear power plants have been performed since 1974 at the Heissdampfreaktor (HDR) Test Facility in Kahl/Main, Federal Republic of Germany. The U. S. Nuclear Regulatory Commission, Office of Research (NRC/RES) has cooperated with the HDR Safety Project (PHDR) of the Kernforschungszentrum Karlsruhe (KfK) in the performance of seismic or dynamic testing of the containment and subsystems in the HDR facility. During the first phase of seismic tests relatively low-level excitation tests were performed on the containment. In the second phase high-level excitation tests were performed. In the tests performed in 1986, denoted as SHAG, the reactor building was subjected to very high levels of dynamic excitation [1,2]. Simulated earthquake excitation tests, denoted SHAM, were performed during April–May 1988 on the Versuchskreislauf (VKL) piping system in the HDR reactor building [3]. The major objectives of the SHAM tests were to study the behavior of a full-scale in-plant piping system subjected to a range of seismic excitation levels (from design levels to those that might induce either failure of pipe supports or plasticity in the pipe runs) and to establish seismic margins for piping and pipe supports.

Besides the major objective noted above, validation/verification of analytical methods with experimental data has been one of the important goals of both PHDR and NRC/RES. Data obtained from the SHAG and SHAM tests have been used to validate analytical methods for piping response calculation. The use of SHAG data for verifying piping response calculations has been reported earlier [4,5].

This report describes an effort to evaluate the subsystem analysis module of the SMACS code [6] using some of the SHAM test data. The SMACS module is a linear finite-element program derived from the SAP4 code and capable of calculating the response of nuclear power plant subsystems subjected to multiple, independent, acceleration excitation. The evaluation is based on a comparison of computational results of simulation of SHAM tests with corresponding test measurements.

2 Piping Analysis Method of SMACS Code

The SMACS (Seismic Methodology Analysis Chain with Statistics) links the calculations of seismic input, soil-structure interaction, major structure response, and subsystem response. The analysis of response of piping systems accounts for independent multisupport excitations and is the focus of the present verification effort. The analysis is based on the pseudostatic-mode method.

The unknown absolute nodal displacement is defined as the sum of a pseudostatic and a dynamic part. The pseudostatic part is the response induced in the system due to support motions, excluding inertia effects. The dynamic part is the response due to inertia effects only. The pseudostatic modes are influence coefficients that relate the pseudostatic part to unit support motions. An eigenfunction expansion is used to determine the dynamic part. For a more detailed description of the pseudostatic method, reference may be made to [7].

A static analysis run of a finite-element code, based on the SAP4 program, computes the pseudostatic modes, and a modal analysis run of the same code computes the eigenfunction expansion assuming proportional damping. The response recovery runs compute the two parts of the response for specified modal damping and combine them to give the total response for prescribed independent support accelerations. Both the prescribed accelerations and the computed total responses (accelerations, displacements, and forces) are in the form of time histories. Modal damping, as a percentage of critical damping, may be prescribed for each modal frequency or specified on the basis of the Pressure Vessels Research Committee (PVRC) criteria. These criteria specify that the modal damping, in percent of critical damping, is to be 5% for modes of frequencies less than 10 Hz, 2% for those of frequencies greater than 20 Hz, and linearly interpolated for modes of frequencies between these points.

In the first attempt to verify the subsystem-analysis module of SMACS, the SHAG test data were used [4,5]. In the SHAG experiments a large coast-down shaker installed on the operating floor applied a dynamic force to the building which, in turn, imparted excitation to the VKL piping system through the pipe supports. The details of the comparisons between experimental and calculational results are given in [5]. Whereas the analysis underestimated the response if measured anchor point motions were prescribed as input excitation, it overestimated the response if measured pipe accelerations at support attachment points were used as input excitation. As extraneous pipe runs connecting to other systems were left in place during the SHAG tests, the uncertainty associated with the boundary conditions of the system made it difficult to realistically simulate the SHAG tests. A test in which the piping system boundaries and the input excitation were more unambiguously defined would be a better source of data for

code verification. In the SHAM tests the VKL system was modified to clearly define its boundaries and the seismic excitation was directly applied to the VKL system at two locations on the pipe. The SHAM tests are considered to be more appropriate for verifying analytical methods.

3 Description of SHAM Tests

3.1 Test Configurations

Figure 1 shows the VKL piping system as used in the SHAM test series. The pipe runs of the VKL, excluding the HDU vessel, extend about 10 m in the vertical direction, about 11.5 m in the x direction, and about 6 m in the z direction. The pipes are of stainless steel, ranging from 100 to 300 mm in diameter. The HDU vessel was fixed at its base, and a displacement restraint in the x and z directions was provided by a structural frame located about one-third of the height of the vessel from its top. The DF15 manifold was directly attached to the floor, as indicated schematically in Fig. 1. Six different seismic support configurations, designed by different participants in the SHAM experiments [3], were used during the dynamic tests. Figure 1 shows a configuration typical of U.S. nuclear power plants, with struts and snubbers, and is designated as the NRC configuration for identification purpose only. The supports for this system were designed by the Idaho National Engineering Laboratory. The only other support configuration covered in this paper is designated as the KWU configuration and is shown in Fig. 2. Siemens, Offenbach, Germany, designed the support system for this [8]. The differences between the NRC and KWU configurations are that the latter had no snubbers at all, had one less strut – H3 having been removed – and had larger struts for H9, H10, and H11. Details about the other configurations not covered in this report, are given in [3].

3.2 Simulation of Seismic Excitation

During the SHAM tests, the dynamic excitation was applied to two different points of the piping along the x direction, with the H5 and H25 servohydraulic actuators, as shown in Figs. 1 and 2. The excitation system included a computer-controlled hydraulic actuating/control system to produce a prescribed displacement history at the actuators. The excitation histories represented an integral multiple of a hypothetical safe-shutdown earthquake (SSE) with a peak acceleration of 0.6 g. Figures 3(a) and 3(b) show the prescribed displacement and acceleration histories for 100% SSE excitation and Fig. 3(c) shows the response spectrum, for 4% damping, of the acceleration. The recorded accelerations on the two actuators turned out to be somewhat different from the one shown in Fig.3(b) and also from each other.

The tests covered a range of excitation levels from 100 to 800% SSE, with the higher levels inducing plastic strains in the pipe. An excitation level of 800% SSE means that the amplitudes of the hypothetical SSE acceleration history were scaled up by a factor of eight, while the duration and the wave form of the history

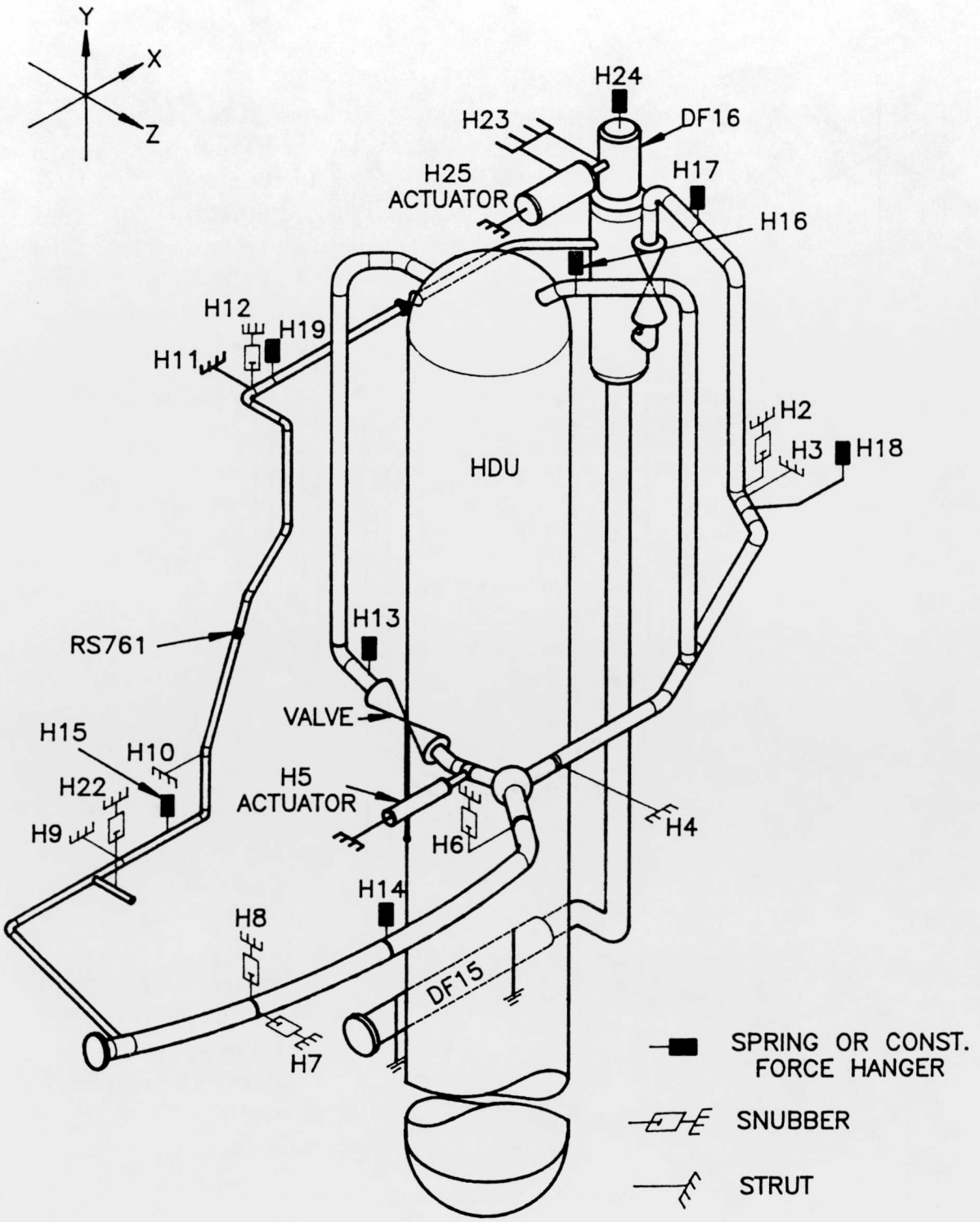

Fig. 1. VKL Piping System with NRC Support Configuration

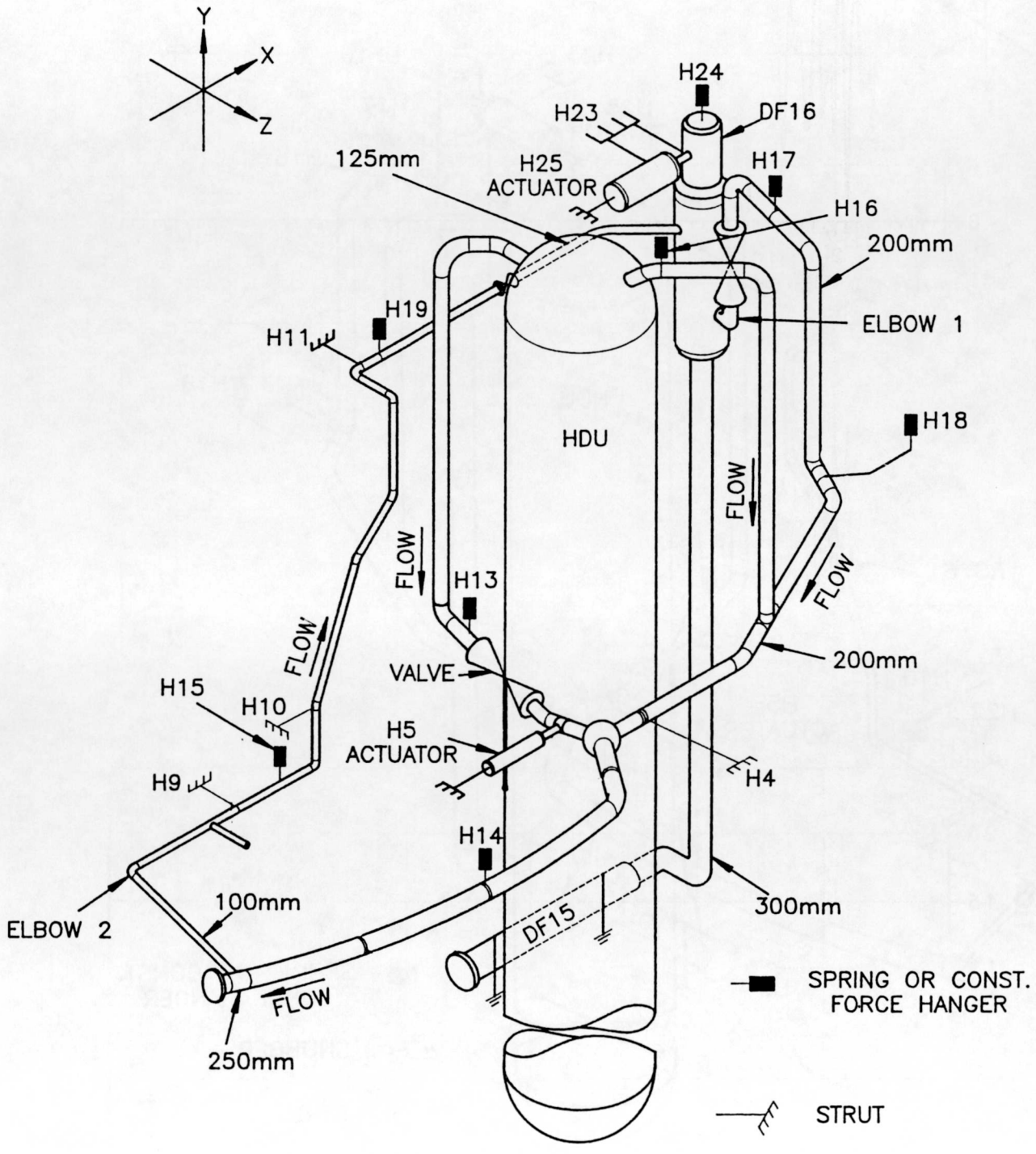

Fig. 2. VKL Piping System with KWU Support Configuration

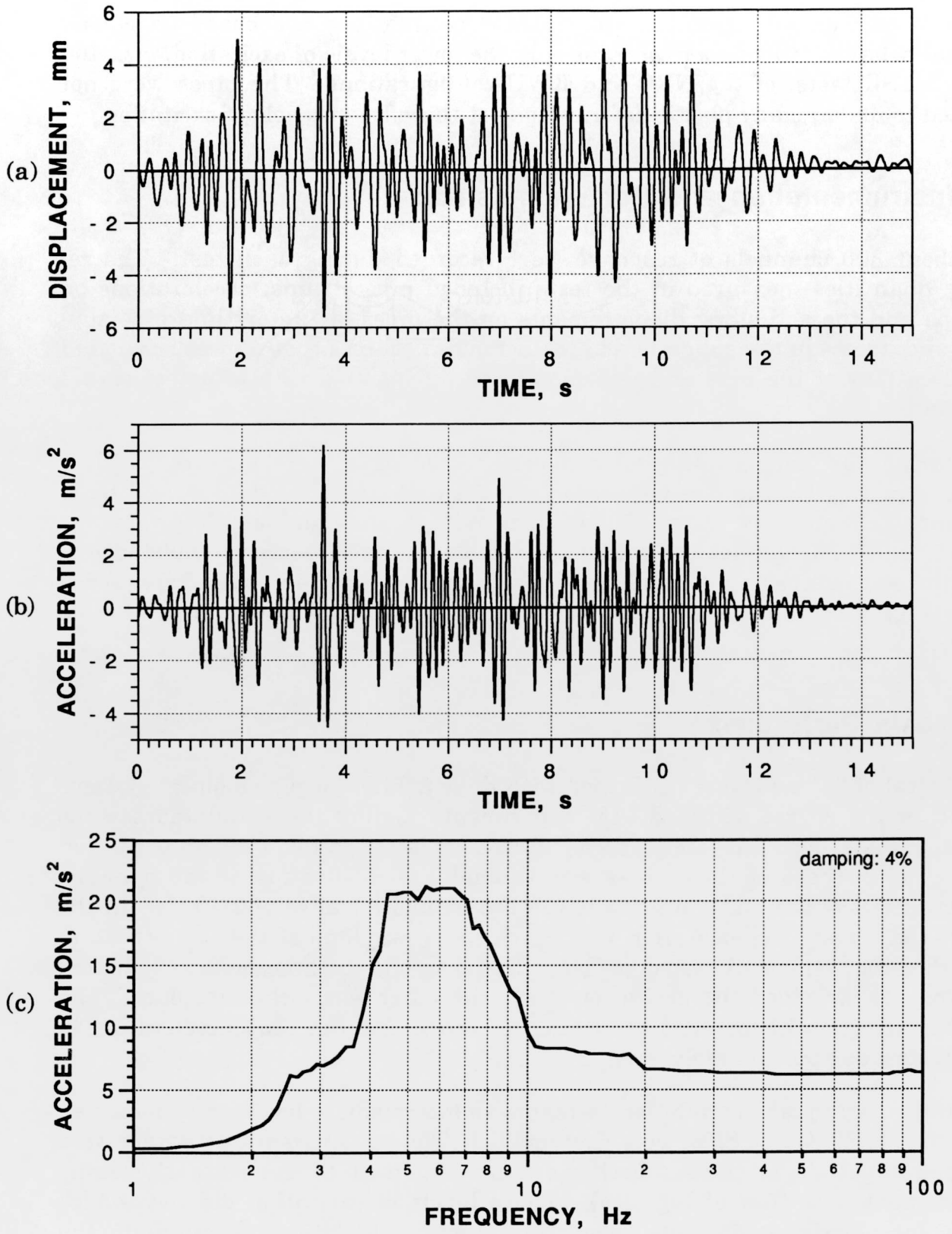

Figure 3. Prescribed Excitation: (a) Displacement History (b) Acceleration History (c) Acceleration Response Spectra

remained unchanged. Because the SMACS calculations are based on elastic material behavior, this paper concerns only the lower levels of excitation, viz., 100 to 300% SSE tests, of the NRC and KWU configurations. The pipes were not expected to undergo any plastic deformations at these lower levels of excitation.

3.3 Instrumentation and Data Acquisition

About 300 channels of response were recorded during each test. The response quantities measured in the tests included pipe strains; accelerations on the pipe and the actuators; displacements on the pipes, actuators and pipe supports; and forces in the supports and the actuators. Stress coating was applied at some locations of the pipe and was monitored during the tests to detect severe deformation.

During the analog-to-digital conversion, the data were acquired with a sampling rate of 625 samples per second. In the first stage, the data were filtered to eliminate frequencies above 100 Hz. For storage, the data sampling rate was reduced to 205.66 samples per second, giving a sampling interval of 0.0048624 s. After the application of a second stage low-pass filter that eliminated frequency contents greater than 60 Hz, the data became available in the form of time histories.

3.4 Tests Performed

A total of 51 tests were performed with the six different pipe support systems of VKL in the course of the SHAM experiment. Before the simulated seismic excitation tests, each pipe support system was subjected to two random excitation tests. The purpose of these tests was to enable identification of the dynamic characteristics of the test configuration in the frequency range of 2-40 Hz. In the first of these tests the excitation was provided by only one of the two actuators while the other remained locked in place. In the second test, the previously locked actuator now provided the excitation while the other was locked in place. The random excitation history had a duration of 120 s, and the peak acceleration in these tests was approximately 0.3 g.

In the earthquake simulation tests, low to intermediate level excitations, i.e., from 100% to 300/400% SSE, were first applied. The two hydraulic actuators were operated together in phase; both were programmed to generate the same displacement, i.e., that of Fig. 3(a). These levels of excitation did not induce significant plastic strain thus permitting elastic calculations to simulate the tests.

The high-level excitation tests (up to 800% SSE) on the NRC and KWU configurations followed after the previous set of tests. These tests produced plastic strains in the pipe and support failures.

Important results of the SHAM tests are summarized in [3]. Only those that are pertinent to the present subject are given in this report in Chapter 5 where the results of the calculation are compared with the measurements.

4 Analytical Simulation of SHAM Tests

4.1 Introduction

Prior to the performance of the tests, the subsystem module of the SMACS code was used for predicting the response of the NRC configuration. These predictions were made mainly for the purpose of test planning. As the analytical method requires the input excitation to be acceleration, rather than displacement, the acceleration history of Fig. 3(b) was specified as input at the two actuators. The results were obtained as histories of various response quantities, i.e., accelerations, displacements, support forces and pipe stresses. The results of the pretest calculations were discussed in [3].

Comparison of pretest predictions with test results showed that the analysis generally tended to underpredict the response. The differences between the actual test excitation and the one assumed in the analyses were suspected to be a reason for the underpredictions. Therefore it was decided that for the posttest calculations for code verification, it would be more appropriate to use the actual or measured excitation of the actuators as input. Except for the use of this set of measured quantities, the first posttest calculations are to be considered blind.

The first set of posttest calculations, the results of which were summarized in [9], did not include any response calculations other than accelerations because of the baseline drift in the other type of calculated response quantities. A second set of posttest calculations were made after overcoming the problem of baseline drift, as described later. This set of calculations was not blind in the strict sense because the comparisons of the results of the first set of calculations with test results did influence the assumptions regarding the damping in the system.

However, the finite-element models for the two configurations were devised blind to the experimental results, and no physical properties other than damping were adjusted to better match the test measurements. For the posttest calculations, only minor changes were made in the pretest model to reflect the actual boundary conditions of the DF15 manifold, and the stiffness of the spring hangers was revised as additional information became available after the tests.

4.2 The Finite-element Model

The systems shown in Figs. 1 and 2 were modeled with pipe and truss elements only. The HDU vessel, the DF15 and DF16 manifolds, the spherical tee, and the valves were all approximated with pipe elements. The connection of the

HDU vessel to the pipe nozzles at its top was represented by artificial pipe elements of equivalent stiffness and zero mass density. Concentrated masses were added to the appropriate nodes to represent the actual mass of the parts represented by such artificial elements. A similar technique was used for modeling the tees and the valves. The model comprised 126 straight pipe elements and 28 curved pipe elements. The total mass of the system as modeled, including the concentrated masses, was 78,400 kg.

The pipe supports were modeled with truss elements. The constant-force hangers H16, H17, H18, and H19 were ignored since they were assumed not to respond to dynamic excitation. Although appropriate stiffness was assumed to represent each of the remaining pipe supports, no distinction was made as to the behavior of struts, snubbers, and spring hangers when subjected to dynamic excitation. The nodes corresponding to the wall ends of truss elements were constrained from translation. The pipe ends of the truss elements were located at the appropriate pipe nodes.

In the model of the NRC configuration, H23, like all other struts, was represented by a single truss element. The strut H23 was, however, modeled with two truss elements in the KWU configuration. The pipe ends of the two truss elements were connected each to one of two beam elements that, in turn, were connected to the pipe. The connection of these beam elements to the pipe allowed for free rotation of the former about the axis of the latter. The two ways of modeling H23 were exactly equivalent.

Displacement and rotation restraints were specified at the appropriate nodes of the elements representing the HDU vessel and the DF15 manifold. The excitation was applied directly on the pipe as prescribed accelerations at the two nodes corresponding to the actuator attachment points.

The finite-element model for the KWU configuration was obtained by deleting the elements representing the snubbers and the strut that were dropped from the NRC configuration. Appendix A contains sample input files for the two support configurations and a brief description of the files.

4.3 Tests Simulated and the Excitation

Table 1 shows the tests that were simulated in the posttest calculations. For the first set of posttest calculations, the accelerations measured at the two actuator locations were used as the input excitation. As noted above, this resulted in a large baseline drift in all the computed response quantities except accelerations. The corrections obtained by conventional means of baseline correction such as polynomial trend removal and high-pass filtering were found not to completely

Table 1. SHAM tests simulated in posttest calculations

Test No.	Support Configuration	Excitation Level, % SSE
T41.21.1	KWU	100
T41.21.2	KWU	300
T41.31.2	NRC	100
T41.31.3	NRC	200

remove the trend in the computed results. It was found that drift-free results could be obtained if accelerations *derived* from displacement histories measured at H5 and H25 were used in the place of measured accelerations. It must be noted here that in tests the hydraulic actuators were actually displacement-controlled [3]. The second derivative of the displacement history was obtained by determining a natural cubic spline function for the displacement history. Because the baseline drift was sensitive to the starting time of the input excitation (acceleration) histories, a parameter study was performed to determine the starting time that would minimize the drift in the integrated quantities.

Figures 4 to 7, show the spectral acceleration (for 4% damping) input used in the calculations. Spectra, rather than histories, are given because they are more illustrative than histories for making comparisons. The solid-line curves of Figs. 4-7, denoted as the target acceleration, show the spectrum for the acceleration history that was *intended* to be the excitation at both H5 and H25. These curves are simply scaled from the response spectrum given in Fig. 3(c). The scale factor is unity for 100% SSE excitation, 2 for 200% SSE excitation, and so on. The pretest calculations were made with the corresponding acceleration histories as input. The dotted line curves of Figs. 4-7 show the response spectra for the recorded acceleration histories at H5 and H25. For the first set of posttest calculations, the recorded acceleration histories were used as input. The dashed line curves of these figures show the spectra for the acceleration histories derived as the second derivative of the recorded displacement histories. The second set of posttest calculations were made with the derived acceleration histories as input.

A number of observations are suggested by these figures. First, the excitation at the two actuators is not identical in any of the tests simulated, whether one uses the recorded or the derived acceleration. This observation confirms the need for a calculational method for independent, multi-support input excitation.

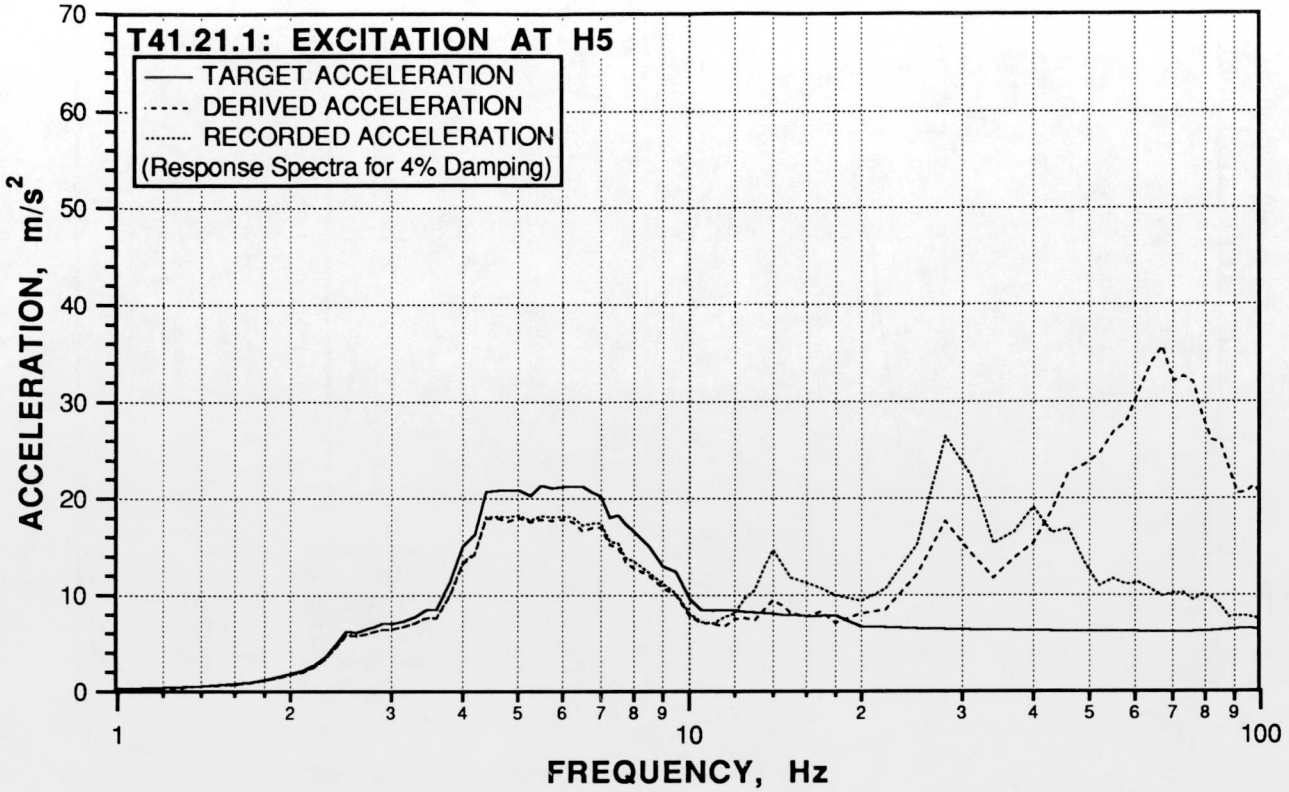

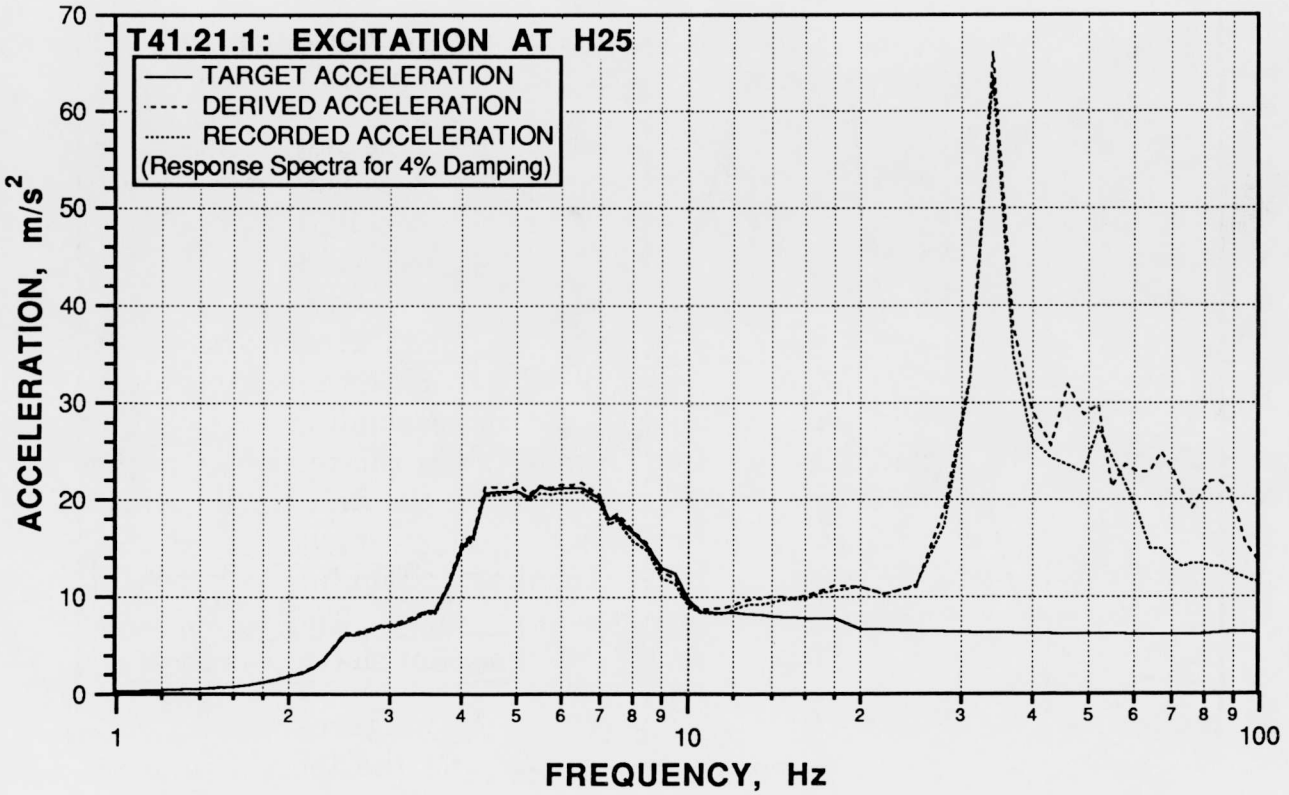

Figure 4. Comparison of Response Spectra of Input Acceleration: Test T41.21.1

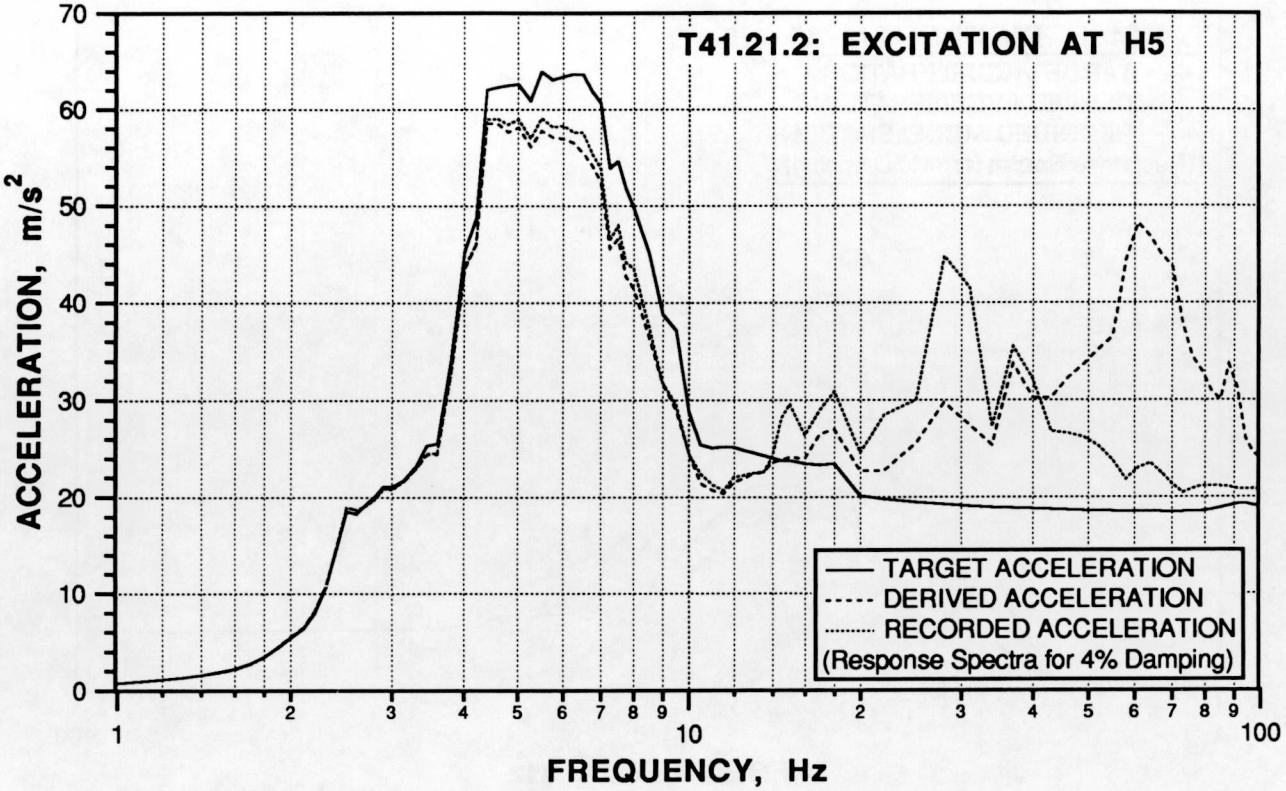

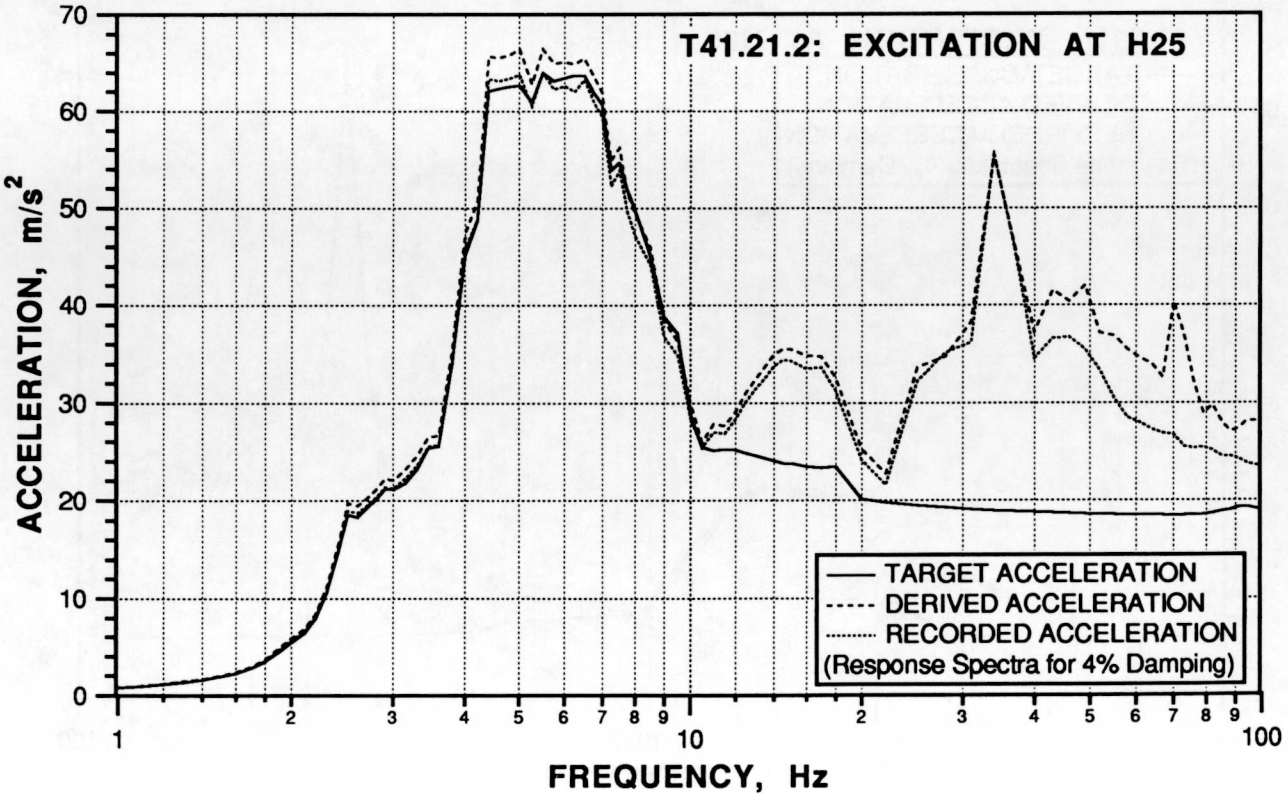

Figure 5. Comparison of Response Spectra of Input Acceleration: Test T41.21.2

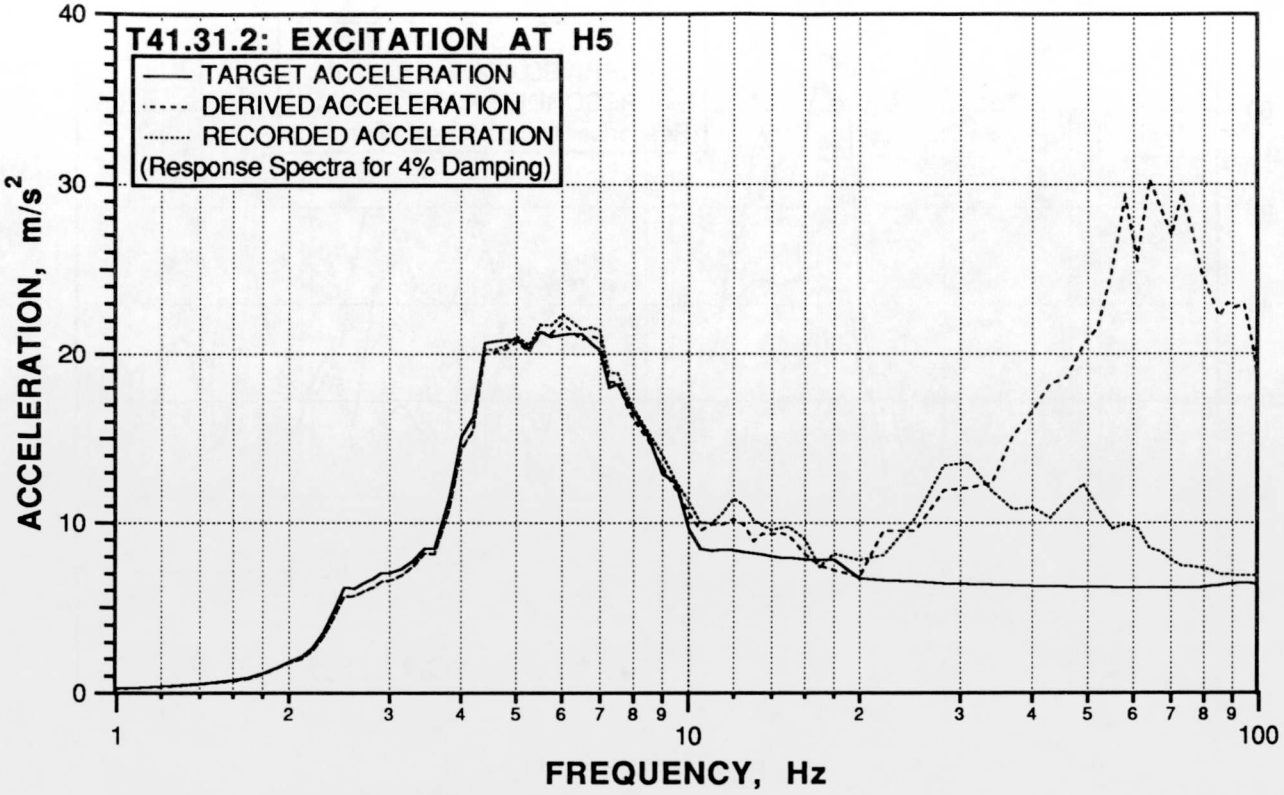

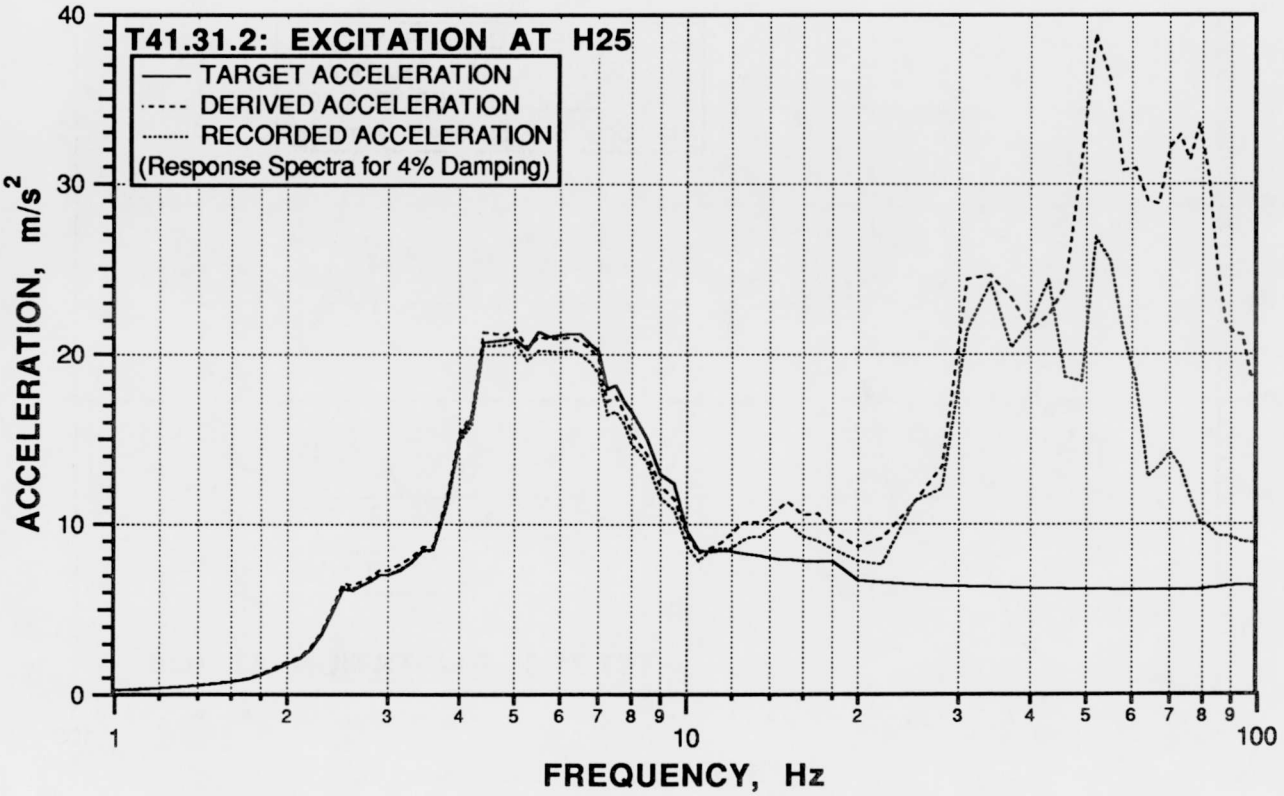

Figure 6. Comparison of Response Spectra of Input Acceleration: Test T41.31.2

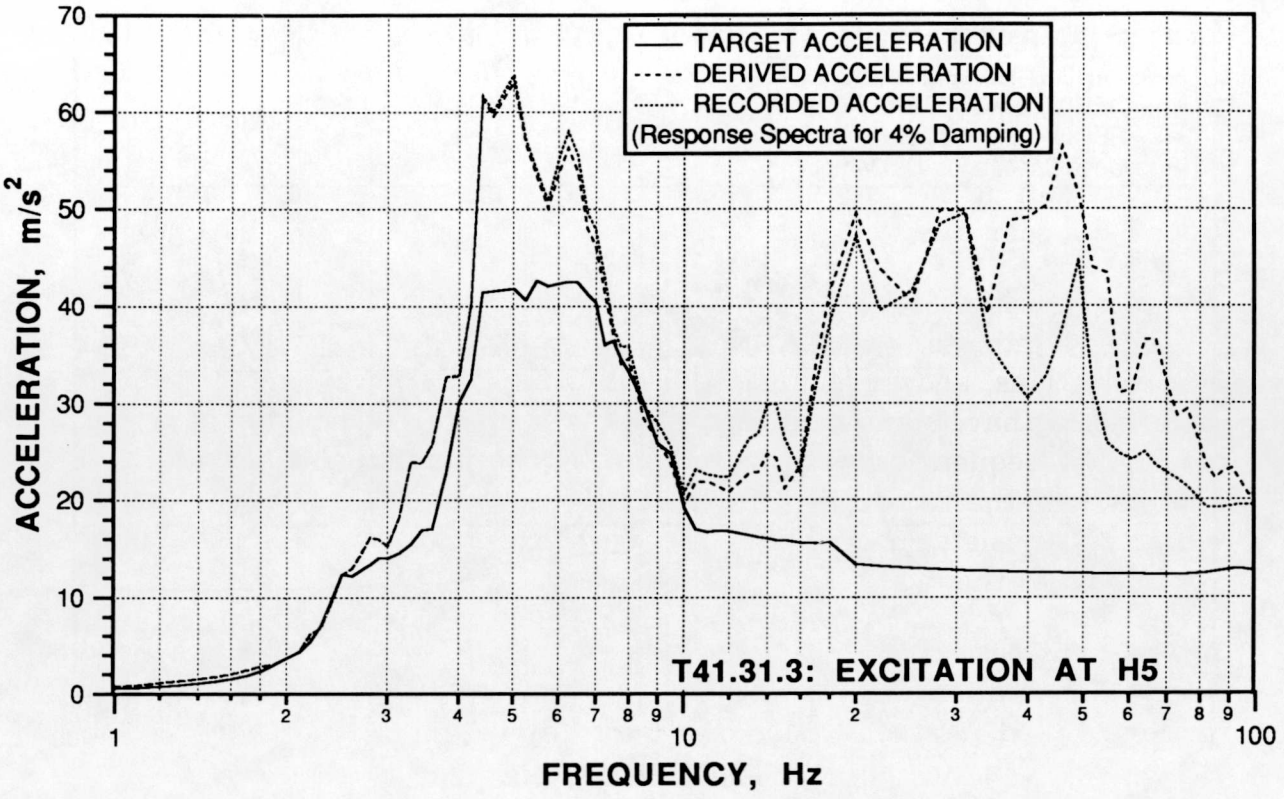

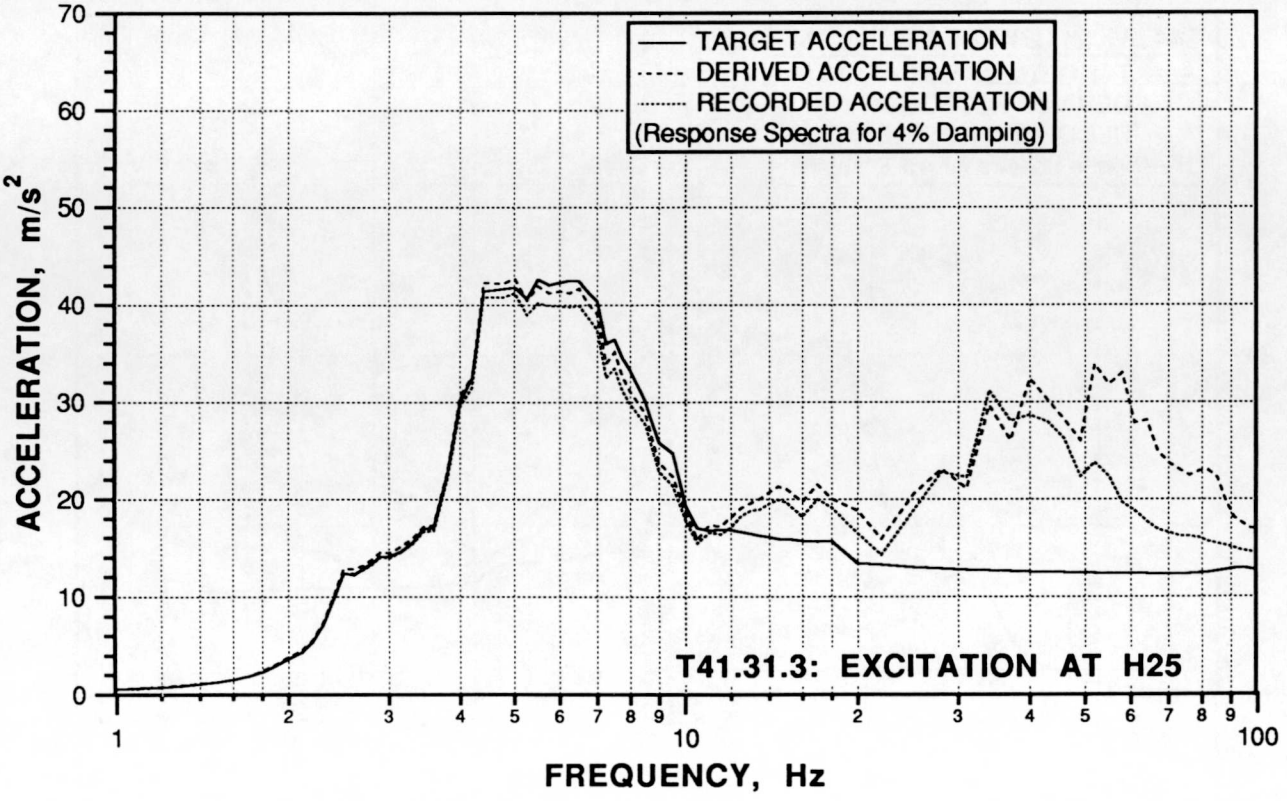

Figure 7. Comparison of Response Spectra of Input Acceleration: Test T41.31.3

Second, in most of the tests, the actual excitation was generally close to the target excitation for frequencies below about 10 Hz. At higher frequencies, the deviation of the measured and derived accelerations at H5 and H25 becomes quite significant for all tests. Third, the derived accelerations show greater deviations from the target than do the recorded accelerations. Finally, in many cases, the higher frequency peaks dominate the derived accelerations.

It was noted earlier that after low-pass filtering, frequency contents greater than 60 Hz were eliminated from the recorded data. The response spectra of the recorded accelerations, shown in Figs. 4-7, confirm this. However, the derived accelerations clearly have significant contents almost up to 100 Hz. It is apparent that these higher frequencies were introduced by the numerical manipulations involved in deriving the second derivatives. By specifying the number of modes included in the analysis or a cut-off frequency, the contribution of these higher-frequency contents to the response can be controlled.

The first set of posttest calculations were made with only 25 modes included for response determination. For the second set of calculations, a cut-off frequency of 60 Hz was specified. A set of calculations were also made with a higher cut-off frequency, i.e., 200 Hz, and the results of these were reported in [10]. For the purpose of the present report, i.e., code verification, it is important that the inputs to the code should be as close to the physical input as possible. Therefore the emphasis here is on the results of the second set of calculations.

5 Results of Calculations and Comparison with Measurements

5.1 Natural Frequencies and Modal Damping

The eigenfunction run of the SMACS subsystem analysis yields the normal modes of the piping system. In this run homogeneous displacement conditions are specified at all boundary degrees of freedom including those that correspond to the H5 and H25 actuators. The random excitation tests of the SHAM series were primarily intended for experimental determination of the modal parameters. Schrammel et al. [11] applied a parameter identification technique to the input-output data from these tests to obtain the modal frequency and damping values for both the KWU and NRC configurations. However, as one or more of the snubbers of the NRC configuration failed or malfunctioned during the random excitation tests, the modal parameters identified for this configuration are not appropriate for comparison with the corresponding analytical results. For the NRC configuration, the calculations gave 45 modes for up to 60 Hz. The first ten modal frequencies, in Hz, of this configuration, determined from the calculations, are as follows: 5.64, 5.66, 8.06, 8.21, 8.79, 9.49, 10.75, 10.93, 15.04, and 15.79. For the KWU configurations, the calculations showed that 47 modes were present up to 60 Hz.

Table 2 gives natural frequencies calculated by SMACS and the frequencies and damping determined from the tests for the KWU configuration for up to 10 Hz. The order of the modes from the calculations are denoted with Roman numerals, as opposed to the order of the test-identified modes which are denoted with Arabic numerals. This is to emphasize that the same order number **does not** necessarily imply the same mode shape. For instance, the first SMACS-determined frequency of 2.15 Hz and the first test-identified frequency of 2.51 Hz may not correspond to the same normal mode, i.e., may not have the same mode-shape vectors.

Up to 12 mode shapes, defined in terms only of two to four mode-shape coefficients, were described by Schrammel and Steinhilber [12]. With the above description as a basis, these authors compared the test-identified modes with those obtained from other analytical investigations. As the SMACS solution process does not provide for easy post-processing of intermediate results, the mode shape information was not analyzed to obtain a description of the analytical modes. This makes it impossible to evaluate the analytical modes by such a comparison. However it is possible to infer some points concerning the modal parameters.

Table 2. Comparison of Modal Parameters of KWU configuration

Order No.	Modal Frequency from SMACS (Hz)	Order No.	Identified Modal Parameters Frequency (Hz)	Damping (%)
i	2.15	1	2.51	3.0
ii	2.68	2	3.33	9.3
iii	3.46	3	3.54	3.1
iv	5.50	4	4.62	3.2
v	5.61	5	5.17	4.6
vi	5.88	6	5.51	6.0
vii	7.07	7	5.89	3.0
viii	7.59	8	6.88	3.2
ix	8.19	9	7.06	3.1
x	9.32	10	7.32	6.2
xi	9.50	11	7.74	4.2
xii	9.83	12	8.28	4.2
		13	8.37	0.9
		14	9.33	3.5
		15	9.63	1.3

Schrammel and Steinhilber [12] note that the the fundamental mode was possibly not excited in the identification tests, due to lack of sufficient energy in the test excitation at about 2 Hz. Four out of five analytical models included in [12] gave the first mode frequency as 2.1 Hz. This frequency is close to that given as the fundamental frequency in the present analysis, i.e., 2.15 Hz. Most other frequencies determined from the SMACS analysis also appear among the frequencies given by other investigators. From Table 2 it is clear that more modes are identified from test data than calculated analytically for frequencies up to 10 Hz. The same is seen to be the case with the analytical results of the five

different investigations reported in [12]. These points increase the confidence that the basic features of the analytical model used in the present case are correct.

It is easier to compare the responses than the modal characteristics in the case of the SMACS results. Moreover from a practical point of view, the responses are more useful quantities than the modal parameters, perhaps with the exception of damping. For the second set of calculations, a uniform modal damping of 3% was assumed. This value would seem to be too low for many modes as indicated by the test-identified values in Table 2.

5.2 Accelerations

Thirty-two channels of response acceleration were computed for each test. They corresponded to 32 channels of measurement at 11 locations distributed over the entire piping system as shown in Fig. 8. The accelerations, except at QB122, were triaxial measurements. The vertical component was not measured at QB122.

As noted before, only acceleration responses were computed in the first set of posttest calculations for which the recorded accelerations were used as input. Two series of computations were made in this set, with the first one assuming PVRC damping criterion and the second one assuming a uniform modal damping of 3% of critical damping. Only the first 25 modes were included for response calculations. This meant that modal truncation occurred at 32 Hz for the NRC configuration, and 26.5 Hz for the KWU configuration. The first set of calculations served mainly to reveal the effect of different damping ratios on the acceleration response. Figures 9-11 show the comparison for acceleration components at gage location RS761 for tests T41.21.1 and T41.31.2, from the first set of calculations. The comparisons for other locations and for other tests were plotted and inspected but not included here.

The acceleration response of the system with PVRC damping was underestimated at most locations. With a uniform damping of 3%, the calculated response became larger, as would be expected. However, at many locations the calculated response was still smaller than the measured response. Generally, the acceleration component in the vertical, i.e., y, direction was significantly underestimated. There were a few locations at which the acceleration was slightly overestimated when the damping was changed to 3% from the levels of the PVRC damping. The underestimation of acceleration response was noted to become quite large at frequencies higher than about 7 Hz.

In the second set of posttest analysis the input excitation used was the set of acceleration histories derived from the recorded displacement. For this set of

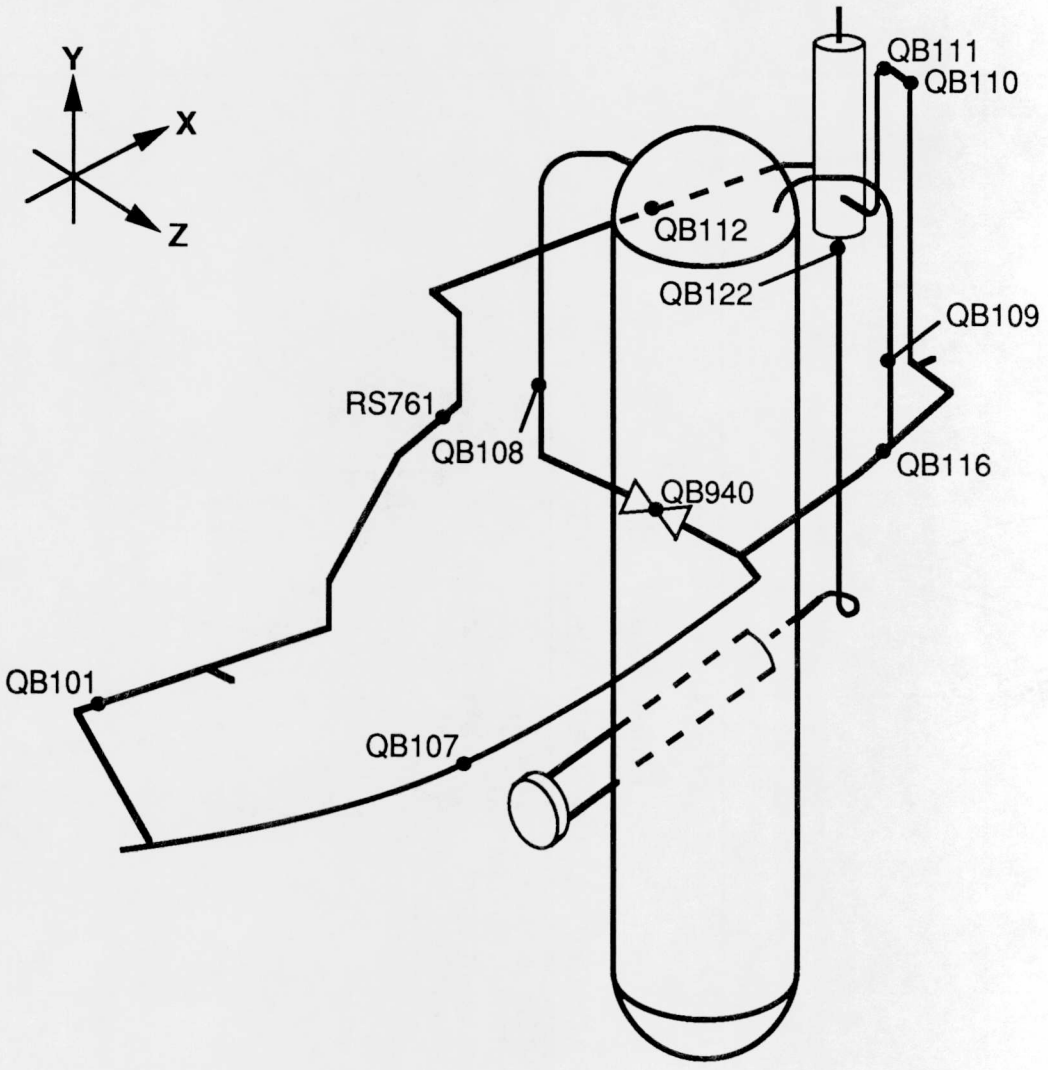

Figure 8. Acceleration Measurement Locations in the VKL Piping System for SHAM Tests

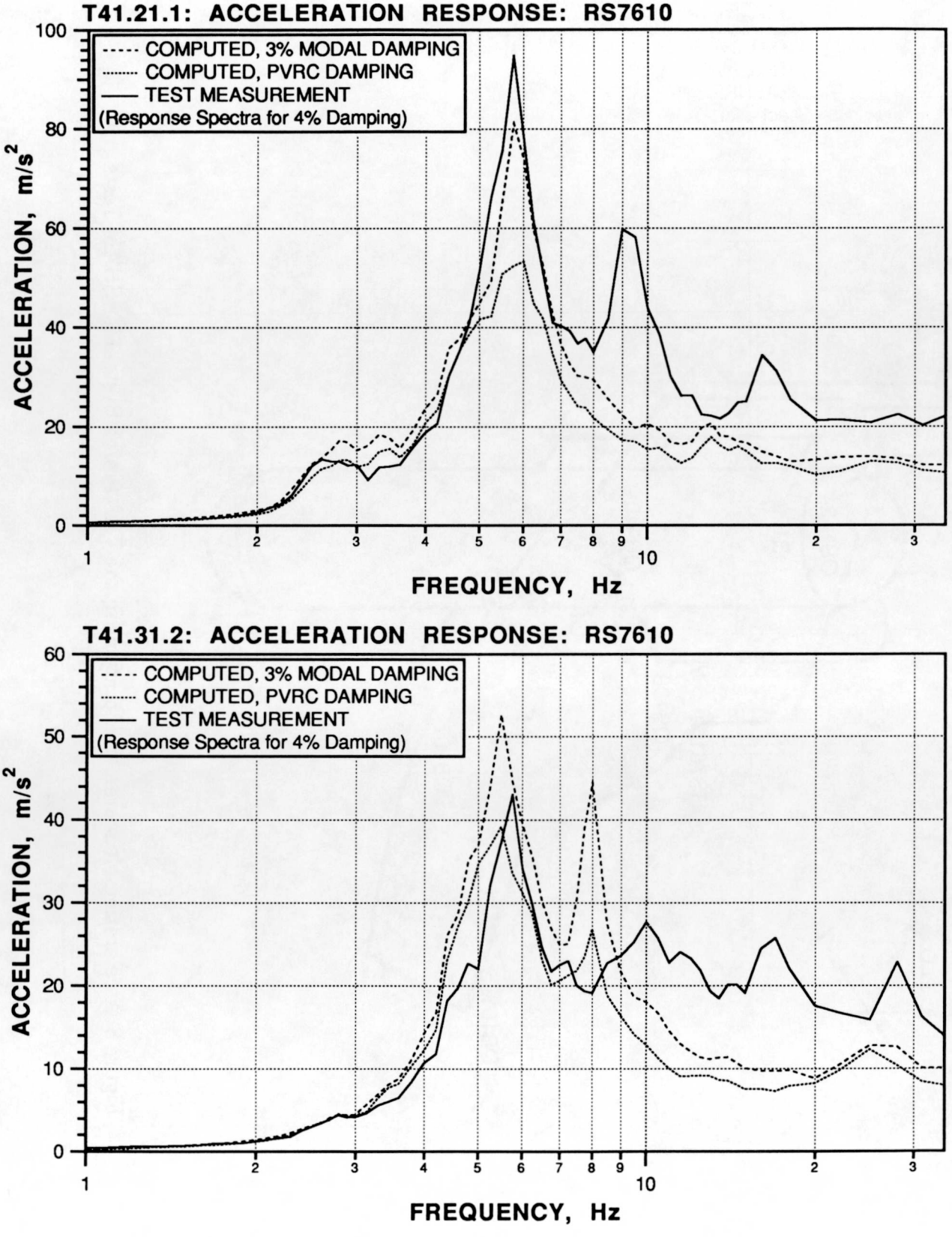

Figure 9. Effect of Damping on Calculated Accleration Response: x component at RS761

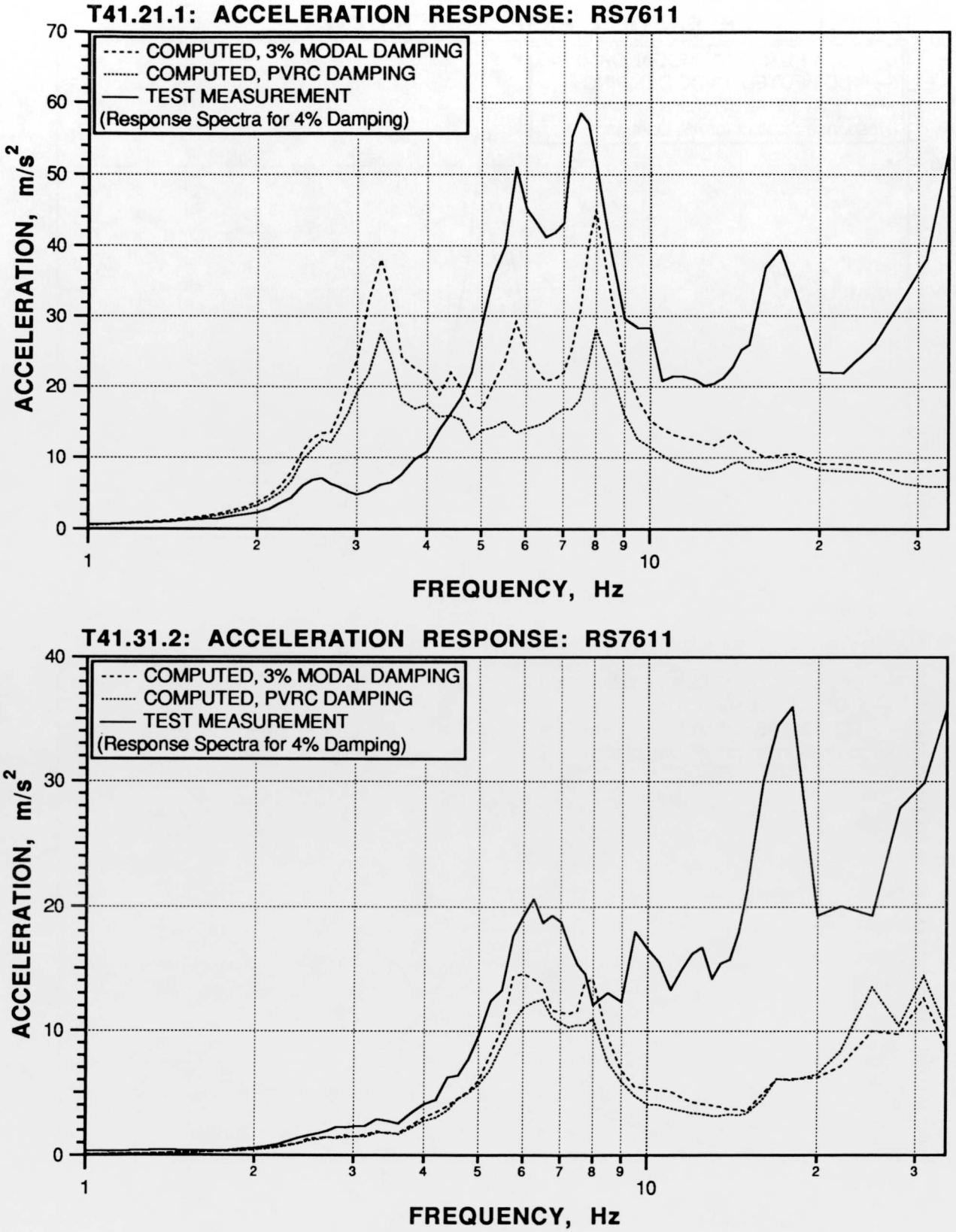

Figure 10. Effect of Damping on Calculated Accleration Response: y component at RS761

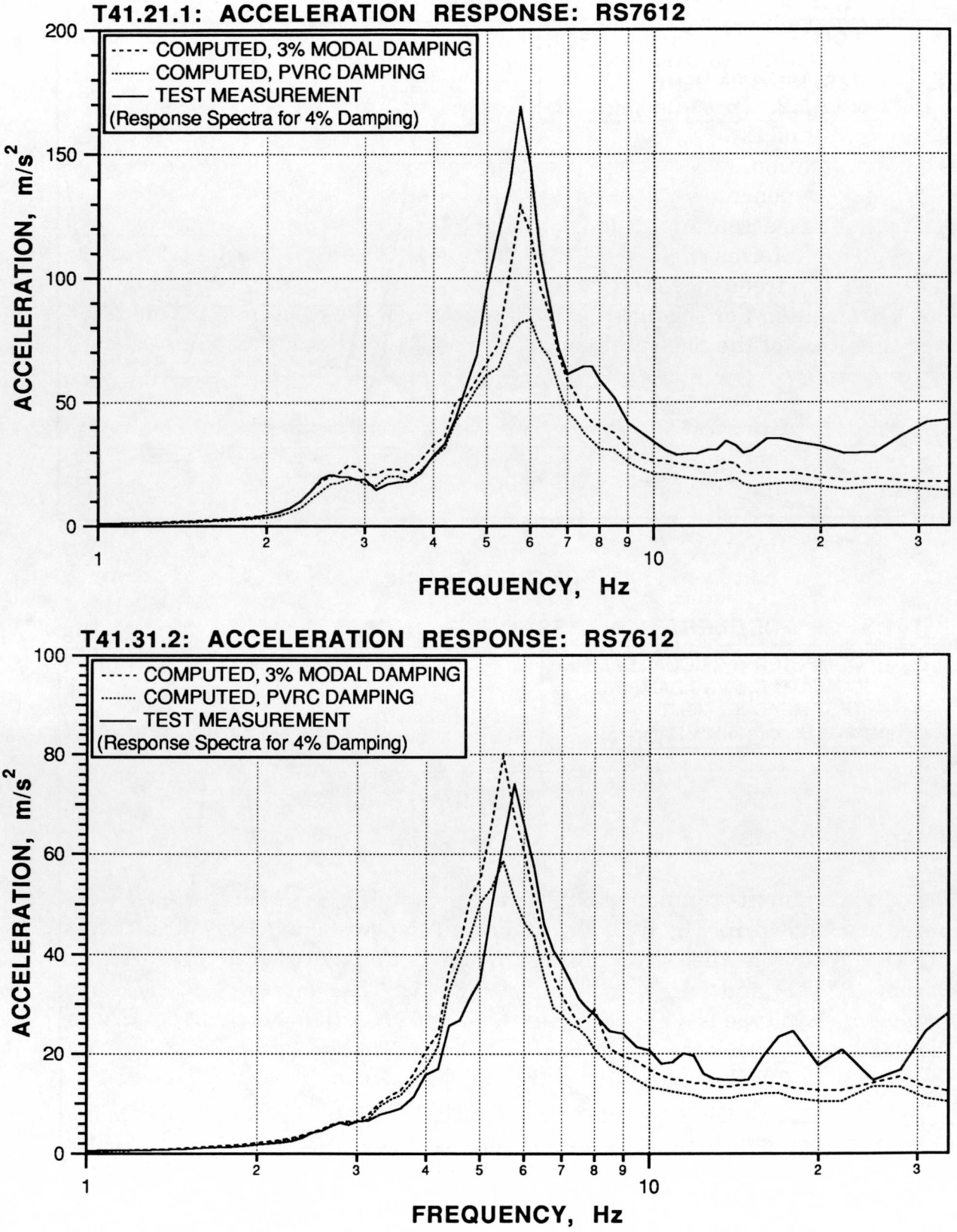

Figure 11. Effect of Damping on Calculated Accleration Response: z component at RS761

runs the cut-off frequency was set at 60 Hz and the systems were assumed to have a uniform modal damping of 3%. Appendix B contains response spectra plots comparing the measured and calculated accelerations at a number of locations for the test T41.31.2. In these plots, the solid line shows the response spectrum (for 4% damping) of the recorded acceleration and the dashed line that of the calculated acceleration. With a few exceptions, the agreement is not good. The spectra of the x component of acceleration at QB110, QB111, and QB116, and that of the z component of acceleration at QB110, QB111, and RS761 show somewhat better agreement in terms of the frequency content of the two sets of data. For the other locations, the frequency distribution of the calculations does not match that of the measurements. For the most part the spectra of the calculated acceleration are lower than that of the measurement. The results from other tests also show a similar pattern.

To make quantitative comparisons, the peak (maximum absolute value) of the acceleration history is selected as the indicator. Table 3 gives the ratio of the calculated to measured peak acceleration for all acceleration channels for the four tests included in this study. Where the ratio is smaller than unity the response is underestimated. The values of the mean and the standard deviation, taken together, are indicators of general nature of the estimates. The calculations generally underestimate the response. The worst underestimates occur for the z component at QB112 and QB122 while the worst overestimates are obtained for the y component at QB108 and QB116. On the average the peaks are underestimated by the range of 22 to 30% for the four tests. The scatter in the values of the ratio, i.e., from channel to channel, is significant as indicated by the standard deviation.

5.3 Displacements

The displacement components for which comparisons are made were distributed as shown in Fig. 12. Two types of displacement transducers were used in the tests on the NRC configuration: linear variable differential transformer (LVDT) and wire-gage transducer [13]. The locations of the more numerous wire-gage type are indicated in Fig.12 by QN1xxx, where xxx is a three-digit identification. The locations of the LVDT type are marked in the figure by QN3xxx (L). Except in the cases of QN1271 and QN1303/QN3303 (L), the last digit of the channel identification indicates the direction of the component, with 1, 2, and 3 denoting x, y, and z directions respectively. For example, QN1011 is the x component at the location shown. As may be noted from this figure, at three of these locations, QN101, QN122, and QN135, the measurement was triaxial. The other measurement points shown corresponded to snubber or strut locations and at each of these points only the component parallel to the axis of the support was measured. Thus QN1271 measured the component of pipe displacement along the

Table 3. Comparing measured and calculated peak values of acceleration histories (Accelerations in m/s^2)

Accel.	Accel.	Test: T41.21.1			Test: T41.21.2			Test: T41.31.2			Test: T41.31.3		
Channel	Comp.	Meas.	Calc.	Ratio	Meas.	Calc.	Ratio	Meas.	Calc.	Ratio	Meas.	Calc.	Ratio
QB1011	X	9.88	4.38	0.444	24.49	10.26	0.419	10.98	6.30	0.574	18.64	11.39	0.611
QB1012	Y	17.78	18.49	1.040	47.68	43.27	0.908	14.39	11.90	0.827	42.36	21.23	0.501
QB1013	Z	16.07	10.97	0.683	37.59	26.46	0.704	11.46	7.29	0.636	25.55	32.91	1.288
QB1071	X	9.52	6.62	0.696	21.58	17.69	0.820	10.59	7.65	0.722	27.19	16.60	0.611
QB1072	Y	5.64	5.48	0.970	13.83	14.14	1.022	8.64	2.73	0.316	16.97	7.39	0.436
QB1073	Z	11.61	8.29	0.714	19.54	17.44	0.893	11.36	9.02	0.794	26.81	21.08	0.786
QB1081	X	11.42	10.49	0.918	29.96	19.79	0.661	9.57	9.98	1.043	32.53	23.33	0.717
QB1082	Y	4.30	8.22	1.914	7.55	10.72	1.420	3.56	6.00	1.685	12.62	7.13	0.565
QB1083	Z	12.04	7.04	0.585	20.74	12.28	0.592	9.00	5.44	0.604	19.82	26.67	1.345
QB1091	X	12.02	5.86	0.487	24.97	15.75	0.631	Faulty			Faulty		
QB1092	Y	4.09	4.44	1.086	8.80	6.16	0.700	3.76	1.84	0.489	10.56	4.04	0.382
QB1093	Z	12.27	4.85	0.396	31.39	12.57	0.400	10.08	3.80	0.377	23.96	10.51	0.439
QB1101	X	25.92	29.74	1.147	72.08	78.77	1.093	34.42	23.06	0.670	52.56	44.70	0.850
QB1102	Y	7.02	3.26	0.465	13.69	6.39	0.467	7.04	5.43	0.771	15.43	4.50	0.292
QB1103	Z	Faulty			Faulty			25.27	23.56	0.932	47.37	43.91	0.927
QB1111	X	23.83	22.46	0.943	56.03	62.94	1.123	22.14	18.76	0.847	40.37	37.14	0.920
QB1112	Y	Faulty			Faulty			Faulty			Faulty		
QB1113	Z	19.58	18.17	0.928	58.76	53.41	0.909	19.14	20.84	1.089	35.49	37.50	1.057
QB1121	X	12.53	8.75	0.698	30.52	22.01	0.721	10.71	8.53	0.796	22.22	14.25	0.641
QB1122	Y	8.07	4.46	0.553	21.62	12.38	0.573	7.00	3.02	0.431	13.23	5.52	0.417
QB1123	Z	28.14	7.07	0.251	46.12	19.42	0.421	30.13	6.13	0.203	40.62	12.05	0.297
QB1161	X	9.08	8.64	0.952	20.22	19.70	0.974	9.82	7.46	0.760	26.96	14.40	0.534
QB1162	Y	3.36	4.52	1.344	5.66	6.25	1.105	3.43	1.88	0.548	11.29	4.07	0.360
QB1163	Z	15.06	5.75	0.382	32.06	12.11	0.378	8.20	5.68	0.693	28.92	18.21	0.630
QB1221	X	11.32	8.50	0.751	29.43	27.52	0.935	11.87	8.83	0.744	21.14	15.14	0.716
QB1223	Z	9.39	2.86	0.304	28.40	7.03	0.247	9.99	2.76	0.276	17.01	4.95	0.291
QB9401	X	10.40	9.08	0.873	25.52	21.28	0.834	7.87	9.97	1.267	21.68	14.48	0.668
QB9402	Y	Faulty			Faulty			Faulty			Faulty		
QB9403	Z	7.46	5.61	0.752	11.75	8.74	0.744	4.51	3.69	0.818	11.15	11.78	1.056
RS7610	X	14.68	12.19	0.830	38.30	34.52	0.901	11.39	9.63	0.845	16.99	19.05	1.121
RS7611	Y	13.63	9.74	0.715	49.17	25.25	0.514	10.25	4.79	0.467	14.37	11.94	0.831
RS7612	Z	23.00	20.10	0.874	47.26	55.55	1.175	12.39	11.56	0.933	23.80	26.55	1.116
Mean				0.783			0.768			0.730			0.704
Std. Dev.				0.343			0.281			0.308			0.302

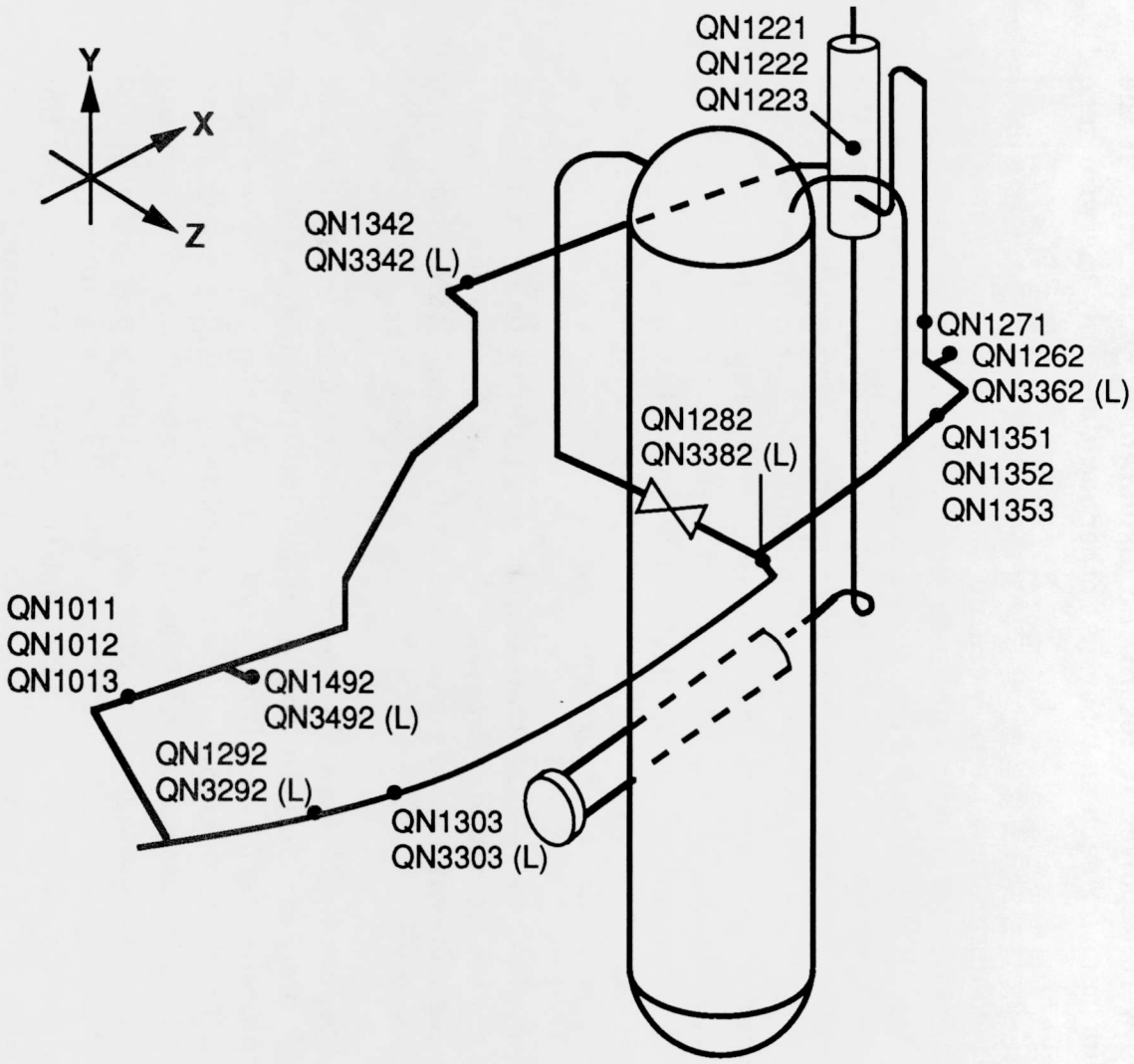

Figure 12. Displacement Components for Comparisons

horizontal strut H3, which made an angle of 45° with x and z axes. Similarly QN1303/QN3303 (L) measured the pipe displacement component along the horizontal snubber H7, which made an angle of 10.18° with the z axis.

The LVDT type transducers were more accurate and more reliable than the wire-gage type. For this reason, the former were used primarily to record the snubber behavior. Thus for the NRC configuration, both the wire-gage and the LVDT transducers were deployed to record the displacement of the pipe at the snubber attachment point for each snubber. At other locations only the wire-gage transducers were used.

For the KWU configuration there were no snubbers and consequently no LVDTs were used. All displacements were measured with wire-gage transducers only. However, though all the snubbers and the strut H3 were absent, all the wire-gage transducers deployed for the NRC configuration (including those along the direction of the missing snubbers and strut) were retained. Consequently, for the KWU configuration, all the displacement measurements were at points where the pipe was not attached to any support. For the NRC configuration, however, only the three locations, QN101, QN122, and QN135, were at points that had no supports attached to the pipe. Because of this difference, two sets of plots are given in Appendix C, the first from test T41.21.1 (KWU configuration) and the second from test T41.31.2 (NRC configuration)

During the tests, the wire-gage transducers were found to be unreliable when the displacements recorded were less than about 5 mm peak-to-peak. Therefore such measurement records were not included for comparison with analytical results.

The figures of Appendix C show the measured displacement in the top plot and the computed displacement in the bottom plot. Considering first the comparison of displacements for the KWU configuration, the two wave forms agree well for most of the compared histories. Amplitudes of displacement are not generally as much underestimated as those of the accelerations. While many histories show some underestimation, only a few, such as QN1013, are overestimated. The displacement component QN1223 seems to be grossly underestimated. However, when we consider that this displacement is along the direction of the strut H23, and was made at a point only a few centimeters away from the point of attachment of this strut to the DF16 manifold, the measured displacement amplitudes seem to be too large to be correct. It is apparent that the clamp attaching H23 to DF16 became loose during the test and permitted a relatively large amount of movement at some point after the excitation began. This movement seems to have been predominantly rotational about the axis of DF16 manifold. Because of the way in which the wire-gage is attached to this manifold, the rotational movement of DF16 would introduce a large error to this

linear measurement. Therefore it is not valid to compare the analytical history with this measurement.

Many, but not all, of the calculated displacement histories show a significantly slower ring down of the motion than the corresponding measurements. This would seem to indicate that the damping assumed might have been too low.

The displacement comparisons for the NRC configuration is best considered by dividing the plots of T41.31.2 in Appendix C into two categories: the wire-gage channels and the LVDT channels. As noted before only those wire-gage channels that recorded displacement amplitudes of about 5 mm or more (peak-to-peak) have been used for making comparisons. Furthermore the measurement at QN1223, though included in Appendix C, is not a valid measurement as discussed before. Of the remaining gages, the measurement at QN1221 is suspect as the record shows one-sided oscillations for no apparent reason. If we ignore the oscillations below the zero-mean line, and compare only the upper half of the measurement history with the corresponding part of the calculated history, we see that the wave forms agree very well and the calculated amplitudes are very close to the recorded ones. Considering the remaining three channels, we notice that the calculations overestimates the amplitudes for all of them. The agreement between the calculated and measured wave forms is only fair. However, unlike in the case of the KWU configuration, the decay of the displacement histories is comparable between test and calculation.

The second set of plots from this test consist of the LVDT channels. All of them measured the displacement along the direction of snubbers. All of them show that the analysis gives far smaller displacements than the measurements. This discrepancy is due to the unexpected behavior of the snubbers. The measurements show that the snubbers did not lock-up and permitted significant travel, approaching a peak-to-peak travel of 6 mm in one case. Most of the records also show that the snubber travel has a tendency to wander instead of to oscillate about the zero-mean line. The analysis assumed that the snubbers lock-up for the entire duration of dynamic excitation and that the pipe displacement is only due to the elastic deformation of the snubber. These comparisons serve only one purpose, namely to show that modeling the snubbers as elastic truss or spring elements is not valid.

To put the amplitude comparisons on a quantitative basis, the peak values of the recorded history were compared with those of the estimated histories for all the four tests. The results are given in Table 4. The LVDT displacement measurements along the snubbers as well as the wire-gage measurements with a peak-to-peak amplitude of less than 5 mm are not included for the quantitative comparisons for the reason noted before. The ratios given in the table are obtained

Table 4. Comparing measured and calculated peak values of displacement histories
(Displacements in mm)

Disp. Channel	Disp. Comp.	Test: T41.21.1			Test: T41.21.2			Test: T41.31.2			Test: T41.31.3		
		Meas.	Calc.	Ratio	Meas.	Calc.	Ratio	Meas.	Calc.	Ratio	Meas.	Calc.	Ratio
QN1011	X	4.25	2.97	0.701	17.10	9.23	0.540	Faulty			3.77	4.59	1.217
QN1012	Y	13.07	11.66	0.892	27.25	37.04	1.359	3.57	4.45	1.247	6.42	8.82	1.373
QN1013	Z	15.38	17.13	1.114	58.97	56.40	0.956	Faulty			Faulty		
QN1221	X	6.43	5.54	0.861	19.05	17.12	0.899	Faulty			12.43	10.80	0.869
QN1351	X	7.92	6.15	0.776	28.44	19.84	0.698	3.51	4.06	1.156	7.43	10.55	1.419
QN1353	Z	7.04	5.69	0.809	26.47	18.86	0.712	3.96	4.63	1.169	12.44	13.62	1.095
QN1271	*, H3	11.77	9.02	0.766	39.90	28.74	0.720						
QN1282	Y, H6	4.83	4.40	0.912	18.71	14.31	0.765						
QN1292	Y, H8	8.61	10.44	1.213	31.53	34.39	1.091						
QN1303	*, H7	14.49	14.15	0.976	51.19	46.64	0.911						
QN1342	Y, H12	6.45	10.05	1.557	25.96	30.82	1.187						
QN1492	Y, H22	12.59	12.21	0.970	31.70	38.56	1.216						
Mean				0.962			0.921			-------			1.194
Std. Dev.				0.238			0.249			-------			0.223

* These displacement components were parallel to the axis of the indicated strut (H3) or snubber (H7) for all tests. Even when the respective support was absent, QN1271 measured the horizontal component inclined an angle of 45° to the x and z axes, and QN1303 measured the horizontal component making an angle of 10.18° to the z axis.

by dividing the calculated peak value by the measured peak. The mean values of this ratio for the KWU configuration tests shows that the peak values are underestimated by up to about 8%. The test T41.31.2 on the NRC configuration (100% SSE loading) had too few valid channels to compute the mean value for this ratio. However all the valid results from this test as well as the mean value from the test T 41.31.3, show that the peak displacements are overestimated by about 20%. The standard deviation values show that the scatter is of the order of about 25%. The nature of the displacement estimates is significantly better than those for acceleration estimates as may be seen by comparing the bottom lines of Tables 3 and 4. Another interesting point is that though the accelerations are underestimated, the displacements are overestimated for the NRC configuration.

5.4 Support Forces

Force in Snubbers

The first part of Appendix D contains plots comparing the measured and calculated snubber force histories for test T41.31.2. The plots for the test T41.31.3 are similar.

The plots show that the analysis does not estimate the snubber forces very well. Almost all the calculated histories underestimate the force in the snubbers. Moreover, many of the recorded histories show that the snubber force amplitude was very small or almost zero for small durations intermittently during the tests. It seems that the snubbers did not remain continually locked for the duration of the excitation. The linear analysis, however, assumes that the snubber behaves like a strut during the entire test and consequently shows the force to continually oscillate without the amplitude staying near zero for any length of time.

Table 5 presents a quantitative comparison of the peak force values. The peak values are underestimated by as much as 76% in one case. QA3262 (H2) is the significant exception in both tests. It is not obvious why the force in this snubber is overestimated by a factor as high as 2.6. It is mainly because of this outlier, the mean value and the standard deviation are much higher than the other histories would suggest.

Force in Struts

The second part of Appendix D gives the comparison of strut forces from the same test as above, i.e., T41.31.2. Among the plots in this part,the measured force history identified as QA1513 is actually the sum of the recorded force histories of

Table 5. Comparing measured and calculated peak values of Snubber Force histories (Force in kN)

Channel ID	Snubber	Test: T41.31.2			Test: T41.31.3		
		Meas.	Calc.	Ratio	Meas.	Calc.	Ratio
QA3262	H2	3.35	7.82	2.337	9.18	24.02	2.616
QA3282	H6	5.61	2.76	0.492	8.28	10.26	1.239
QA3292	H8	6.13	1.44	0.235	10.60	3.30	0.311
QA3303	H7	11.07	6.10	0.551	17.92	16.74	0.934
QA3342	H12	1.06	0.86	0.816	3.38	1.67	0.494
QA3492	H22	1.84	1.06	0.574	5.07	2.32	0.457
Mean				0.834			1.008
Std. Dev.				0.759			0.860

the two struts making up the strut H23. It became necessary to do this because the analysis model for the NRC configuration represented H23 with a single truss element.

The calculations significantly underestimate the force in struts also. The recorded history for QA1243 (H4) shows that the force remained close to zero continually for intermittent and small durations. This suggests that there were small gaps in the connections of the strut to the pipe. Obviously the linear model could not represent such behavior. Even though the other histories do not show this as clearly, it was likely that small gaps were present in the other struts.

The third part of Appendix D contains comparison plots for strut forces for the test T41.21.1. This test was on the KWU configuration which had no snubbers and one less strut (H3) than the NRC configuration. The analytical estimates of forces in the all the struts, including H4 (i.e., QA1243), were lower than the measurement for this configuration.

Considering now the two struts of H23, we note that the test measurements QA1513 and QA1517 are clearly different from each other. The unequal forces in the two struts of H23 show that the pipe clamp of H23 did not permit completely free rotation about the axis of DF16. However, though the clamp-to-pipe connection was intended to be tight, i.e., permitting no relative rotation, it appears that during the tests the friction between the clamp and pipe was overcome and some relative rotation did take place [13]. In linear analysis it is obviously not possible to model such nonlinear behavior as friction. A choice had to be made between a joint that is fully tight or one that allows free rotation. The latter was selected in the present model because that is consistent with the modeling of all the other supports.

Table 6 gives a summary of the peak value comparisons for all the four tests. If we compare the values of standard deviation from Table 5 to that of Table 6, we might then note that although the strut forces are significantly underestimated like the snubber forces, the scatter in the estimates is lower for the struts than for the snubbers.

5.5 Bending Stresses in Pipe

Strain measurements were made at a number of locations during the tests. These may be broadly classified into three categories: sections of straight pipe, sections of elbows, and special sections such as on valves or nozzle welds. Among these the ones that are most appropriate for comparison with SMACS calculations are the measurements on straight pipe sections. The strain distributions at other sections are much more complex than those assumed by the simplified Euler beam theory formulas. The SMACS calculations give results in terms of moments and forces at specified sections. It is valid only at straight pipe sections to apply the simple beam formulas to obtain the stresses from these moments and forces. Consequently the comparisons of bending stresses are made only for the measurement locations at straight pipe locations. These locations are shown in Fig. 13.

At each of the cross sections shown in Fig. 13, six strain gages were mounted as shown in Fig. 14. Strain gage 5, which is not visible in the figure, is placed as the mirror image of gage 4 about gage 1. By designating the pipe axis as local coordinate 3, we define a local coordinate system as shown in Fig. 14. Then the bending stresses σ_{b1} and σ_{b2} are given by

$$\sigma_{b1} = \frac{1}{2}(\varepsilon_1 - \varepsilon_6)E$$

$$\sigma_{b2} = \frac{1}{2}(\varepsilon_2 - \varepsilon_3)E,$$

where ε_1, ε_2, ε_3, and ε_6 are the longitudinal strains recorded by the strain gages 1, 2, 3, and 6 respectively, and E is the Youngs modulus.

The corresponding calculated bending stresses are obtained from the simple beam formulas as

Table 6. Comparing measured and calculated peak values of Strut Force histories
(Force in kN)

		Test: T41.21.1			Test: T41.21.2			Test: T41.31.2			Test: T41.31.3		
Channel ID	Strut	Meas.	Calc.	Ratio	Meas.	Calc.	Ratio	Meas.	Calc.	Ratio	Meas.	Calc.	Ratio
QA3271	H3							6.37	5.41	0.849	21.20	16.55	0.780
QA1243	H4	18.03	11.49	0.637	38.87	24.67	0.635	11.48	6.41	0.558	26.75	18.77	0.702
QA3313	H9	2.82	2.49	0.882	9.25	7.67	0.829	1.65	1.04	0.627	2.76	2.69	0.974
QA3321	H10	3.51	3.21	0.914	11.70	9.98	0.853	2.33	1.70	0.731	5.29	4.73	0.894
QA3333	H11	4.35	2.03	0.465	10.42	6.56	0.629	4.23	1.95	0.461	7.23	3.70	0.512
QA1513	H23							37.12	14.68	0.395	75.58	29.79	0.394
QA1513	H23/1	31.25	7.71	0.247	60.62	22.23	0.367						
QA1517	H23/2	22.54	7.71	0.342	55.68	22.23	0.399						
Mean				0.581			0.618			0.604			0.709
Std. Dev.				0.278			0.205			0.169			0.222

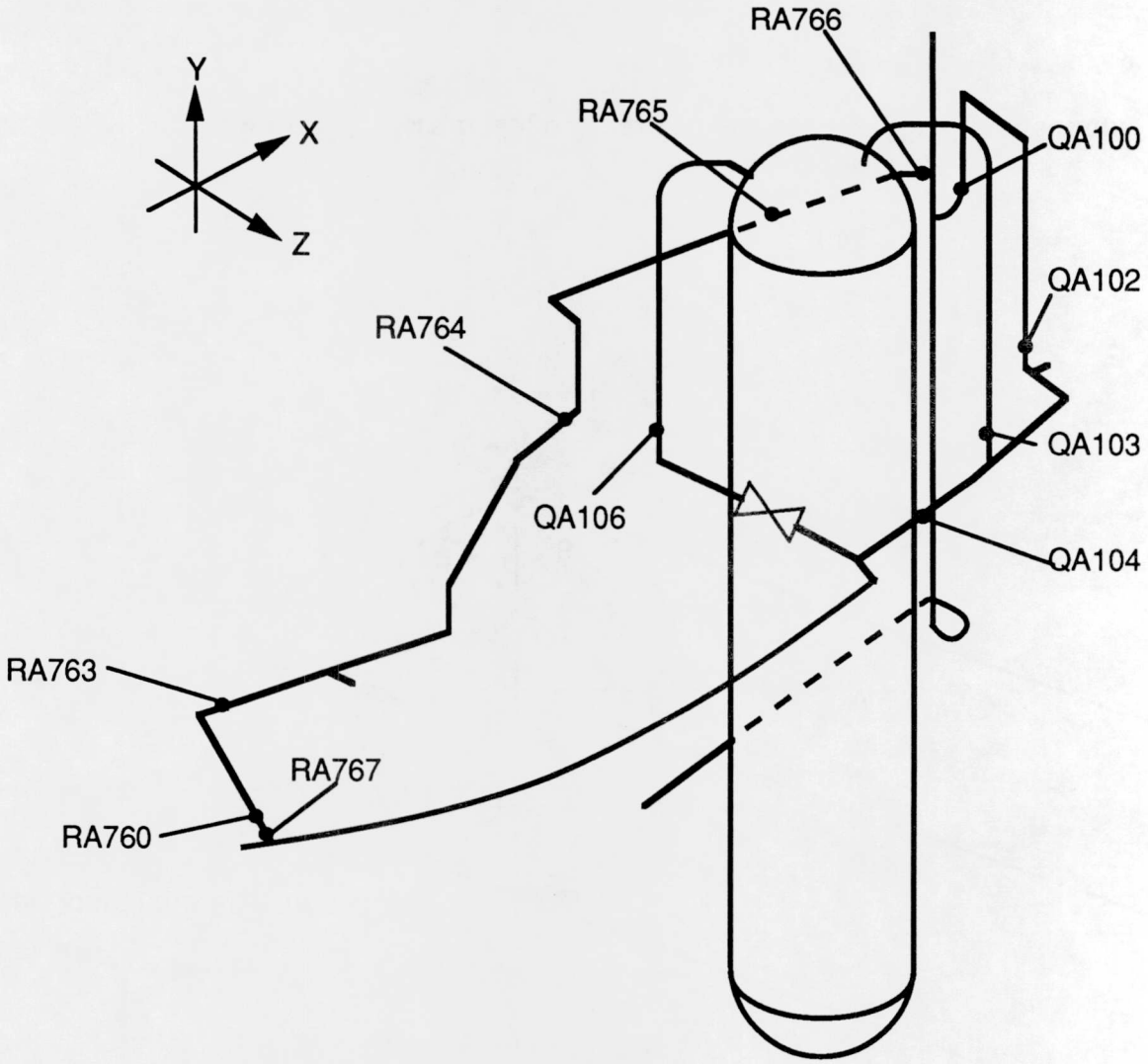

Figure 13. Strain Measurement Locations Selected for Stress Comparisons

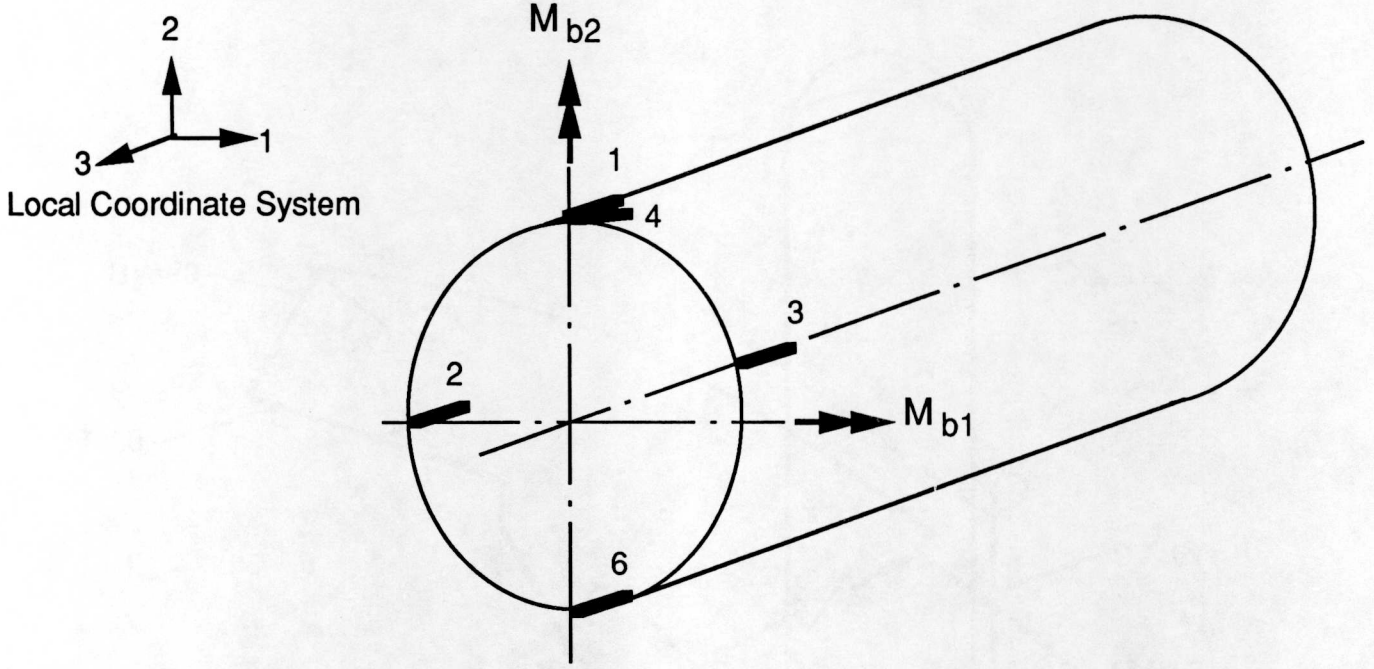

Figure 14. Strain Gage Arrangement at Straight Pipe Sections

$$\sigma_{b1} = \frac{M_{b1}}{Z}$$

$$\sigma_{b2} = \frac{M_{b2}}{Z},$$

where M_{b1} and M_{b2} are the bending moments about the local 1 and 2 axes respectively and is the section modulus of the pipe cross section. The section modulus is expressed as

$$Z = \frac{\pi\left(r_o^4 - r_i^4\right)}{4r_o},$$

where r_o and r_i are the outer and inner radius of the pipe section, respectively. To make appropriate comparisons, it was necessary to match the local coordinate system of Fig. 14 with that of the SMACS calculations.

The first part of Appendix E consists of plots of bending stresses σ_{b1} and σ_{b2}, from test measurements and SMACS calculations for test T41.21.1 (KWU configuration, 100% SSE), for the 11 locations shown in Fig.13. In general, the computed stress histories are underestimated at almost all locations. The greatest underestimate occurs for σ_{b2} at RA765, in the 100 mm diameter pipe (see Fig. 2 for pipe size). For the pipe runs with 200 mm diameter pipe, the only exception occurs at QA106 where the calculated σ_{b1} is slightly overestimated. For the 100 mm diameter pipe sections, the exceptions are that σ_{b1} is overestimated at RA766 and σ_{b2} is overestimated at RA763 for the first half of the history. The same pattern of comparisons was observed from the stress history plots for test T41.21.2.

However, the pattern that emerged from the tests on the NRC configuration was slightly different. The second part of Appendix E contains plots of bending stresses σ_{b1} and σ_{b2}, from test measurements and SMACS calculations for test T41.31.2. As for the KWU configuration, most computed histories have lower amplitudes than the test histories. The difference between test and calculation, is the greatest for σ_{b2} at QA106, in the 200 mm pipe. For the 200 mm diameter pipe runs, the exception to the rule of underestimates occurs only for σ_{b2} at QA104. However, for the 100 mm pipe, σ_{b1} is overestimated at all locations except RA765 and RA766. In addition to the amplitude differences, the decay or the 'ring down' is generally slower in the calculated stresses than in the test stresses. The same observations as above also hold for the other test on the NRC configuration, T41.31.3.

Table 7 presents a numerical comparison of the peak value of the resultant bending stress in the pipe for the 11 locations. The resultant bending stress, σ_{br}, is defined by

$$\sigma_{br} = \sqrt{\left(\sigma_{b1}{}^2 + \sigma_{b2}{}^2\right)}.$$

The data in the table confirms that the bending stresses are generally underestimated. The standard deviation values show that the scatter in the values of the ratio is not as large as it was for accelerations or support forces, indicating that there is more spatial consistency in estimating stresses than the other response quantities.

Table 7. Comparing measured and calculated peak values of resultant bending stress histories (Stress in MPa)

Stress at	Pipe Dia. (mm)	Test: T41.21.1			Test: T41.21.2			Test: T41.31.2			Test: T41.31.3		
		Meas.	Calc.	Ratio	Meas.	Calc.	Ratio	Meas.	Calc.	Ratio	Meas.	Calc.	Ratio
QA100	200	65.73	57.42	0.874	178.83	175.71	0.983	68.50	49.10	0.717	122.58	97.74	0.797
QA102	200	31.80	29.36	0.923	106.54	91.45	0.858	37.12	31.59	0.851	77.04	67.22	0.873
QA103	200	28.61	23.90	0.835	86.74	74.01	0.853	28.13	21.02	0.747	58.78	58.53	0.996
QA104	200	21.21	16.46	0.776	82.19	47.18	0.574	8.55	10.04	1.175	27.13	32.38	1.194
QA106	200	14.48	16.04	1.107	53.50	52.36	0.979	8.57	4.97	0.580	15.37	14.51	0.944
RA760	100	48.64	46.86	0.963	175.62	147.78	0.841	27.95	24.47	0.876	98.33	90.58	0.921
RA763	100	45.63	48.17	1.056	176.97	157.17	0.888	17.61	16.99	0.965	59.50	57.83	0.972
RA764	100	30.31	21.86	0.721	100.38	68.76	0.685	12.98	11.46	0.883	24.18	22.56	0.933
RA765	100	34.28	19.59	0.572	90.92	61.58	0.677	33.04	16.65	0.504	63.74	32.71	0.513
RA766	100	50.06	32.30	0.645	147.45	99.75	0.677	47.76	25.46	0.533	95.55	50.21	0.525
RA767	100	55.05	46.89	0.852	208.61	147.87	0.709	31.30	24.48	0.782	111.65	90.59	0.811
Mean				0.848			0.793			0.783			0.862
Std. Dev.				0.164			0.135			0.199			0.199

6 Discussion and Conclusions

It is clear from the comparisons discussed in the previous chapter that the analytical results are characterized by underestimation of response in general. Furthermore, the spatial consistency of the response estimates is uneven, as indicated by the generally significant standard deviation values for the ratio of calculated to measured peak value. However, the error in estimating the different response quantities is not the same and it is possible to discern a pattern regarding this. Table 8 summarizes the results given in Tables 3 through 7. Even though the peak values do not necessarily characterize a history, they are important from a design perspective and therefore are significant.

Table 8. Ratio of calculated peak value to measured peak value

	Acceleration		Displacement		Snubber Force		Strut Force		Bending Stress	
Test No.	Mean	σ	Mean	σ	Mean	σ	Mean	σ	Mean	σ
T41.21.1	0.783	0.343	0.962	0.238	-----	-----	0.581	0.278	0.848	0.164
T41.21.2	0.768	0.281	0.921	0.249	-----	-----	0.618	0.205	0.793	0.135
T41.31.2	0.730	0.308	-----	-----	0.834	0.759	0.604	0.169	0.783	0.199
T41.31.3	0.704	0.302	1.194	0.223	1.008	0.860	0.709	0.222	0.862	0.199

As a class, the snubber forces are the most poorly estimated response as indicated by σ values that are almost as large as the mean values. Because of this the mean values are not good indicators of accuracy of calculation. The strut forces are also seriously underestimated although the relatively lower value for σ shows a greater spatial consistency of the estimates.

It is not difficult to see why support forces are the most poorly estimated among the responses. First of all, linear models ignore the fact that there are gaps in the attachment devices for any kind of supports. These gaps give rise to impacts when they close and provide no restraint until they remain fully close or fully open. Furthermore the behavior of mechanical snubbers is more complex than is assumed in the analysis. The actual force-displacement relationship for snubbers is not linear and is characterized by a hysteresis-type curve. Moreover the snubbers do not lock up instantaneously under dynamic excitation whereas the model assumes that the snubbers and struts behave the same way under dynamic excitation.

In addition to the gaps, the connection by pipe clamps introduces additional nonlinearity to the system. The 'stick and slip' behavior of the pipe clamp at H23

seems to have caused additional nonlinearity in the behavior of the two struts of H23. The fact that the forces in the two struts of H23 were not the same shows that the pipe clamp for H23 transmitted some torque to DF16, to which H23 is attached. As the clamp was not welded to DF16, only friction provided for this torque transfer. It stands to reason that when this torque exceeded the friction capacity, the clamp would begin to rotate. Information on torque capacity of frictional clamps is not normally available and even if available such information could not be used in a linear analysis. A linear analysis is thus incapable of modeling the complex behavior of supports. It may be noted that other similar linear analysis, the results of which were summarized in [12], also generally underestimated the support forces.

The acceleration estimates, besides being smaller than the measurement, also suffer from the lack of spatial consistency as shown by the relatively high values of σ. It has not been possible to trace the discrepancy between test and calculation to any specific experimental or modeling deficiency. Again, linear analyses by other investigators, reported in [12], also underestimate accelerations.

The underestimation of the displacements was not as severe as that of the acceleration responses for the KWU configuration. In fact the displacement estimates, as a category, for the KWU configuration were the closest to the measurement. The displacement results for the NRC configuration were overestimated almost for all measurement locations. Since the main difference between the two systems is the presence or absence of snubbers, it seems that the inherent limitations of a linear code – that make it impossible to model the complexity of snubber behavior – might also be responsible for the overestimation of displacements for the NRC configuration.

The maximum resultant bending stress calculated has, as a class, less discrepancy than the accelerations and support forces, though this response is also underestimated. As seen from Table 8, these estimates have the greatest spatial consistency indicated by the relatively low values of σ. That most of the pipe locations at which the bending stresses were measured were not near a support might be a contributing factor for the better comparisons. The other linear analyses reported in [12] also gave better estimates for bending stress than acceleration or support force.

In general, the integrated response quantities (displacement and stress) are better estimated than the other two (acceleration and support force). As noted in [12], this was so for all the other linear analysis estimates also. As the process of integration tends to enhance the contribution from the lower rather than the higher frequency contents in any time history, the possible presence of the latter in the test measurements might be responsible for this. These higher frequencies are attributed to the inherent nonlinearities in the system [12].

The proper value of damping ratio remains to be investigated further. The first set of calculations, discussed in Section 5.2, showed that the PVRC criteria resulted in underestimation of acceleration response. However, the second set of calculations, which is mainly the subject of this report, and for which a uniform damping of 3% was used, shows that though the acceleration responses get closer to the measurement, the slower decay of the calculated displacement and stress histories seems to indicate that this damping value might be too small for the KWU configuration and appropriate for the NRC configuration. On the other hand, without a separate parameter study, it is not possible to determine what proportion of the underestimation of responses is attributable to the damping used.

Concluding Remarks

Obviously the discrepancy between test results and calculated estimates cannot all be attributed to the calculational method. There are uncertainties in the experimental data and analytical model that may have contributed to the differences. It was noted that it became necessary to use acceleration inputs at H5 and H25 that were derived from the test-measured actuator displacements. The process of differentiation of the displacement histories introduced spurious high frequencies into the resulting acceleration histories. So the cut-off frequency was set at a low 60 Hz in the analysis. This illustrates the likelihood of artificial elements being introduced into the test data due to digitization and numerical processing of the data. These artificial elements that add to the inherent high frequency contents could be responsible for a significant portion of the discrepancies because either the input to the calculations contained errors or the test measurement with which comparison is made contains errors. This is especially so for peak value comparisons. Comparison of Table 8 with a similar table in [10] shows that the mean values of the ratio between estimate and measurement decreased by up to 20% for acceleration response when the cut-off frequency was reduced from 200 Hz to 60 Hz. Some of the calculated peak values of support force dropped by almost 50%.

The uncertainties in the finite element model relates to the representation of components that are not pipes with pipe elements. The nozzles, spherical tee, and the dome of HDU, etc have all been represented by artificial pipe elements. Estimating the stiffness of these artificial elements is based more on the judgment of the analyst than on any separate analyses. The uncertainty regarding the nonlinear nature of the connection of the pipe to support elements was also noted before. It is also possible that the other boundaries, such as fixed boundaries, are not realistically modeled.

Because of the uncertainties present in the other elements of the analytical and experimental process, it has not been possible to verify the SMACS piping calculation code as a separate element. However, the effort should be considered as an attempt to verify the whole process that is typical of a design calculation with a linear code. The present exercise has shown that the process could result in significant underestimation of responses in general and support forces in particular. The neglecting of the nonlinear behavior of the connection between pipe and support members appears to be the primary deficiency of linear analysis method of the SMACS and other such programs.

An effort is now underway to determine whether a nonlinear finite-element code, capable of modeling gaps and material nonlinearity, can better simulate a higher level excitation SHAM test. It is expected that the results of that study will throw some light on the contribution of nonlinearities on response estimates.

References

1. Malcher, L., and Kot, C. A., "HDR Phase II Vibrational Experiments," *Proceedings of the U.S. NRC 14th Water Reactor Safety Information Meeting,* NUREG/CP-0082, Vol. 3, pp. 295-312, Gaithersburg, MD, October 27-31, 1986.

2. Kot, C. A., Malcher, L., and Steinhilber, H., "Vibrational Experiments at the HDR: SHAG Results and Planning for SHAM," *Proceedings of the U.S. NRC 15th Water Reactor Safety Information Meeting,* NUREG/CP-0091, Vol. 3, pp. 251-277, Gaithersburg, MD, October 26-29, 1987.

3. Kot, C. A., Srinivasan, M. G., Hsieh, B. J., Malcher, L., Schrammel, D., Steinhilber, H., and Costello, J. F., "SHAM: High-Level Seismic Tests of Piping at the HDR," *Nuclear Engineering and Design*, Vol. 118, pp. 305-318, 1990.

4. Hsieh, B. J., Kot, C. A., and Srinivasan, M. G., "Vibration Testing and Analysis of a Multiply Supported Piping System," *Transactions of the 9th International Conference on Structural Mechanics in Reactor Technology, Volume K2, Seismic Response Analysis of Nuclear Power Plant Systems,* pp. 969-974, A. A. Balkema, Rotterdam, 1987.

5. Hsieh, B. J., Kot, C. A., and Srinivasan, M. G., "Comparison of Analysis and Vibration Test Results for a Multiply-supported Piping System," *Seismic Engineering - 1989, Design, Analysis, Testing and Qualification Methods,* pp. 293-301, The 1989 ASME Pressure Vessels and Piping Conference, Honolulu, Hawaii, 1989.

6. Maslenikov, O. R., Johnson, J. J., Tiong, L. W., Mraz, M. J., Bumpus, S., and Gerhard, M. A., "SMACS - A System of Computer Programs for Probabilistic Seismic Analysis of Structures and Subsystems," UCID-20413, Vol.1, Lawrence Livermore Laboratory, 1985.

7. Johnson, J. J., Goudreau, G. L., Bumpus, S. E., and Maslenikov, O. R., "Phase I Final Report— SMACS—Seismic Methodology Analysis Chain with Statistics (Project VIII)," NUREG/CR-2015, Vol. 9, Lawrence Livermore Laboratory, 1981.

8. Habip, M. A., "HDR/SHAM Tests: Seismic Design of the Experimental Piping without Snubbers," Siemens, Offenbach, Technical Report No. UED 24/88/0227, December 1989, PHDR Working Report No. 4.357/89 (in German).

9. Srinivasan, M. G., Kot, C. A., and Hsieh, B. J., "Response of HDR-VKL Piping System to Seismic Test Excitations - Comparison of Analytical Predictions and Test Measurements," *Transactions of the Tenth International Conference on Structural Mechanics in Reactor Technology,* Vol. K2, pp. 751-756, August 1989.

10. Srinivasan, M. G., Kot, C. A., and Hsieh, B. J., "Analytical Simulation of Seismic Testing of VKL Piping System at the HDR Test Facility," *Seismic Engineering - 1990, The 1990 Pressure Vessels and Piping Conference, Nashville, Tennessee*, PVP-Vol. 197, ASME, New York, NY, pp. 175-182, 1990.

11. Schrammel, D., Steinhilber, H., Flade, D., and Waldner, K., "Damping Behavior of a Piping System with Various Support Concepts and with Increasing Earthquake-like Loading," Contribution No. 4, pp. 159-191, 13th Status Report of the HDR Safety Programme of the Kernforschungszentrum Karlsruhe, December 1989 (in German).

12. Schrammel, D., and Steinhilber, H., "Structural Dynamic Investigations at the HDR, Earthquake Experiments at High Levels of Excitation of a Piping System with Various Support Configurations," Evaluation Report Test Group: SHAM, Technical Topical Report PHDR No. 96 - 90, Kernforschungszentrum Karlsruhe, September 1990 (in German with English summary).

13. Schrammel, D., Steinhilber, H., and Malcher, L., "Servo Hydraulic Excitation of Mechanical Components," Quick Look Report, Test Group: SHAM, Test: T41, Technical Topical Report PHDR No. 86 - 88, Kernforschungszentrum Karlsruhe, pp. 67-69, October 1988 (in German).

APPENDIX A

Description of Finite Element Models

Description of Input File:

This is one of the input files to a SMACS run and contains the information on the complete finite element model. This file is included only to provide complete documentation for future reference. The format of this files is based on that for input to SAP IV. A brief description of the file is given below.

The first part of the file gives the node numbers, boundary condition or master-to-slave conditions at the node, and the nodal coordinates in a global Cartesian coordinate system.

The second part contains element descriptions. The KWU configuration is made up of three type of elements: truss, beam, and pipe . The NRC configuration has only truss and pipe elements. Records pertaining to each type are arranged in one block. The first block pertains to truss elements. The first part of this block contains the stiffness information, Young's Modulus and cross sectional area, for the truss elements and the second part contains the connectivity of truss elements. The next block describes the beam elements, where applicable. The first part of this block gives the material properties, Young's Modulus, Poisson's Ratio, and mass density. The second part contains cross sectional properties in terms of areas and area moments of inertia. The third part is made up of element connectivity cards, which also have the information on end-release codes to provide for hinged ends etc. The next block of cards applies to pipe elements. The first part of this block has a set of material property cards, containing Young's Modulus and Poisson's Ratio. The second part contains section property cards. Each card has the values for outer diameter and thickness of cross section, a shape factor for shear distortion, weight per unit length, and mass per unit length. The final part of this block consists of pipe element cards containing information on element connectivity, and pressure in the pipe. These cards pertain to either tangent elements (denoted by T) or elbow elements (denoted by B). Each elbow element has an additional card containing the radius of the elbow and the center of radius.

The last part of the file contains the information on concentrated masses associated with appropriate nodes.

Consistent units were used: millimeter for length, Newton for force, and seconds for time. This implies the choice of metric tonne for mass. The consistent unit for pressure and stress is MPa.

KWU Configuration

```
POSTTEST ANALYSIS,SHAM T41.21.1&2,KWU CONFIG,REV. MODEL 1,DIFF INPUTS
  172    3    0   50    1    0    0    0    1                                                    1
    1    1    1    1    1    1    1    4800.0    15020.0    5700.0    0
    2                                   4800.0    15772.0    5700.0    0
    3                                   4800.0    18831.5    5700.0    0
    4                                   4800.0    21891.0    5700.0    0
    5    1         1                    4800.0    24950.0    5700.0    0
    6                                   4800.0    27207.0    5700.0    0
    7                                   4160.8    27753.2    5252.3    0
   10                                   4053.5    27844.9    5177.2    0
   12                                   3910.2    27900.0    5076.9    0
   14                                   3821.0    27900.0    5014.7    0
   16                                   3571.0    27595.0    4840.0    0
   18                                   3571.0    27495.0    4840.0    0
   20                                   3571.0    27430.0    4840.0    0
   22                                   3571.0    26745.0    4840.0    0
   24                                   3571.0    25598.3    4840.0    0
   26                                   3571.0    24451.7    4840.0    0
   28                                   3571.0    23305.0    4840.0    0
   30                                   3466.7    23000.0    5126.6    0
   33                                   3297.3    23000.0    5591.7    0
   36                                   3037.3    23000.0    6305.9    0
   41                                   3037.3    21933.0    6305.9    0
   40                                   2778.0    23000.0    7018.1    0
   44                                   2764.2    23000.0    7175.5    0
 4710002                                2809.4    23000.0    7431.0    0
   53                                   2824.7    23000.0    7517.9    0
   49                                   2903.0    23000.0    7961.0    0
   45                                   3333.0    23000.0    7961.0    0
   42                                   3700.3    23000.0    7961.0    0
   38                                   3852.8    23000.0    7920.2    0
   34                                   4727.3    23000.0    7415.4    0
   31                                   5601.2    23000.0    6911.0    0
   29                                   5861.0    23000.0    6761.0    0
   27                                   5861.0    23300.0    6761.0    0
   25                                   5861.0    24373.7    6761.0    0
   23                                   5861.0    25447.5    6761.0    0
   21                                   5861.0    26521.2    6761.0    0
   19                                   5861.0    27075.0    6761.0    0
   17                                   5861.0    27595.0    6761.0    0
   15                                   5645.3    27900.0    6545.3    0
   13                                   5568.0    27900.0    6468.0    0
   11                                   5444.3    27844.9    6344.3    0
    8                                   5351.6    27753.1    6251.6    0
   32                                   6121.1    23000.0    6611.5    0
   35                                   6211.3    23000.0    6559.7    0
   39                                   6308.9    23000.0    6470.6    0
   43                                   6439.7    23000.0    6284.6    0
   46                                   6615.0    23305.0    6035.0    0
   51                                   6615.0    23905.0    6035.0    0
   55                                   6615.0    25500.0    6035.0    0
   57                                   6615.0    26597.5    6035.0    0
   59                                   6615.0    27695.0    6035.0    0
   61                                   6789.9    28000.0    5785.1    0
   63                                   7151.1    28000.0    5268.9    0
   65                                   7326.0    27695.0    5019.0    0
   68                                   7326.0    26925.0    5019.0    0
   70                                   7326.0    26400.0    5019.0    0
   72                                   7326.0    25875.0    5019.0    0
   74                                   7326.0    25455.0    5019.0    0
   76                                   7501.0    25150.0    4769.2    0
   78                                   7613.0    25150.0    4609.5    0
   80                                   7762.3    25150.0    4396.5    0
   54                                   2581.6    23000.0    8344.0    0
```

56							2436.1	23000.0	8517.3	0
58							2210.4	23000.0	8647.6	0
60							1545.5	23000.0	8764.8	0
62							172.1	23000.0	8898.4	0
64							-1205.4	23000.0	8818.0	0
66							-2303.4	23000.0	8596.8	0
69							-2390.3	23000.0	8573.5	0
71							-2544.9	23000.0	8532.1	0
73							-2719.7	23000.0	8485.2	0
75							-2797.0	23000.0	8464.5	0
77							-2904.7	23000.0	8277.1	0
79							-2698.3	23000.0	7520.5	0
81							-2492.0	23000.0	6763.9	0
83							-2285.6	23000.0	6007.4	0
85							-2138.5	23000.0	5895.0	0
87							-1318.0	23000.0	5895.0	0
89							-497.5	23000.0	5895.0	0
91							323.0	23000.0	5895.0	0
94							430.5	23000.0	5895.0	0
97							583.0	23152.5	5895.0	0
99							583.0	23707.5	5895.0	0
101							708.2	23860.0	5807.9	0
104							1480.1	23860.0	5270.5	0
106							2252.1	23860.0	4733.1	0
108							3024.1	23860.0	4195.6	0
110							3153.9	23943.6	4140.0	0
112							3480.7	24491.3	4140.0	0
114							3807.5	25038.9	4140.0	0
117							3829.0	25117.0	4140.0	0
118							3829.0	26265.7	4140.0	0
115							3829.0	26411.6	4032.1	0
113							3977.5	26455.0	3885.9	0
111							4553.3	26455.0	3870.2	0
109							5129.1	26455.0	3854.4	0
107							5289.0	26455.0	3850.0	0
105							5289.0	26350.0	3850.0	0
103							5449.0	26350.0	3850.0	0
100							5729.0	26350.0	3850.0	0
98							6179.7	26350.0	3850.0	0
96							6545.0	26350.0	3850.0	0
92							7093.0	26350.0	3850.0	0
90							7242.9	26350.0	3850.0	0
88							7338.2	26350.0	3875.5	0
86							7693.3	26350.0	4080.6	0
84	0	0	0	0	0	0	7900.0	26350.0	4200.0	0
82							7900.0	25150.0	4200.0	0
9							4800.0	28159.5	5700.0	0
93	1	1	1				323.0	23930.0	5895.0	0
67	1	1	1				-1205.4	24000.0	8818.0	0
37	1	1	1				3434.2	24000.0	5215.9	0
48							6718.2	23305.0	5887.5	0
50	1	1	1				3458.0	23000.0	7107.0	0
52	1	1	1	1	1	1	6013.0	23905.0	5433.0	0
95	1	1	1	0	0	0	163.0	23000.0	7057.0	0
102	1	1	1	0	0	0	1345.0	23570.0	5895.0	0
116	1	1	1	0	0	0	3977.5	26455.0	3206.5	0
119							3829.0	25691.3	4140.0	0
120							7900.0	17900.0	2300.0	0
121	1	1	1	1	0	0	7550.0	17900.0	2300.0	0
122							7200.0	17900.0	2300.0	0
123							6500.0	17900.0	2300.0	0
124							6130.0	17900.0	2300.0	0
125							5800.0	17900.0	2300.0	0
126							4750.0	17900.0	2300.0	0

```
127    1    1    1    1    1    1    4400.0   17900.0    2300.0    0
128                                   7925.3   17900.0    2300.0    0
129                                   8406.8   17900.0    3034.3    0
130                                   8109.3   17900.0    3718.5    0
131    0    0    1    0    0    0    7900.0   18425.0    4200.0    0
132                                   7900.0   19462.5    4200.0    0
133                                   7900.0   20500.0    4200.0    0
134                                   7900.0   21537.5    4200.0    0
135                                   7900.0   22575.0    4200.0    0
136                                   7900.0   23612.5    4200.0    0
137                                   7900.0   24650.0    4200.0    0
138                                   7900.0   25750.0    4200.0    0
139                                   7900.0   26850.0    4200.0    0
140                                  -2945.0   23000.0    8424.9    0
141                                  -3093.0   23000.0    8385.2    0
142    1    1    1                    7671.0   27250.0    3644.4    0
143    1    1    1    1    1    1    6718.2   22600.0    5887.5    0
144    1    1    1    1    1    1    2581.6   23965.2    8344.0    0
145    1    1    1    1    1    1   -1398.0   23000.0    7791.0    0
146    1    1    1    1    1    1   -1763.0   23985.0    8724.0    0
147    1    1    1    1    1    1    3977.5   27096.0    3885.9    0
148    1    1    1    1    1    1   -1077.0   23584.0    6055.0    0
149                                   7900.0   27250.0    4200.0    0
15010001                              7900.0   27550.0    4200.0    0
151                                   7900.0   28150.0    4200.0    0
152                                   3458.0   23000.0    7961.0    0
153                                  -1572.0   23000.0    8760.0    0
154                                  -1763.0   23000.0    8724.0    0
155                                  -1077.0   23000.0    5895.0    0
156                                    163.0   23000.0    5895.0    0
157                                  -1077.0   23000.0    6055.0    0
158                                    583.0   23570.0    5895.0    0
159                                   3434.2   23000.0    5215.9    0
160                                   3571.0   23755.0    4840.0    0
161                                   4243.5   23000.0    7696.1    0
162                                   5861.0   23750.0    6761.0    0
163                                   6615.0   23705.7    6035.0    0
164                                   7326.0   25725.0    5019.0    0
165                                   6962.9   26350.0    3850.0    0
166                                   2835.4   23860.0    4327.0    0
167                                  -1908.5   23000.0    5895.0    0
168                                  -2845.2   23000.0    8054.9    0
169                                   7671.0   27250.0    4200.0    0
170                                   8129.0   27250.0    4200.0    0
171    1    1    1                    8129.0   27250.0    3644.4    0
172  149  149  149  149    0  149    7900.0   27250.0    4200.0    0
  1    9    6
  1 210000.0       0.0              1945.80
  2   1000.0       0.0               263.00
  3   1000.0       0.0                79.00
  4   1000.0       0.0                15.00
  5 210000.0       0.0              1945.80
  6 210000.0       0.0               506.70



  1  152   50    1
  2  159   37    2
  3   64   67    3
  4   91   93    4
  5  169  142    5
  6  156   95    6
  7  158  102    6
```

```
 8  113  116    6
 9  170  171    5
 2    4    2    0    2
 1  210000.0       0.3       0.0       0.0
 2  210000.0     0.305    7.9E-9       0.0
 1   5806.44    4838.7    4838.7 1076374.5 6321514.8  312173.6
 2  25965.26  12982.63  12982.63709477190.354738595.354738595.



 1  169  172  150    1    1    0    0    0    0000111000000
 2  172  170  150    1    1    0    0    0    0000000000111
 3  139  149  170    2    2    0    0    0    0000000000000
 4  149  150  170    2    2    0    0    0    0000000000000
 9  152   11    1   41
 1    1  HDU          BHW 38        20 GR C
     0.   215000.      0.28
 2    1  DR201/2/3    1.4550        20 GR C
     0.   210000.      0.28
 3    1  DR108/D14    1.4961        20 GR C
     0.   199400.      0.29
 4    1  VN-R23       1.5415        20 GR C
     0.   212500.      0.29
 5    1  DR109        1.4961        20 GR C
     0.   200000.      0.29
 6    1  D15          1.4981/HG     20 GR C
     0.   195600.      0.28
 7    1  TRUNNIONS AT H2A, H22       316 SS
     0.   193150.    0.2667
 8    1  NOT IN USE IN THIS CASE    20 GR C
     0.     1000.      0.30
 9    1  NOT IN USE IN THIS CASE    20 GR C
     0.        1.      0.30
10    1       AN11 UND ATS   PDL/285 GRAD C
       175000.      .305   17.00E-06
11    1       AN11 UND ATS DR105/ 20 GRAD C
       210000.      .305   17.00E-06
 1   1855.0      45.0           44.4724   0.0045334 HDU ZYL.
 2    325.0      30.0            2.9739   0.0003031 HDU STUTZEN
 3    219.1      13.6            1.1074   0.0001129 DR201/108 G
 4    225.7      17.5            1.3122   0.0001338 DR201/108 B
 5    219.1      13.6            1.1074   0.0001129 DR201/108 G
 6    225.7      17.5            1.3122   0.0001338 DR201/108 B
 7    217.5      15.0            1.1525   0.0001175 DR202 VKL612
 8    219.1      12.8            1.0748   0.0001096 DR202 VKL621
 9    276.1      17.6            1.7217   0.0001755 DR203 G
10    281.0      20.0            1.8865   0.0001923 DR203 B
11    114.3       6.1            0.3391   0.0000346 VN-R23 G
12    115.9       7.9            0.3834   0.0000391 VN-R23 B
13    114.3       7.3            0.3646   0.0000372 VN-R23 VKL601
14    139.0       9.0            0.5063   0.0000516 DR-109 G
15    145.7      11.1            0.5926   0.0000604 DR-109 B
16    321.0      16.5  0.000001                    DF21 DA=219
17   1088.8      6.82  2.000000                    DF21 DA=273
18    295.0      30.0            2.5314   0.0002580 DF22 GRUNDROHR
19    230.7      20.0            1.4526   0.0001481 DF22 ABZWEIG
20    355.6      25.0                              D14
21    241.0      25.0            1.7451   0.0001779 DF16 ABZW. DR108
22    515.4      2.52  0.700000                    REDUZIERUNG
23    120.0      12.5                              D15
24    241.0      25.0            1.7451   0.0001779 DF16 ABZW. DR109
25     15.0      3.00                              NOT IN USE
26     15.0      2.56                              NOT IN USE
27   1779.5      94.5  1.000000                    HDU-BODEN F. EL.
```

28	2000.0	99.00	0.000001			HDU-HAUBE F. EL.
29	139.0	9.4		0.5165	0.0000527	DR-109 G VKL616
30	2000.0	100.0				DF16 F. EL.
31	219.1	15.4		1.1796	0.0001202	DR201/108 G NR13
32	300.0	60.0	2.000000			VENTIL
33	100.0	9.25	2.000000			H5 (ZYLINDERSTEIF.)
34	114.3	8.56		0.2186	0.0000223	TRUNNION AT H2A
35	60.3	3.91		0.0533	0.0000054	TRUNNION AT H22
36	38.1	5.56	2.000000			NOT IN USE
37	50.8	4.98	2.000000			NOT IN USE
38	457.0	41.0		5.0612	0.00051592	SAMMLER
39	355.6	25.0		2.5882	0.00026383	DR105 ROHR
40	361.0	28.0		2.8443	0.00028994	DR105 BOGEN
41	470.0	50.0		5.6691	0.00057789	DF16 FORMST.

1.0

1T	1	2	1	27		6.895
2T	2	3	1	1		6.895
3T	3	4	1	1		6.895
4T	4	5	1	1		6.895
5T	5	6	1	1		6.895
6T	6	7	1	28		6.895
7T	7	10	1	2		6.895
8B	10	12	2	6		6.895
305.00		CC	3909.90		27595.00	5077.40
9T	12	14	2	5		6.895
10B	14	16	2	6		6.895
305.00		CC	3821.00		27595.00	5014.70
11T	16	18	2	5		6.895
12T	18	20	2	7		6.895
13T	20	22	2	7		6.895
14T	22	24	2	3		6.895
15T	24	26	2	3		6.895
16T	26	160	2	3		6.895
17B	28	30	2	6		6.895
305.00		CC	3466.70		23305.00	5126.60
18T	30	159	2	5		6.895
19T	33	36	2	32		6.895
20T	36	41	2	32		6.895
21T	36	40	2	32		6.895
22B	40	44	2	6		6.895
305.00		CC	3064.60		23000.00	7122.50
23T	44	47	2	8		6.895
24T	47	53	2	8		6.895
25T	53	49	2	16		6.895
26T	49	45	2	16		6.895
27T	45	152	2	5		6.895
28B	42	38	2	6		6.895
305.00		CC	3700.30		23000.00	7656.00
29T	38	161	2	5		6.895
30T	34	31	2	5		6.895
31T	31	29	2	18		6.895
32T	29	27	2	19		6.895
33T	27	162	2	3		6.895
34T	25	23	2	3		6.895
35T	23	21	2	3		6.895
36T	21	19	2	31		6.895
37T	19	17	2	3		6.895
38B	17	15	2	4		6.895
305.00		CC	5645.30		27595.00	6545.30
39T	15	13	2	3		6.895

40B	13	11	2	4		6.895
305.00		CC	5568.00		27595.00	6468.00
41T	11	8	1	2		6.895
42T	8	6	1	28		6.895
43T	29	32	2	18		6.895
44T	32	35	3	3		6.895
45B	35	39	3	4		6.895
305.00		CC	6059.40		23000.00	6295.30
46T	39	43	3	3		6.895
47B	43	46	3	4		6.895
305.00		CC	6439.70		23305.00	6284.60
48T	46	163	3	3		6.895
49T	51	55	3	3		6.895
50T	55	57	3	3		6.895
51T	57	59	3	3		6.895
52B	59	61	3	4		6.895
305.00		CC	6789.90		27695.00	5785.10
53T	61	63	3	3		6.895
54B	63	65	3	4		6.895
305.00		CC	7151.10		27695.00	5268.90
55T	65	68	3	20		6.895
56T	68	70	3	20		6.895
57T	70	72	3	20		6.895
58T	72	164	3	3		6.895
59B	74	76	3	4		6.895
305.00		CC	7501.00		25455.00	4769.20
60T	76	78	3	3		6.895
61T	78	80	3	21		6.895
62T	49	54	2	16		6.895
63T	54	56	2	9		6.895
64B	56	58	2	10		6.895
381.00		CC	2144.30		23000.00	8272.40
65T	58	60	2	9		6.895
66B	60	62	2	9		6.895
8900.00		CC	.10		23000.00	.00
67B	62	64	2	9		6.895
8900.00		CC	.10		23000.00	.00
68B	64	153	2	9		6.895
8900.70		CC	.20		23000.00	-.70
69T	66	69	2	9		6.895
70T	69	71	2	9		6.895
71T	71	73	2	9		6.895
72T	73	75	2	9		6.895
73T	140	77	4	11		6.895
74T	77	168	4	11		6.895
75T	79	81	4	11		6.895
76T	81	83	4	11		6.895
77B	83	85	4	12		6.895
152.50		CC	-2138.50		23000.00	6047.50
78T	85	167	4	11		6.895
79T	87	155	4	11		6.895
80T	155	89	4	11		6.895
81T	91	94	4	11		6.895
82B	94	97	4	12		6.895
152.50		CC	430.50		23152.50	5895.00
83T	97	158	4	11		6.895
84B	99	101	4	12		6.895
152.50		CC	708.20		23707.50	5807.90
85T	101	104	4	11		6.895
86T	104	106	4	11		6.895
87T	106	166	4	11		6.895
88B	108	110	4	12		6.895
152.50		CC	3052.20		24004.30	4236.00
89T	110	112	4	11		6.895

```
 90T  112  114    4   11                6.895
 91B  114  117    4   12                6.895
   152.50   CC   3676.50  25117.00    4140.00
 92T  117  119    4   11                6.895
 93T  119  118    4   11                6.895
 94B  118  115    4   12                6.895
   152.50   CC   3829.00  26265.70    3987.50
 95B  115  113    4   12                6.895
   152.50   CC   3981.50  26410.40    4031.70
 96T  113  111    4   11                6.895
 97T  111  109    4   11                6.895
 98T  109  107    6   23                6.895
 99T  107  105    6   23                6.895
100T  105  103    6   23                6.895
101T  103  100    5   14                6.895
102T  100   98    5   14                6.895
103T   98   96    5   14                6.895
104T   96  165    5   29                6.895
105T   92   90    5   14                6.895
106B   90   88    5   15                6.895
   190.50   CC   7242.90  26350.00    4040.50
107T   88   86    5   24                6.895
108T   86   84   11   24                6.895
109T   84  139   11   41                6.895
110T   82   80   11   21                6.895
111T    6    9    1   27                6.895
112T  120  121   10   38                6.895
113T  121  122   10   38                6.895
114T  122  123   10   38                6.895
115T  123  124   10   38                6.895
116T  124  125   10   38                6.895
117T  125  126   10   38                6.895
118T  126  127   10   38                6.895
119T  120  128   11   39                6.895
120B  128  129   11   40                6.895
   525.00   CC   7925.30  17900.00    2825.00
121T  129  130   11   39                6.895
122B  130  131   11   40                6.895
   525.00   CC   8109.30  18425.00    3718.50
123T  131  132   11   39                6.895
124T  132  133   11   39                6.895
125T  133  134   11   39                6.895
126T  134  135   11   39                6.895
127T  135  136   11   39                6.895
128T  136  137   11   39                6.895
129T   82  138   11   41                6.895
130T  138   84   11   41                6.895
131T   82  137   11   41                6.895
132T   75  140    2    9                6.895
133T  140  141    2    9                6.895
134T   46   48    7   34
135T  155  157    7   35
136T  152   42    2    5                6.895
137B  153  154    2    9                6.895
  8900.00   CC        .10  23000.00       .00
138B  154   66    2    9                6.895
  8900.00   CC        .10  23000.00       .00
139T   89  156    4   11                6.895
140T  156   91    4   11                6.895
141T  158   99    4   11                6.895
142T  159   33    2    5                6.895
143T  160   28    2    3                6.895
144T  161   34    2    5                6.895
145T  162   25    2    3                6.895
```

```
146T  163   51     3     3                6.895
147T  164   74     3     3                6.895
148T  165   92     5    29                6.895
149T  166  108     4    11                6.895
150T  167   87     4    11                6.895
151T  168   79     4    11                6.895
152T  150  151    11    39                6.895
   2    0   4.94279   4.94279   4.94279
   5    0   1.41125   1.41125   1.41125
   6    0   3.36254   3.36254   3.36254
   9    0   2.47495   2.47495   2.47495
  10    0   0.05000   0.05000   0.05000
  11    0   0.05000   0.05000   0.05000
  36    0   0.56000   0.56000   0.56000
  41    0   0.28000   0.28000   0.28000
  49    0   0.40045   0.40045   0.40045
  60    0   0.02500   0.02500   0.02500
  69    0   0.00619   0.00619   0.00619
  70    0   0.90000   0.90000   0.90000
  71    0   0.00308   0.00308   0.00308
 107    0   0.09124   0.09124   0.09124
 120    0       0.5       0.5       0.5
 122    0 0.0054335 0.0054335 0.0054335
 123    0 0.0054335 0.0054335 0.0054335
 125    0 0.0054335 0.0054335 0.0054335
 127    0      0.62      0.62      0.62
 138    0      0.35      0.35      0.35
 149    0     0.075     0.075     0.075


   0    0   35                 60.0
```

NRC Configuration

```
POSTTEST ANALYSIS,SHAM T41.31.2&3,NRC CONFIG,REV. MODEL L,DIFF INPUTS
  168    2    0  140    1    0    0    0    1                                        1
    1    1    1    1    1    1    1    4800.0   15020.0    5700.0    0
    2                                   4800.0   15772.0    5700.0    0
    3                                   4800.0   18831.5    5700.0    0
    4                                   4800.0   21891.0    5700.0    0
    5    1         1                    4800.0   24950.0    5700.0    0
    6                                   4800.0   27207.0    5700.0    0
    7                                   4160.8   27753.2    5252.3    0
   10                                   4053.5   27844.9    5177.2    0
   12                                   3910.2   27900.0    5076.9    0
   14                                   3821.0   27900.0    5014.7    0
   16                                   3571.0   27595.0    4840.0    0
   18                                   3571.0   27495.0    4840.0    0
   20                                   3571.0   27430.0    4840.0    0
   22                                   3571.0   26745.0    4840.0    0
   24                                   3571.0   25598.3    4840.0    0
   26                                   3571.0   24451.7    4840.0    0
   28                                   3571.0   23305.0    4840.0    0
   30                                   3466.7   23000.0    5126.6    0
   33                                   3297.3   23000.0    5591.7    0
   36                                   3037.3   23000.0    6305.9    0
   41                                   3037.3   21933.0    6305.9    0
   40                                   2778.0   23000.0    7018.1    0
   44                                   2764.2   23000.0    7175.5    0
 4710002                                2809.4   23000.0    7431.0    0
   53                                   2824.7   23000.0    7517.9    0
   49                                   2903.0   23000.0    7961.0    0
   45                                   3333.0   23000.0    7961.0    0
   42                                   3700.3   23000.0    7961.0    0
   38                                   3852.8   23000.0    7920.2    0
   34                                   4727.3   23000.0    7415.4    0
   31                                   5601.2   23000.0    6911.0    0
   29                                   5861.0   23000.0    6761.0    0
   27                                   5861.0   23300.0    6761.0    0
   25                                   5861.0   24373.7    6761.0    0
   23                                   5861.0   25447.5    6761.0    0
   21                                   5861.0   26521.2    6761.0    0
   19                                   5861.0   27075.0    6761.0    0
   17                                   5861.0   27595.0    6761.0    0
   15                                   5645.3   27900.0    6545.3    0
   13                                   5568.0   27900.0    6468.0    0
   11                                   5444.3   27844.9    6344.3    0
    8                                   5351.6   27753.1    6251.6    0
   32                                   6121.1   23000.0    6611.5    0
   35                                   6211.3   23000.0    6559.7    0
   39                                   6308.9   23000.0    6470.6    0
   43                                   6439.7   23000.0    6284.6    0
   46                                   6615.0   23305.0    6035.0    0
   51                                   6615.0   23905.0    6035.0    0
   55                                   6615.0   25500.0    6035.0    0
   57                                   6615.0   26597.5    6035.0    0
   59                                   6615.0   27695.0    6035.0    0
   61                                   6789.9   28000.0    5785.1    0
   63                                   7151.1   28000.0    5268.9    0
   65                                   7326.0   27695.0    5019.0    0
   68                                   7326.0   26925.0    5019.0    0
   70                                   7326.0   26400.0    5019.0    0
   72                                   7326.0   25875.0    5019.0    0
   74                                   7326.0   25455.0    5019.0    0
   76                                   7501.0   25150.0    4769.2    0
   78                                   7613.0   25150.0    4609.5    0
   80                                   7762.3   25150.0    4396.5    0
   54                                   2581.6   23000.0    8344.0    0
```

56							2436.1	23000.0	8517.3	0
58							2210.4	23000.0	8647.6	0
60							1545.5	23000.0	8764.8	0
62							172.1	23000.0	8898.4	0
64							-1205.4	23000.0	8818.0	0
66							-2303.4	23000.0	8596.8	0
69							-2390.3	23000.0	8573.5	0
71							-2544.9	23000.0	8532.1	0
73							-2719.7	23000.0	8485.2	0
75							-2797.0	23000.0	8464.5	0
77							-2904.7	23000.0	8277.1	0
79							-2698.3	23000.0	7520.5	0
81							-2492.0	23000.0	6763.9	0
83							-2285.6	23000.0	6007.4	0
85							-2138.5	23000.0	5895.0	0
87							-1318.0	23000.0	5895.0	0
89							-497.5	23000.0	5895.0	0
91							323.0	23000.0	5895.0	0
94							430.5	23000.0	5895.0	0
97							583.0	23152.5	5895.0	0
99							583.0	23707.5	5895.0	0
101							708.2	23860.0	5807.9	0
104							1480.1	23860.0	5270.5	0
106							2252.1	23860.0	4733.1	0
108							3024.1	23860.0	4195.6	0
110							3153.9	23943.6	4140.0	0
112							3480.7	24491.3	4140.0	0
114							3807.5	25038.9	4140.0	0
117							3829.0	25117.0	4140.0	0
118							3829.0	26265.7	4140.0	0
115							3829.0	26411.6	4032.1	0
113							3977.5	26455.0	3885.9	0
111							4553.3	26455.0	3870.2	0
109							5129.1	26455.0	3854.4	0
107							5289.0	26455.0	3850.0	0
105							5289.0	26350.0	3850.0	0
103							5449.0	26350.0	3850.0	0
100							5729.0	26350.0	3850.0	0
98							6179.7	26350.0	3850.0	0
96							6545.0	26350.0	3850.0	0
92							7093.0	26350.0	3850.0	0
90							7242.9	26350.0	3850.0	0
88							7338.2	26350.0	3875.5	0
86							7693.3	26350.0	4080.6	0
84	0	0	0	0	0	0	7900.0	26350.0	4200.0	0
82							7900.0	25150.0	4200.0	0
9							4800.0	28159.5	5700.0	0
93	1	1	1				323.0	23930.0	5895.0	0
67	1	1	1				-1205.4	24000.0	8818.0	0
37	1	1	1				3434.2	24000.0	5215.9	0
48							6718.2	23305.0	5887.5	0
50	1	1	1				3458.0	23000.0	7107.0	0
52	1	1	1	0	0	0	6013.0	23905.0	5433.0	0
95	1	1	1	0	0	0	163.0	23000.0	7057.0	0
102	1	1	1	0	0	0	1345.0	23570.0	5895.0	0
116	1	1	1	0	0	0	3977.5	26455.0	3206.5	0
119							3829.0	25691.3	4140.0	0
120							7900.0	17900.0	2300.0	0
121	1	1	1	1	0	0	7550.0	17900.0	2300.0	0
122							7200.0	17900.0	2300.0	0
123							6500.0	17900.0	2300.0	0
124							6130.0	17900.0	2300.0	0
125							5800.0	17900.0	2300.0	0
126							4750.0	17900.0	2300.0	0

```
127    1    1    1    1    1    1    4400.0   17900.0   2300.0    0
128                                   7925.3   17900.0   2300.0    0
129                                   8406.8   17900.0   3034.3    0
130                                   8109.3   17900.0   3718.5    0
131    0    0    1    0    0    0    7900.0   18425.0   4200.0    0
132                                   7900.0   19462.5   4200.0    0
133                                   7900.0   20500.0   4200.0    0
134                                   7900.0   21537.5   4200.0    0
135                                   7900.0   22575.0   4200.0    0
136                                   7900.0   23612.5   4200.0    0
137                                   7900.0   24650.0   4200.0    0
138                                   7900.0   25750.0   4200.0    0
139                                   7900.0   26850.0   4200.0    0
140                                  -2945.0   23000.0   8424.9    0
141                                  -3093.0   23000.0   8385.2    0
142    1    1    1                    7900.0   27250.0   3644.4    0
143    1    1    1                    6718.2   22600.0   5887.5    0
144    1    1    1                    2581.6   23965.2   8344.0    0
145    1    1    1                   -1398.0   23000.0   7791.0    0
146    1    1    1                   -1763.0   23985.0   8724.0    0
147    1    1    1                    3977.5   27096.0   3885.9    0
148    1    1    1                   -1077.0   23584.0   6055.0    0
149                                   7900.0   27250.0   4200.0    0
15010001                              7900.0   27550.0   4200.0    0
151                                   7900.0   28150.0   4200.0    0
152                                   3458.0   23000.0   7961.0    0
153                                  -1572.0   23000.0   8760.0    0
154                                  -1763.0   23000.0   8724.0    0
155                                  -1077.0   23000.0   5895.0    0
156                                    163.0   23000.0   5895.0    0
157                                  -1077.0   23000.0   6055.0    0
158                                    583.0   23570.0   5895.0    0
159                                   3434.2   23000.0   5215.9    0
160                                   3571.0   23755.0   4840.0    0
161                                   4243.5   23000.0   7696.1    0
162                                   5861.0   23750.0   6761.0    0
163                                   6615.0   23705.7   6035.0    0
164                                   7326.0   25725.0   5019.0    0
165                                   6962.9   26350.0   3850.0    0
166                                   2835.4   23860.0   4327.0    0
167                                  -1908.5   23000.0   5895.0    0
168                                  -2845.2   23000.0   8054.9    0
  1   15    9
  1  210000.0        0.0              1945.80
  2    1000.0        0.0               263.00
  3    1000.0        0.0                79.00
  4    1000.0        0.0                15.00
  5  210000.0        0.0              3891.60
  6  210000.0        0.0               506.70
  7  210000.0        0.0               285.02
  8  210000.0        0.0               412.30
  9  210000.0        0.0               214.58



  1  152   50    1
  2  159   37    2
  3   64   67    3
  4   91   93    4
  5  149  142    5
  6   51   52    6
  7  156   95    7
  8  158  102    7
```

```
 9  113  116    7
10   48  143    8
11   54  144    9
12  153  145    8
13  154  146    9
14  113  147    9
15  157  148    9
 9  154   11    1   41
 1    1  HDU          BHW 38        20 GR C
     0.   215000.       0.28
 2    1  DR201/2/3    1.4550        20 GR C
     0.   210000.       0.28
 3    1  DR108/D14    1.4961        20 GR C
     0.   199400.       0.29
 4    1  VN-R23       1.5415        20 GR C
     0.   212500.       0.29
 5    1  DR109        1.4961        20 GR C
     0.   200000.       0.29
 6    1  D15          1.4981/HG     20 GR C
     0.   195600.       0.28
 7    1  TRUNNIONS AT H2A, H22       316 SS
     0.   193150.    0.2667
 8    1  NOT IN USE IN THIS CASE    20 GR C
     0.     1000.       0.30
 9    1  NOT IN USE IN THIS CASE    20 GR C
     0.        1.       0.30
10    1       AN11 UND ATS   PDL/285 GRAD C
       175000.      .305   17.00E-06
11    1       AN11 UND ATS DR105/ 20 GRAD C
       210000.      .305   17.00E-06
 1   1855.0      45.0          44.4724   0.0045334 HDU ZYL.
 2    325.0      30.0           2.9739   0.0003031 HDU STUTZEN
 3    219.1      13.6           1.1074   0.0001129 DR201/108 G
 4    225.7      17.5           1.3122   0.0001338 DR201/108 B
 5    219.1      13.6           1.1074   0.0001129 DR201/108 G
 6    225.7      17.5           1.3122   0.0001338 DR201/108 B
 7    217.5      15.0           1.1525   0.0001175 DR202 VKL612
 8    219.1      12.8           1.0748   0.0001096 DR202 VKL621
 9    276.1      17.6           1.7217   0.0001755 DR203 G
10    281.0      20.0           1.8865   0.0001923 DR203 B
11    114.3       6.1           0.3391   0.0000346 VN-R23 G
12    115.9       7.9           0.3834   0.0000391 VN-R23 B
13    114.3       7.3           0.3646   0.0000372 VN-R23 VKL601
14    139.0       9.0           0.5063   0.0000516 DR-109 G
15    145.7      11.1           0.5926   0.0000604 DR-109 B
16    321.0      16.5  0.000001                     DF21 DA=219
17   1088.8      6.82  2.000000                     DF21 DA=273
18    295.0      30.0           2.5314   0.0002580 DF22 GRUNDROHR
19    230.7      20.0           1.4526   0.0001481 DF22 ABZWEIG
20    355.6      25.0                               D14
21    241.0      25.0           1.7451   0.0001779 DF16 ABZW. DR108
22    515.4      2.52  0.700000                     REDUZIERUNG
23    120.0      12.5                               D15
24    241.0      25.0           1.7451   0.0001779 DF16 ABZW. DR109
25     15.0      3.00                               NOT IN USE
26     15.0      2.56                               NOT IN USE
27   1779.5      94.5  1.000000                     HDU-BODEN F. EL.
28   2000.0     99.00  0.000001                     HDU-HAUBE F. EL.
29    139.0       9.4           0.5165   0.0000527 DR-109 G VKL616
30   2000.0     100.0                               DF16 F. EL.
31    219.1      15.4           1.1796   0.0001202 DR201/108 G NR13
32    300.0      60.0  2.000000                     VENTIL
33    100.0      9.25  2.000000                     H5 (ZYLINDERSTEIF.)
34    114.3      8.56           0.2186   0.0000223 TRUNNION AT H2A
```

35	60.3	3.91		0.0533	0.0000054	TRUNNION AT H22
36	38.1	5.56	2.000000			NOT IN USE
37	50.8	4.98	2.000000			NOT IN USE
38	457.0	41.0		5.0612	0.00051592	SAMMLER
39	355.6	25.0		2.5882	0.00026383	DR105 ROHR
40	361.0	28.0		2.8443	0.00028994	DR105 BOGEN
41	470.0	50.0		5.6691	0.00057789	DF16 FORMST.

1.0

1T	1	2	1	27		6.895
2T	2	3	1	1		6.895
3T	3	4	1	1		6.895
4T	4	5	1	1		6.895
5T	5	6	1	1		6.895
6T	6	7	1	28		6.895
7T	7	10	1	2		6.895
8B	10	12	2	6		6.895
305.00		CC	3909.90		27595.00	5077.40
9T	12	14	2	5		6.895
10B	14	16	2	6		6.895
305.00		CC	3821.00		27595.00	5014.70
11T	16	18	2	5		6.895
12T	18	20	2	7		6.895
13T	20	22	2	7		6.895
14T	22	24	2	3		6.895
15T	24	26	2	3		6.895
16T	26	160	2	3		6.895
17B	28	30	2	6		6.895
305.00		CC	3466.70		23305.00	5126.60
18T	30	159	2	5		6.895
19T	33	36	2	32		6.895
20T	36	41	2	32		6.895
21T	36	40	2	32		6.895
22B	40	44	2	6		6.895
305.00		CC	3064.60		23000.00	7122.50
23T	44	47	2	8		6.895
24T	47	53	2	8		6.895
25T	53	49	2	16		6.895
26T	49	45	2	16		6.895
27T	45	152	2	5		6.895
28B	42	38	2	6		6.895
305.00		CC	3700.30		23000.00	7656.00
29T	38	161	2	5		6.895
30T	34	31	2	5		6.895
31T	31	29	2	18		6.895
32T	29	27	2	19		6.895
33T	27	162	2	3		6.895
34T	25	23	2	3		6.895
35T	23	21	2	3		6.895
36T	21	19	2	31		6.895
37T	19	17	2	3		6.895
38B	17	15	2	4		6.895
305.00		CC	5645.30		27595.00	6545.30
39T	15	13	2	3		6.895
40B	13	11	2	4		6.895
305.00		CC	5568.00		27595.00	6468.00
41T	11	8	1	2		6.895
42T	8	6	1	28		6.895
43T	29	32	2	18		6.895
44T	32	35	3	3		6.895
45B	35	39	3	4		6.895

	305.00	CC	6059.40	23000.00	6295.30	
46T	39	43	3	3	6.895	
47B	43	46	3	4	6.895	
	305.00	CC	6439.70	23305.00	6284.60	
48T	46	163	3	3	6.895	
49T	51	55	3	3	6.895	
50T	55	57	3	3	6.895	
51T	57	59	3	3	6.895	
52B	59	61	3	4	6.895	
	305.00	CC	6789.90	27695.00	5785.10	
53T	61	63	3	3	6.895	
54B	63	65	3	4	6.895	
	305.00	CC	7151.10	27695.00	5268.90	
55T	65	68	3	20	6.895	
56T	68	70	3	20	6.895	
57T	70	72	3	20	6.895	
58T	72	164	3	3	6.895	
59B	74	76	3	4	6.895	
	305.00	CC	7501.00	25455.00	4769.20	
60T	76	78	3	3	6.895	
61T	78	80	3	21	6.895	
62T	49	54	2	16	6.895	
63T	54	56	2	9	6.895	
64B	56	58	2	10	6.895	
	381.00	CC	2144.30	23000.00	8272.40	
65T	58	60	2	9	6.895	
66B	60	62	2	9	6.895	
	8900.00	CC	.10	23000.00	.00	
67B	62	64	2	9	6.895	
	8900.00	CC	.10	23000.00	.00	
68B	64	153	2	9	6.895	
	8900.70	CC	.20	23000.00	-.70	
69T	66	69	2	9	6.895	
70T	69	71	2	9	6.895	
71T	71	73	2	9	6.895	
72T	73	75	2	9	6.895	
73T	140	77	4	11	6.895	
74T	77	168	4	11	6.895	
75T	79	81	4	11	6.895	
76T	81	83	4	11	6.895	
77B	83	85	4	12	6.895	
	152.50	CC	-2138.50	23000.00	6047.50	
78T	85	167	4	11	6.895	
79T	87	155	4	11	6.895	
80T	155	89	4	11	6.895	
81T	91	94	4	11	6.895	
82B	94	97	4	12	6.895	
	152.50	CC	430.50	23152.50	5895.00	
83T	97	158	4	11	6.895	
84B	99	101	4	12	6.895	
	152.50	CC	708.20	23707.50	5807.90	
85T	101	104	4	11	6.895	
86T	104	106	4	11	6.895	
87T	106	166	4	11	6.895	
88B	108	110	4	12	6.895	
	152.50	CC	3052.20	24004.30	4236.00	
89T	110	112	4	11	6.895	
90T	112	114	4	11	6.895	
91B	114	117	4	12	6.895	
	152.50	CC	3676.50	25117.00	4140.00	
92T	117	119	4	11	6.895	
93T	119	118	4	11	6.895	
94B	118	115	4	12	6.895	
	152.50	CC	3829.00	26265.70	3987.50	

```
 95B  115  113    4   12                6.895
   152.50   CC   3981.50  26410.40   4031.70
 96T  113  111    4   11                6.895
 97T  111  109    4   11                6.895
 98T  109  107    6   23                6.895
 99T  107  105    6   23                6.895
100T  105  103    6   23                6.895
101T  103  100    5   14                6.895
102T  100   98    5   14                6.895
103T   98   96    5   14                6.895
104T   96  165    5   29                6.895
105T   92   90    5   14                6.895
106B   90   88    5   15                6.895
   190.50   CC   7242.90  26350.00   4040.50
107T   88   86    5   24                6.895
108T   86   84   11   24                6.895
109T   84  139   11   41                6.895
110T   82   80   11   21                6.895
111T    6    9    1   27                6.895
112T  120  121   10   38                6.895
113T  121  122   10   38                6.895
114T  122  123   10   38                6.895
115T  123  124   10   38                6.895
116T  124  125   10   38                6.895
117T  125  126   10   38                6.895
118T  126  127   10   38                6.895
119T  120  128   11   39                6.895
120B  128  129   11   40                6.895
   525.00   CC   7925.30  17900.00   2825.00
121T  129  130   11   39                6.895
122B  130  131   11   40                6.895
   525.00   CC   8109.30  18425.00   3718.50
123T  131  132   11   39                6.895
124T  132  133   11   39                6.895
125T  133  134   11   39                6.895
126T  134  135   11   39                6.895
127T  135  136   11   39                6.895
128T  136  137   11   39                6.895
129T   82  138   11   41                6.895
130T  138   84   11   41                6.895
131T   82  137   11   41                6.895
132T   75  140    2    9                6.895
133T  140  141    2    9                6.895
134T   46   48    7   34
135T  155  157    7   35
136T  152   42    2    5                6.895
137B  153  154    2    9                6.895
  8900.00   CC       .10  23000.00        .00
138B  154   66    2    9                6.895
  8900.00   CC       .10  23000.00        .00
139T   89  156    4   11                6.895
140T  156   91    4   11                6.895
141T  158   99    4   11                6.895
142T  159   33    2    5                6.895
143T  160   28    2    3                6.895
144T  161   34    2    5                6.895
145T  162   25    2    3                6.895
146T  163   51    3    3                6.895
147T  164   74    3    3                6.895
148T  165   92    5   29                6.895
149T  166  108    4   11                6.895
150T  167   87    4   11                6.895
151T  168   79    4   11                6.895
152T  139  149   11   39                6.895
```

```
153T  149  150   11    39                6.895
154T  150  151   11    39                6.895
   2    0   4.94279   4.94279   4.94279
   5    0   1.41125   1.41125   1.41125
   6    0   3.36254   3.36254   3.36254
   9    0   2.47495   2.47495   2.47495
  10    0   0.05000   0.05000   0.05000
  11    0   0.05000   0.05000   0.05000
  36    0   0.56000   0.56000   0.56000
  41    0   0.28000   0.28000   0.28000
  49    0   0.40045   0.40045   0.40045
  60    0   0.02500   0.02500   0.02500
  69    0   0.00619   0.00619   0.00619
  70    0   0.90000   0.90000   0.90000
  71    0   0.00308   0.00308   0.00308
 107    0   0.09124   0.09124   0.09124
 120    0       0.5       0.5       0.5
 122    0 0.0054335 0.0054335 0.0054335
 123    0 0.0054335 0.0054335 0.0054335
 125    0 0.0054335 0.0054335 0.0054335
 127    0      0.62      0.62      0.62
 138    0      0.35      0.35      0.35


   0    0   35              200.0
```

APPENDIX B

Comparisons of Acceleration Spectra

Test: T41.31.2

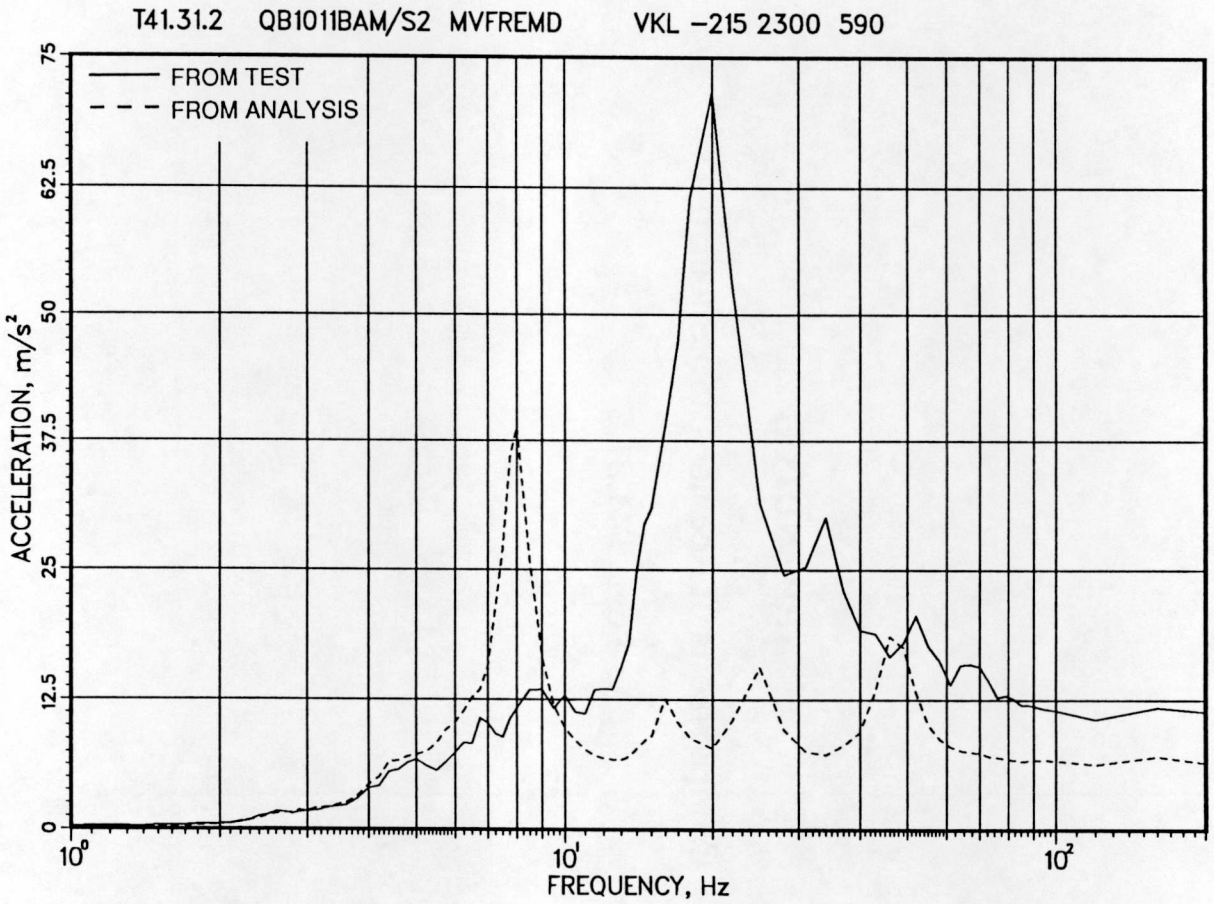
T41.31.2 QB1011BAM/S2 MVFREMD VKL -215 2300 590
FROM TEST
FROM ANALYSIS
ACCELERATION, m/s²
0
12.5
25
37.5
50
62.5
75
10⁰
10¹
10²
FREQUENCY, Hz

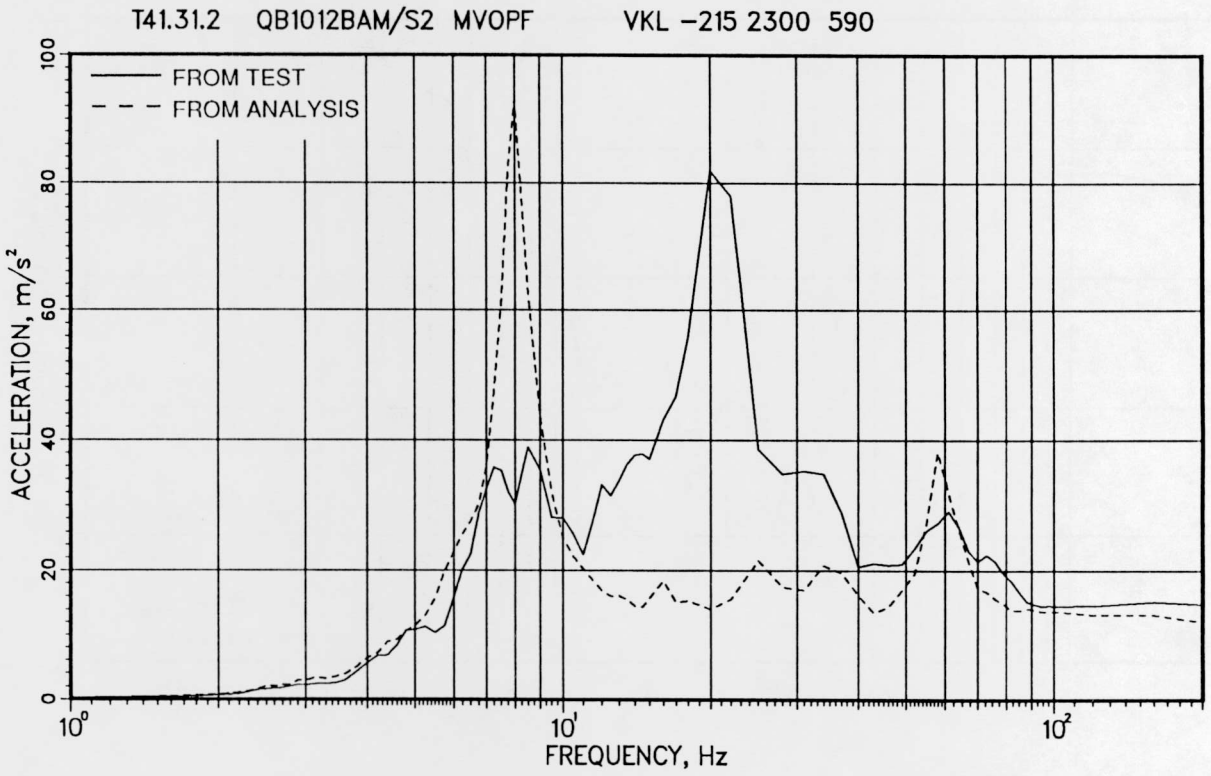
T41.31.2 QB1012BAM/S2 MVOPF VKL −215 2300 590
FROM TEST
FROM ANALYSIS
ACCELERATION, m/s²
0
20
40
60
80
100
10⁰
10¹
10²
FREQUENCY, Hz

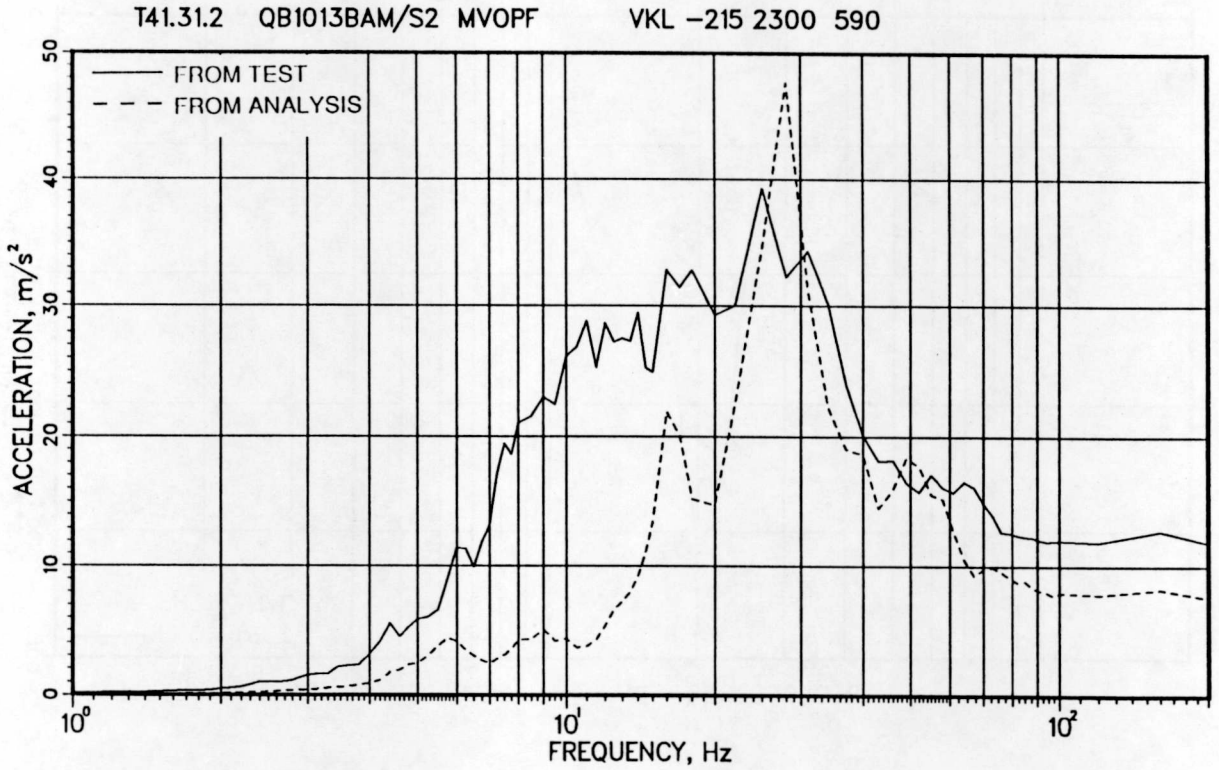
T41.31.2 QB1013BAM/S2 MVOPF VKL −215 2300 590
FROM TEST
FROM ANALYSIS
ACCELERATION, m/s²
0
10
20
30
40
50
10⁰
10¹
10²
FREQUENCY, Hz

T41.31.2 QB1071BAM/S2 MVOPF VKL 44 2300 896
FROM TEST
FROM ANALYSIS
ACCELERATION, m/s²
0
10
20
30
40
10⁰
10¹
10²
FREQUENCY, Hz

T41.31.2 QB1072BAM/S2 MVOPF VKL 44 2300 896
FROM TEST
FROM ANALYSIS
ACCELERATION, m/s²
0
10
20
30
40
10⁰
10¹
10²
FREQUENCY, Hz

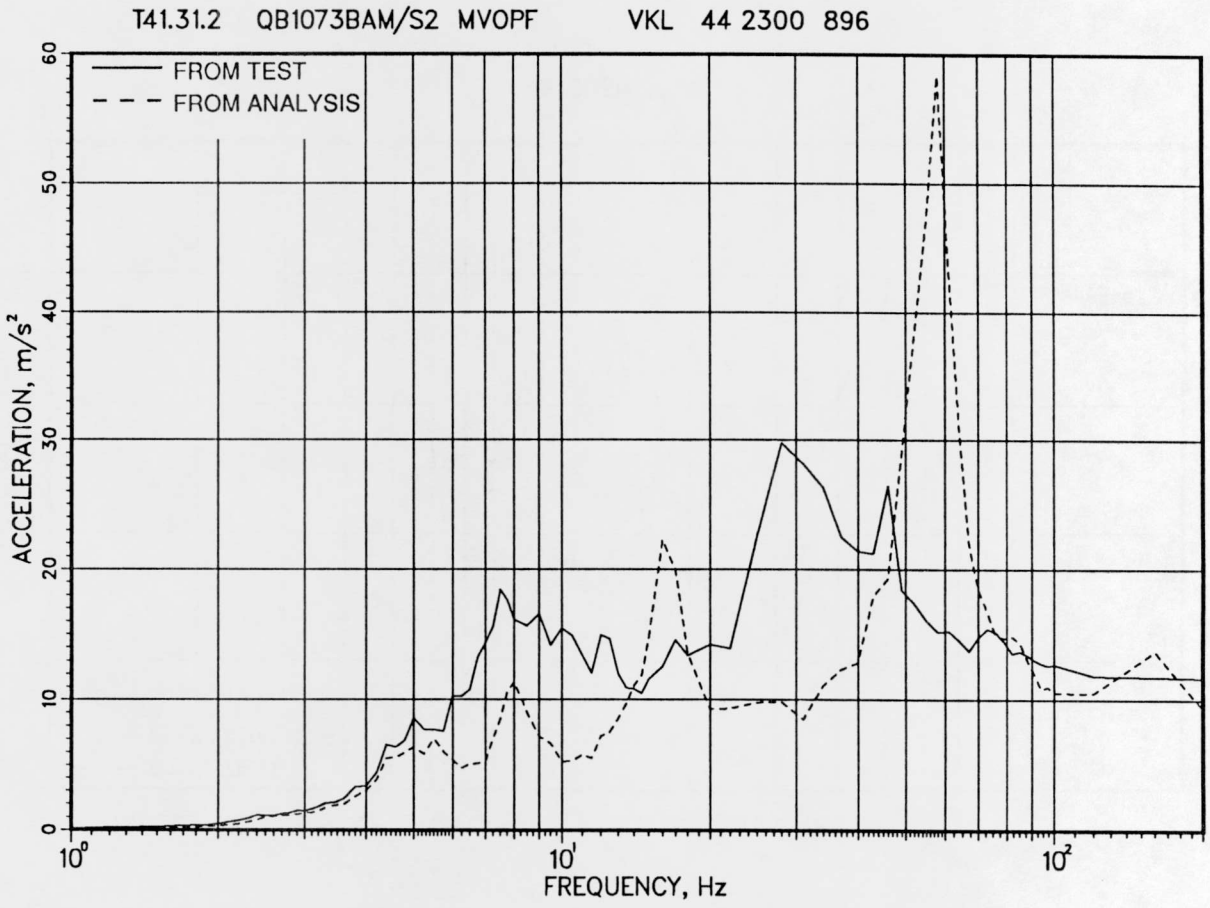
T41.31.2 QB1073BAM/S2 MVOPF VKL 44 2300 896
FROM TEST
FROM ANALYSIS
ACCELERATION, m/s²
0
10
20
30
40
50
60
10⁰
10¹
10²
FREQUENCY, Hz

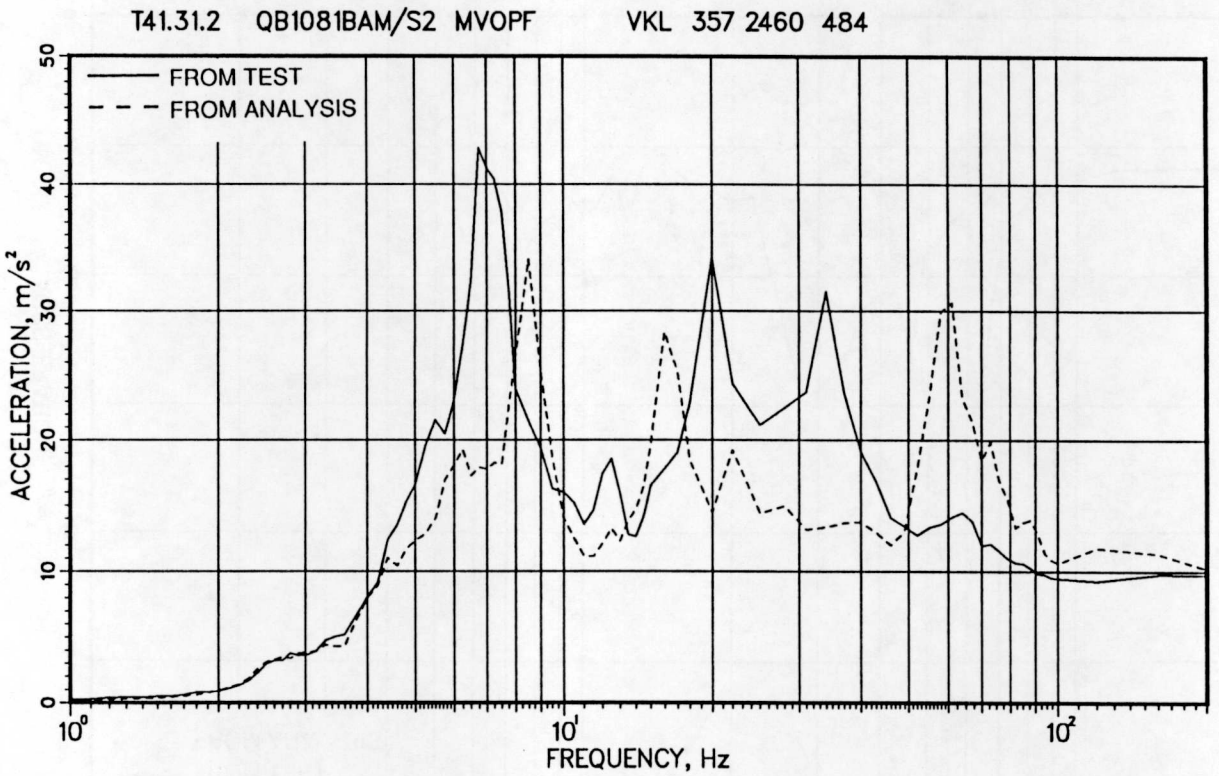
T41.31.2 QB1081BAM/S2 MVOPF VKL 357 2460 484
FROM TEST
FROM ANALYSIS
ACCELERATION, m/s²
0
10
20
30
40
50
10⁰
10¹
10²
FREQUENCY, Hz

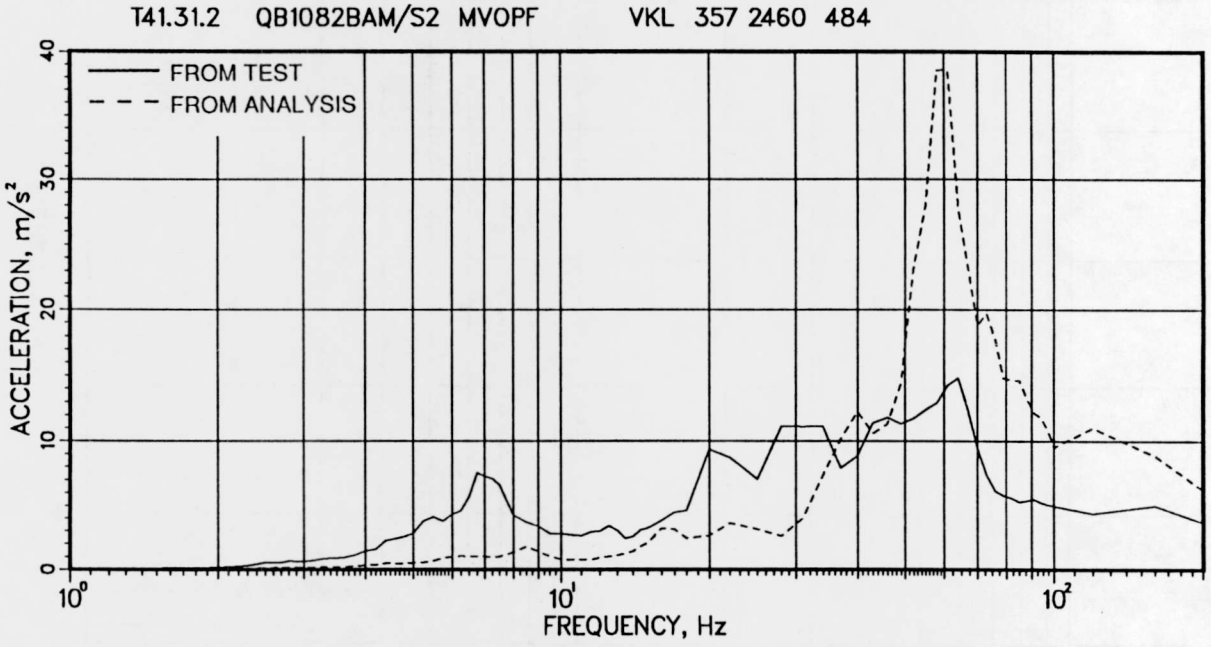
T41.31.2 QB1082BAM/S2 MVOPF VKL 357 2460 484
FROM TEST
FROM ANALYSIS
ACCELERATION, m/s²
0
10
20
30
40
10⁰
10¹
10²
FREQUENCY, Hz

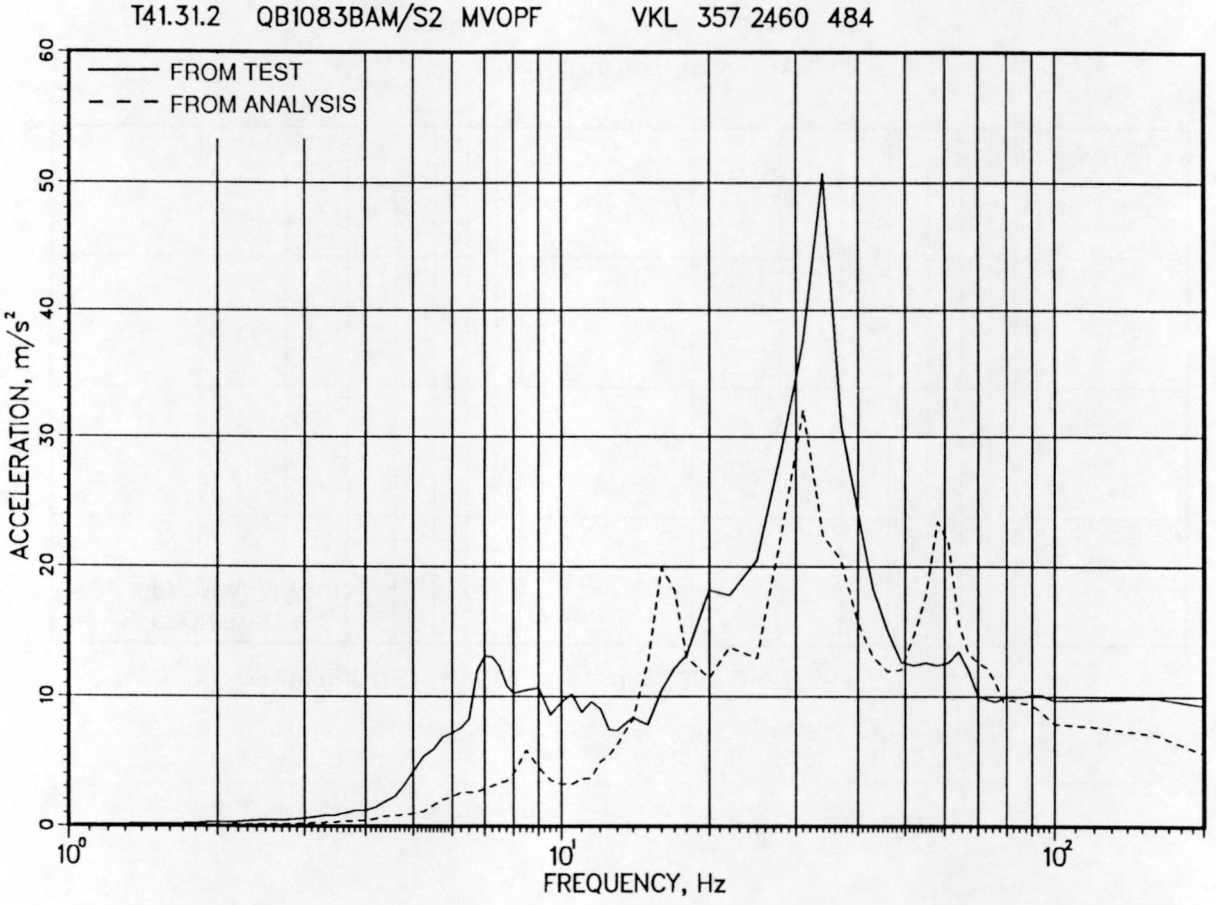
T41.31.2 QB1083BAM/S2 MVOPF VKL 357 2460 484
FROM TEST
FROM ANALYSIS
ACCELERATION, m/s²
0
10
20
30
40
50
60
10⁰
10¹
10²
FREQUENCY, Hz

T41.31.2 QB1092BAM/S2 MVOPF VKL 586 2460 676
FROM TEST
FROM ANALYSIS
ACCELERATION, m/s²
0
5
10
15
20
25
10⁰
10¹
10²
FREQUENCY, Hz

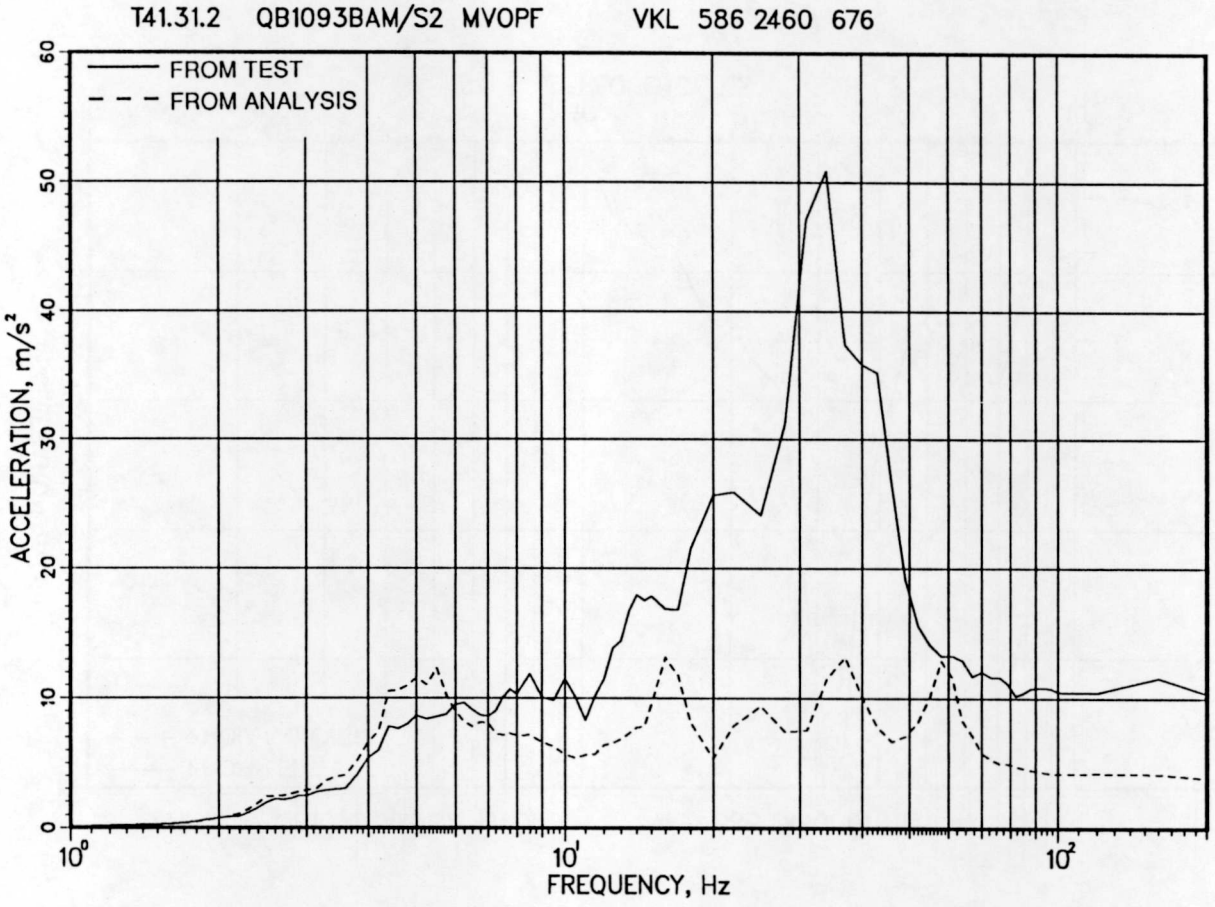
T41.31.2 QB1093BAM/S2 MVOPF VKL 586 2460 676
FROM TEST
FROM ANALYSIS
ACCELERATION, m/s²
0
10
20
30
40
50
60
10⁰
10¹
10²
FREQUENCY, Hz

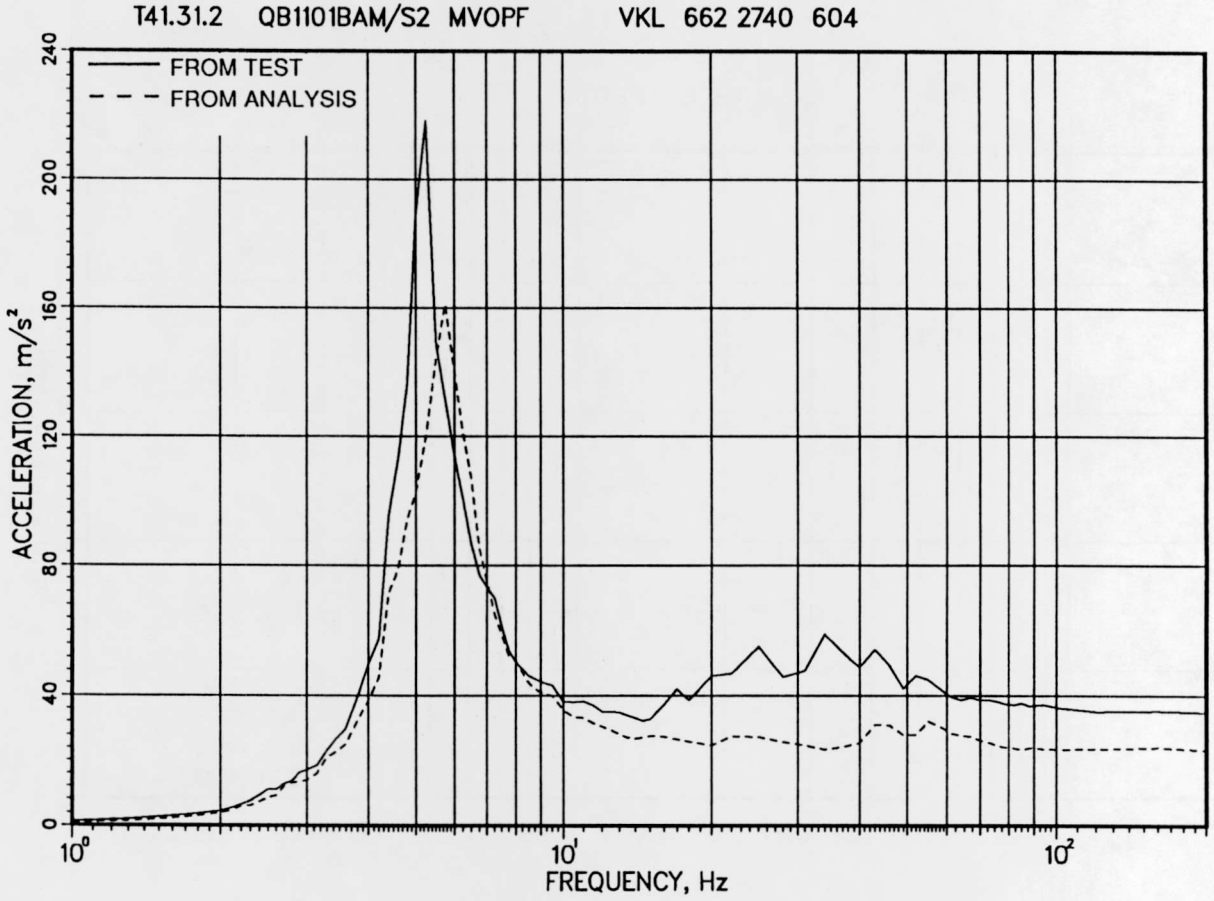
T41.31.2 QB1101BAM/S2 MVOPF VKL 662 2740 604
FROM TEST
FROM ANALYSIS
ACCELERATION, m/s²
0
40
80
120
160
200
240
10⁰
10¹
10²
FREQUENCY, Hz

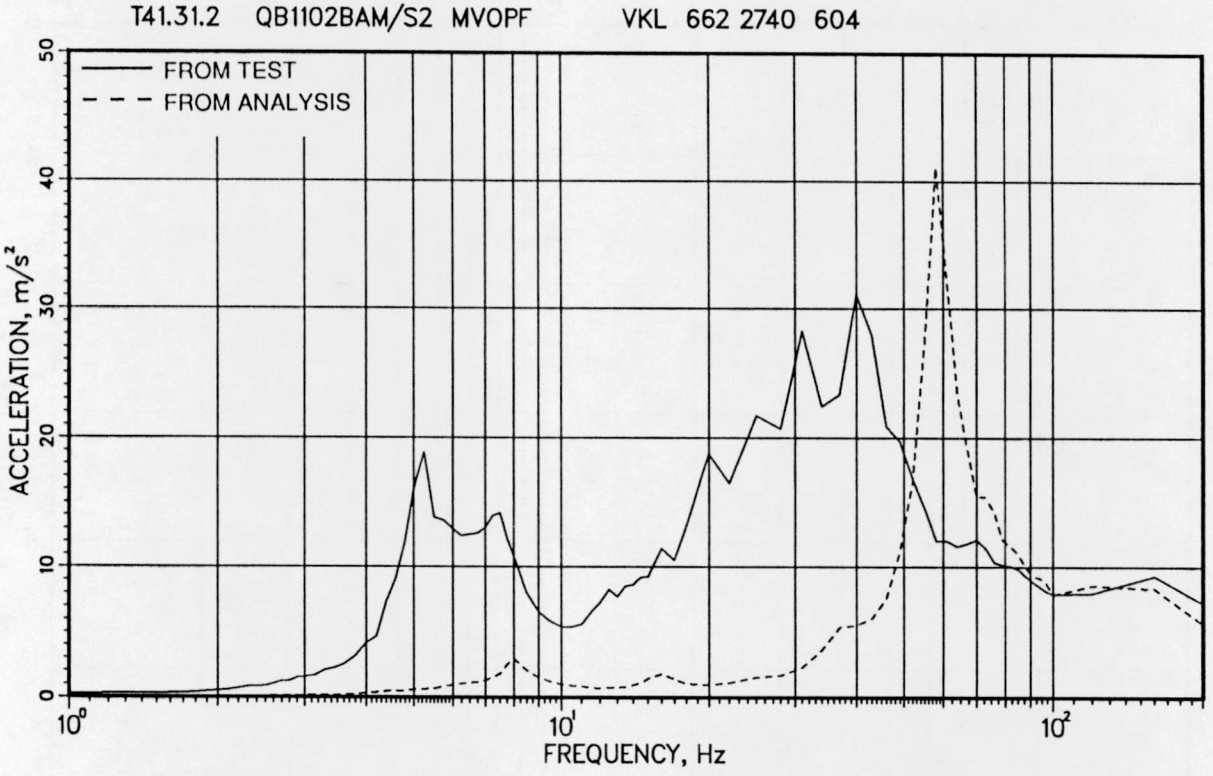
T41.31.2 QB1102BAM/S2 MVOPF VKL 662 2740 604
FROM TEST
FROM ANALYSIS
ACCELERATION, m/s²
0
10
20
30
40
50
10⁰
10¹
10²
FREQUENCY, Hz

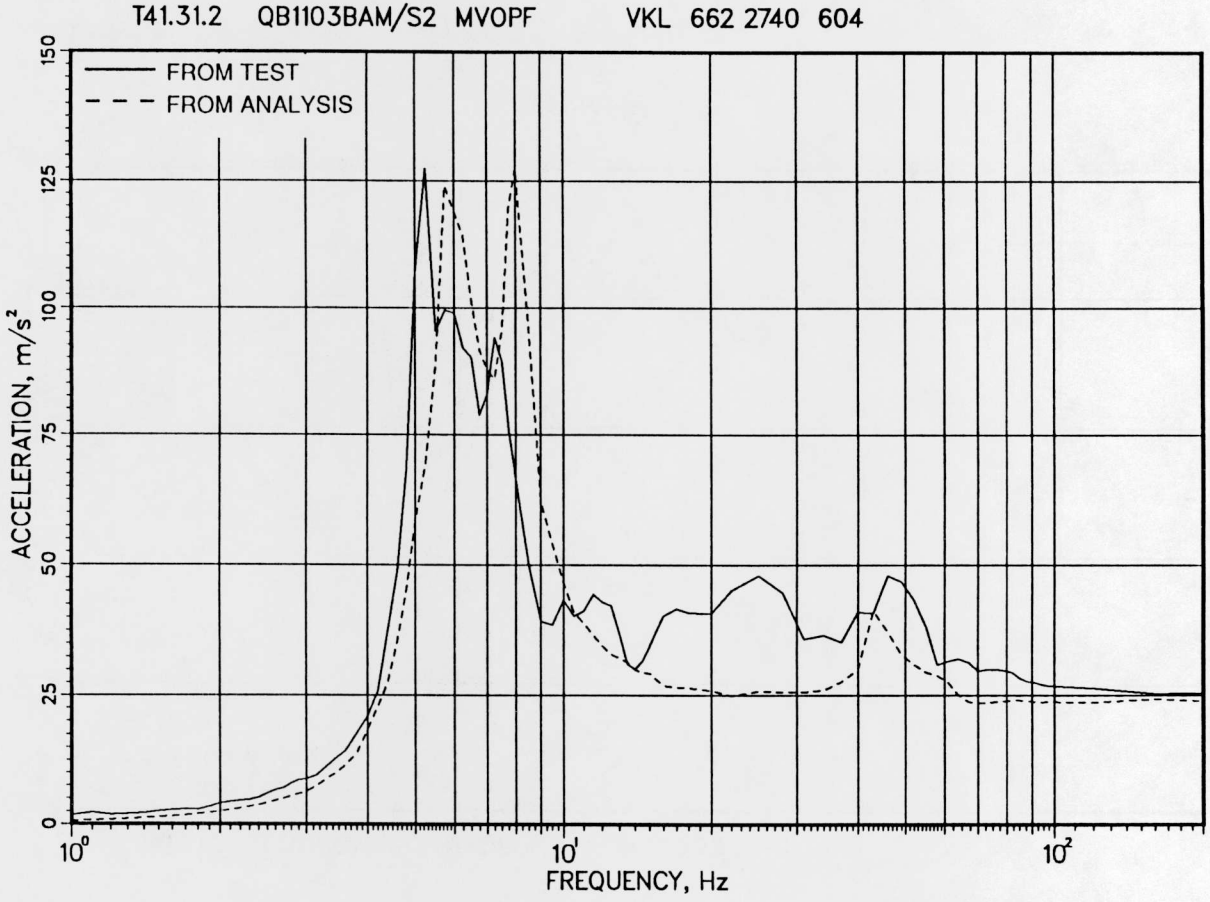
T41.31.2 QB1103BAM/S2 MVOPF VKL 662 2740 604
FROM TEST
FROM ANALYSIS
ACCELERATION, m/s²
0
25
50
75
100
125
150
10⁰
10¹
10²
FREQUENCY, Hz

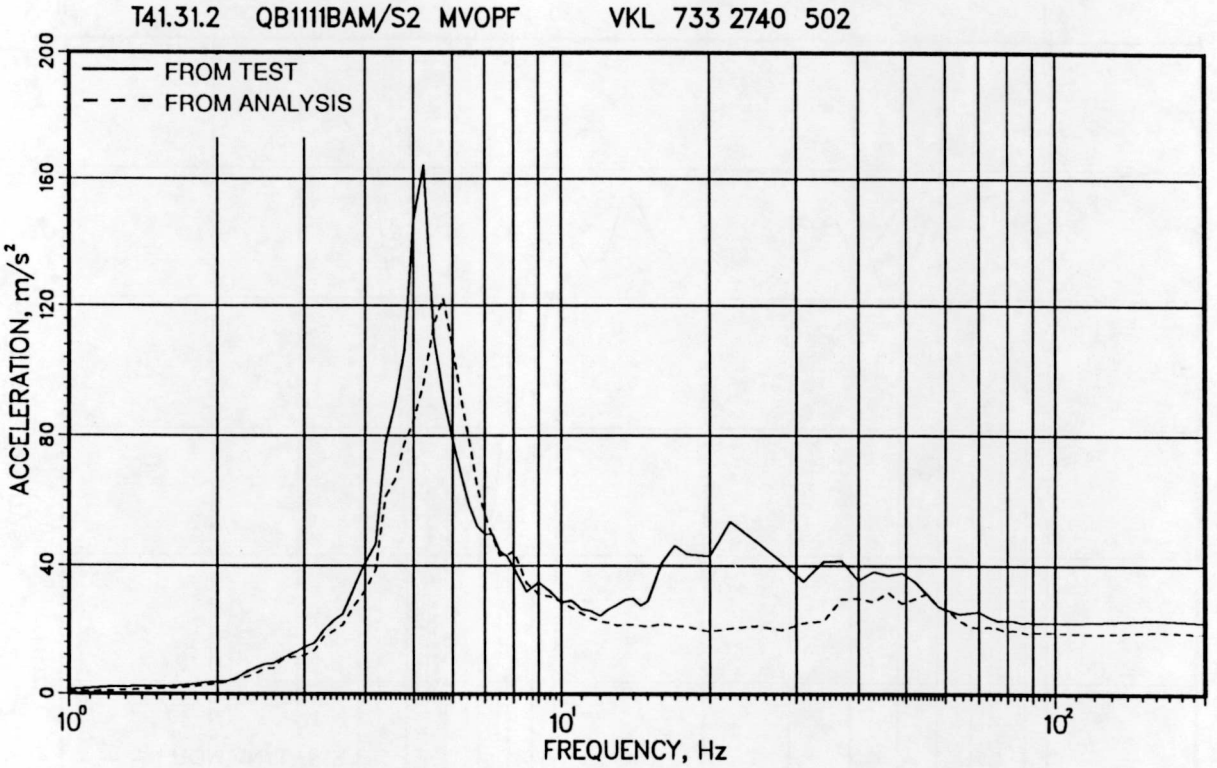
T41.31.2 QB1111BAM/S2 MVOPF VKL 733 2740 502
FROM TEST
FROM ANALYSIS
ACCELERATION, m/s²
0
40
80
120
160
200
10⁰
10¹
10²
FREQUENCY, Hz

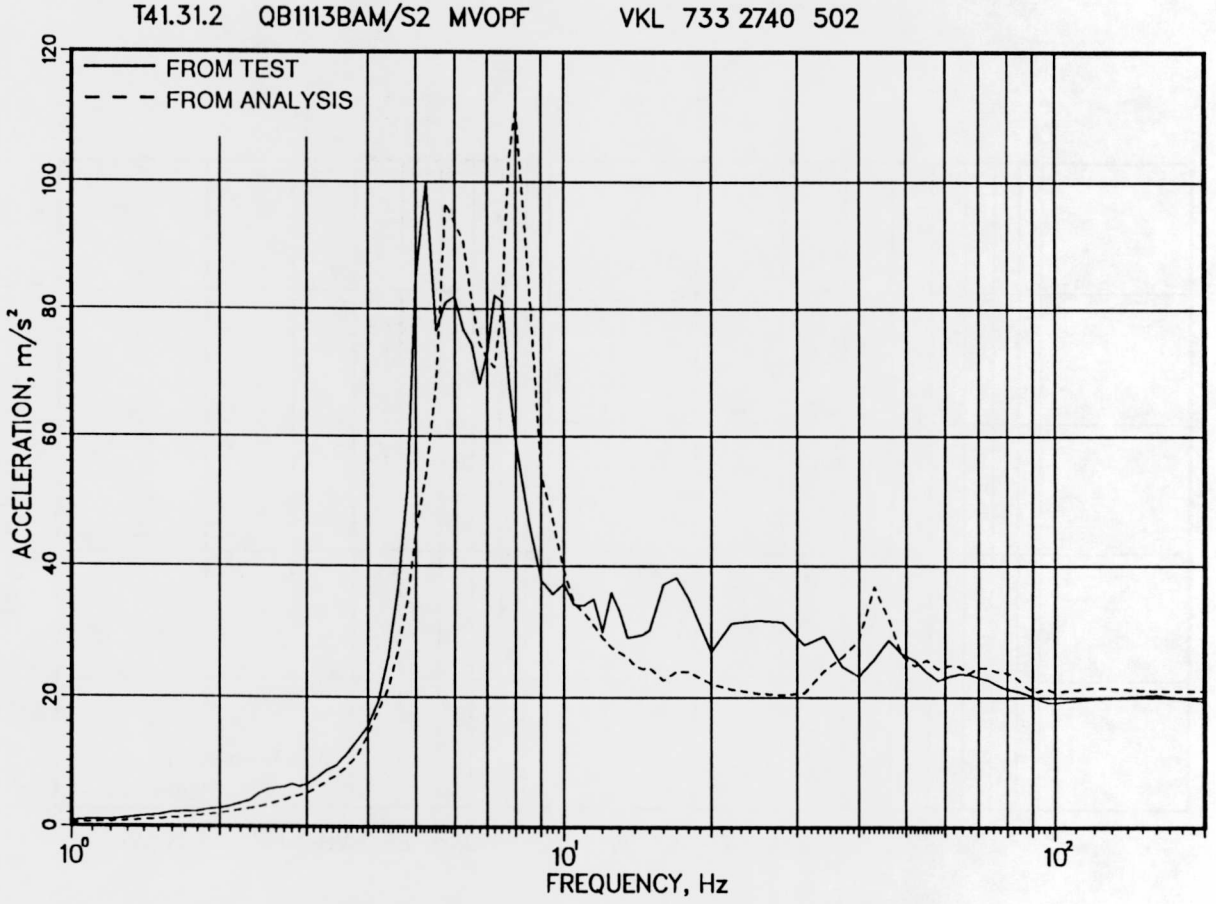
T41.31.2 QB1113BAM/S2 MVOPF VKL 733 2740 502
FROM TEST
FROM ANALYSIS
ACCELERATION, m/s²
0
20
40
60
80
100
120
10⁰
10¹
10²
FREQUENCY, Hz

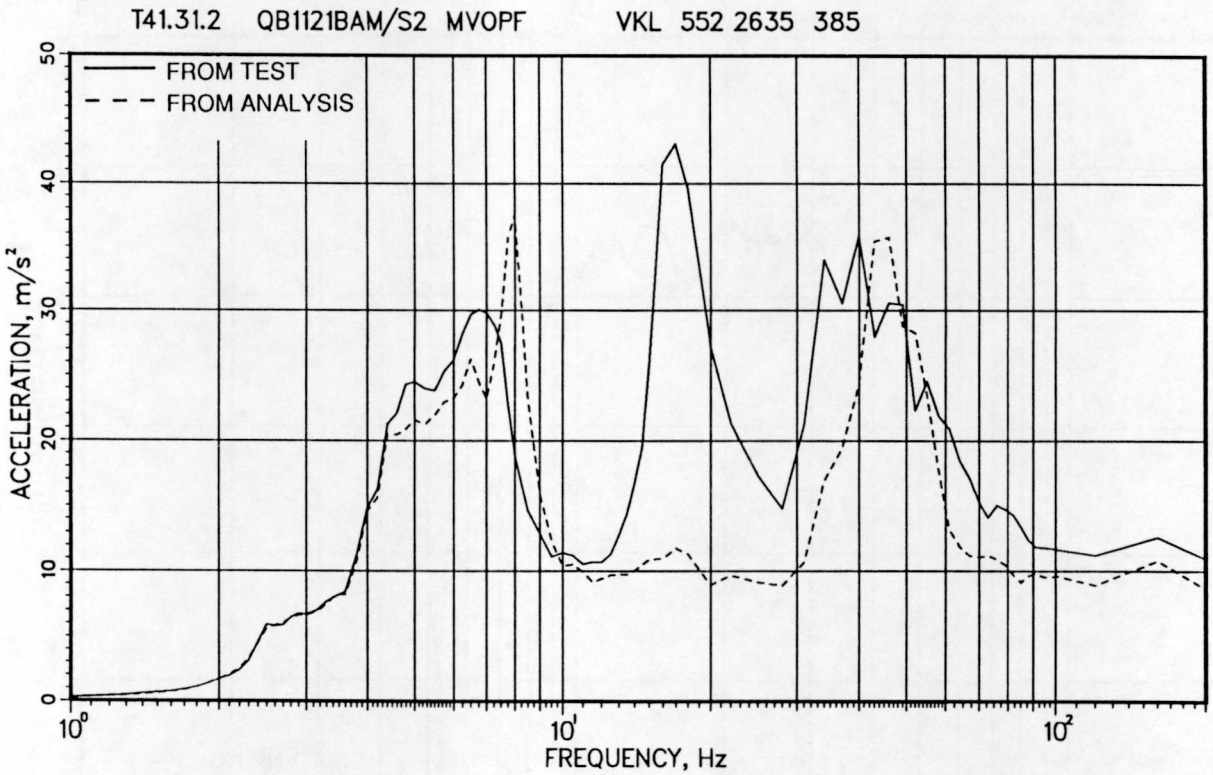
T41.31.2 QB1121BAM/S2 MVOPF VKL 552 2635 385
FROM TEST
FROM ANALYSIS
ACCELERATION, m/s²
0
10
20
30
40
50
10⁰
10¹
10²
FREQUENCY, Hz

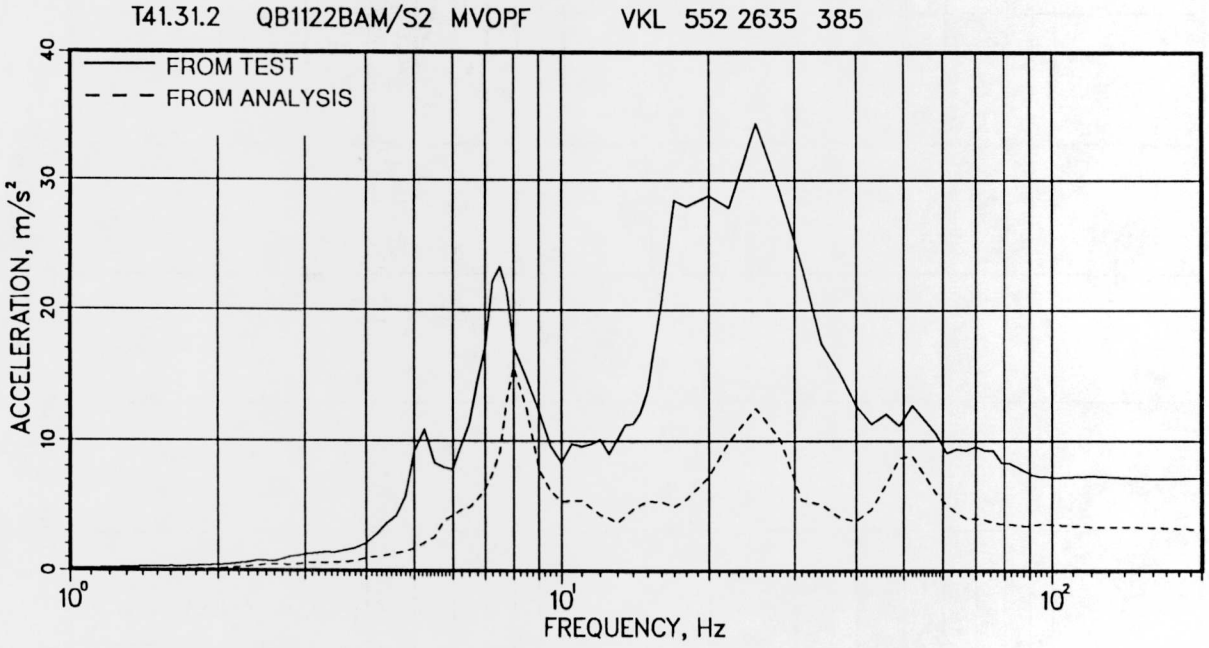
T41.31.2 QB1122BAM/S2 MVOPF VKL 552 2635 385
FROM TEST
FROM ANALYSIS
ACCELERATION, m/s²
0
10
20
30
40
10⁰
10¹
10²
FREQUENCY, Hz

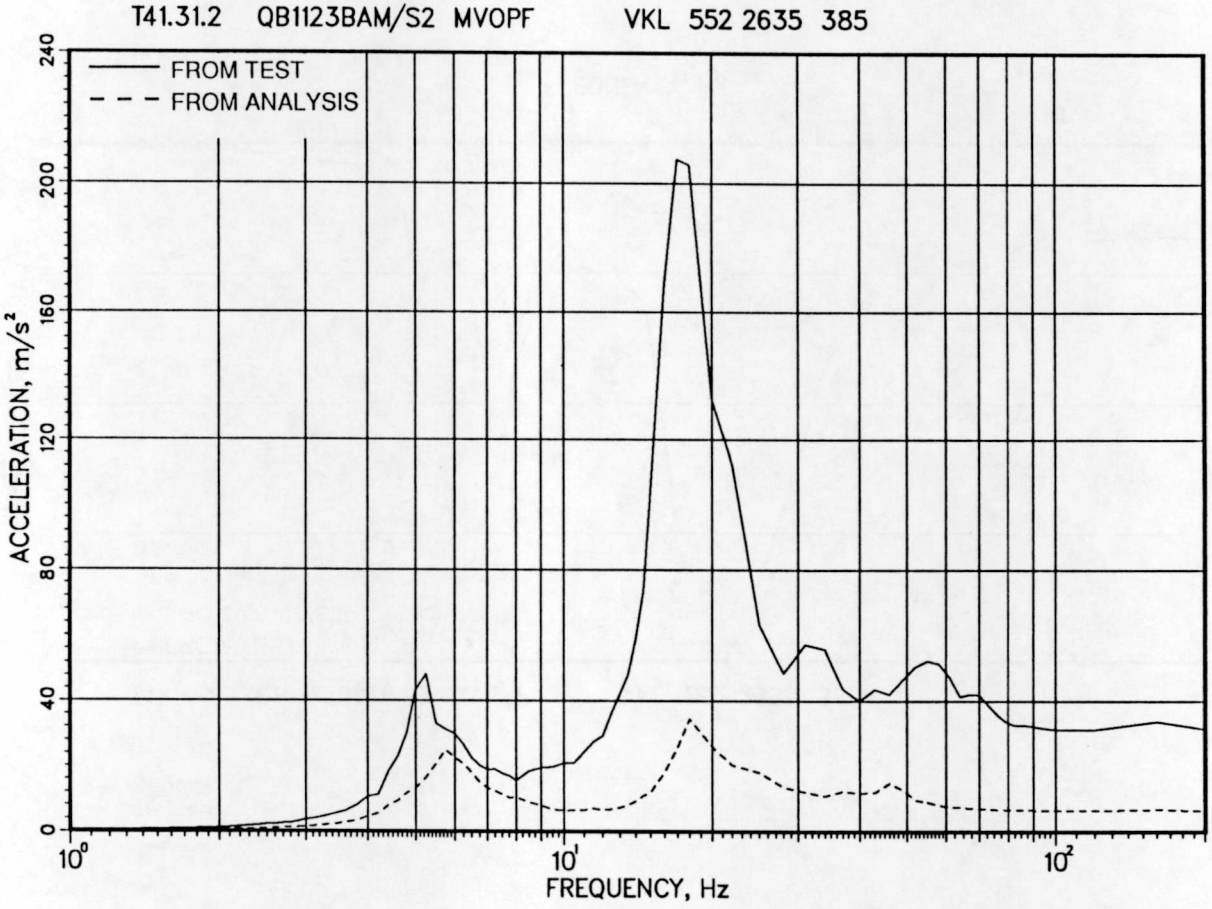
T41.31.2 QB1123BAM/S2 MVOPF VKL 552 2635 385
FROM TEST
FROM ANALYSIS
ACCELERATION, m/s²
0
40
80
120
160
200
240
10⁰
10¹
10²
FREQUENCY, Hz

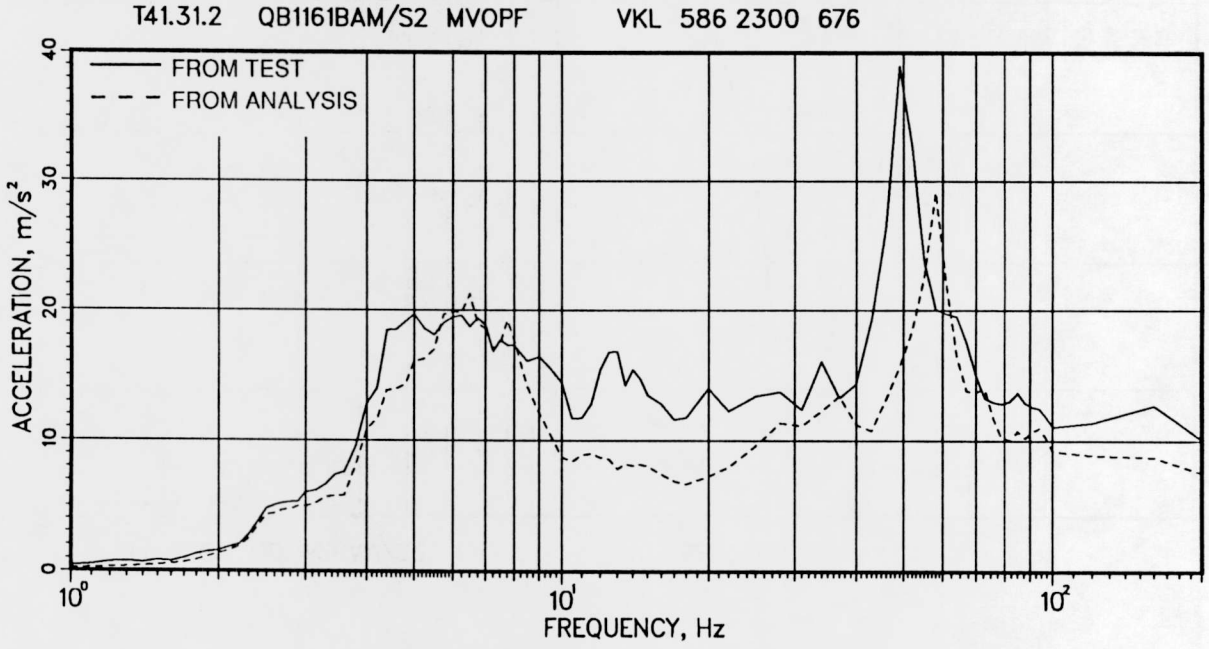
T41.31.2 QB1161BAM/S2 MVOPF VKL 586 2300 676
FROM TEST
FROM ANALYSIS
ACCELERATION, m/s²
0
10
20
30
40
10⁰
10¹
10²
FREQUENCY, Hz

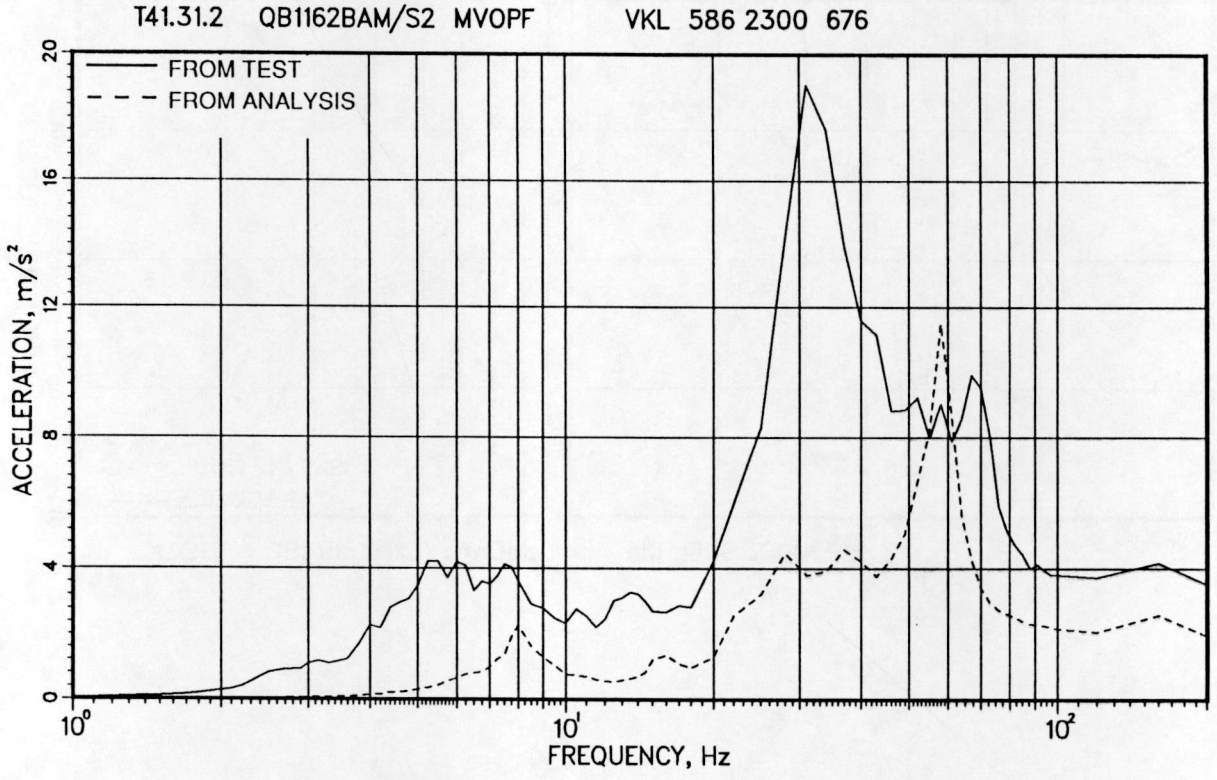
T41.31.2 QB1162BAM/S2 MVOPF VKL 586 2300 676
FROM TEST
FROM ANALYSIS
ACCELERATION, m/s²
0
4
8
12
16
20
10⁰
10¹
10²
FREQUENCY, Hz

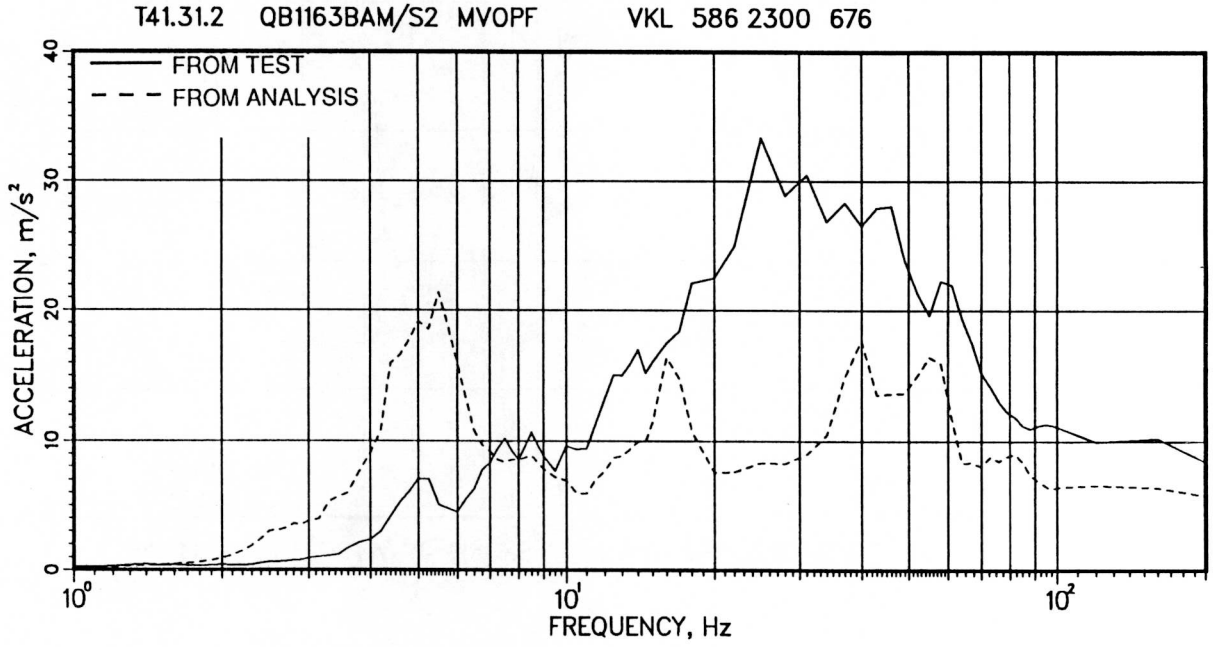
T41.31.2 QB1163BAM/S2 MVOPF VKL 586 2300 676
FROM TEST
FROM ANALYSIS
ACCELERATION, m/s²
0
10
20
30
40
10⁰
10¹
10²
FREQUENCY, Hz

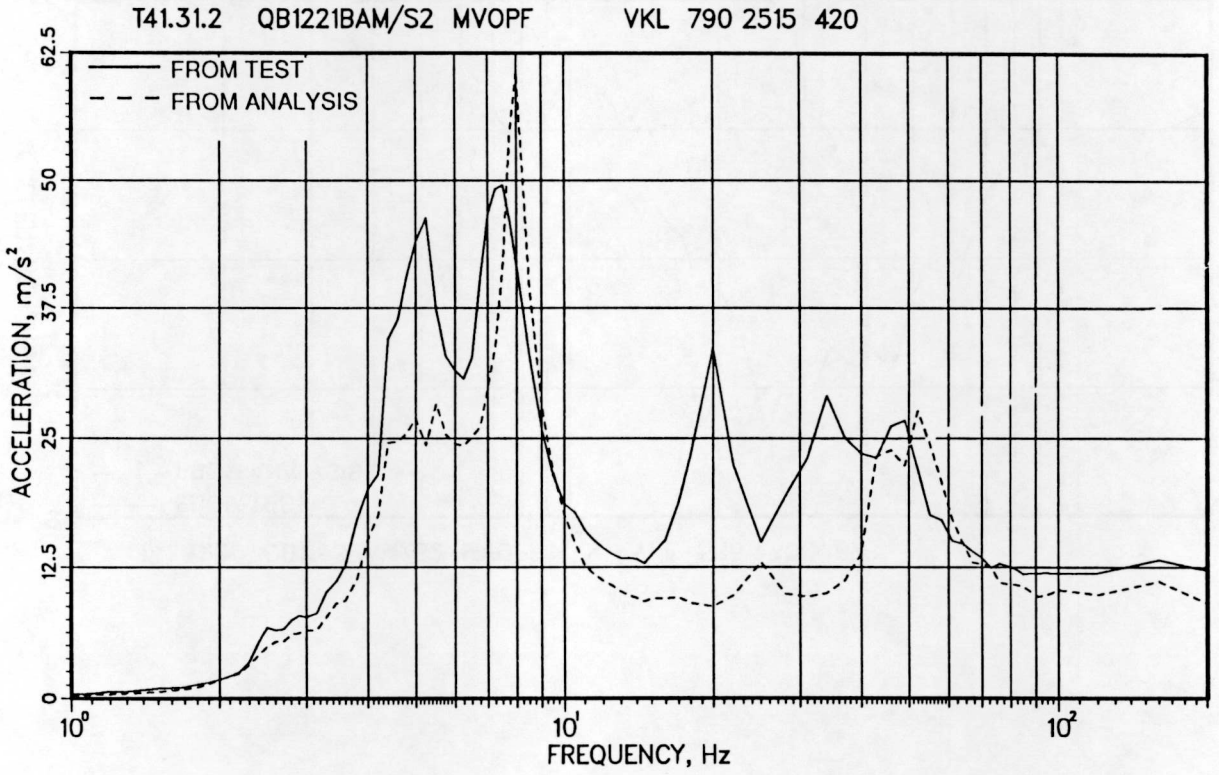
T41.31.2 QB1221BAM/S2 MVOPF VKL 790 2515 420
FROM TEST
FROM ANALYSIS
ACCELERATION, m/s²
62.5
50
37.5
25
12.5
0
10⁰
10¹
10²
FREQUENCY, Hz

T41.31.2 QB1223BAM/S2 MVOPF VKL 790 2515 420
FROM TEST
FROM ANALYSIS
ACCELERATION, m/s²
0
10
20
30
40
10⁰
10¹
10²
FREQUENCY, Hz

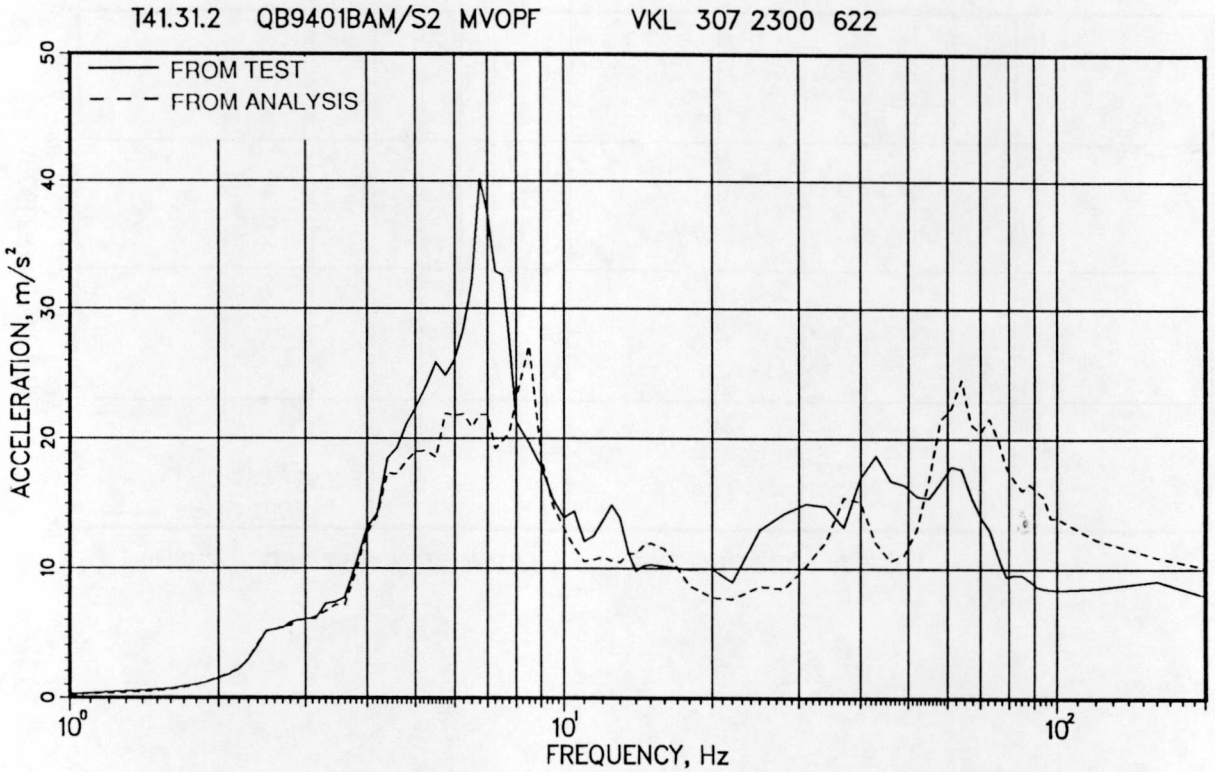
T41.31.2 QB9401BAM/S2 MVOPF VKL 307 2300 622
FROM TEST
FROM ANALYSIS
ACCELERATION, m/s²
0
10
20
30
40
50
10⁰
10¹
10²
FREQUENCY, Hz

T41.31.2 QB9403BAM/S2 MVOPF VKL 307 2300 622
FROM TEST
FROM ANALYSIS
ACCELERATION, m/s²
0
4
8
12
16
10⁰
10¹
10²
FREQUENCY, Hz

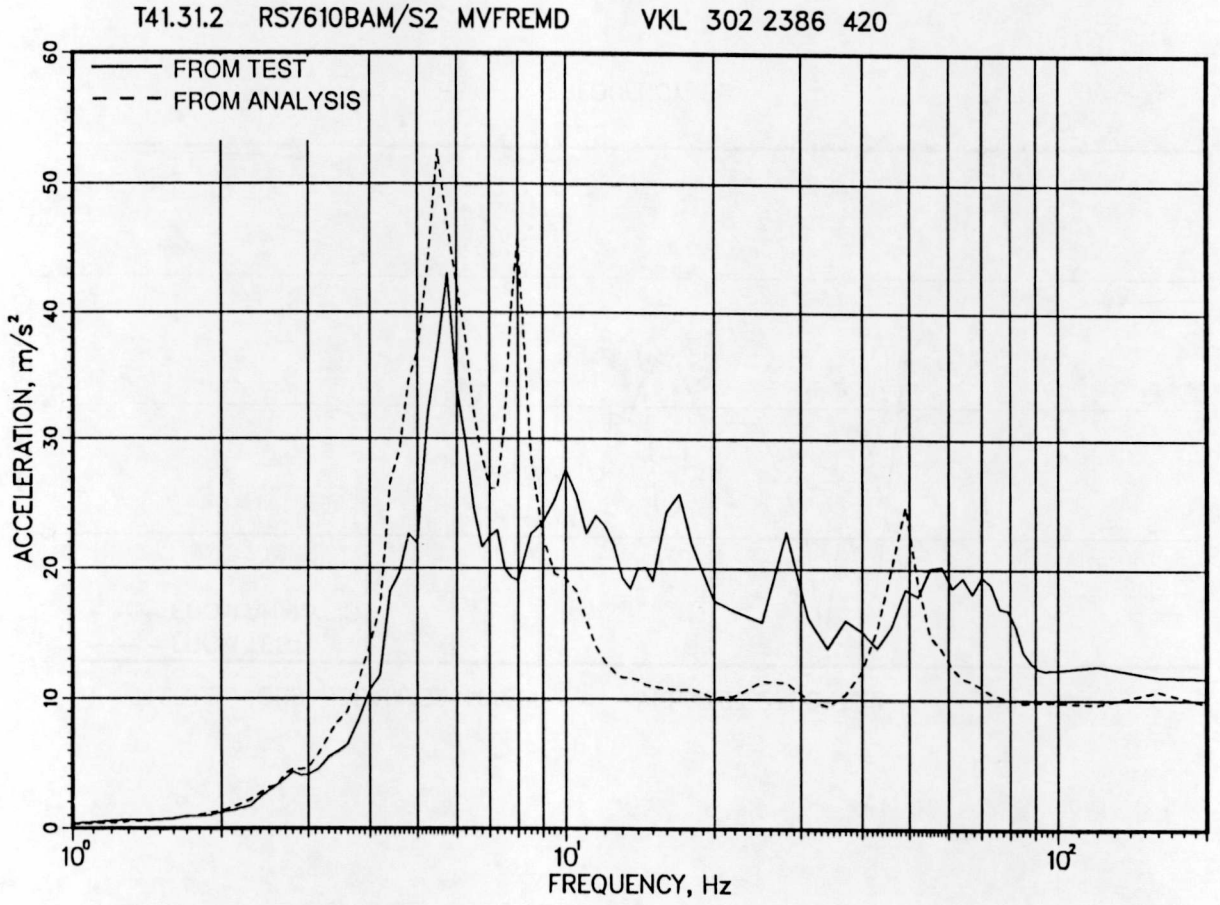
T41.31.2 RS7610BAM/S2 MVFREMD VKL 302 2386 420
FROM TEST
FROM ANALYSIS
ACCELERATION, m/s²
0
10
20
30
40
50
60
10⁰
10¹
10²
FREQUENCY, Hz

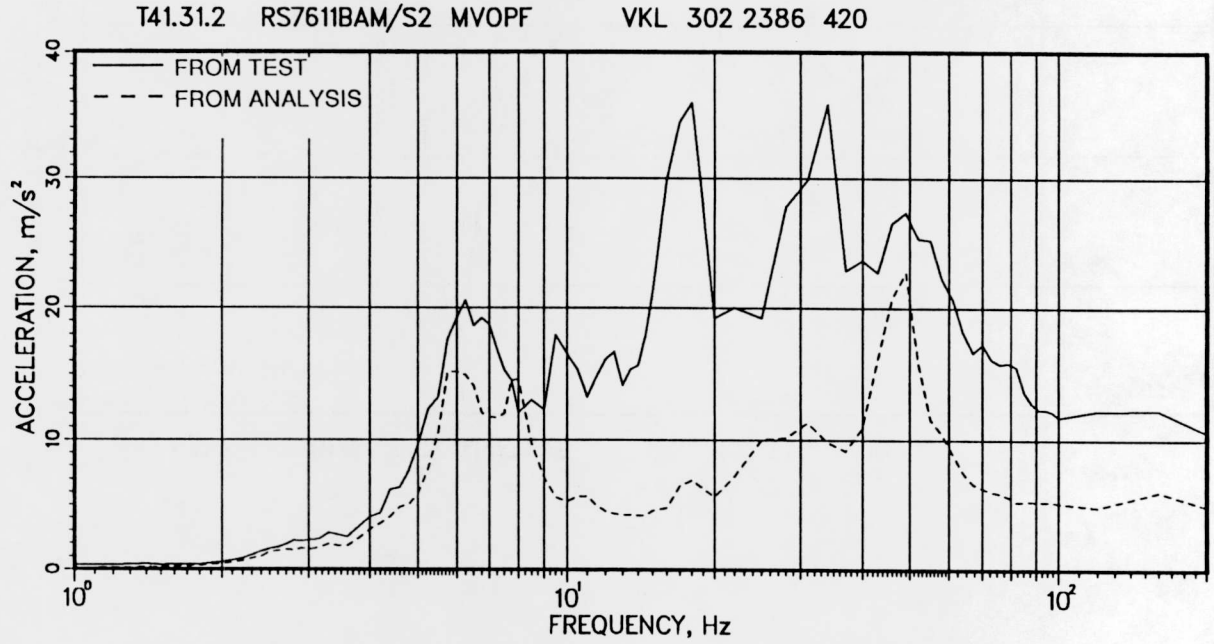
T41.31.2 RS7611BAM/S2 MVOPF VKL 302 2386 420
FROM TEST
FROM ANALYSIS
ACCELERATION, m/s²
0
10
20
30
40
10⁰
10¹
10²
FREQUENCY, Hz

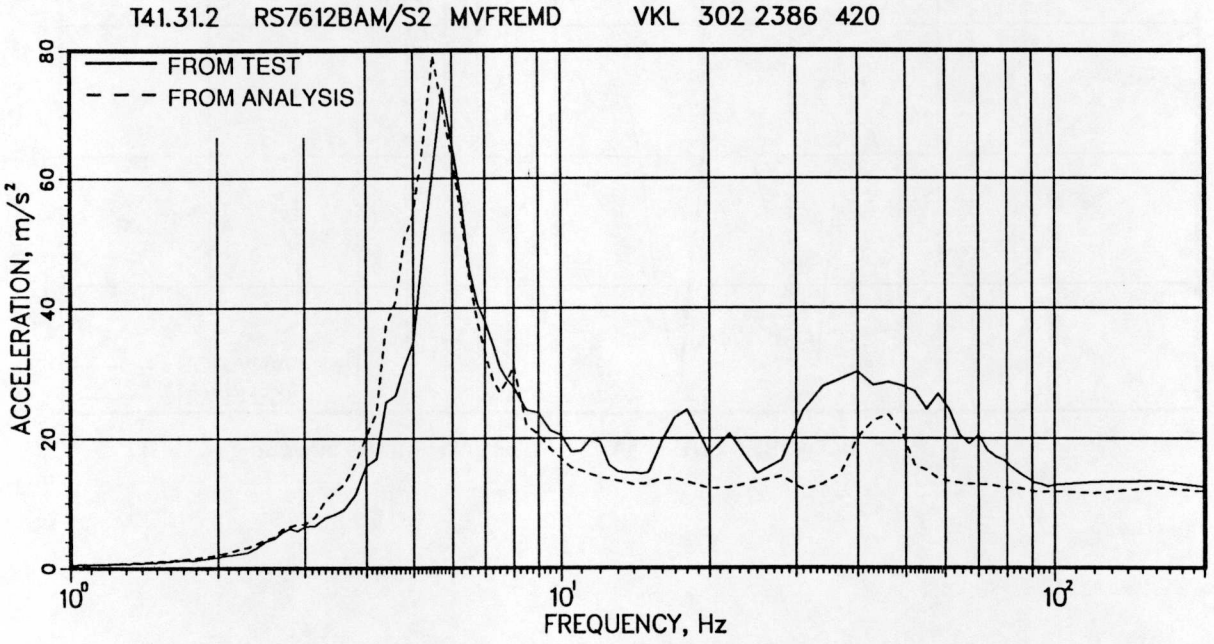
T41.31.2 RS7612BAM/S2 MVFREMD VKL 302 2386 420
FROM TEST
FROM ANALYSIS
ACCELERATION, m/s²
0
20
40
60
80
10⁰
10¹
10²
FREQUENCY, Hz

APPENDIX C

Comparisons of Displacement Histories

Test: T41.21.1

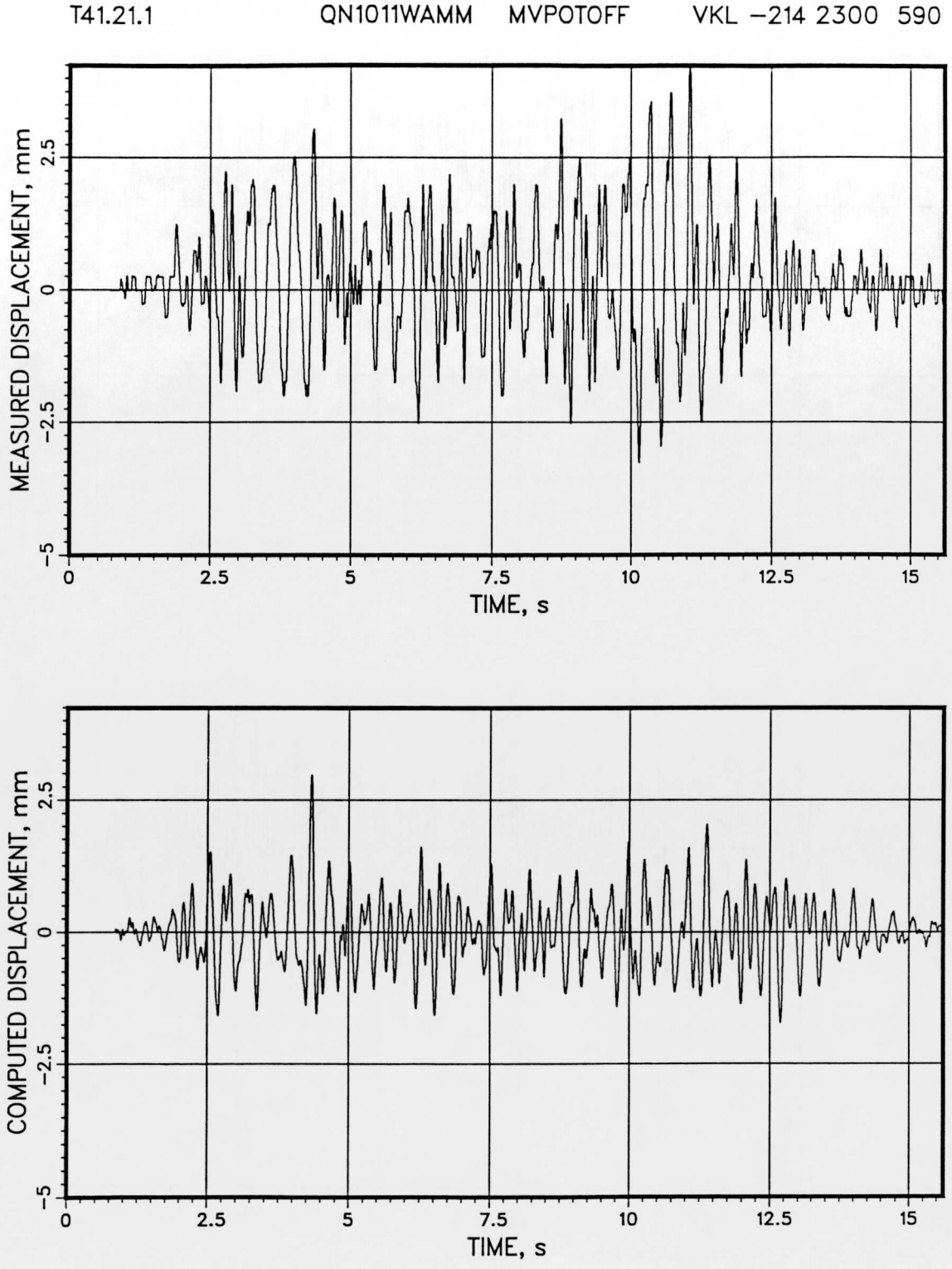
T41.21.1 QN1011WAMM MVPOTOFF VKL −214 2300 590
MEASURED DISPLACEMENT, mm
2.5
0
−2.5
−5
0
2.5
5
7.5
10
12.5
15
TIME, s
COMPUTED DISPLACEMENT, mm
2.5
0
−2.5
−5
0
2.5
5
7.5
10
12.5
15
TIME, s

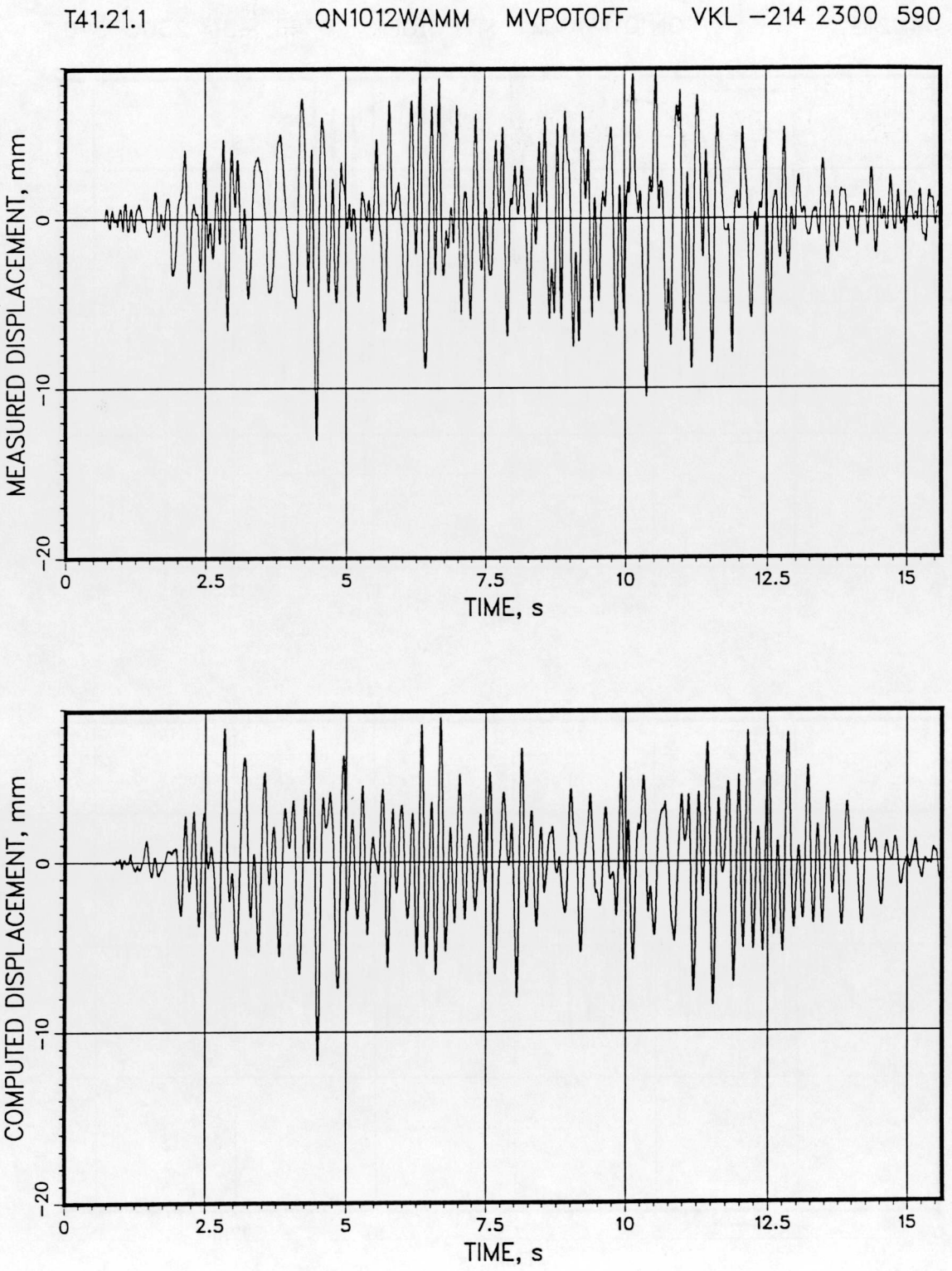
T41.21.1
QN1012WAMM
MVPOTOFF
VKL −214 2300 590
MEASURED DISPLACEMENT, mm
0
−10
−20
0
2.5
5
7.5
10
12.5
15
TIME, s
COMPUTED DISPLACEMENT, mm
0
−10
−20
0
2.5
5
7.5
10
12.5
15
TIME, s

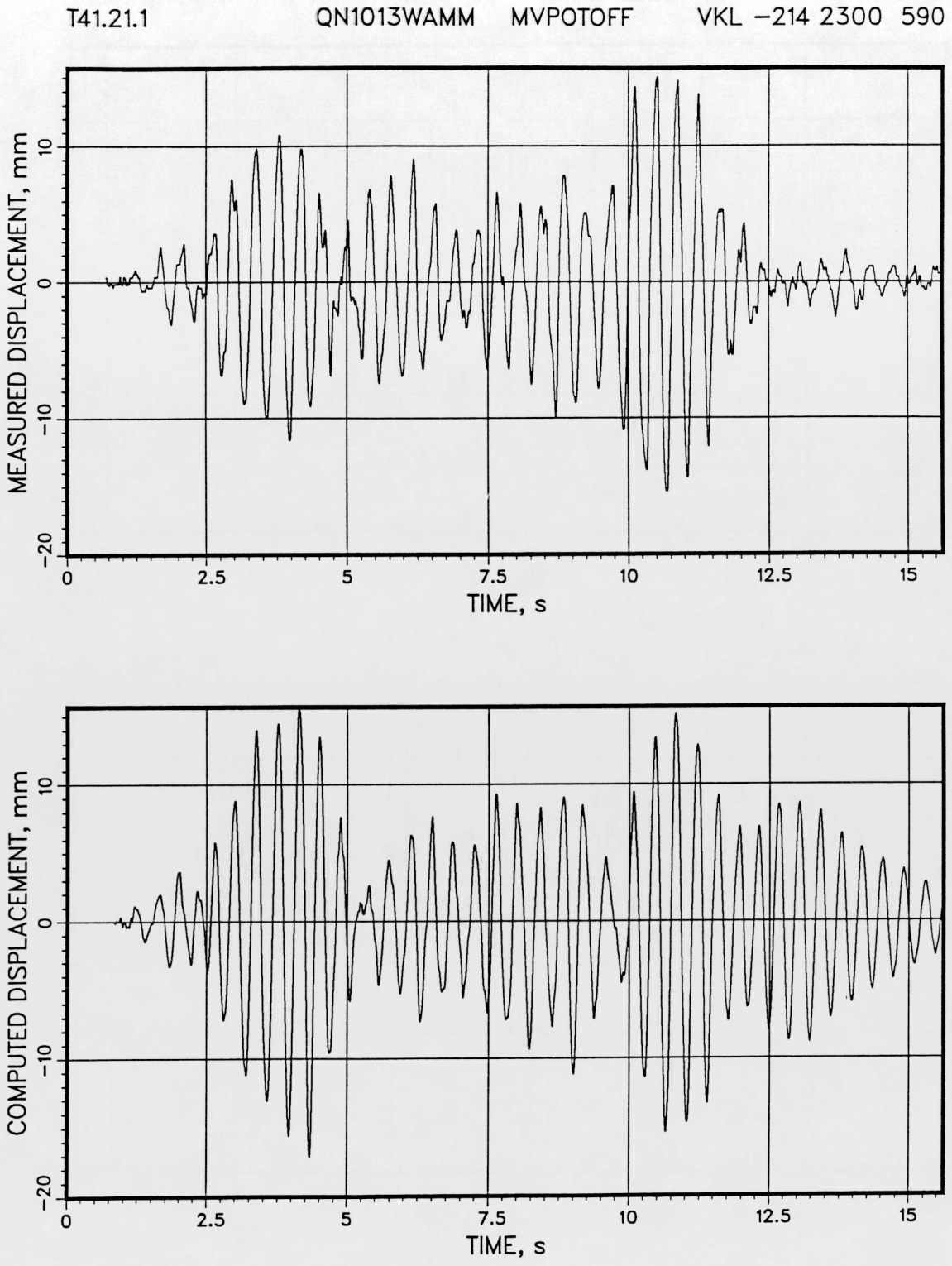
T41.21.1 QN1013WAMM MVPOTOFF VKL −214 2300 590
MEASURED DISPLACEMENT, mm
10
0
−10
−20
0
2.5
5
7.5
10
12.5
15
TIME, s
COMPUTED DISPLACEMENT, mm
10
0
−10
−20
0
2.5
5
7.5
10
12.5
15
TIME, s

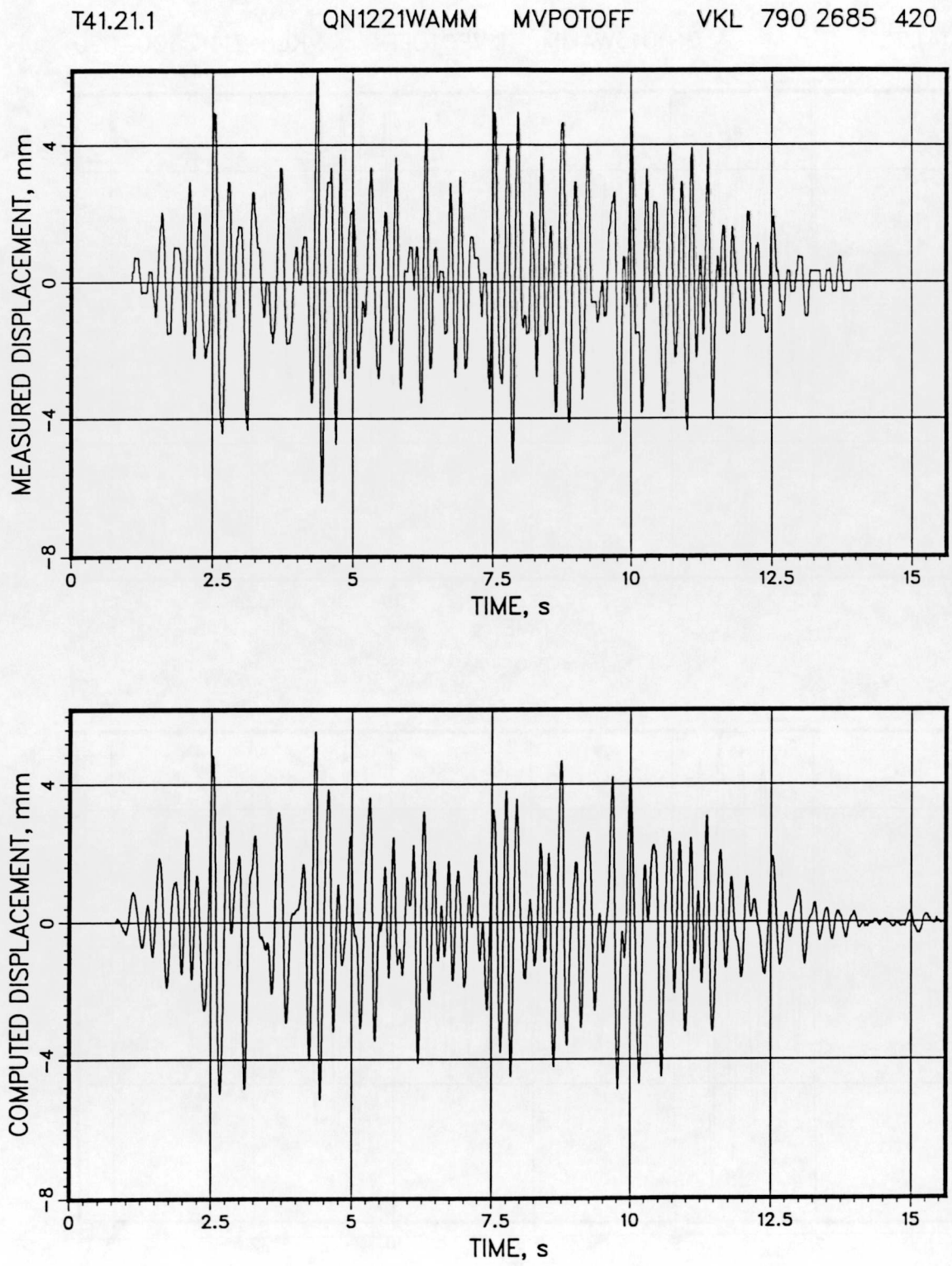
T41.21.1
QN1221WAMM MVPOTOFF
VKL 790 2685 420
MEASURED DISPLACEMENT, mm
4
0
-4
-8
0
2.5
5
7.5
10
12.5
15
TIME, s
COMPUTED DISPLACEMENT, mm
4
0
-4
-8
0
2.5
5
7.5
10
12.5
15
TIME, s

T41.21.1 QN1223WAMM MVPOTOFF VKL 790 2685 420

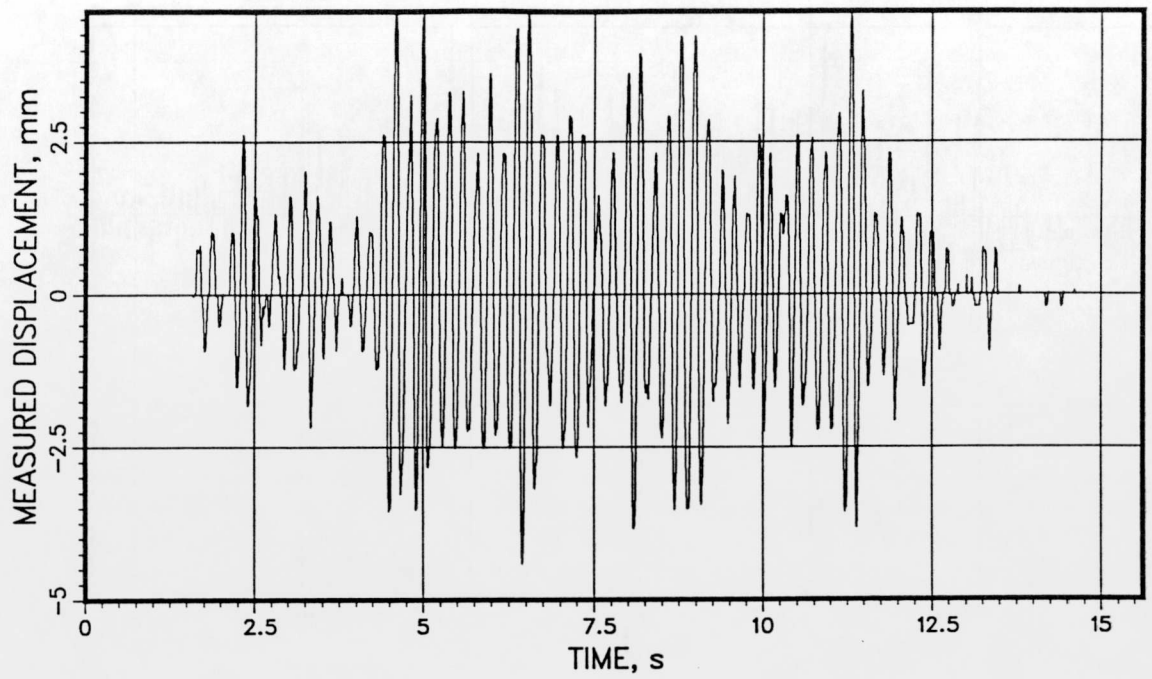

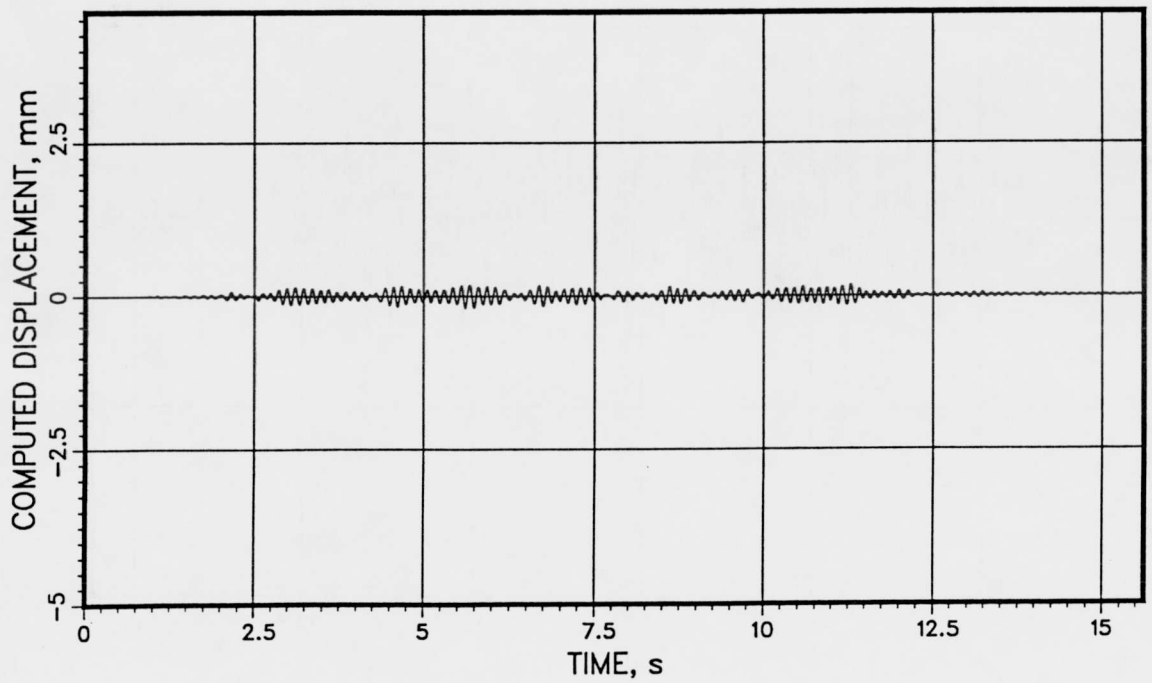

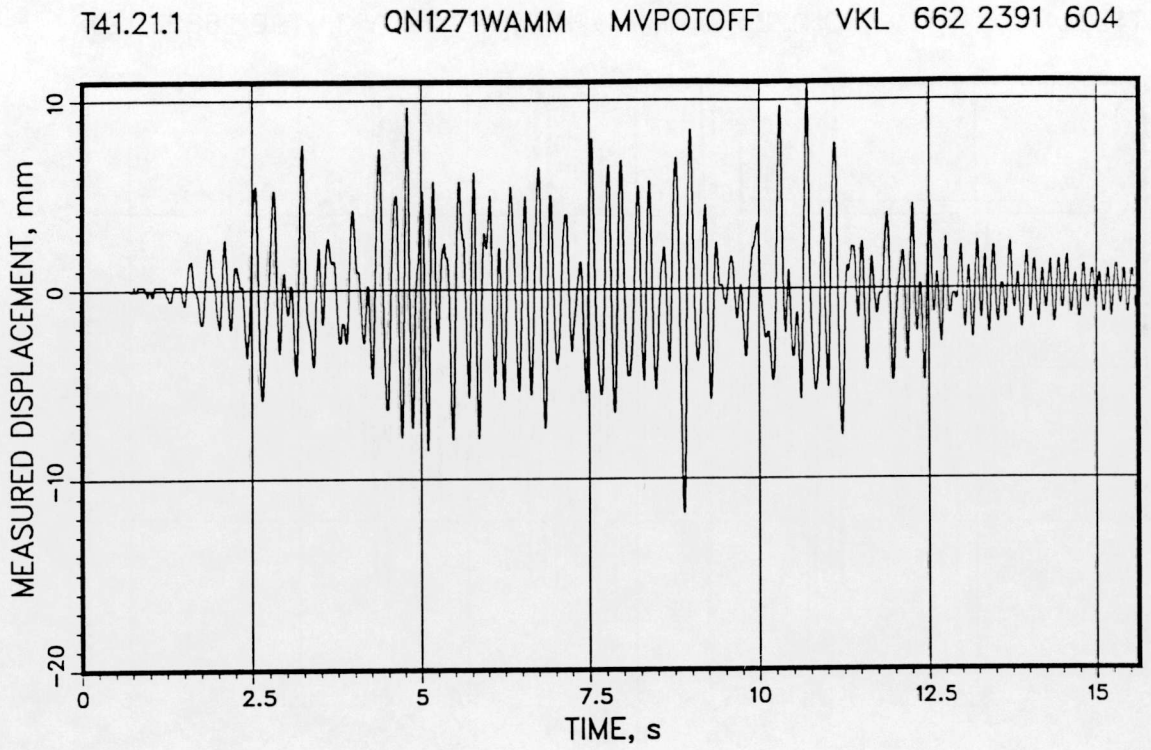
T41.21.1
QN1271WAMM
MVPOTOFF
VKL 662 2391 604
MEASURED DISPLACEMENT, mm
10
0
-10
-20
0
2.5
5
7.5
10
12.5
15
TIME, s

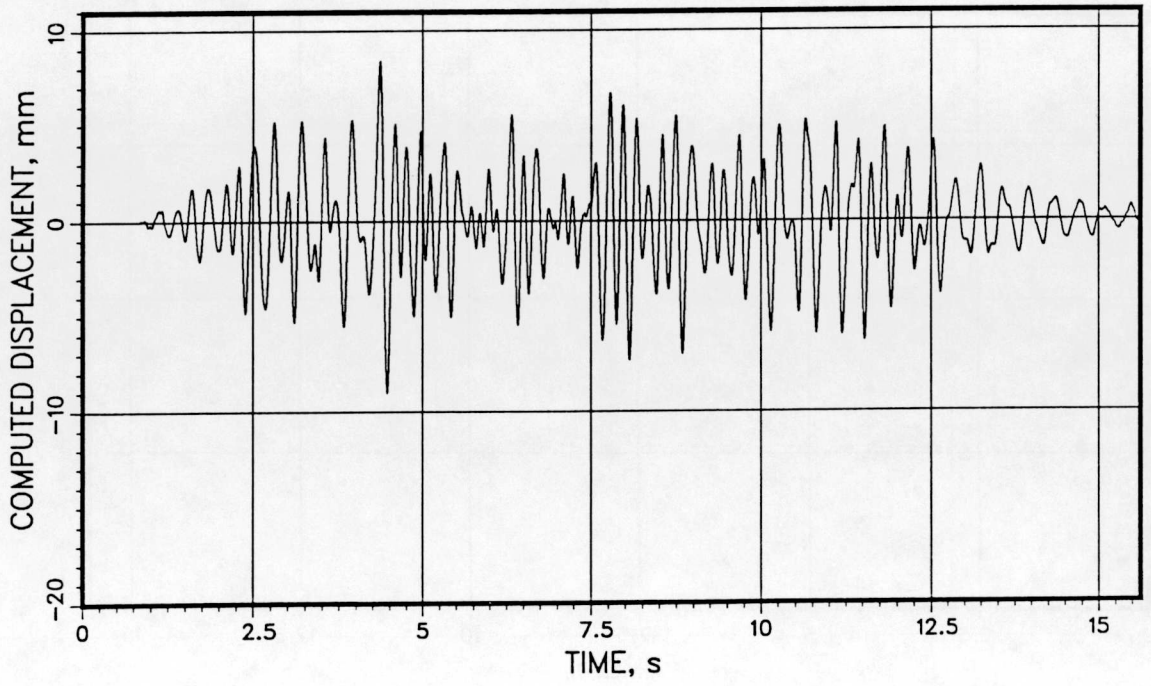
COMPUTED DISPLACEMENT, mm
10
0
-10
-20
0
2.5
5
7.5
10
12.5
15
TIME, s

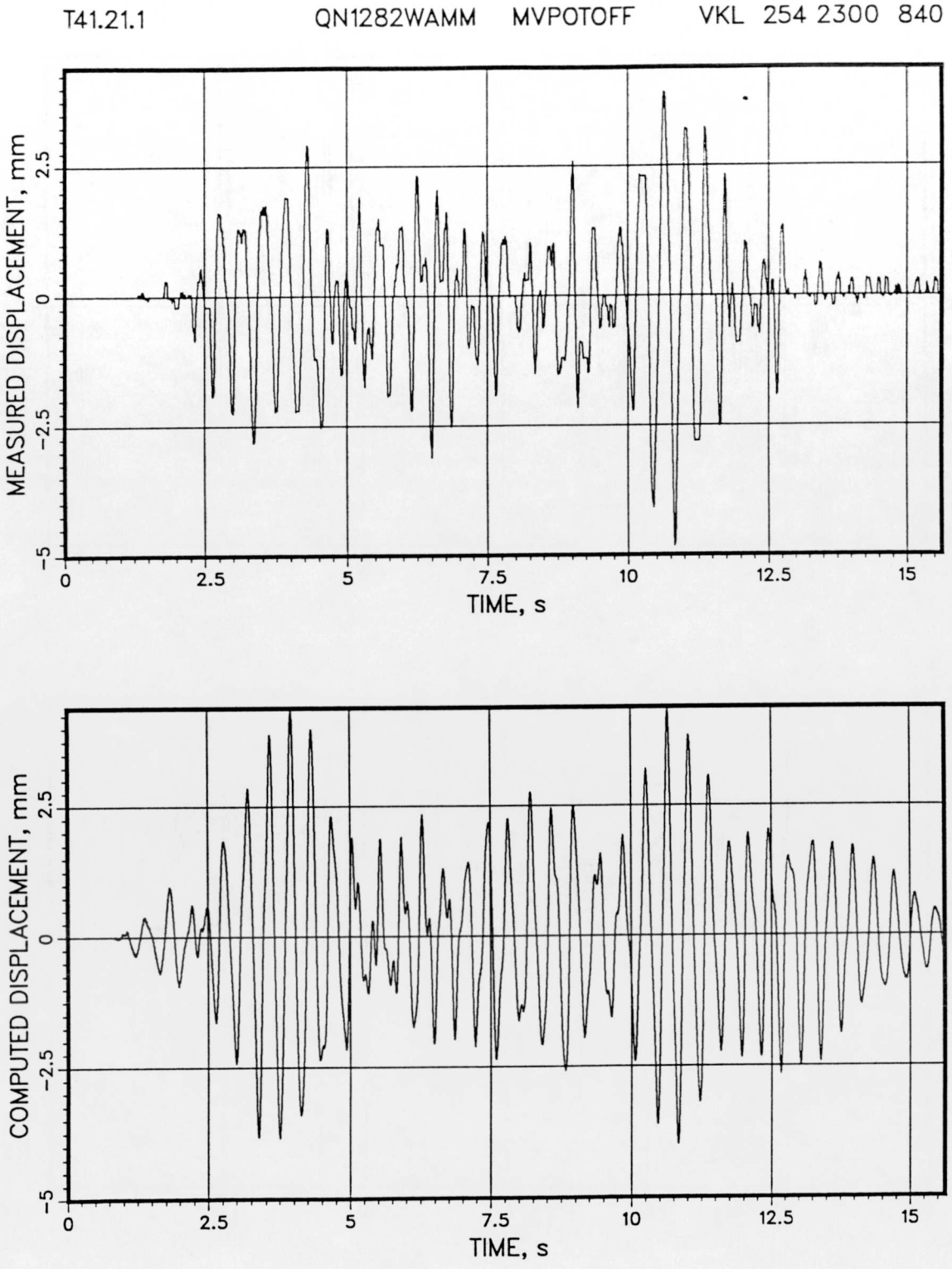
T41.21.1 QN1282WAMM MVPOTOFF VKL 254 2300 840
MEASURED DISPLACEMENT, mm
2.5
0
-2.5
-5
0
2.5
5
7.5
10
12.5
15
TIME, s
COMPUTED DISPLACEMENT, mm
2.5
0
-2.5
-5
0
2.5
5
7.5
10
12.5
15
TIME, s

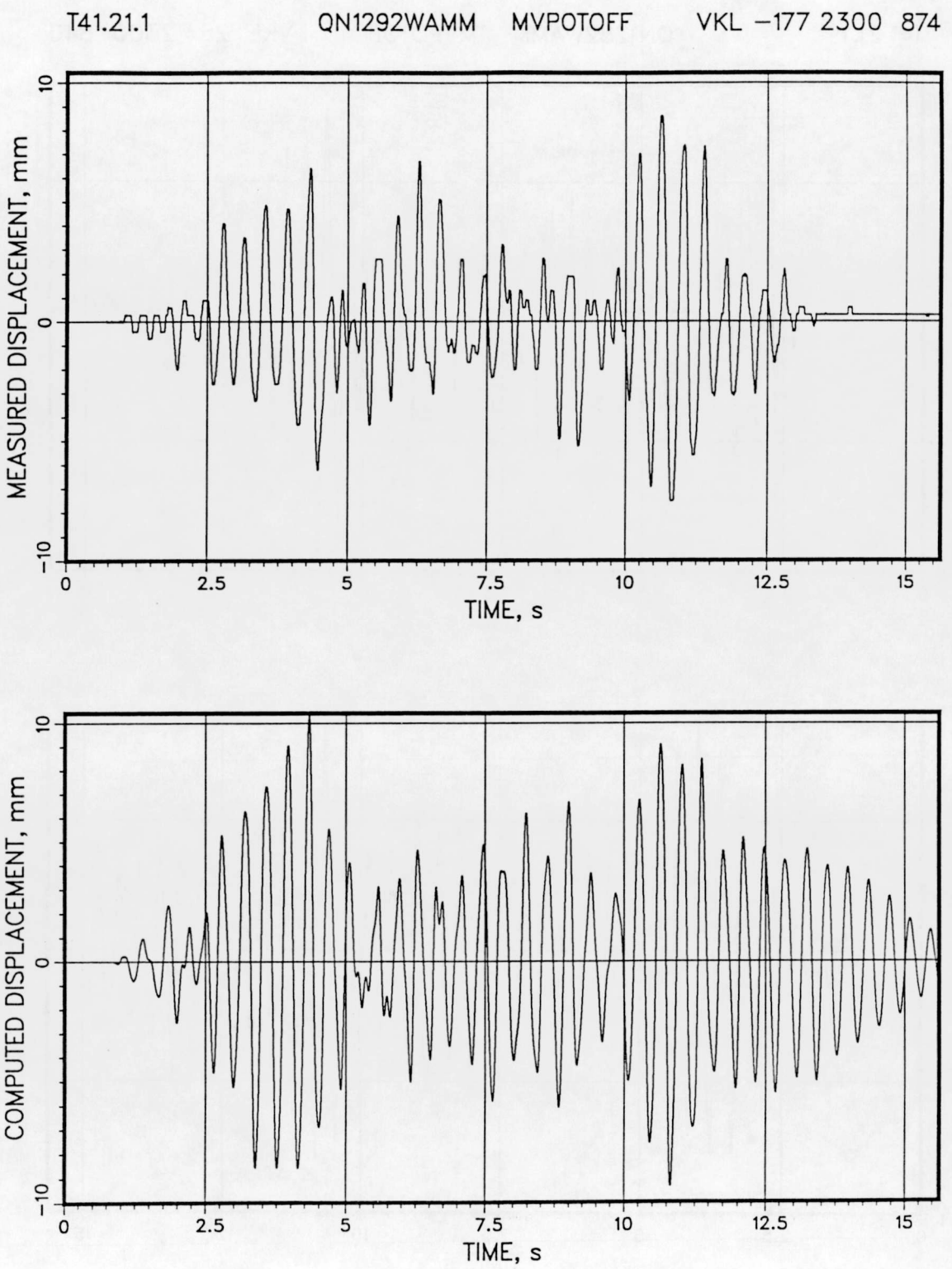
T41.21.1 QN1292WAMM MVPOTOFF VKL −177 2300 874
MEASURED DISPLACEMENT, mm
10
0
−10
0
2.5
5
7.5
10
12.5
15
TIME, s
COMPUTED DISPLACEMENT, mm
10
0
−10
0
2.5
5
7.5
10
12.5
15
TIME, s

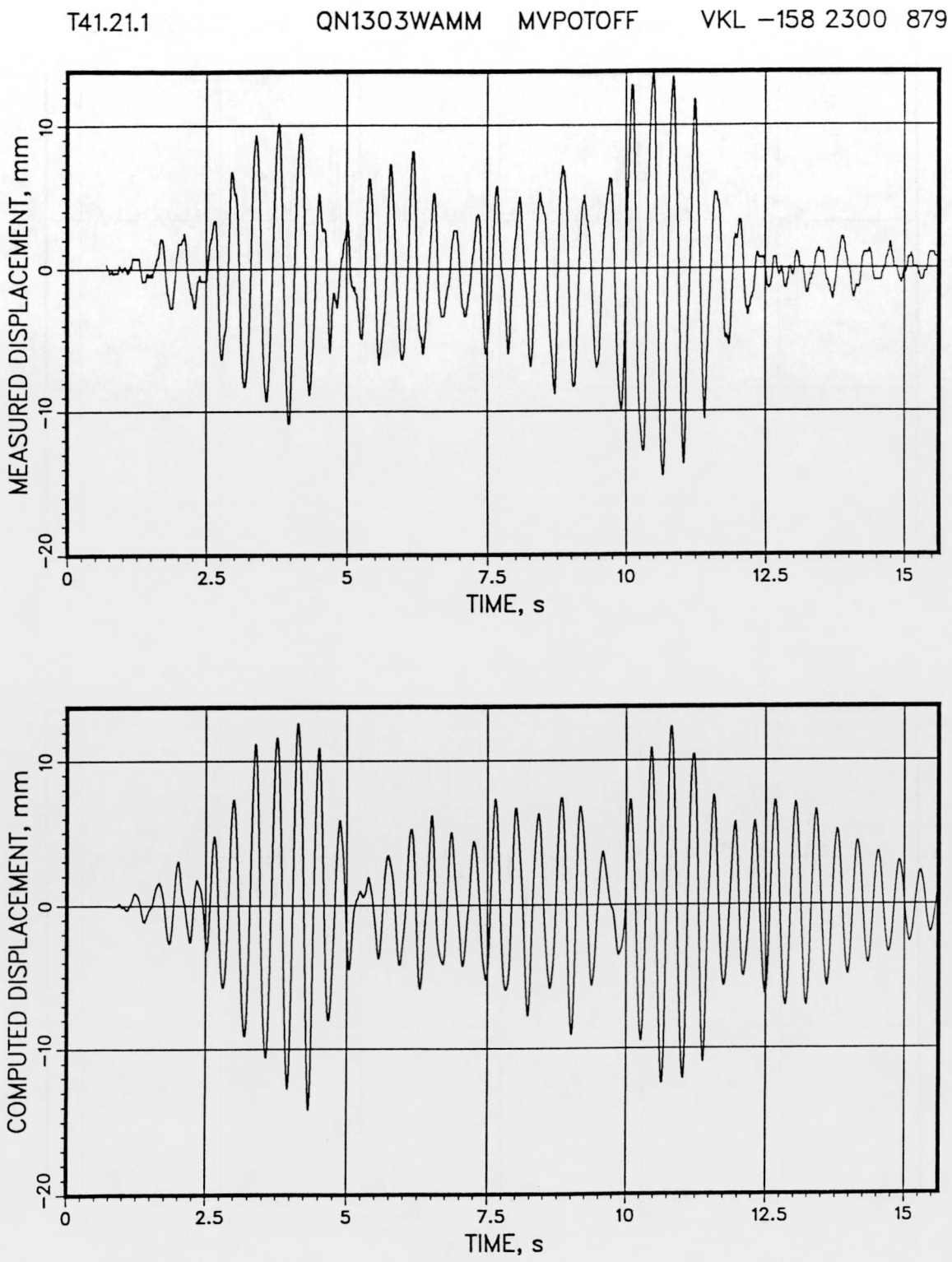
T41.21.1 QN1303WAMM MVPOTOFF VKL −158 2300 879
MEASURED DISPLACEMENT, mm
10
0
-10
-20
0
2.5
5
7.5
10
12.5
15
TIME, s
COMPUTED DISPLACEMENT, mm
10
0
-10
-20
0
2.5
5
7.5
10
12.5
15
TIME, s

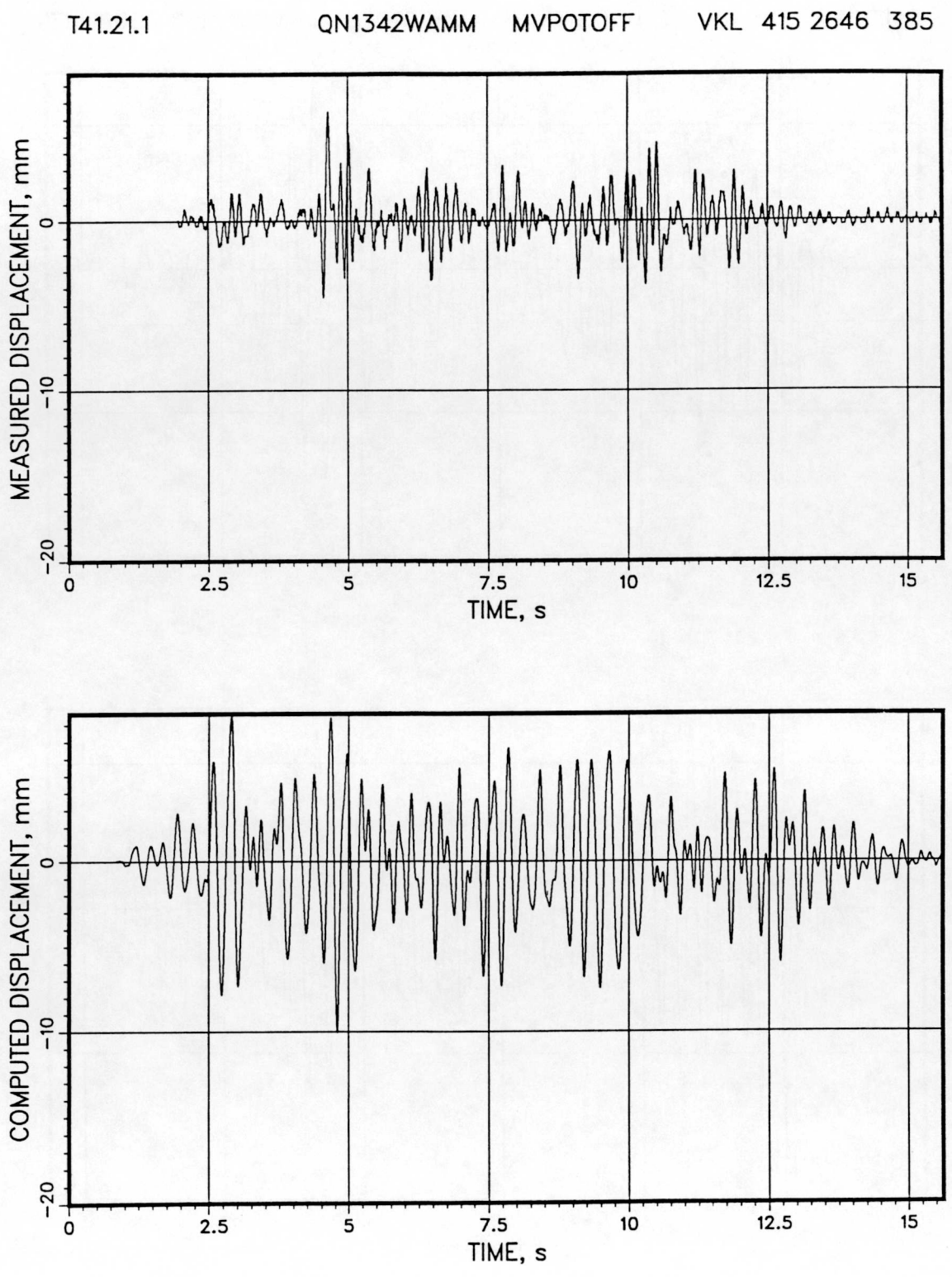
T41.21.1 QN1342WAMM MVPOTOFF VKL 415 2646 385
MEASURED DISPLACEMENT, mm
0
-10
-20
0
2.5
5
7.5
10
12.5
15
TIME, s
COMPUTED DISPLACEMENT, mm
0
-10
-20
0
2.5
5
7.5
10
12.5
15
TIME, s

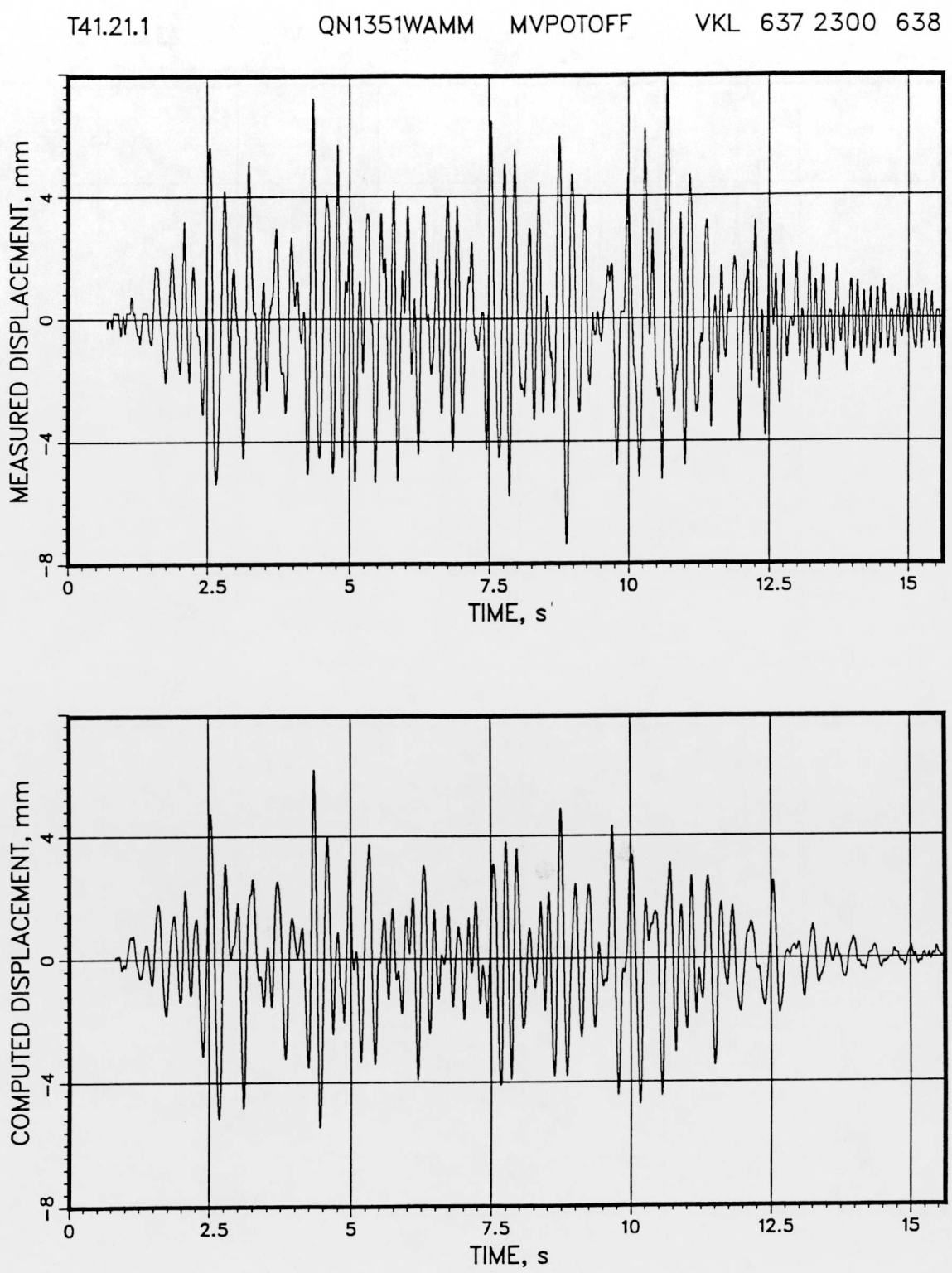
T41.21.1 QN1351WAMM MVPOTOFF VKL 637 2300 638
MEASURED DISPLACEMENT, mm
4
0
-4
-8
0
2.5
5
7.5
10
12.5
15
TIME, s
COMPUTED DISPLACEMENT, mm
4
0
-4
-8
0
2.5
5
7.5
10
12.5
15
TIME, s

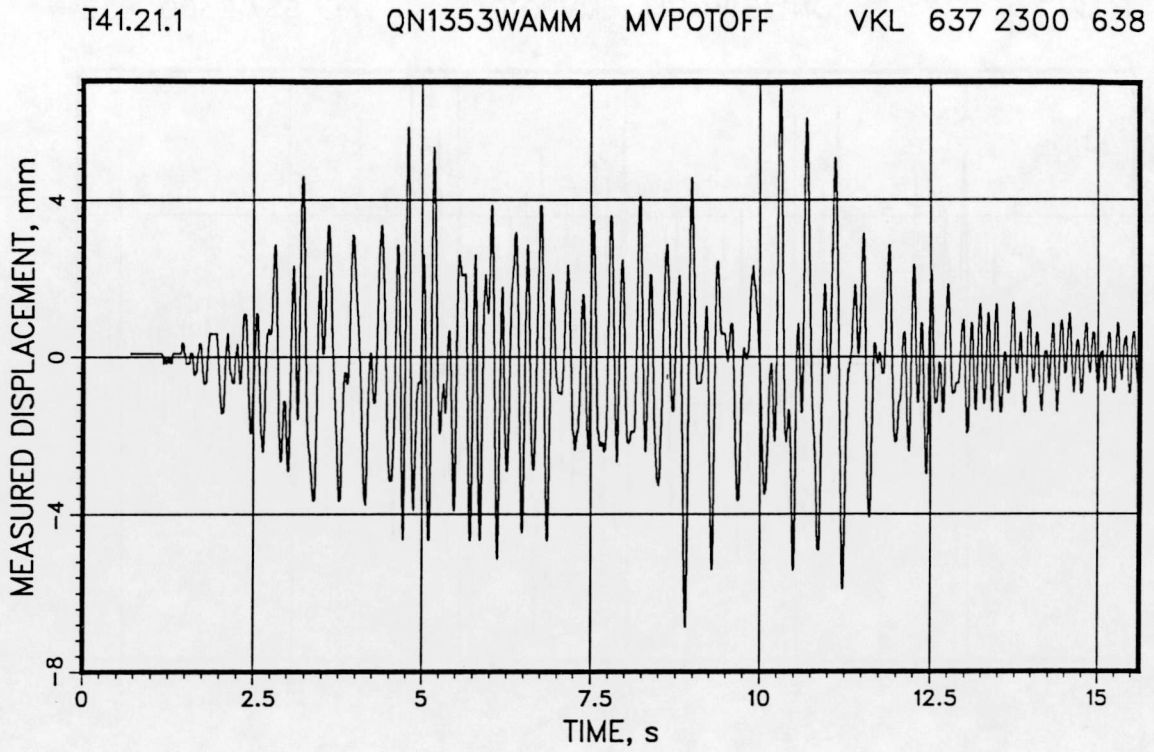
T41.21.1 QN1353WAMM MVPOTOFF VKL 637 2300 638
MEASURED DISPLACEMENT, mm
4
0
-4
-8
0
2.5
5
7.5
10
12.5
15
TIME, s

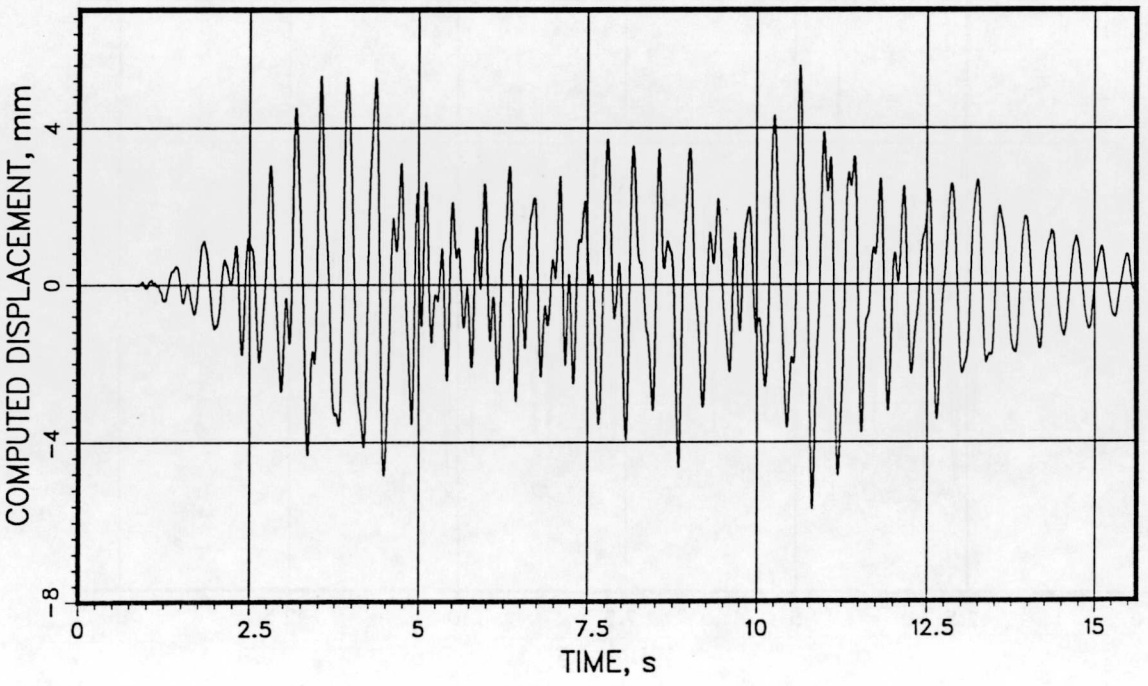
COMPUTED DISPLACEMENT, mm
4
0
-4
-8
0
2.5
5
7.5
10
12.5
15
TIME, s

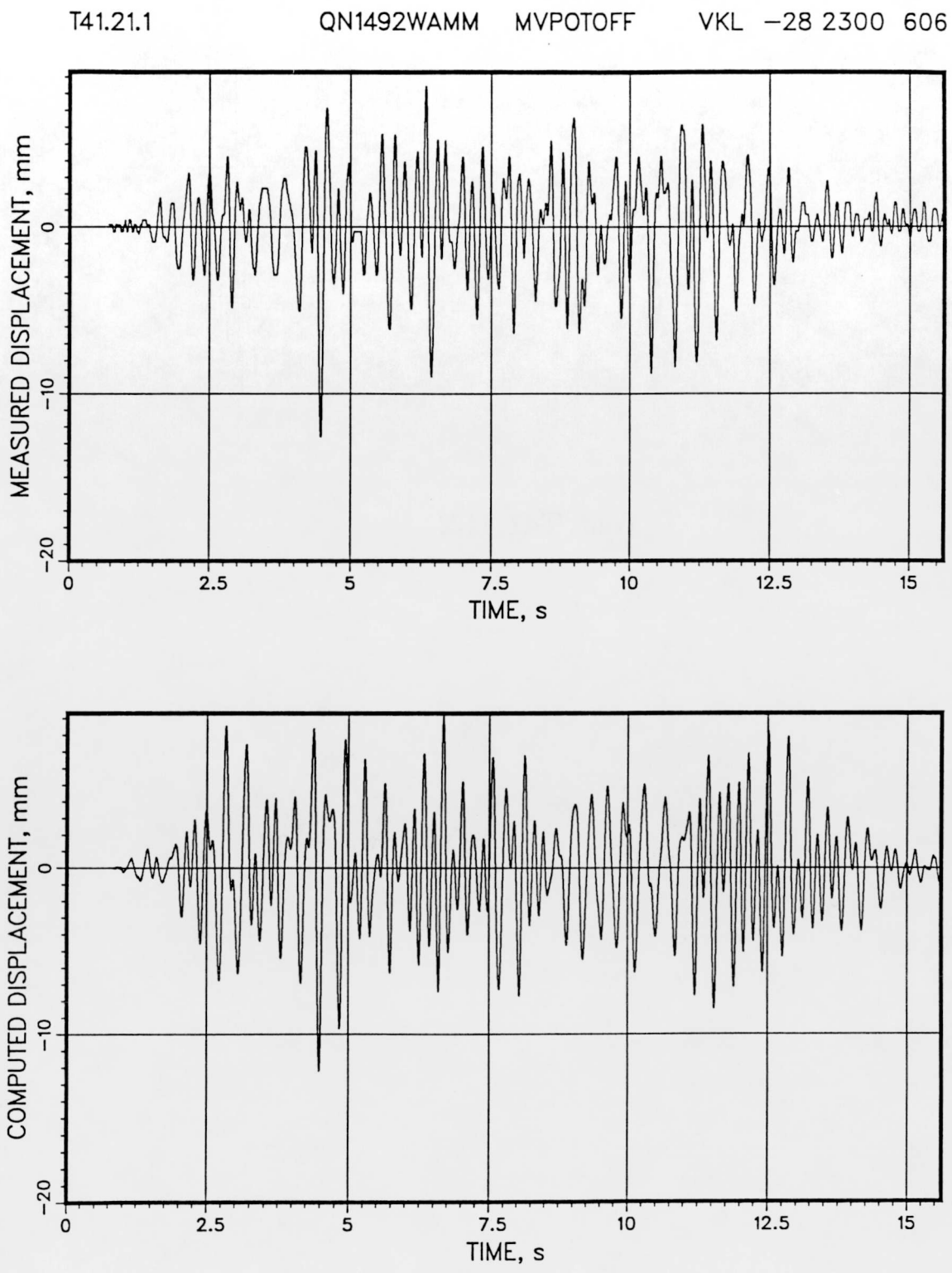
T41.21.1 QN1492WAMM MVPOTOFF VKL −28 2300 606
MEASURED DISPLACEMENT, mm
0
−10
−20
0
2.5
5
7.5
10
12.5
15
TIME, s
COMPUTED DISPLACEMENT, mm
0
−10
−20
0
2.5
5
7.5
10
12.5
15
TIME, s

Test: T41.31.2

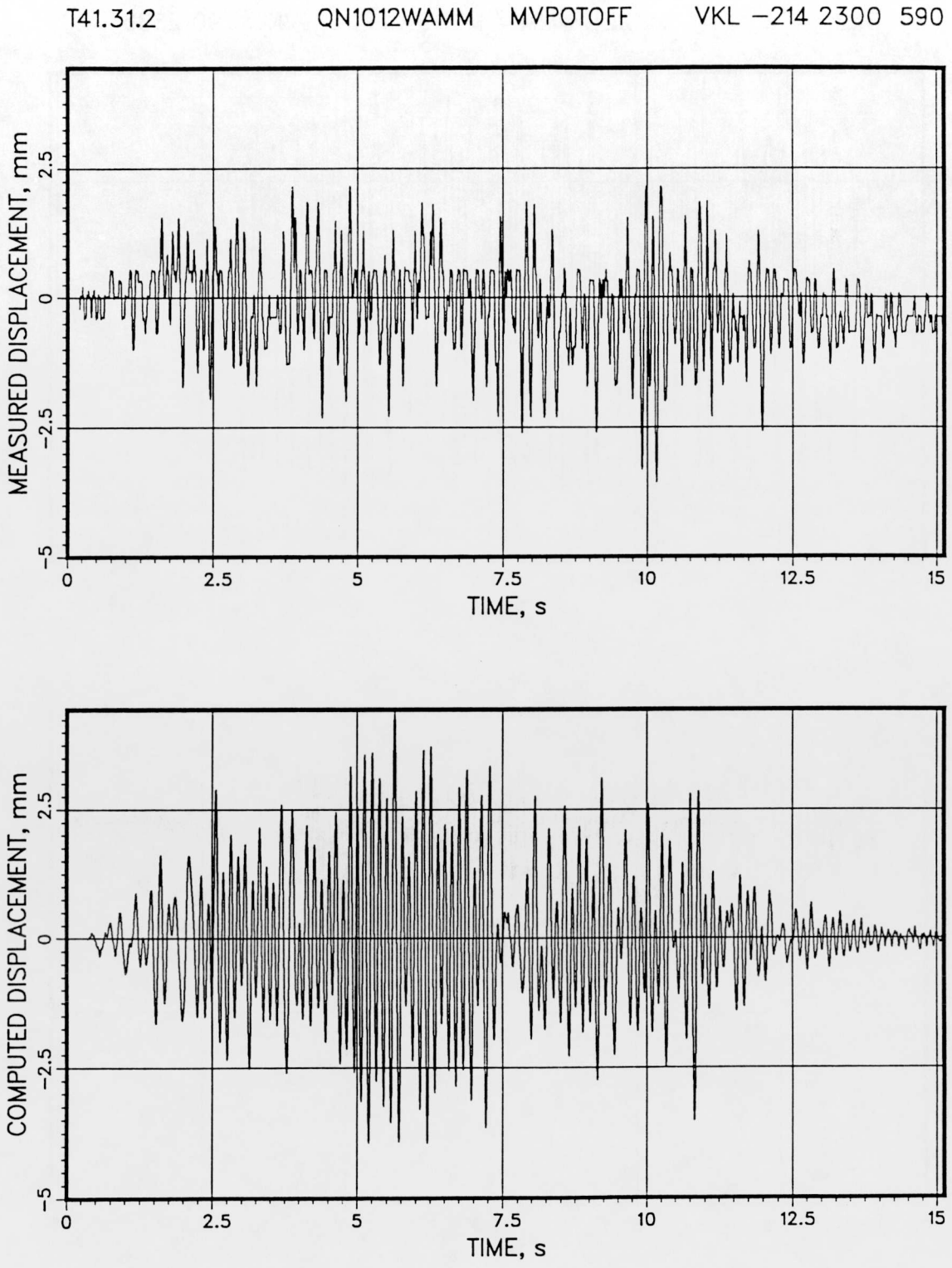
T41.31.2 QN1012WAMM MVPOTOFF VKL −214 2300 590
MEASURED DISPLACEMENT, mm
2.5
0
−2.5
−5
0
2.5
5
7.5
10
12.5
15
TIME, s
COMPUTED DISPLACEMENT, mm
2.5
0
−2.5
−5
0
2.5
5
7.5
10
12.5
15
TIME, s

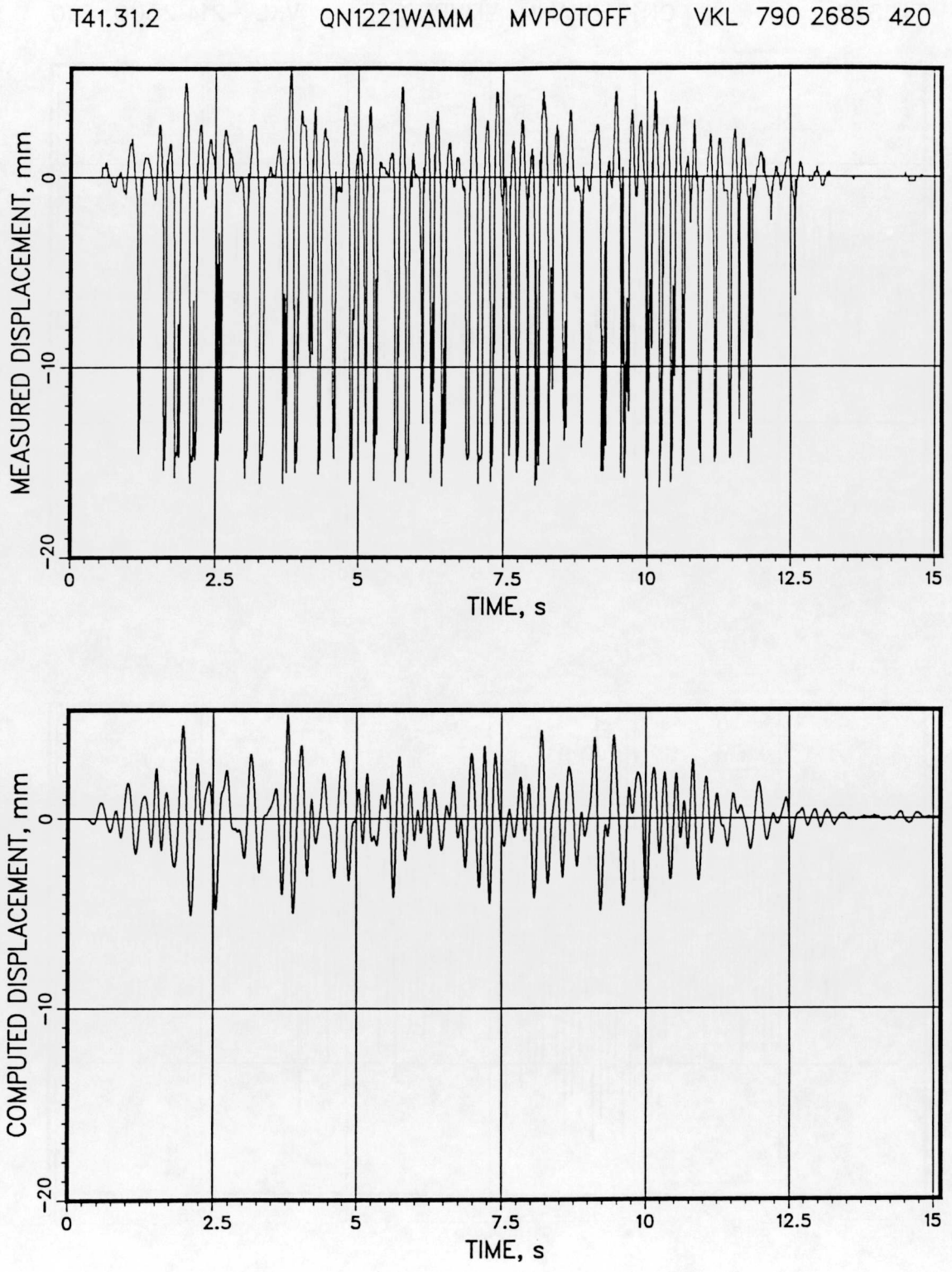
T41.31.2 QN1221WAMM MVPOTOFF VKL 790 2685 420
MEASURED DISPLACEMENT, mm
0
-10
-20
0
2.5
5
7.5
10
12.5
15
TIME, s
COMPUTED DISPLACEMENT, mm
0
-10
-20
0
2.5
5
7.5
10
12.5
15
TIME, s

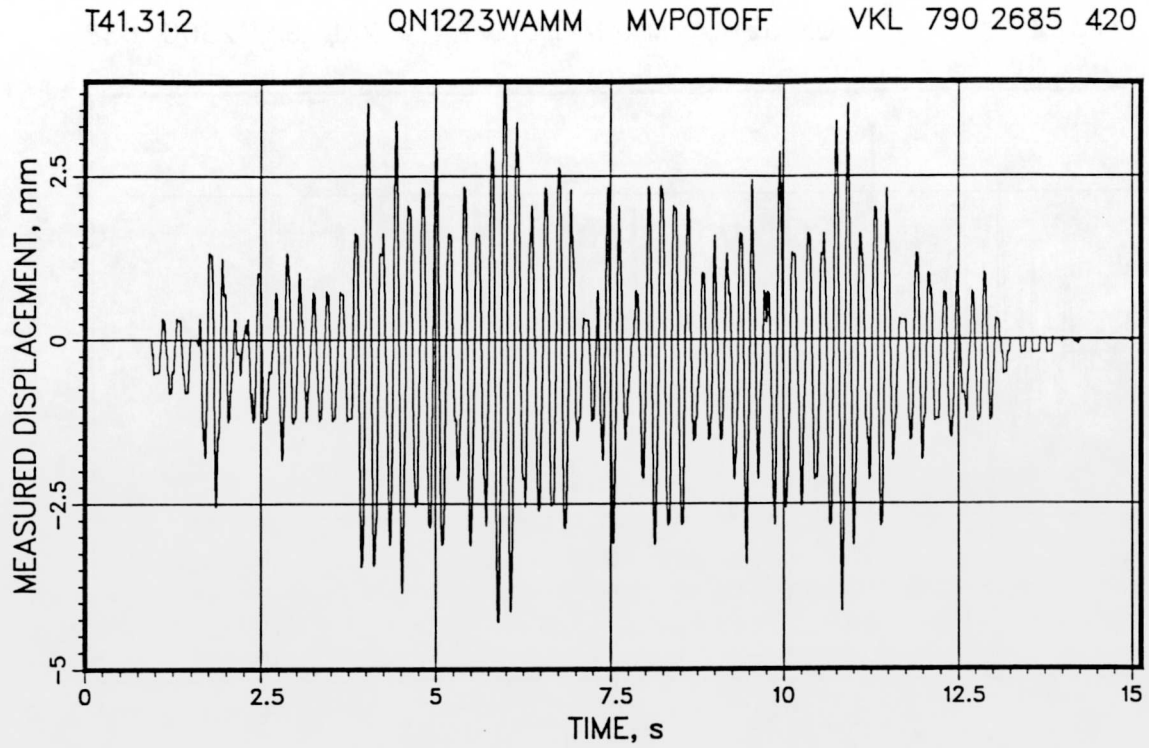
T41.31.2
QN1223WAMM MVPOTOFF
VKL 790 2685 420
MEASURED DISPLACEMENT, mm
2.5
0
-2.5
-5
0
2.5
5
7.5
10
12.5
15
TIME, s

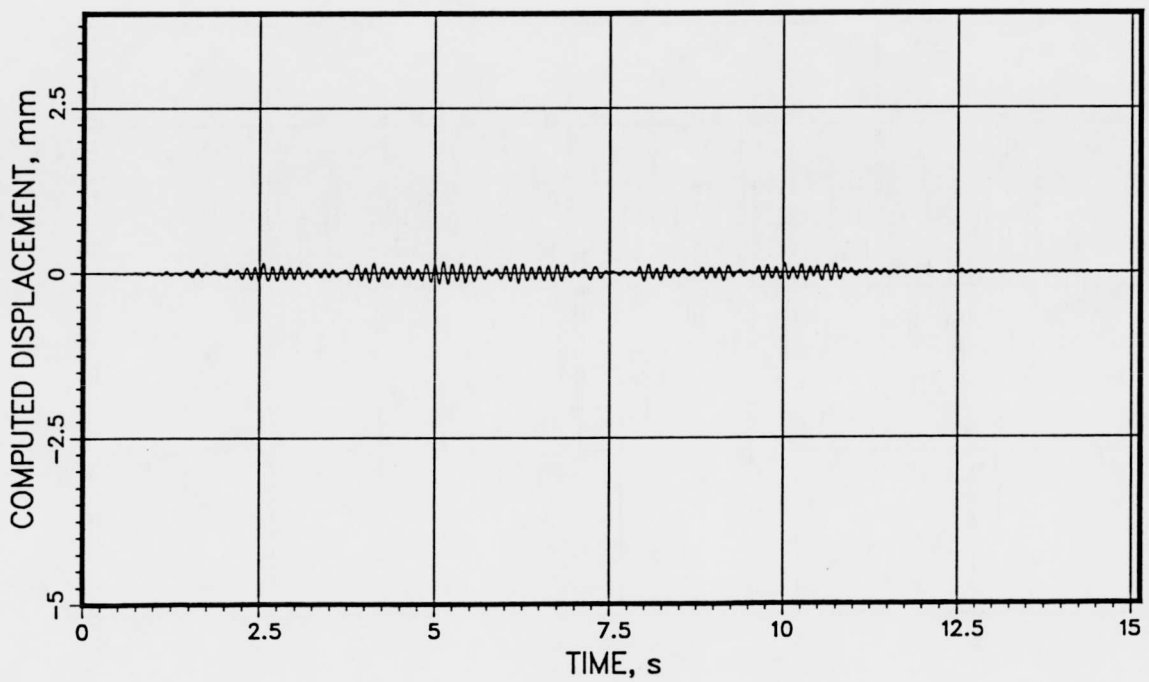
COMPUTED DISPLACEMENT, mm
2.5
0
-2.5
-5
0
2.5
5
7.5
10
12.5
15
TIME, s

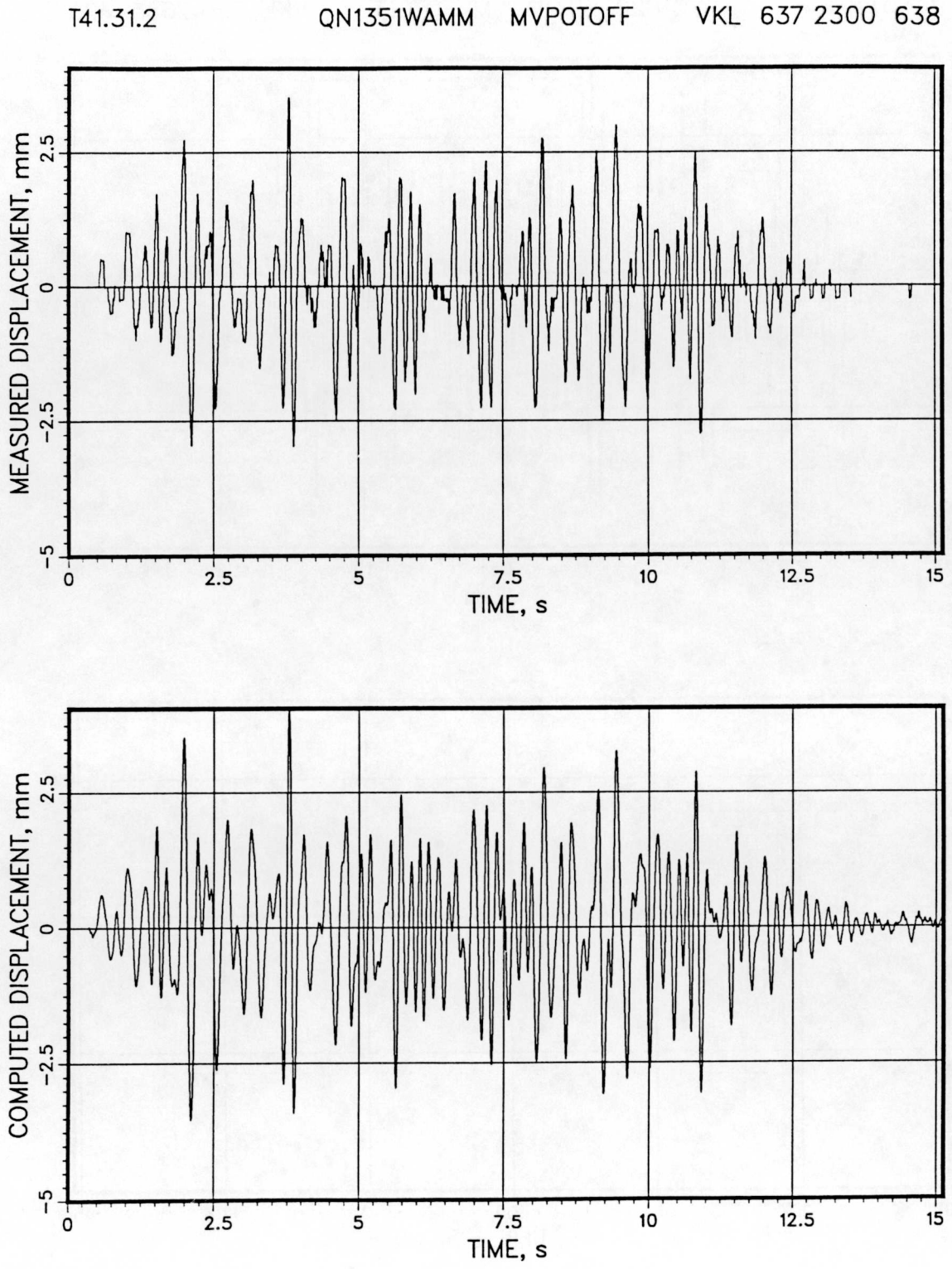
T41.31.2
QN1351WAMM
MVPOTOFF
VKL 637 2300 638
MEASURED DISPLACEMENT, mm
2.5
0
-2.5
-5
0
2.5
5
7.5
10
12.5
15
TIME, s
COMPUTED DISPLACEMENT, mm
2.5
0
-2.5
-5
0
2.5
5
7.5
10
12.5
15
TIME, s

T41.31.2 QN1353WAMM MVPOTOFF VKL 637 2300 638

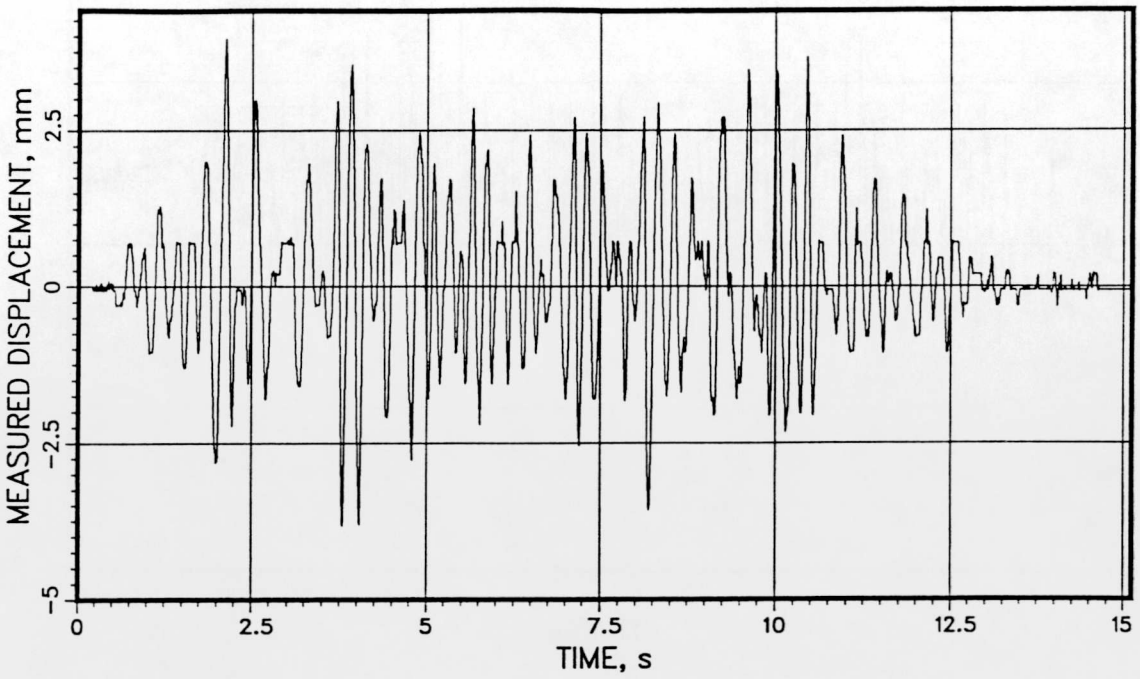

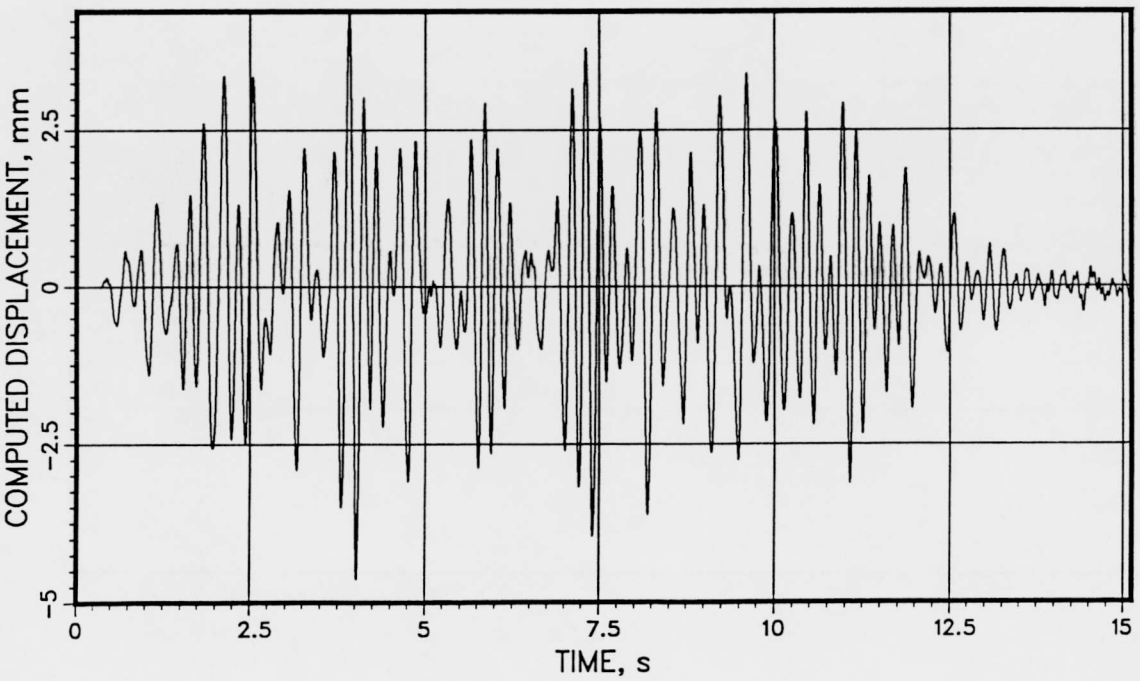

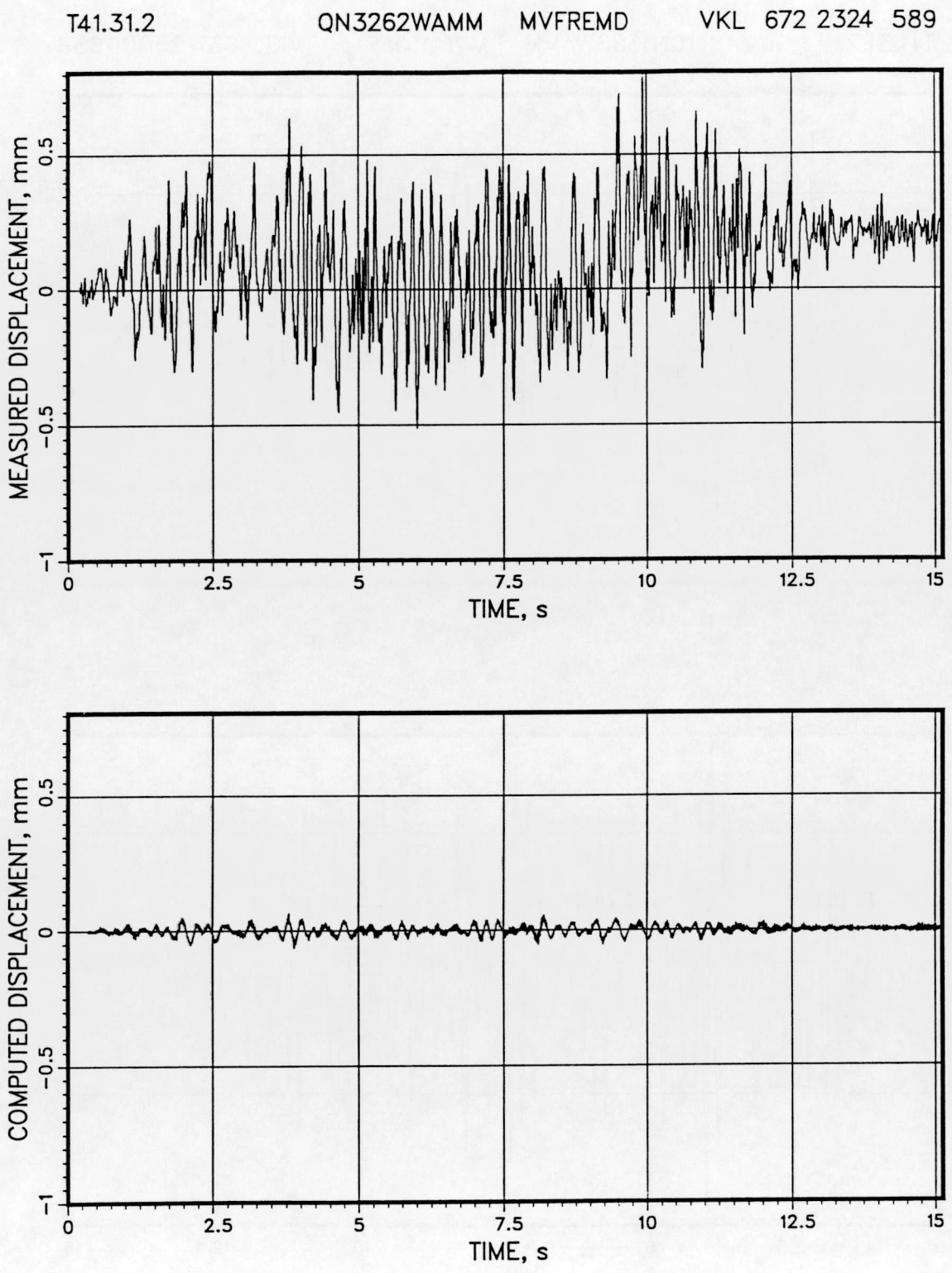
T41.31.2
QN3262WAMM
MVFREMD
VKL 672 2324 589
MEASURED DISPLACEMENT, mm
0.5
0
-0.5
-1
0
2.5
5
7.5
10
12.5
15
TIME, s
COMPUTED DISPLACEMENT, mm
0.5
0
-0.5
-1
0
2.5
5
7.5
10
12.5
15
TIME, s

T41.31.2 QN3282WAMM MVFREMD VKL 254 2300 840

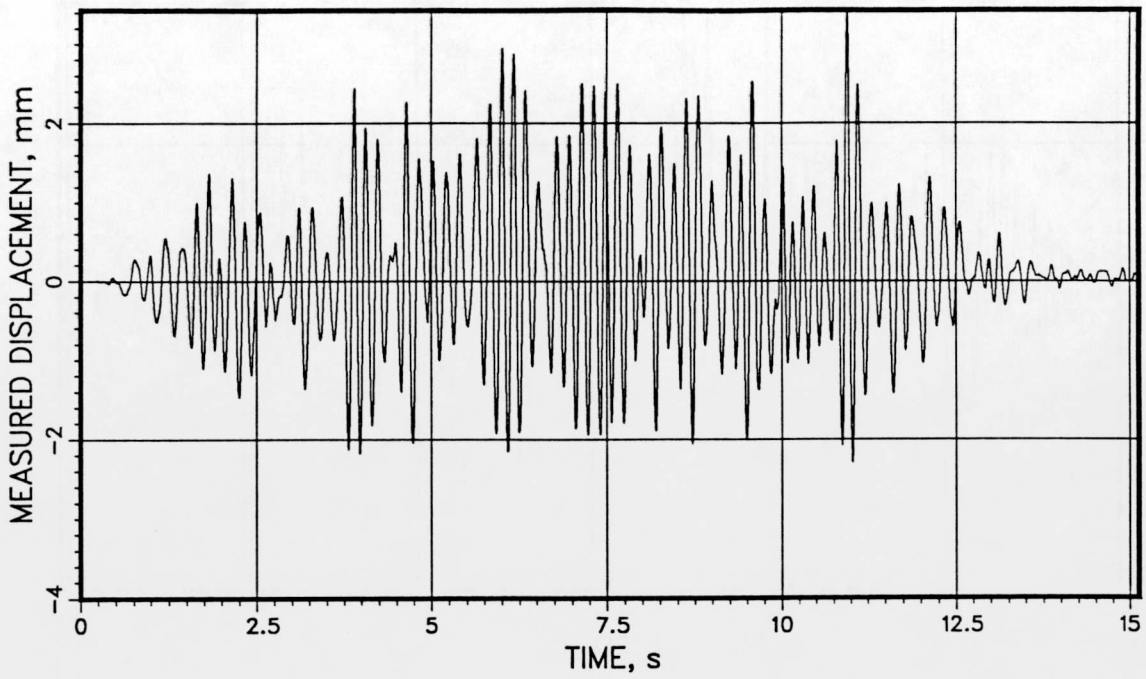

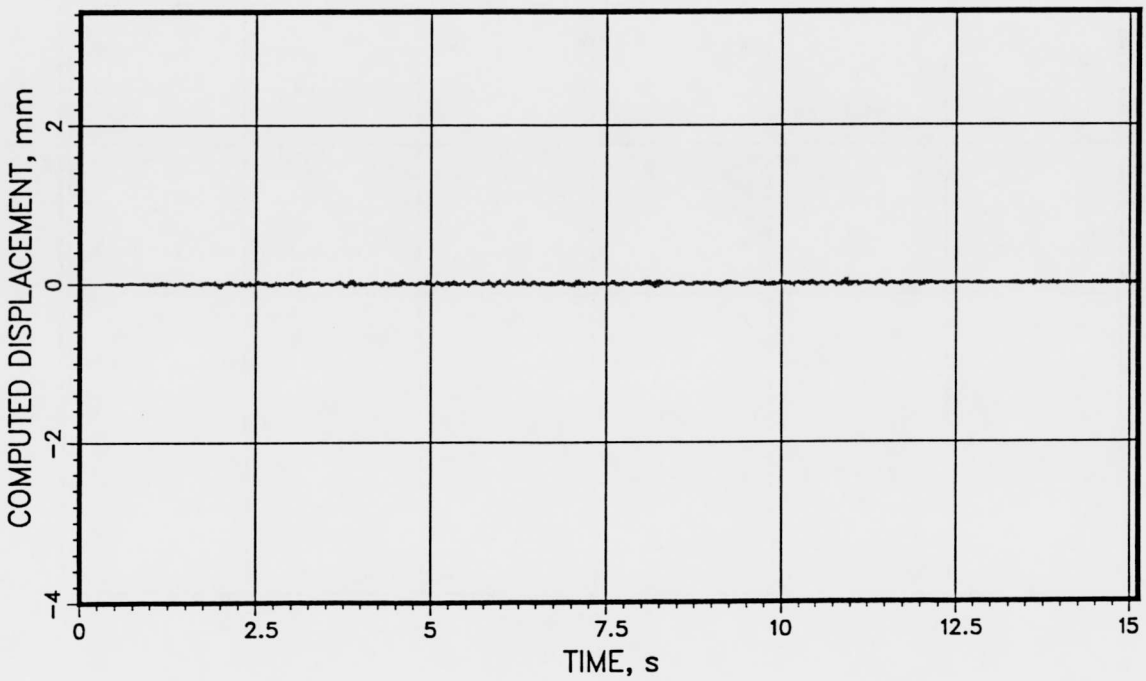

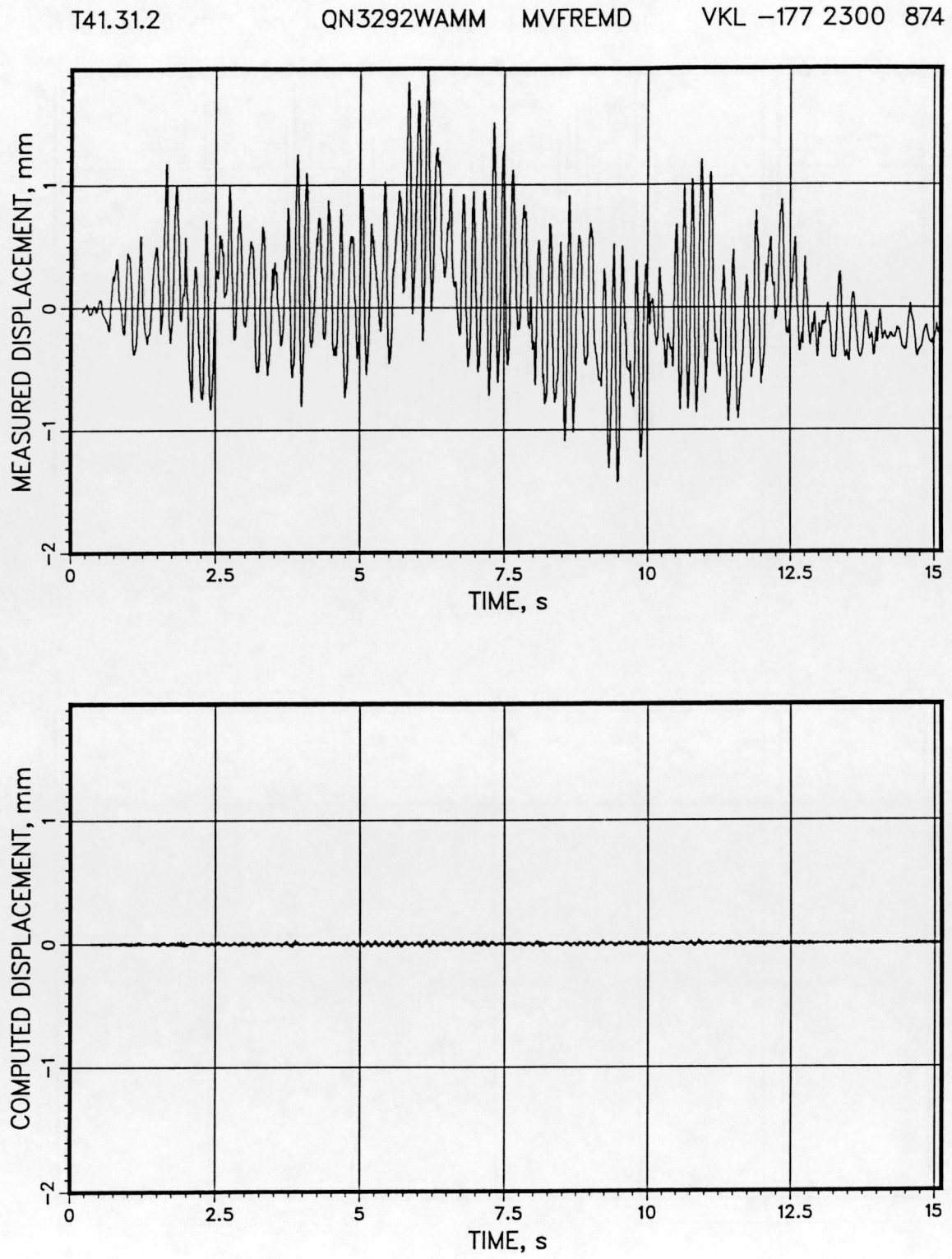
T41.31.2
QN3292WAMM MVFREMD
VKL −177 2300 874
MEASURED DISPLACEMENT, mm
1
0
−1
−2
0
2.5
5
7.5
10
12.5
15
TIME, s
COMPUTED DISPLACEMENT, mm
1
0
−1
−2
0
2.5
5
7.5
10
12.5
15
TIME, s

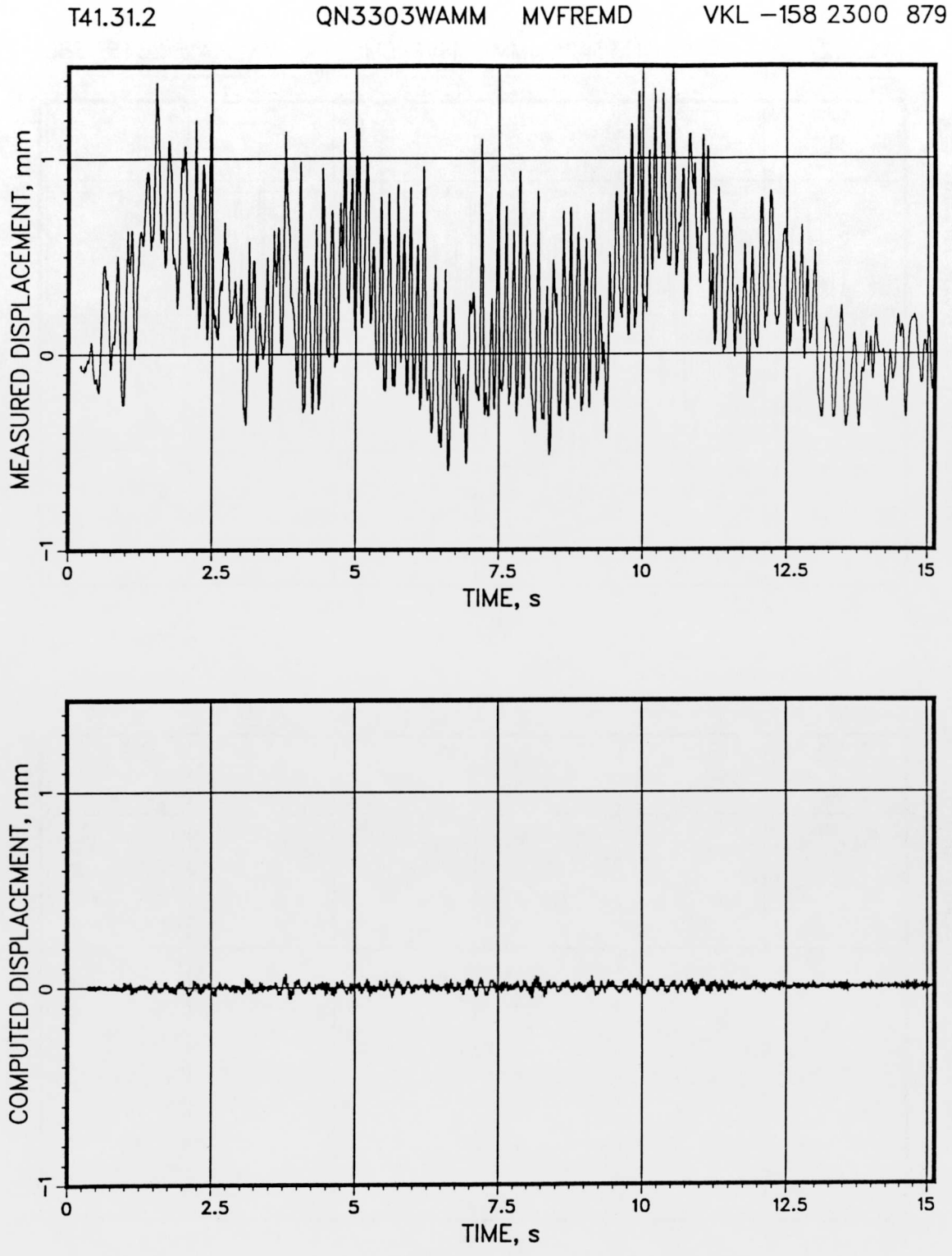
T41.31.2
QN3303WAMM MVFREMD
VKL −158 2300 879
MEASURED DISPLACEMENT, mm
1
0
−1
0
2.5
5
7.5
10
12.5
15
TIME, s
COMPUTED DISPLACEMENT, mm
1
0
−1
0
2.5
5
7.5
10
12.5
15
TIME, s

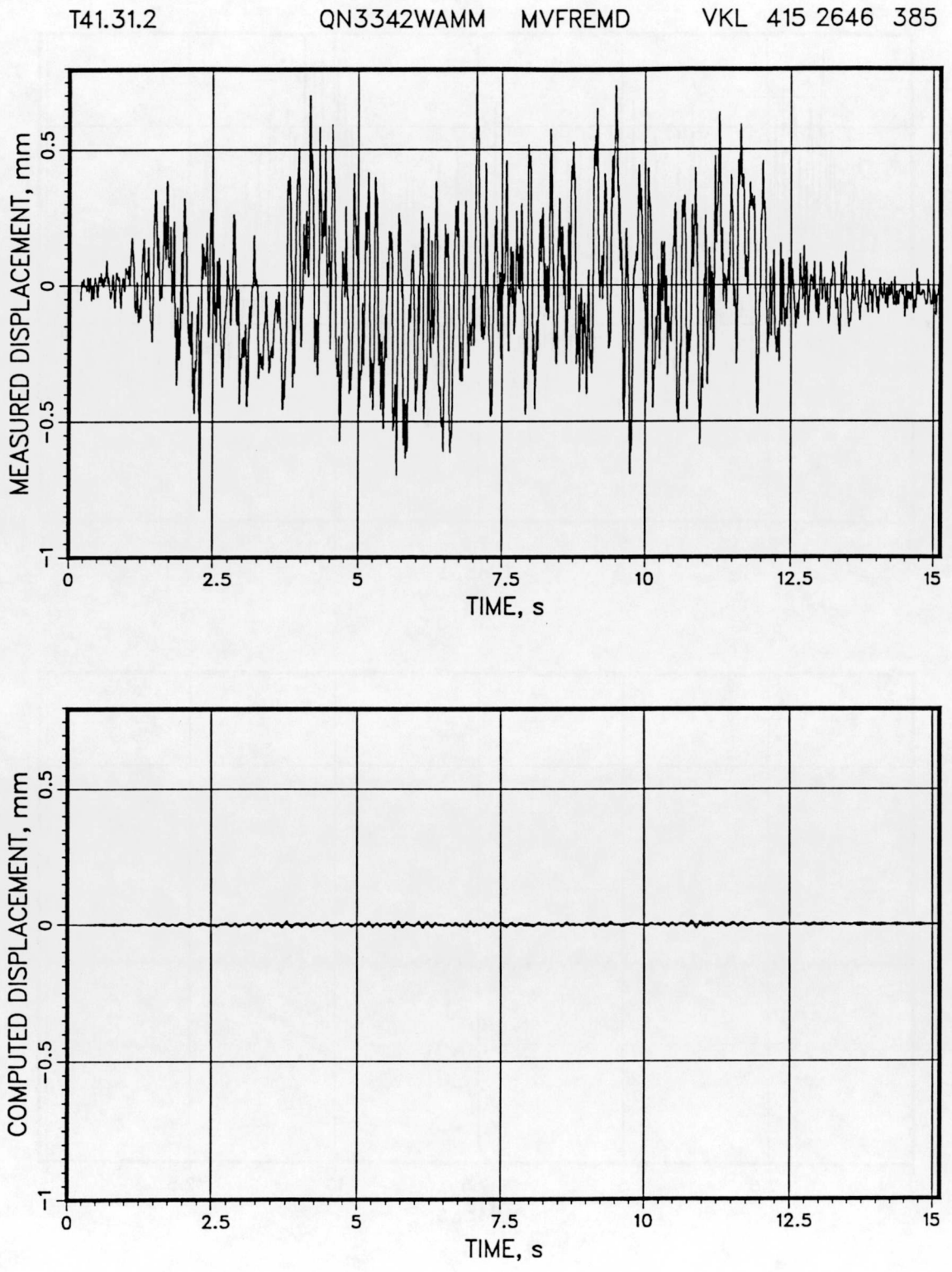
T41.31.2 QN3342WAMM MVFREMD VKL 415 2646 385
MEASURED DISPLACEMENT, mm
0.5
0
-0.5
-1
0
2.5
5
7.5
10
12.5
15
TIME, s
COMPUTED DISPLACEMENT, mm
0.5
0
-0.5
-1
0
2.5
5
7.5
10
12.5
15
TIME, s

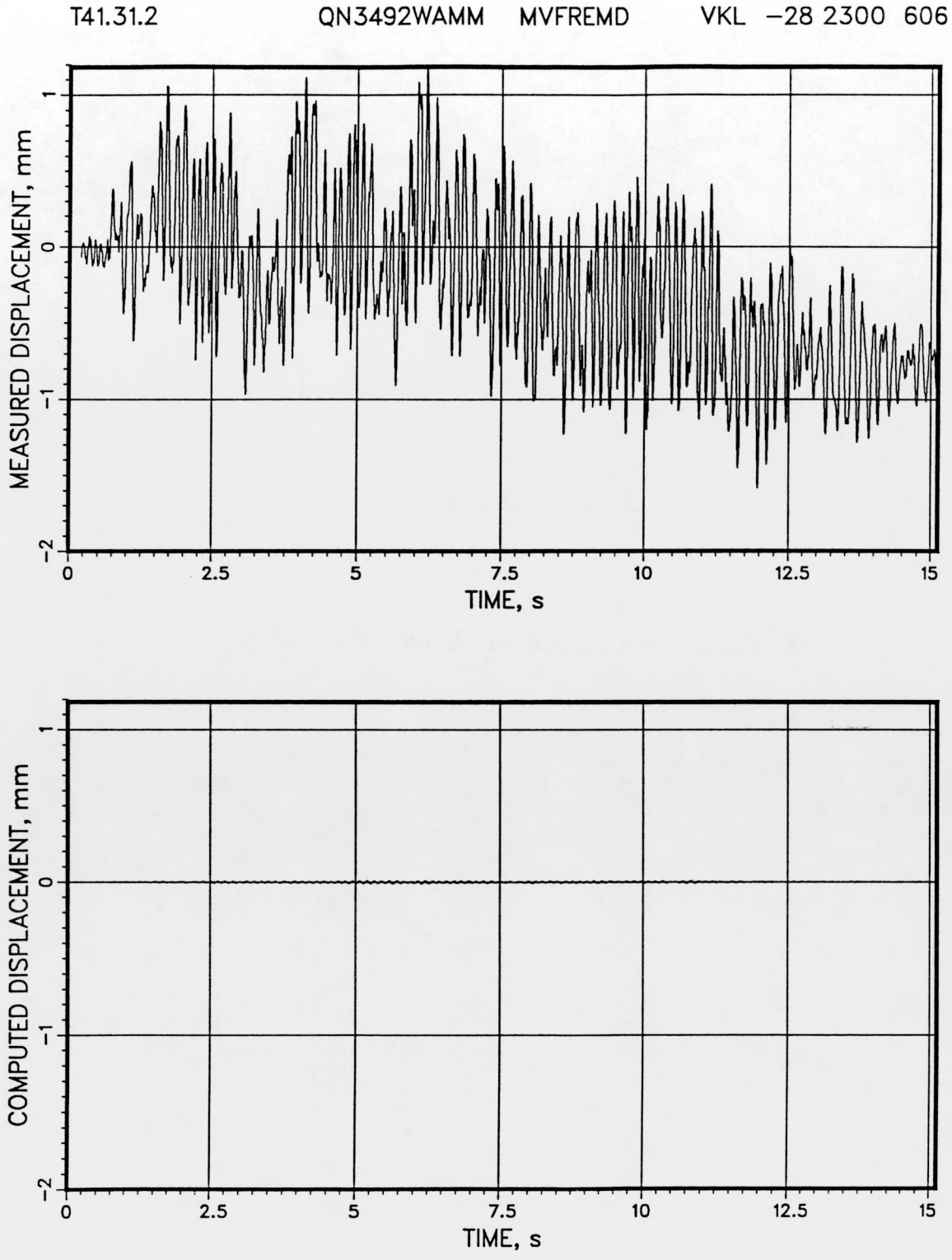
T41.31.2
QN3492WAMM MVFREMD
VKL −28 2300 606
MEASURED DISPLACEMENT, mm
1
0
−1
−2
0
2.5
5
7.5
10
12.5
15
TIME, s
COMPUTED DISPLACEMENT, mm
1
0
−1
−2
0
2.5
5
7.5
10
12.5
15
TIME, s

APPENDIX D

Comparisons of Support Force Histories

Force in Snubbers
Test: T41.31.2

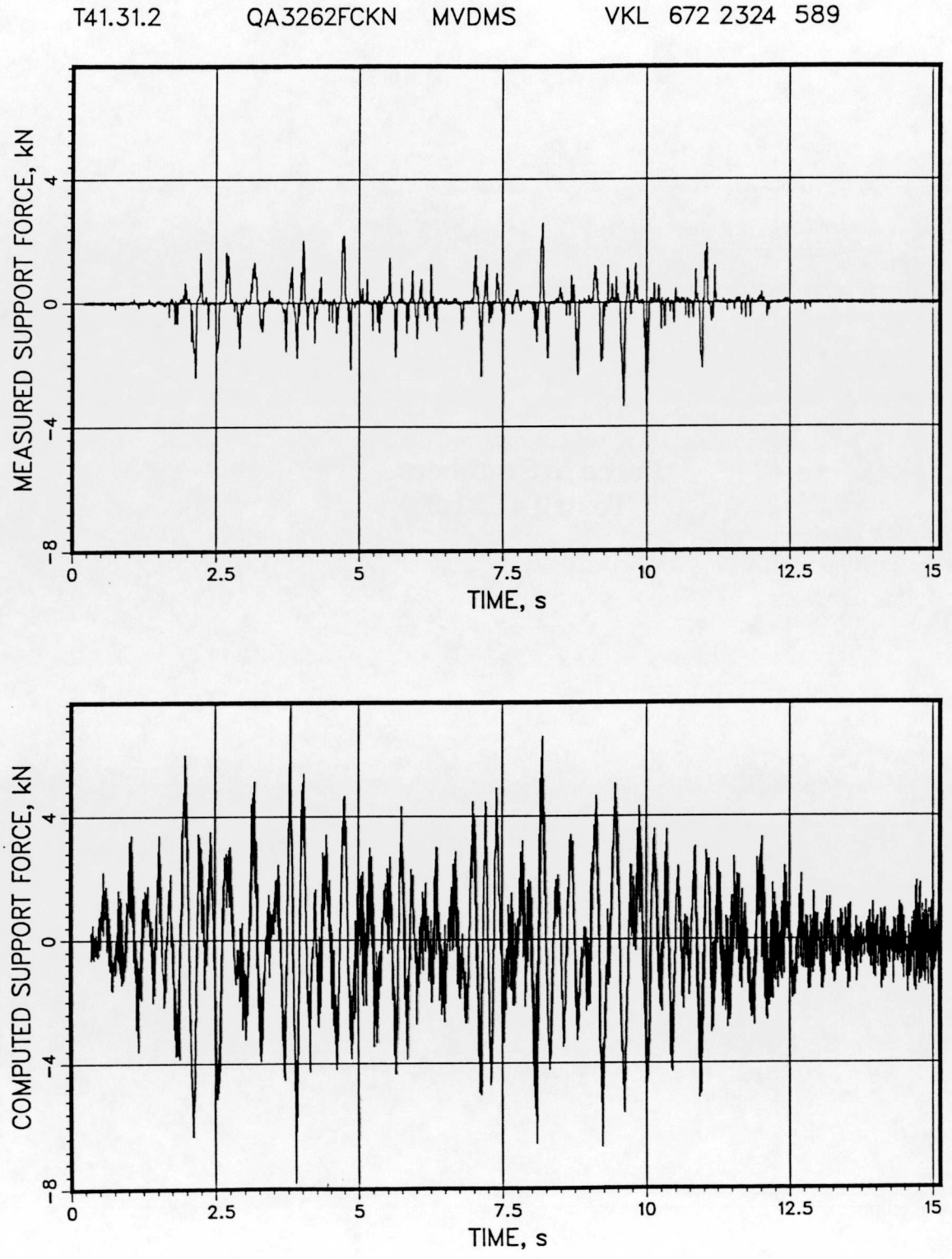
T41.31.2 QA3262FCKN MVDMS VKL 672 2324 589
MEASURED SUPPORT FORCE, kN
4
0
-4
-8
0
2.5
5
7.5
10
12.5
15
TIME, s
COMPUTED SUPPORT FORCE, kN
4
0
-4
-8
0
2.5
5
7.5
10
12.5
15
TIME, s

T41.31.2 QA3282FCKN MVDMS VKL 254 2300 840

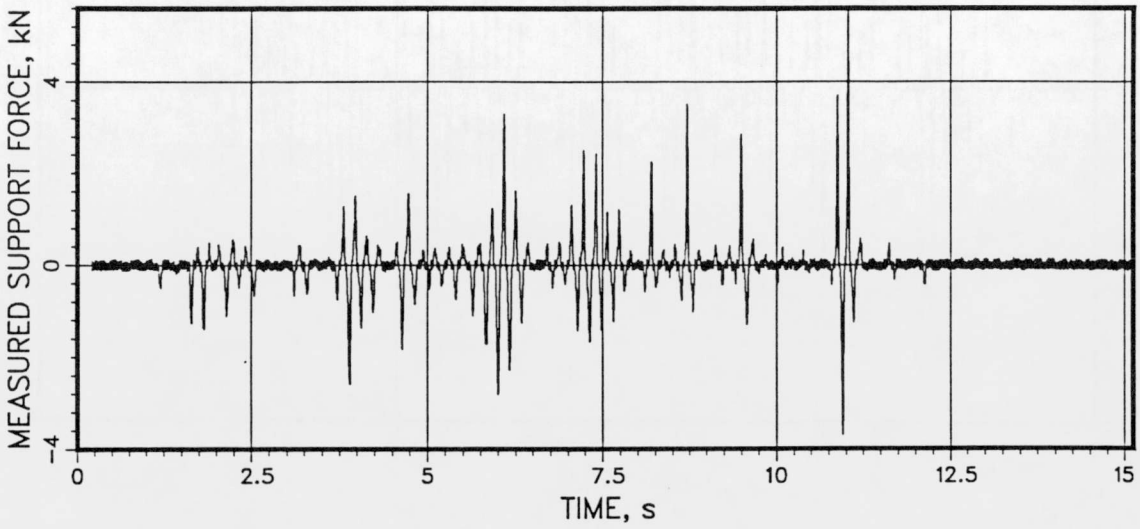

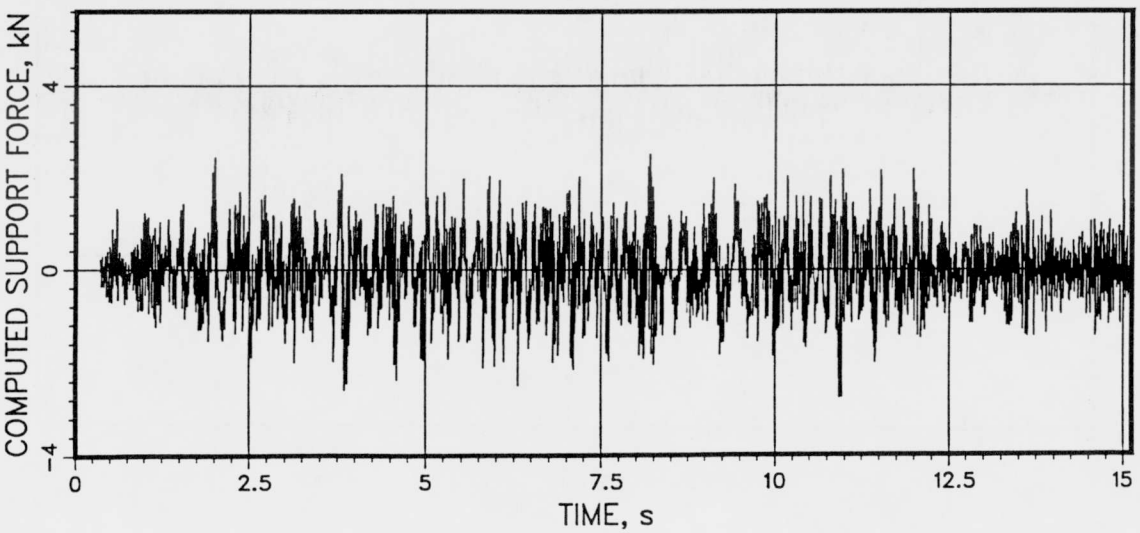

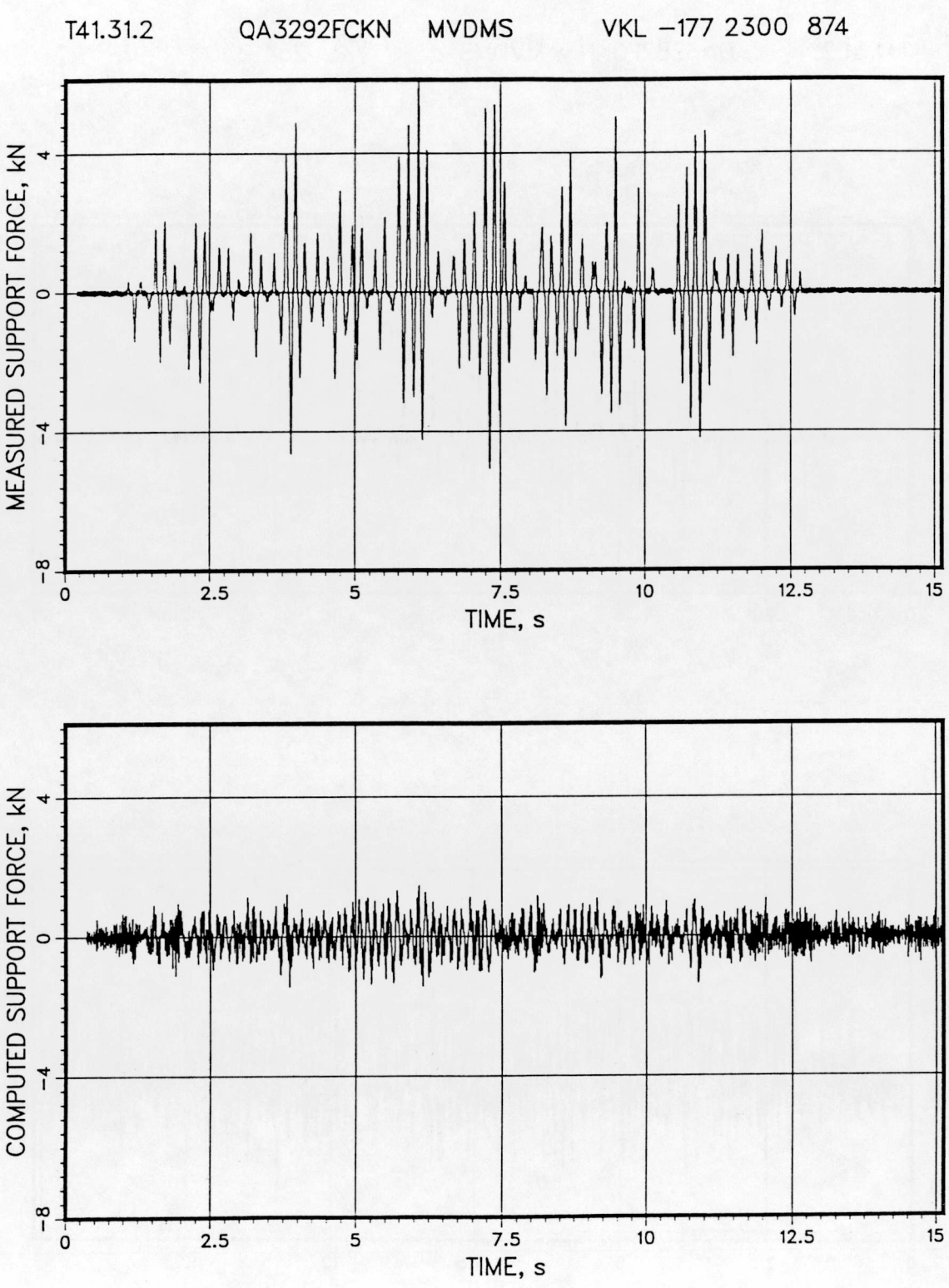
T41.31.2 QA3292FCKN MVDMS VKL −177 2300 874
MEASURED SUPPORT FORCE, kN
4
0
−4
−8
0
2.5
5
7.5
10
12.5
15
TIME, s
COMPUTED SUPPORT FORCE, kN
4
0
−4
−8
0
2.5
5
7.5
10
12.5
15
TIME, s

T41.31.2 QA3303FCKN MVDMS VKL −158 2300 879

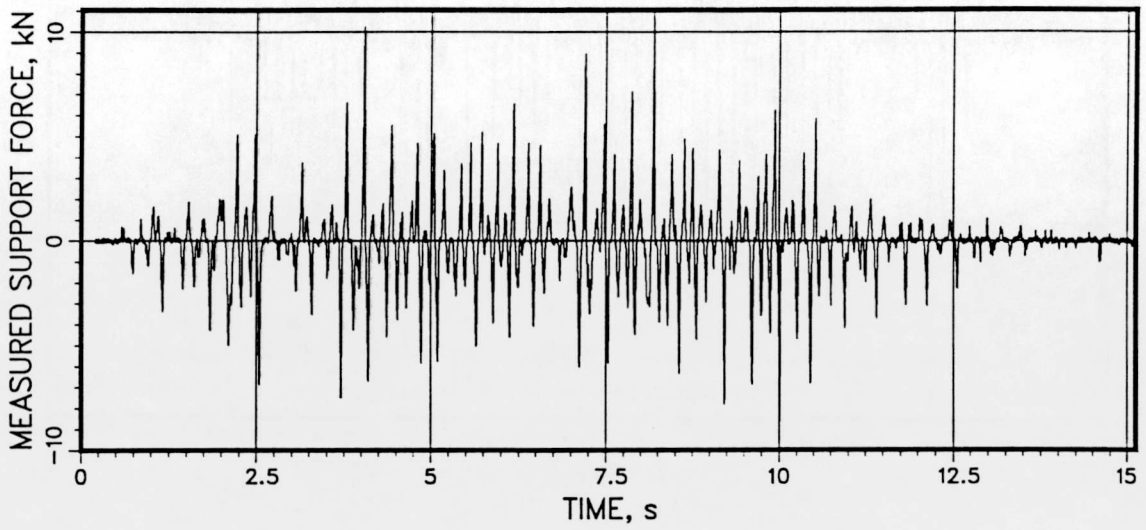

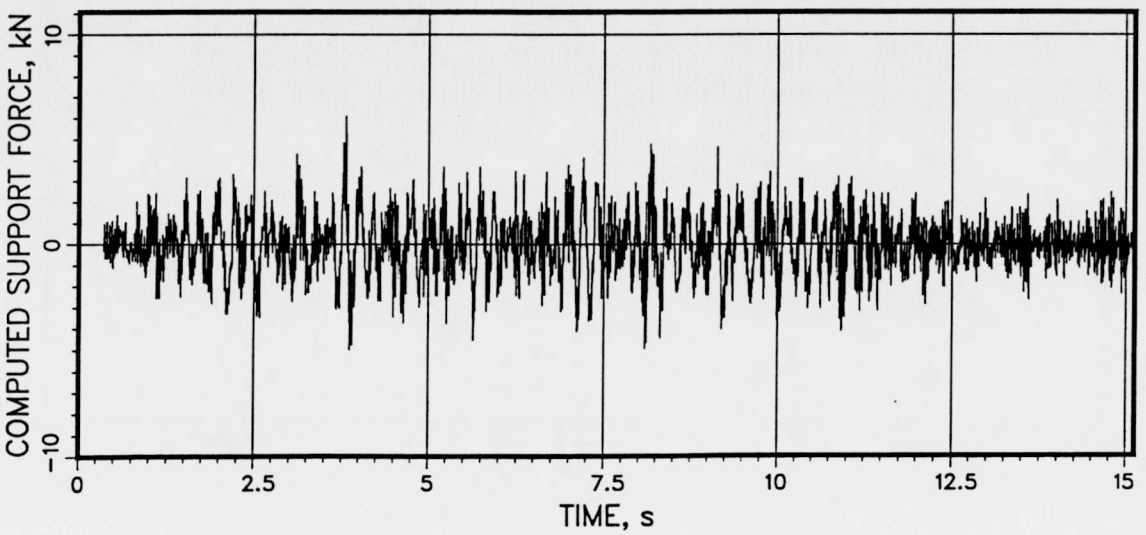

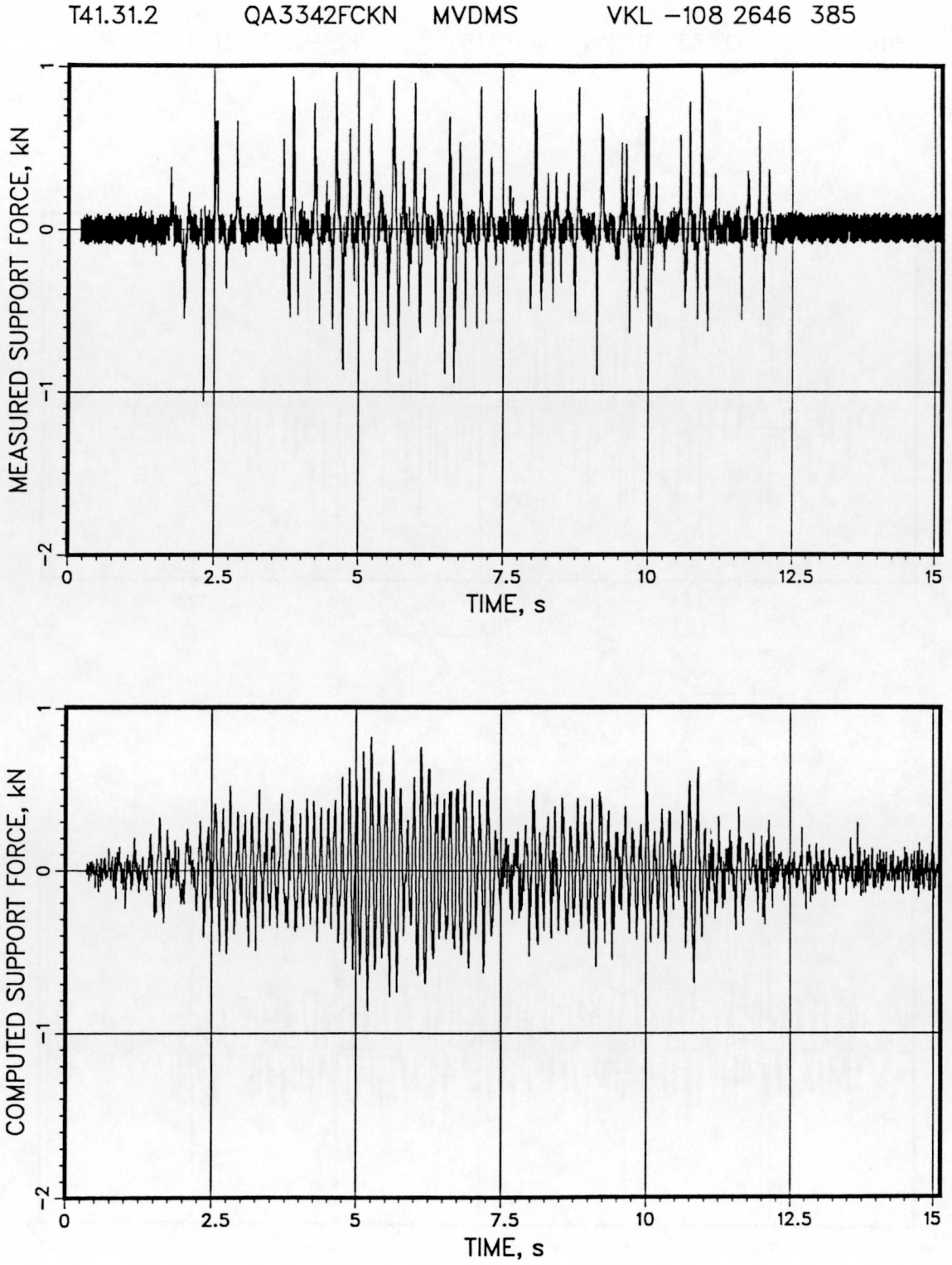
T41.31.2 QA3342FCKN MVDMS VKL −108 2646 385
MEASURED SUPPORT FORCE, kN
1
0
−1
−2
0
2.5
5
7.5
10
12.5
15
TIME, s
COMPUTED SUPPORT FORCE, kN
1
0
−1
−2
0
2.5
5
7.5
10
12.5
15
TIME, s

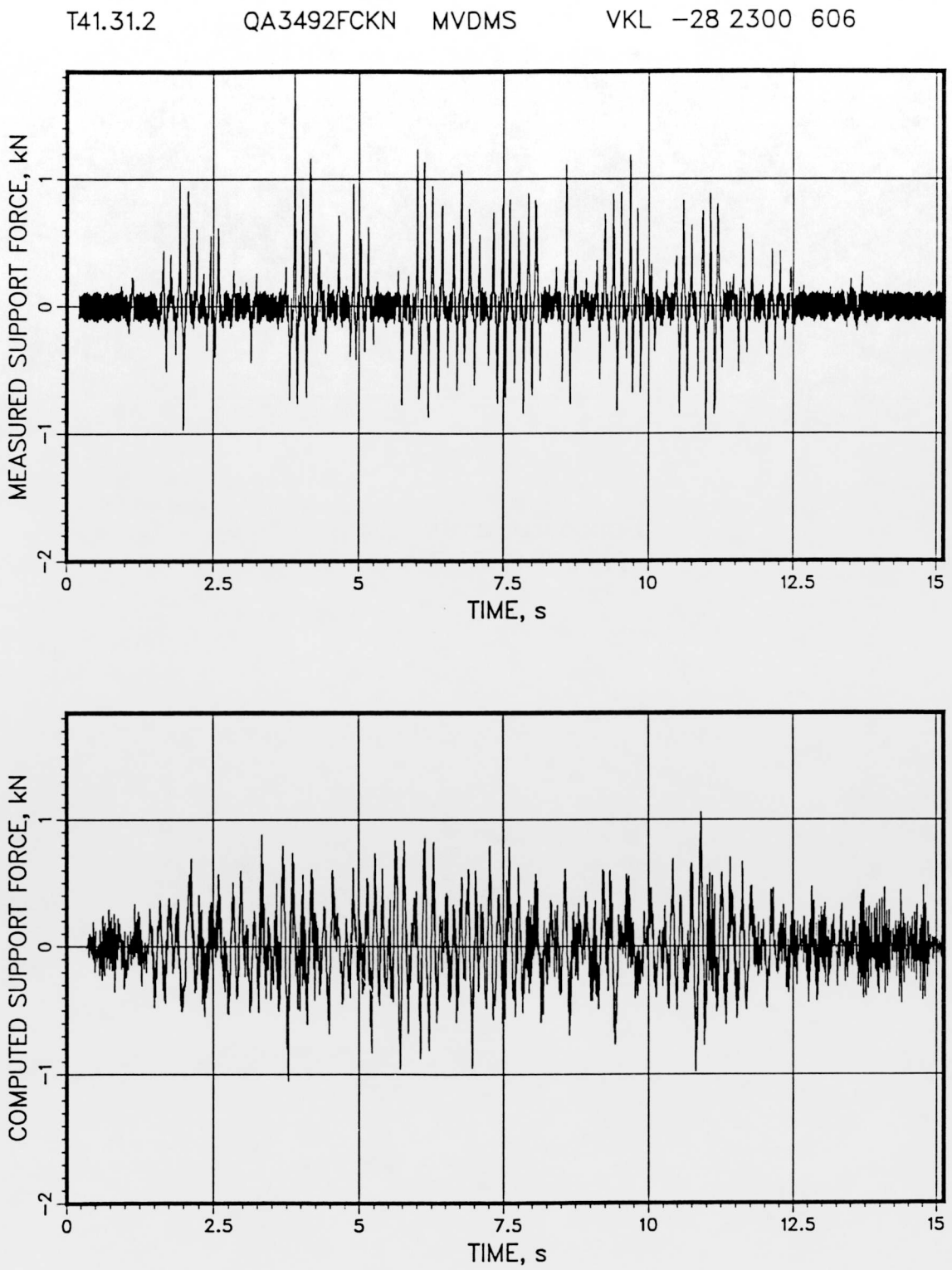
T41.31.2 QA3492FCKN MVDMS VKL −28 2300 606
MEASURED SUPPORT FORCE, kN
1
0
−1
−2
0
2.5
5
7.5
10
12.5
15
TIME, s
COMPUTED SUPPORT FORCE, kN
1
0
−1
−2
0
2.5
5
7.5
10
12.5
15
TIME, s

Force in Struts
Test: T41.31.2

T41.31.2 QA1243FCKN MVDMS VKL 346 2300 796

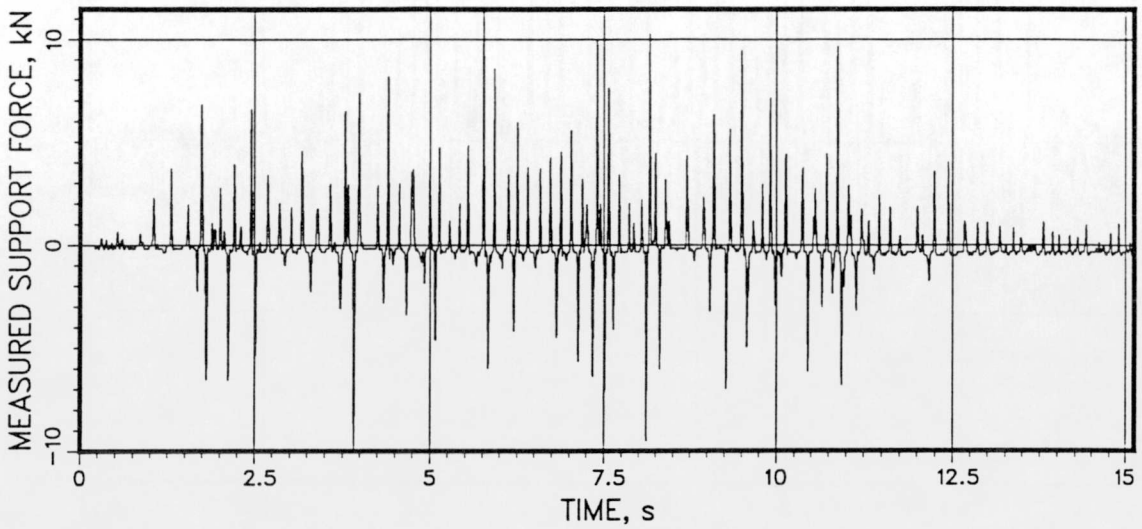

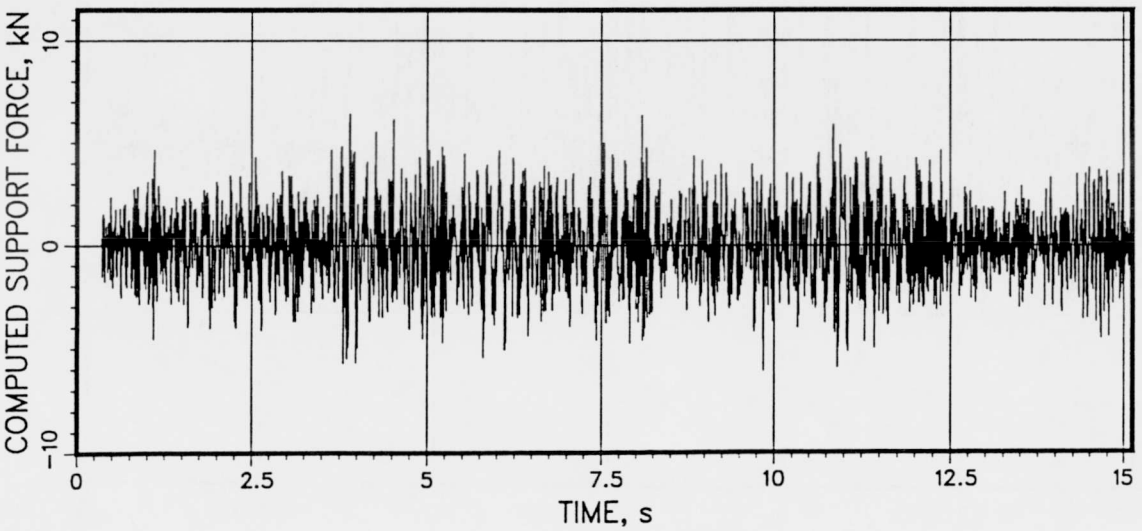

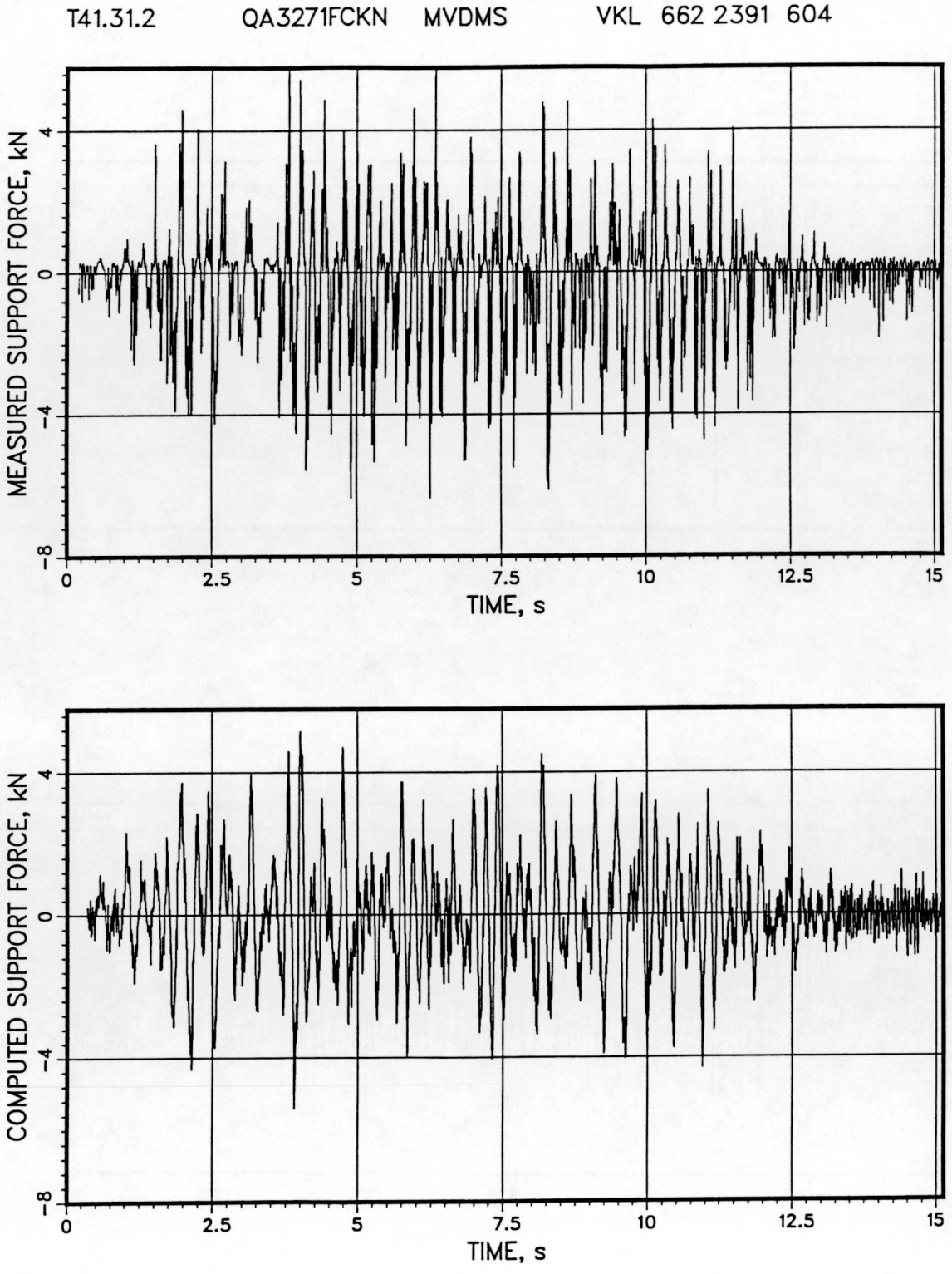
T41.31.2 QA3271FCKN MVDMS VKL 662 2391 604
MEASURED SUPPORT FORCE, kN
4
0
-4
-8
0
2.5
5
7.5
10
12.5
15
TIME, s
COMPUTED SUPPORT FORCE, kN
4
0
-4
-8
0
2.5
5
7.5
10
12.5
15
TIME, s

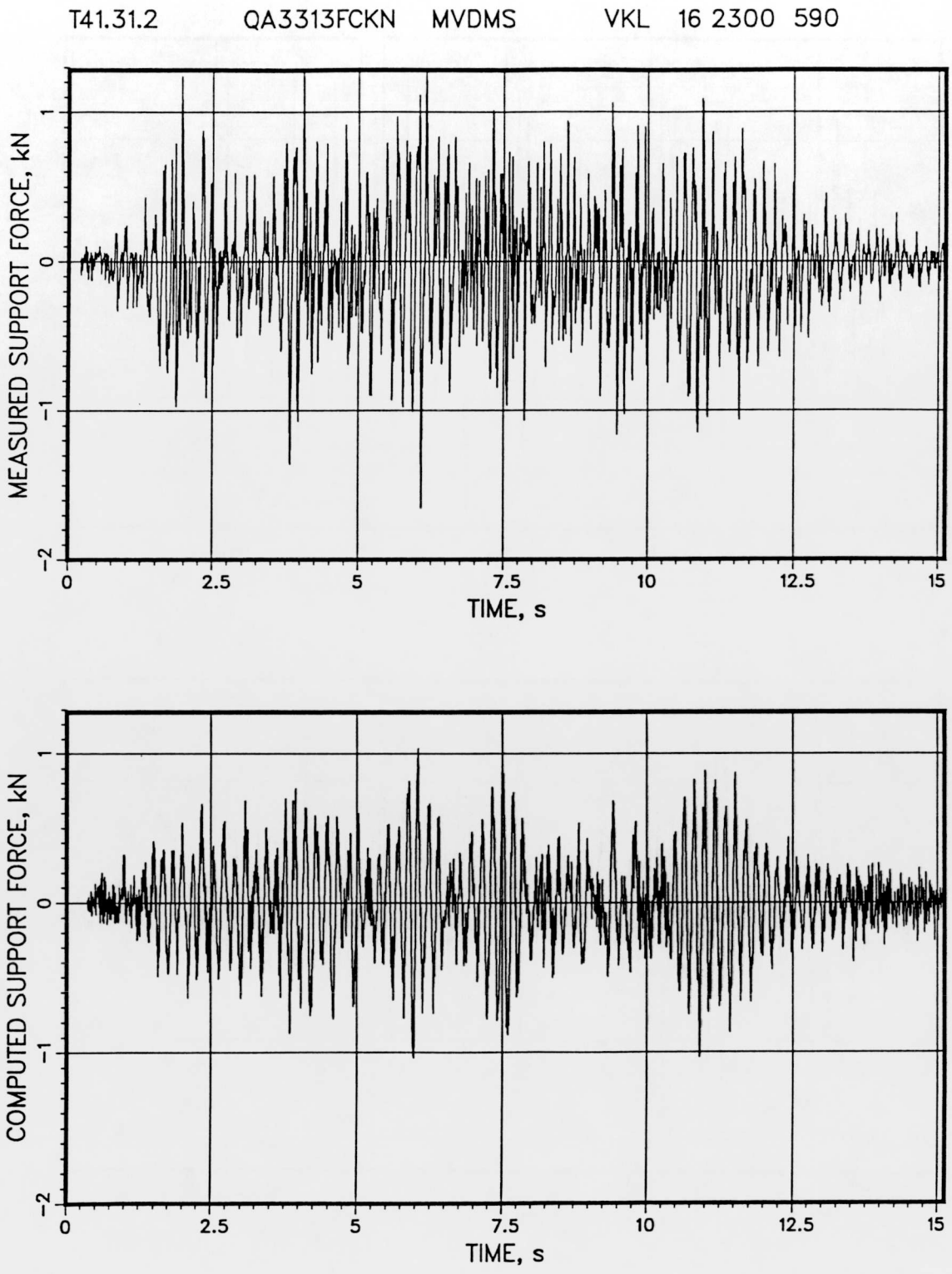
T41.31.2 QA3313FCKN MVDMS VKL 16 2300 590
MEASURED SUPPORT FORCE, kN
1
0
-1
-2
0
2.5
5
7.5
10
12.5
15
TIME, s
COMPUTED SUPPORT FORCE, kN
1
0
-1
-2
0
2.5
5
7.5
10
12.5
15
TIME, s

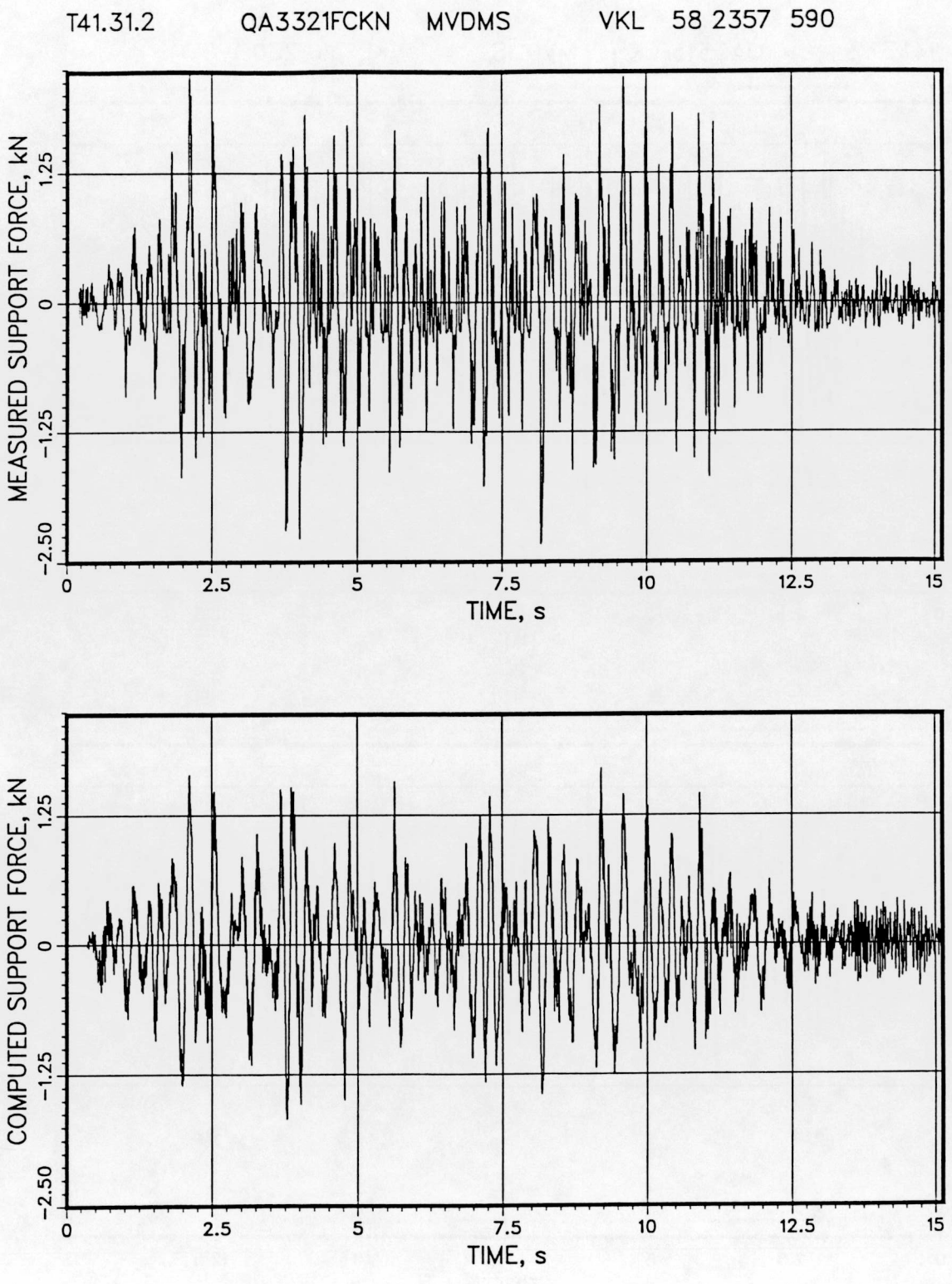
T41.31.2 QA3321FCKN MVDMS VKL 58 2357 590
MEASURED SUPPORT FORCE, kN
1.25
0
-1.25
-2.50
0
2.5
5
7.5
10
12.5
15
TIME, s
COMPUTED SUPPORT FORCE, kN
1.25
0
-1.25
-2.50
0
2.5
5
7.5
10
12.5
15
TIME, s

T41.31.2 QA3333FCKN MVDMS VKL 406 2646 385

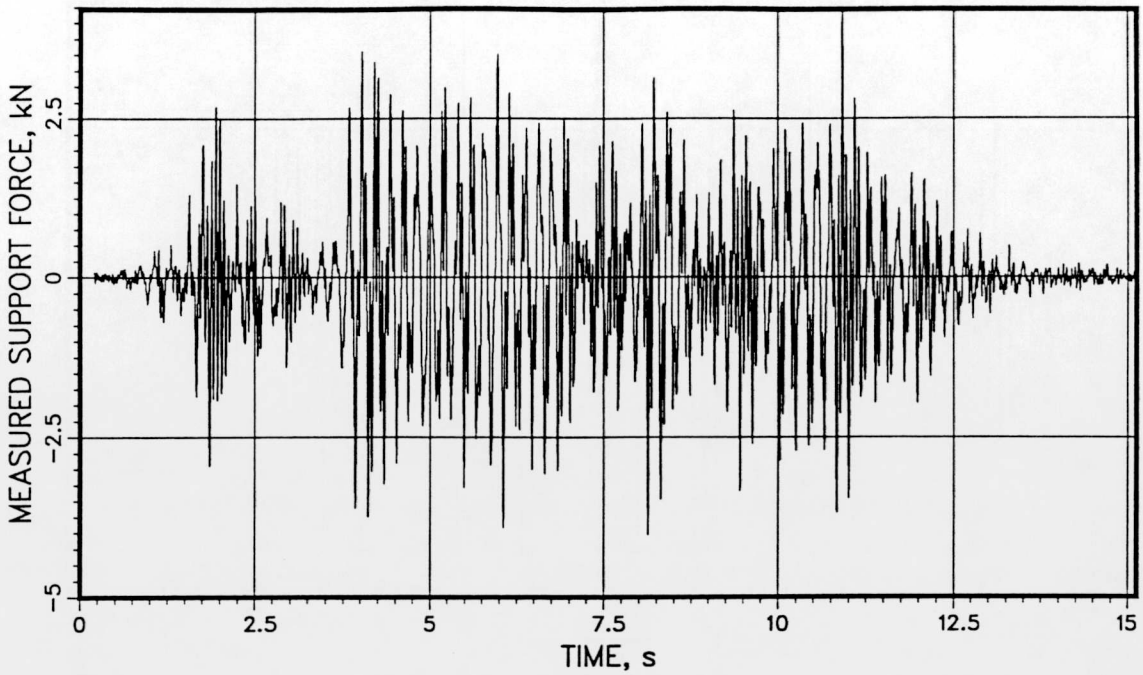

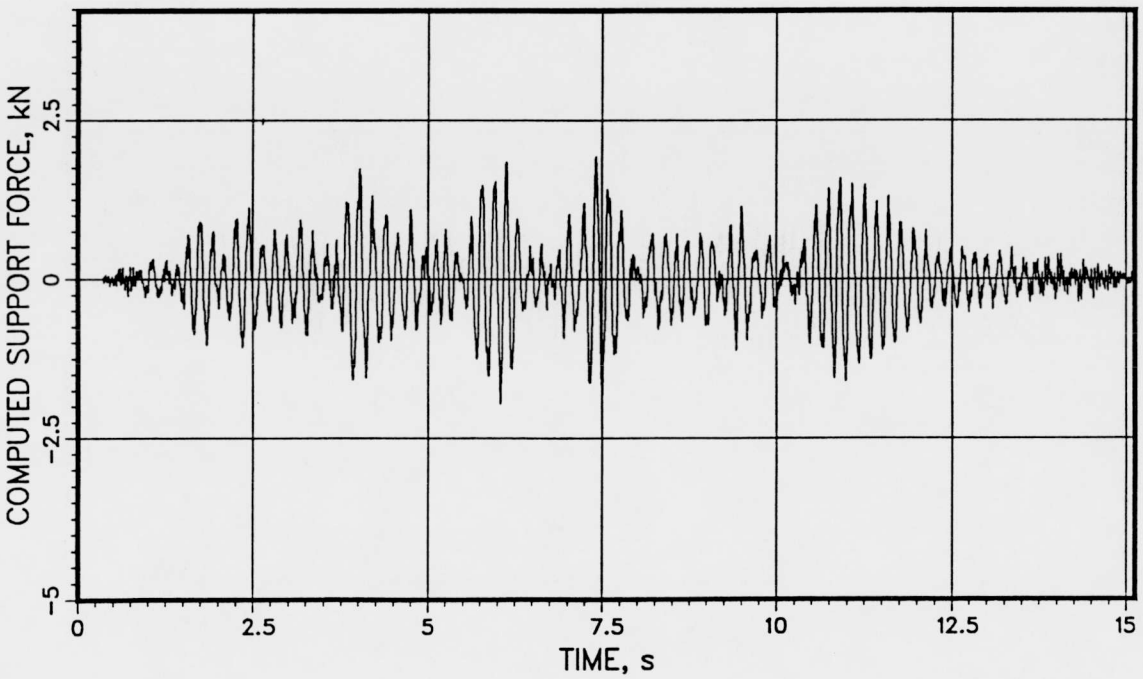

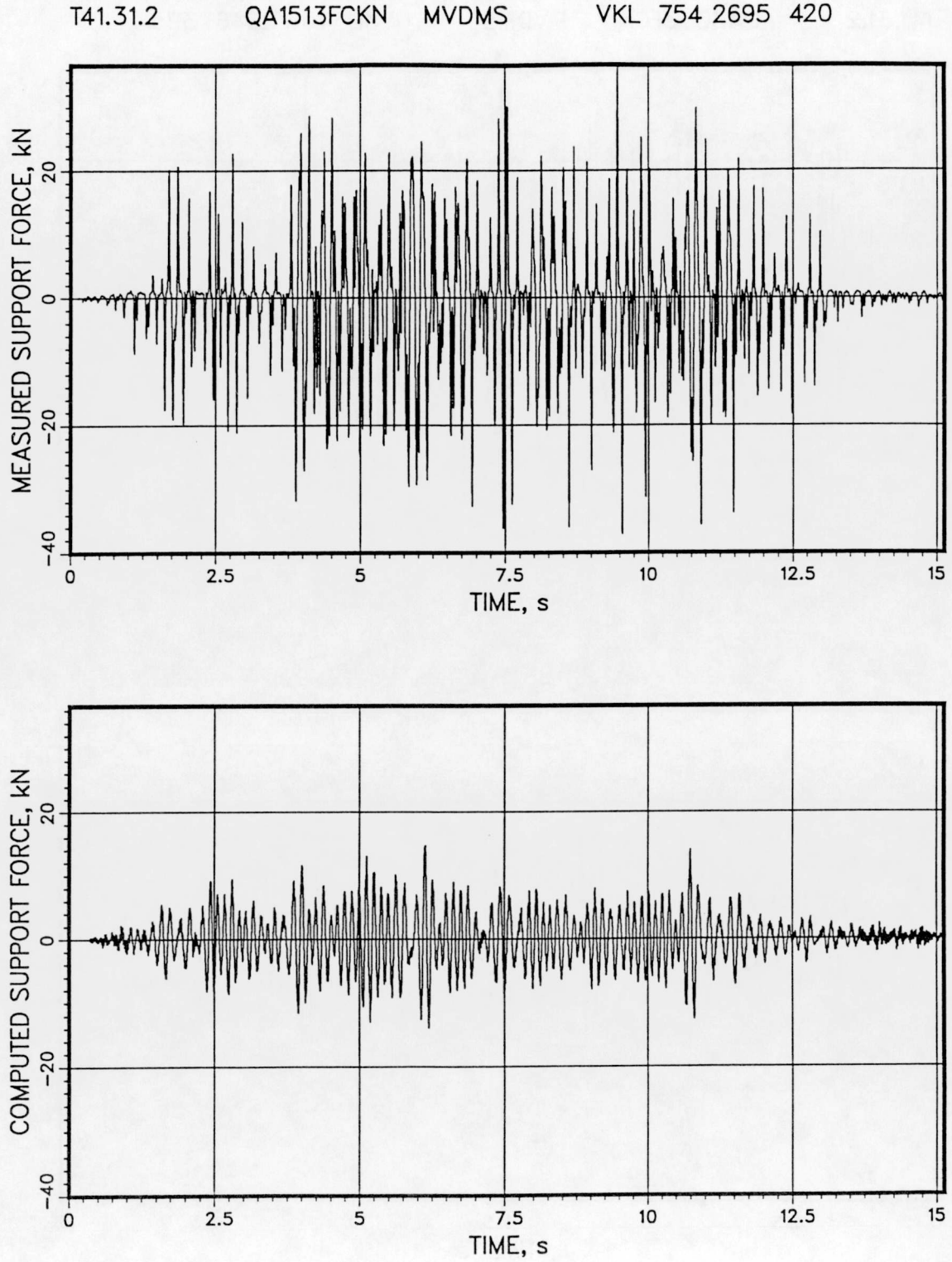
T41.31.2 QA1513FCKN MVDMS VKL 754 2695 420
MEASURED SUPPORT FORCE, kN
20
0
-20
-40
0
2.5
5
7.5
10
12.5
15
TIME, s
COMPUTED SUPPORT FORCE, kN
20
0
-20
-40
0
2.5
5
7.5
10
12.5
15
TIME, s

Force in Struts
Test: T41.21.1

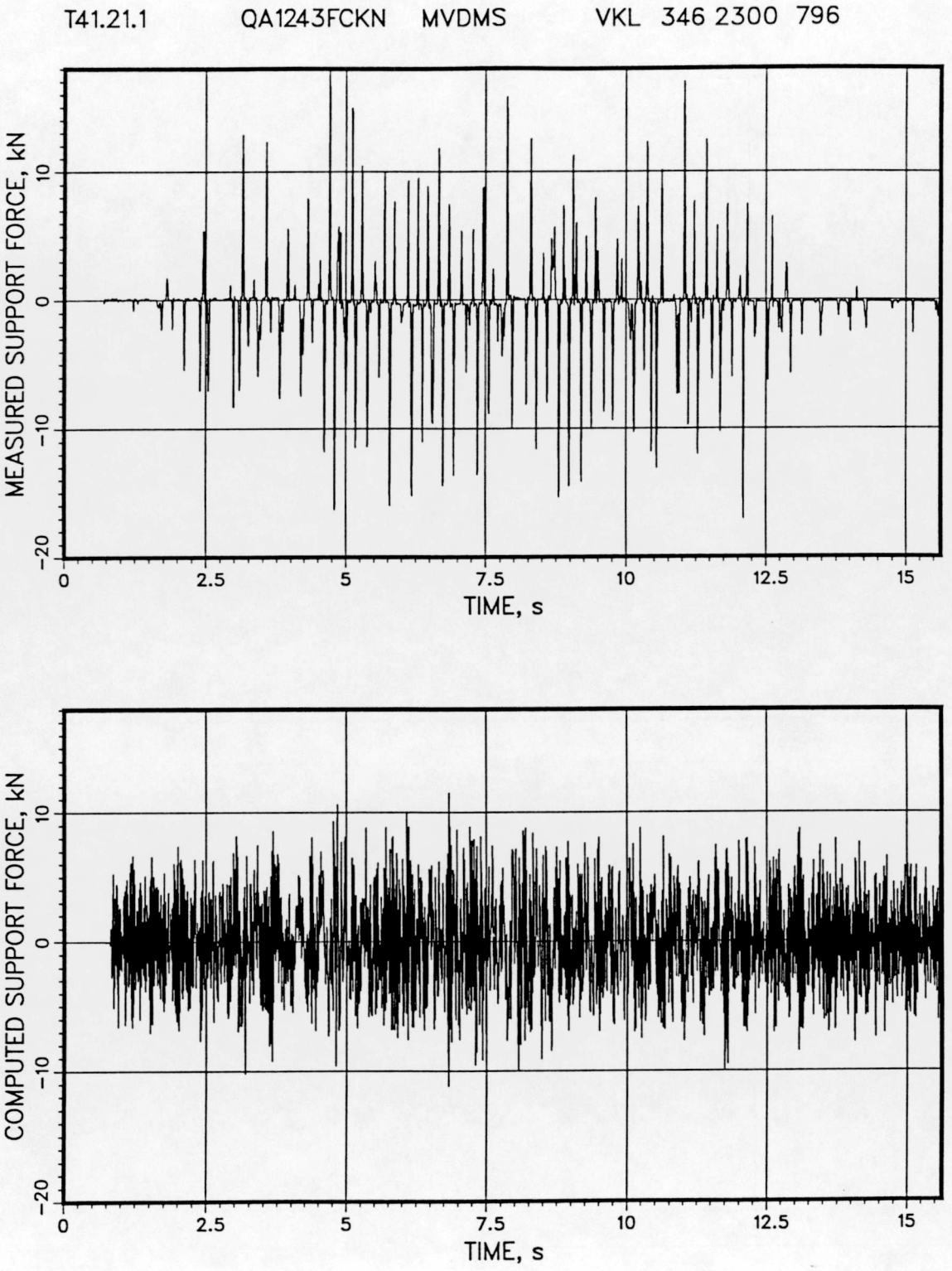
T41.21.1 QA1243FCKN MVDMS VKL 346 2300 796
MEASURED SUPPORT FORCE, kN
10
0
-10
-20
0
2.5
5
7.5
10
12.5
15
TIME, s
COMPUTED SUPPORT FORCE, kN
10
0
-10
-20
0
2.5
5
7.5
10
12.5
15
TIME, s

T41.21.1 QA3313FCKN MVDMS VKL 16 2300 590

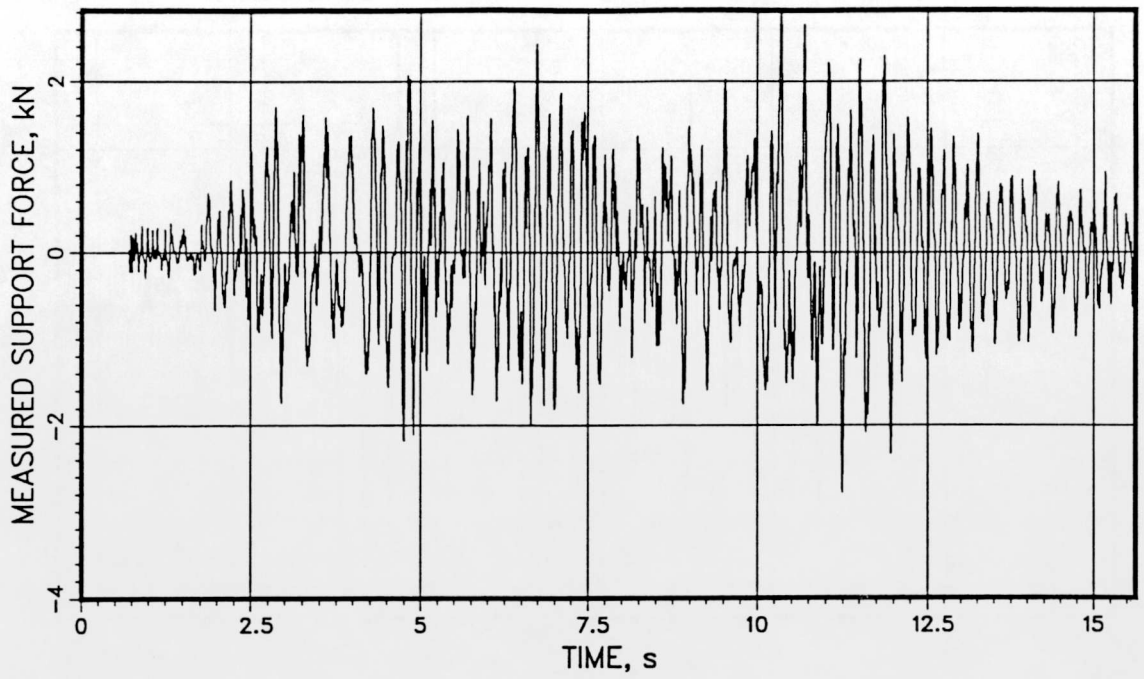

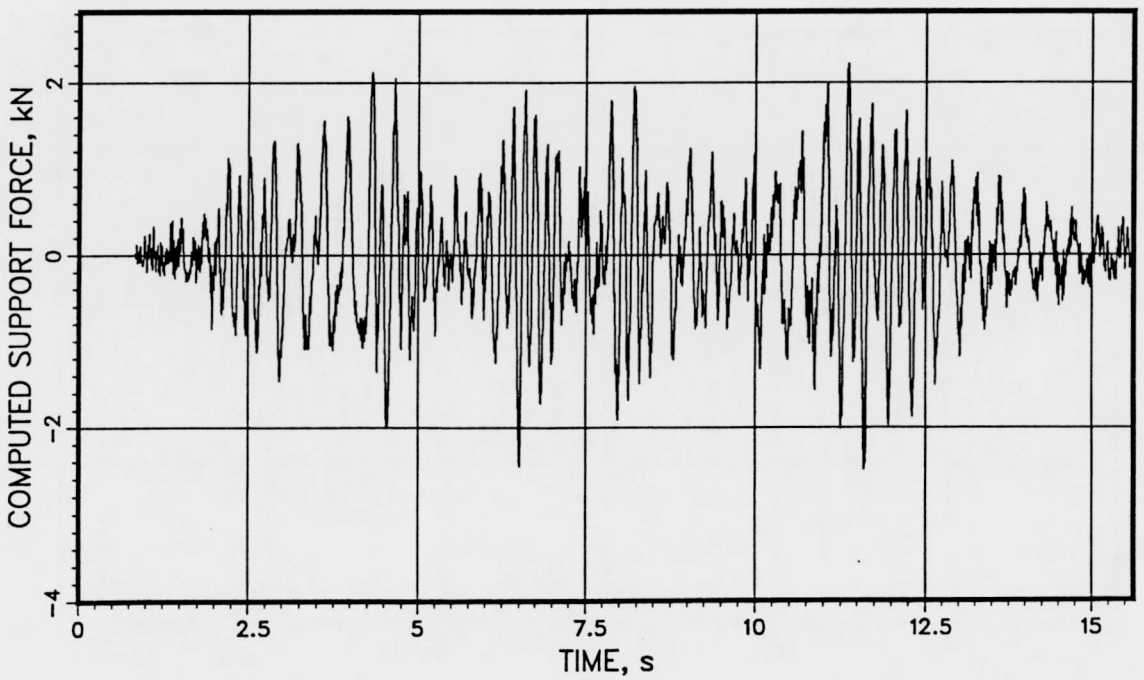

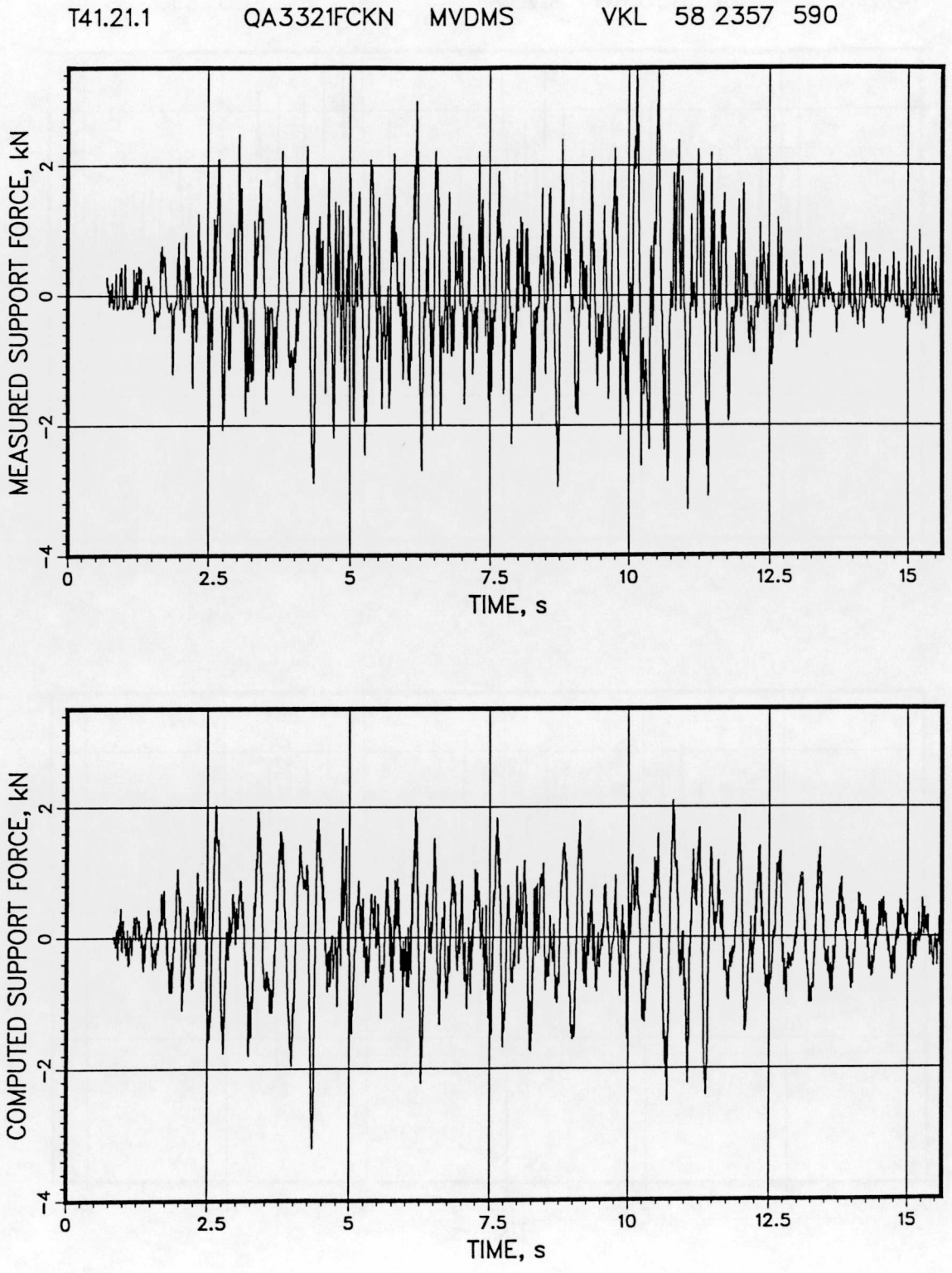
T41.21.1 QA3321FCKN MVDMS VKL 58 2357 590
MEASURED SUPPORT FORCE, kN
2
0
-2
-4
0
2.5
5
7.5
10
12.5
15
TIME, s
COMPUTED SUPPORT FORCE, kN
2
0
-2
-4
0
2.5
5
7.5
10
12.5
15
TIME, s

T41.21.1 QA3333FCKN MVDMS VKL 406 2646 385

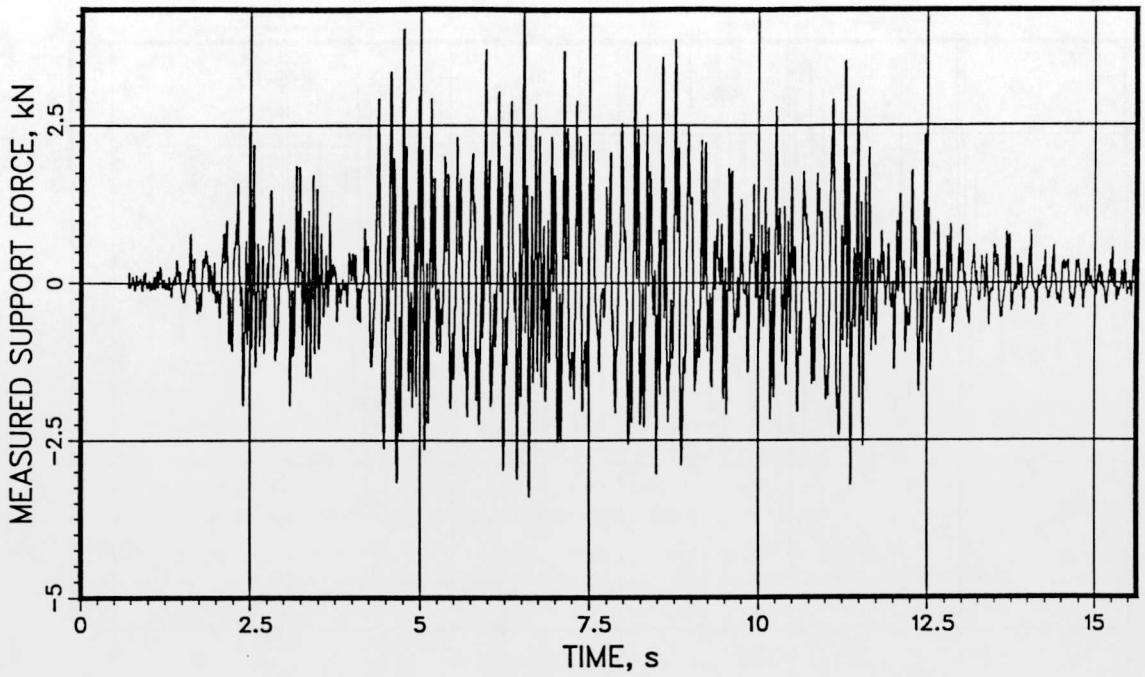

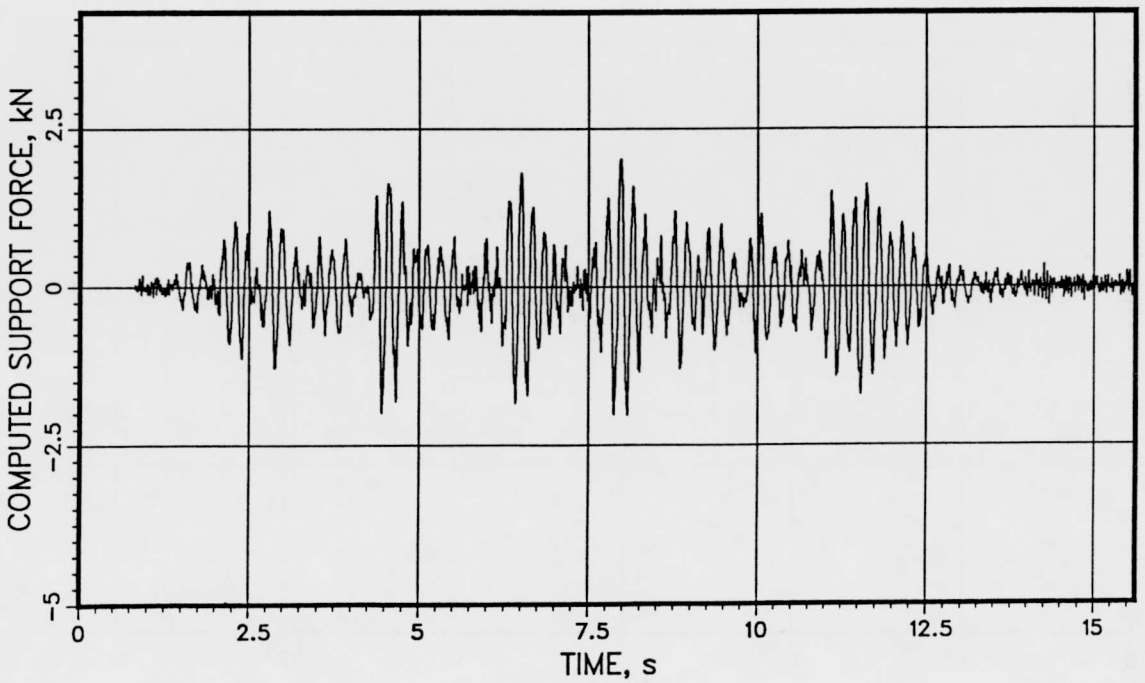

T41.21.1 QA1513FCKN MVDMS VKL 754 2695 420

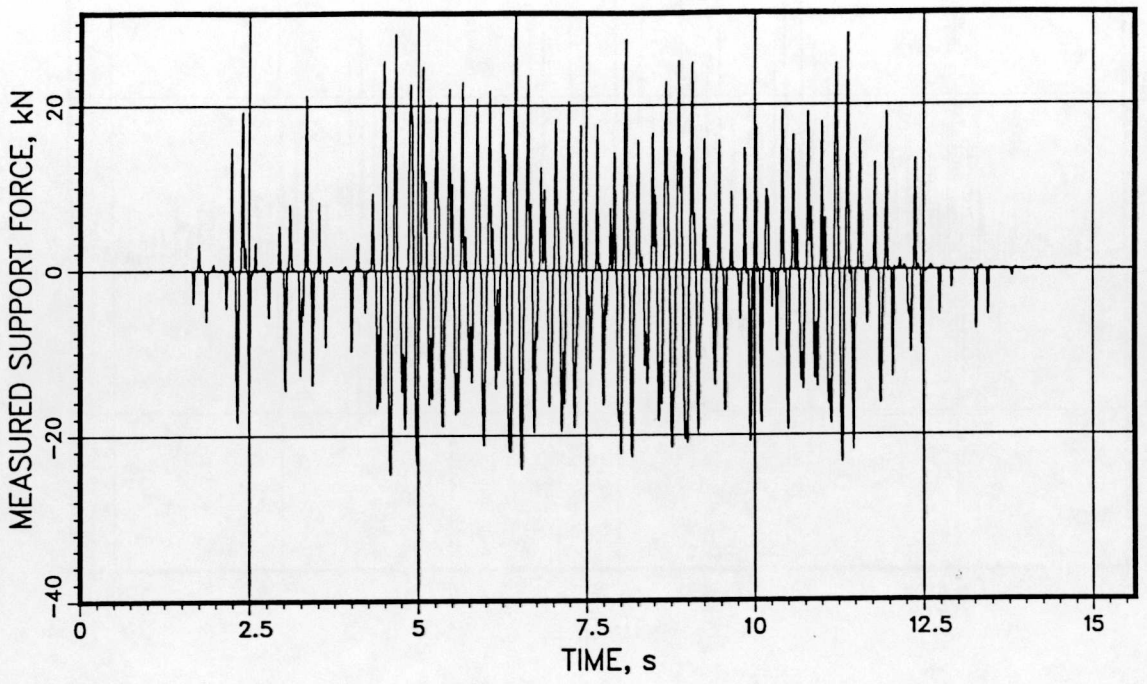

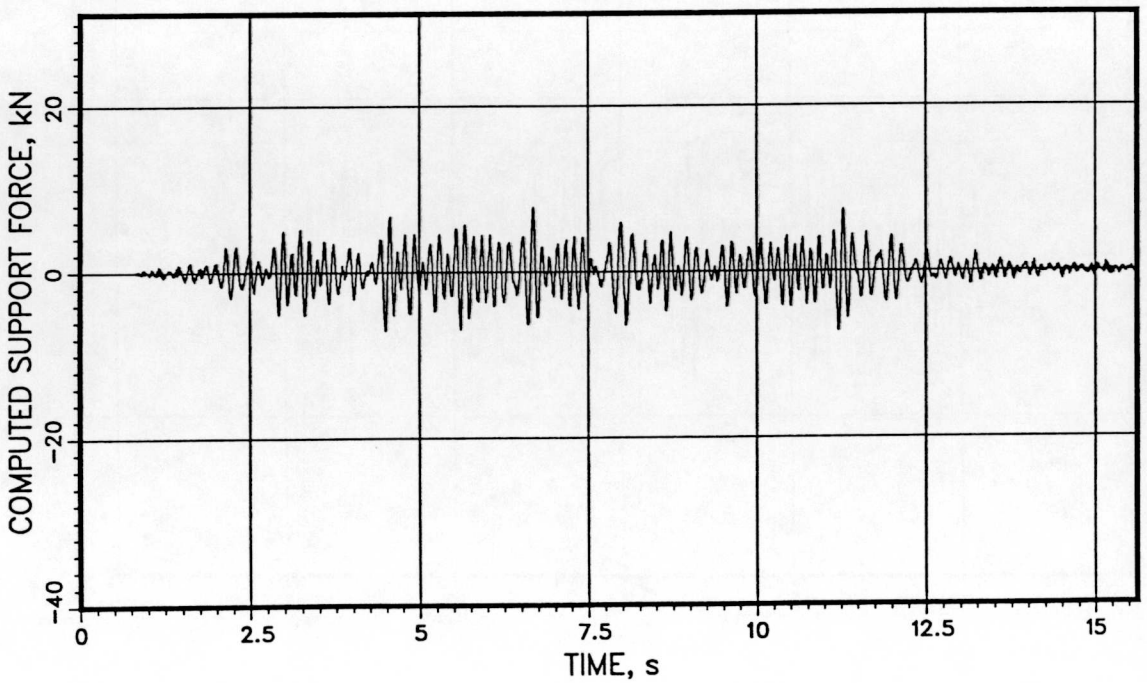

T41.21.1 QA1517FCKN MVDMS VKL 826 2695 420

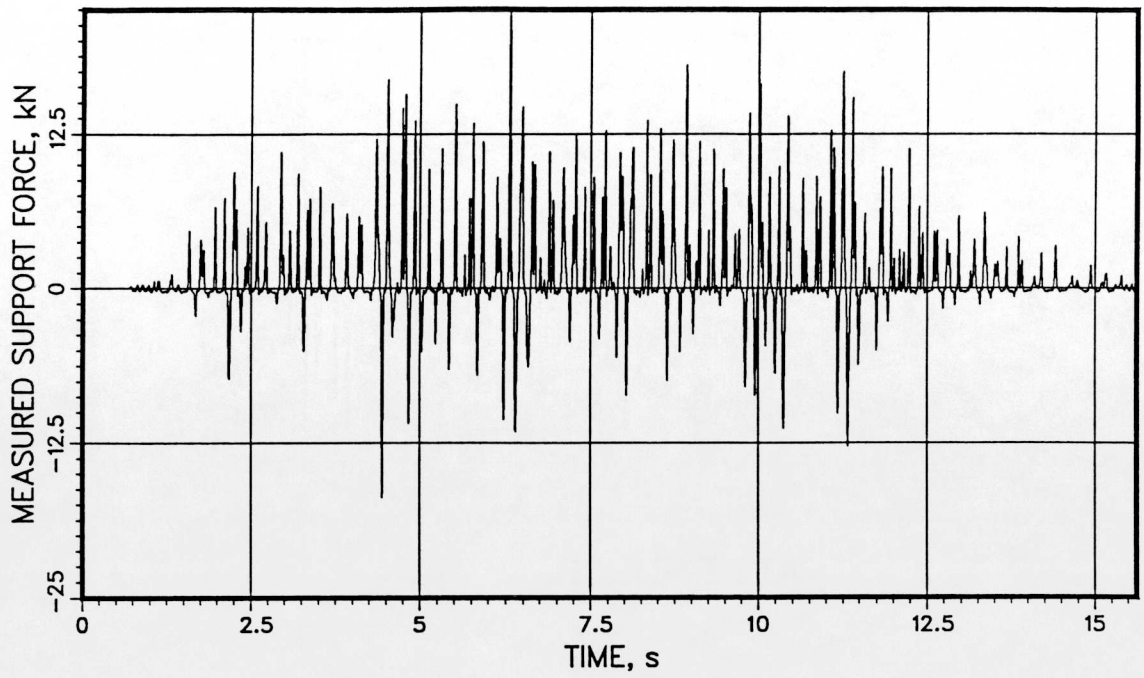

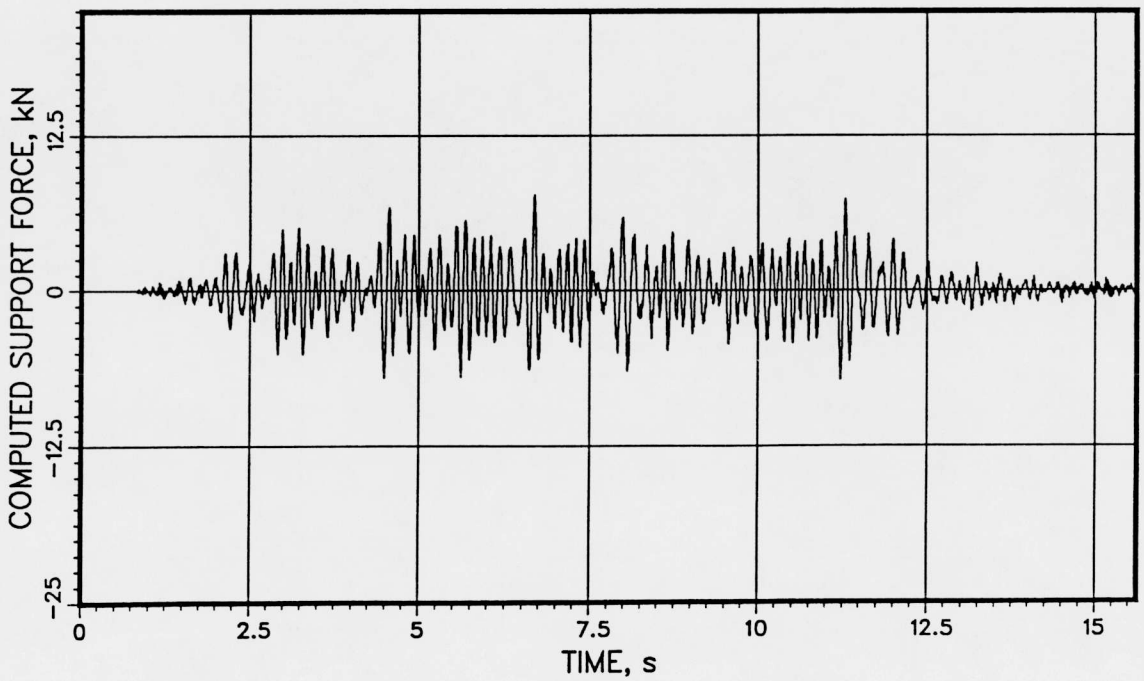

APPENDIX E

Comparisons of Bending Stresses in Pipe

Test: T41.21.1

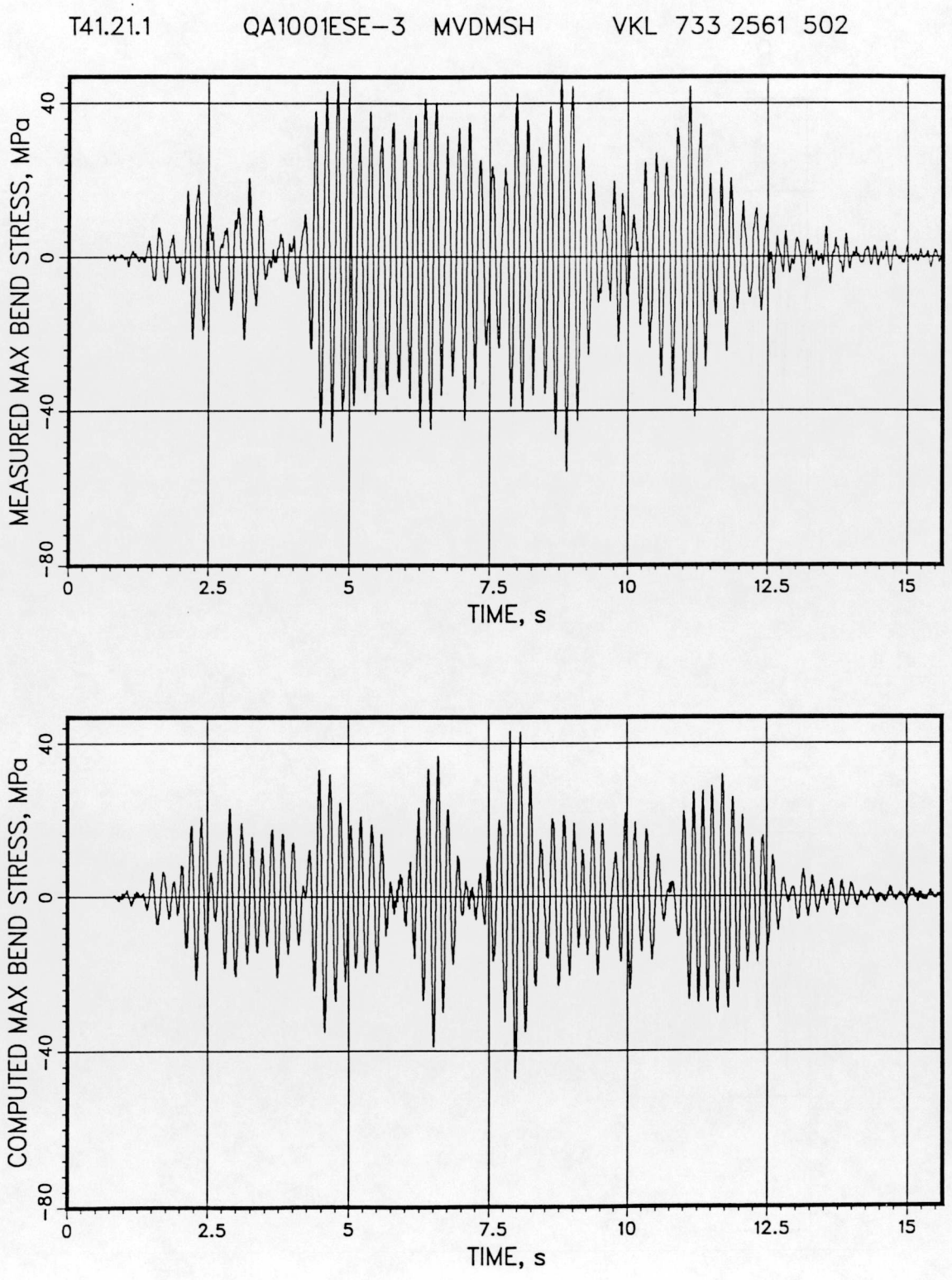
T41.21.1 QA1001ESE-3 MVDMSH VKL 733 2561 502
MEASURED MAX BEND STRESS, MPa
40
0
-40
-80
0
2.5
5
7.5
10
12.5
15
TIME, s
COMPUTED MAX BEND STRESS, MPa
40
0
-40
-80
0
2.5
5
7.5
10
12.5
15
TIME, s

T41.21.1 QA1002ESE-3 MVDMSH VKL 733 2561 502

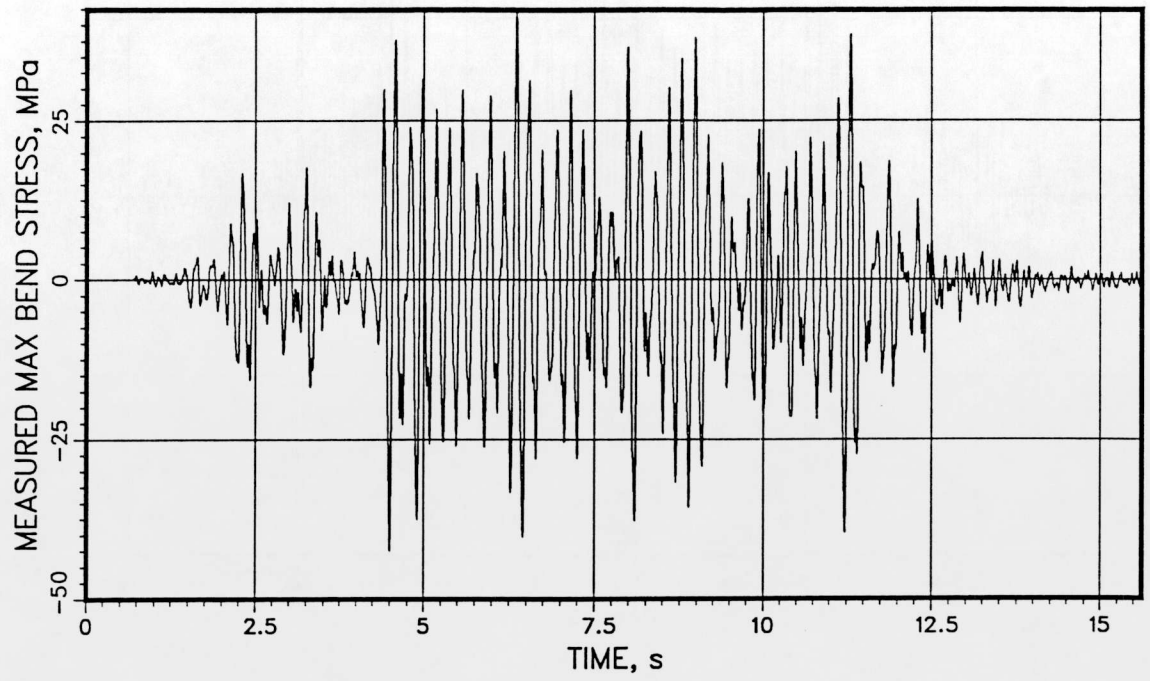

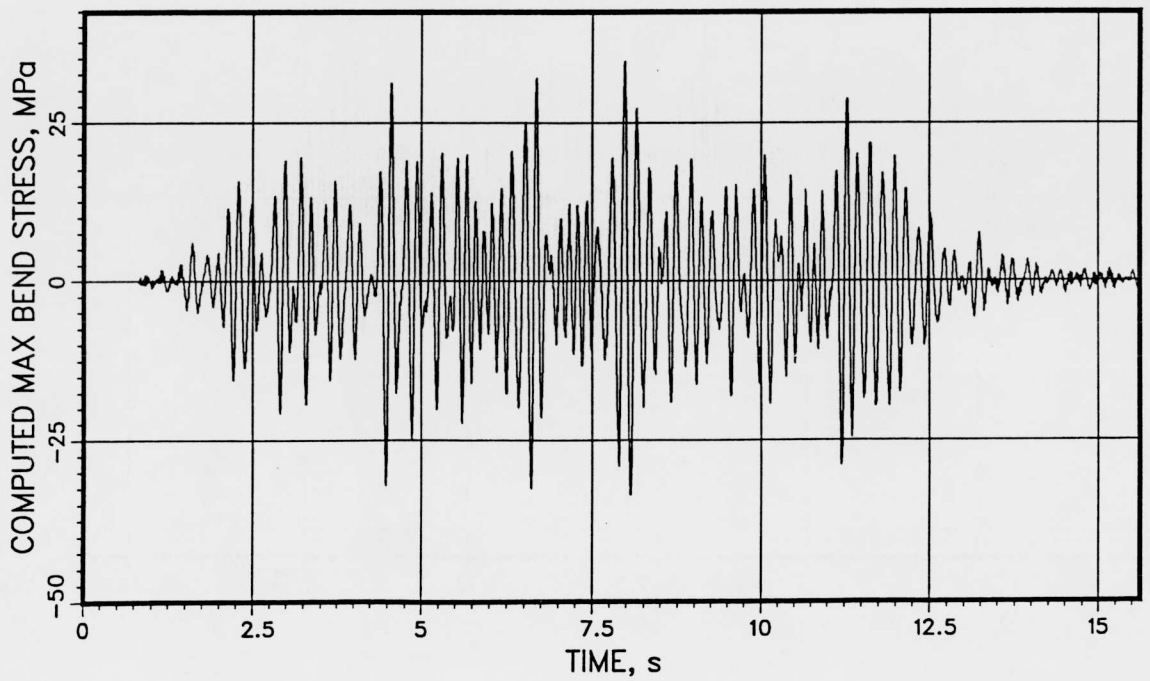

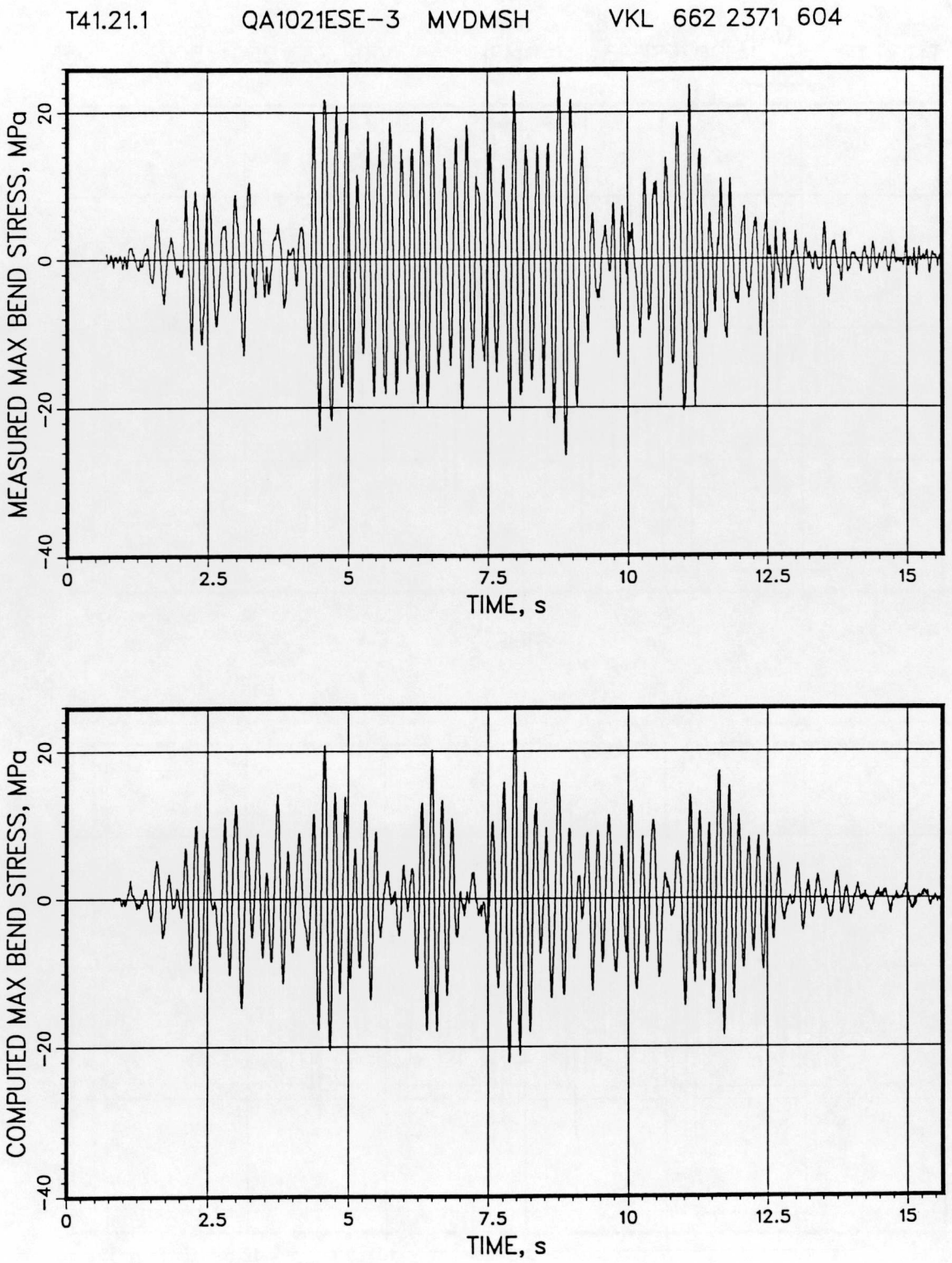
T41.21.1 QA1021ESE-3 MVDMSH VKL 662 2371 604
MEASURED MAX BEND STRESS, MPa
20
0
-20
-40
0
2.5
5
7.5
10
12.5
15
TIME, s
COMPUTED MAX BEND STRESS, MPa
20
0
-20
-40
0
2.5
5
7.5
10
12.5
15
TIME, s

T41.21.1 QA1022ESE−3 MVDMSH VKL 662 2371 604

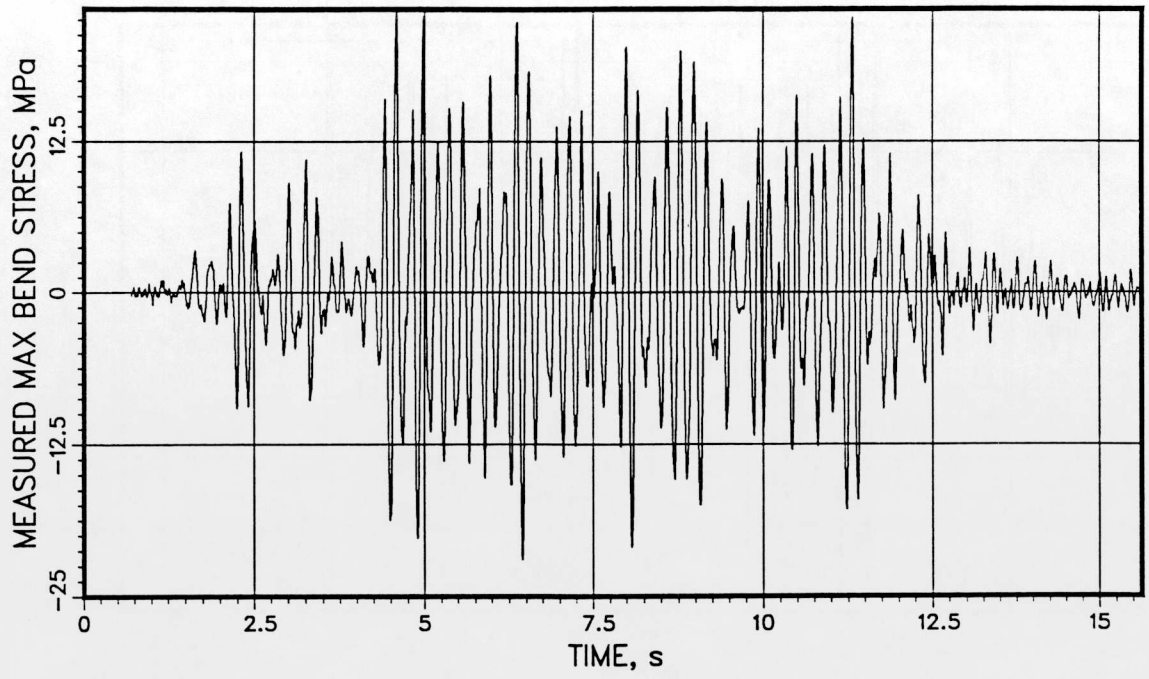

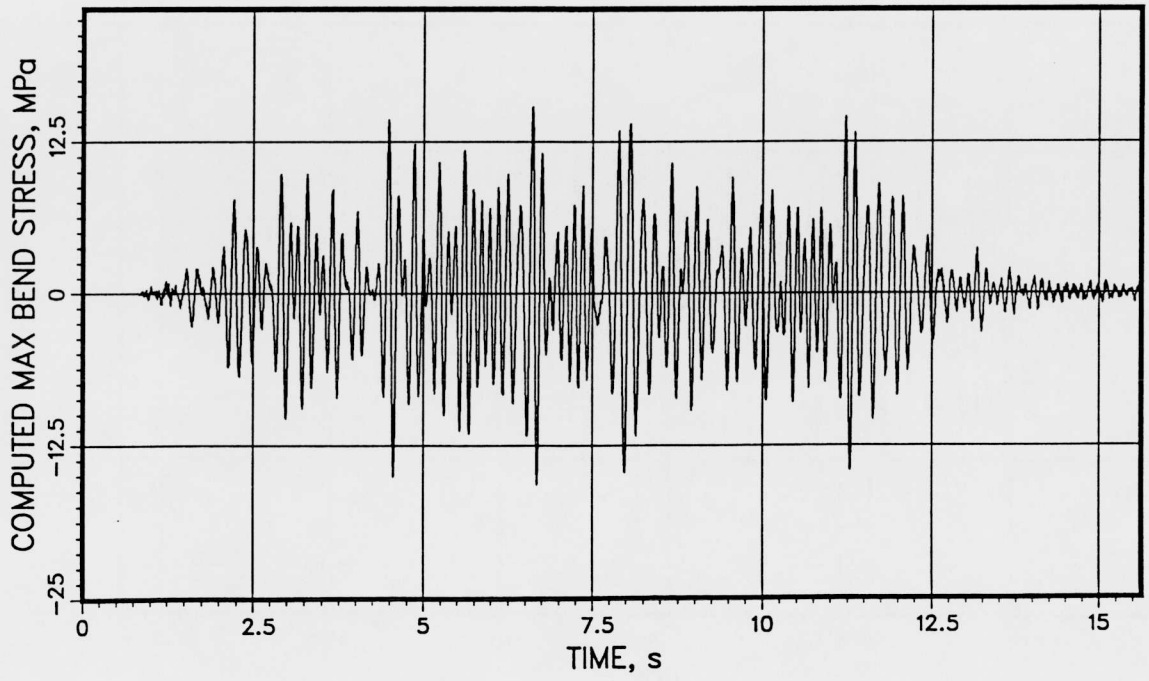

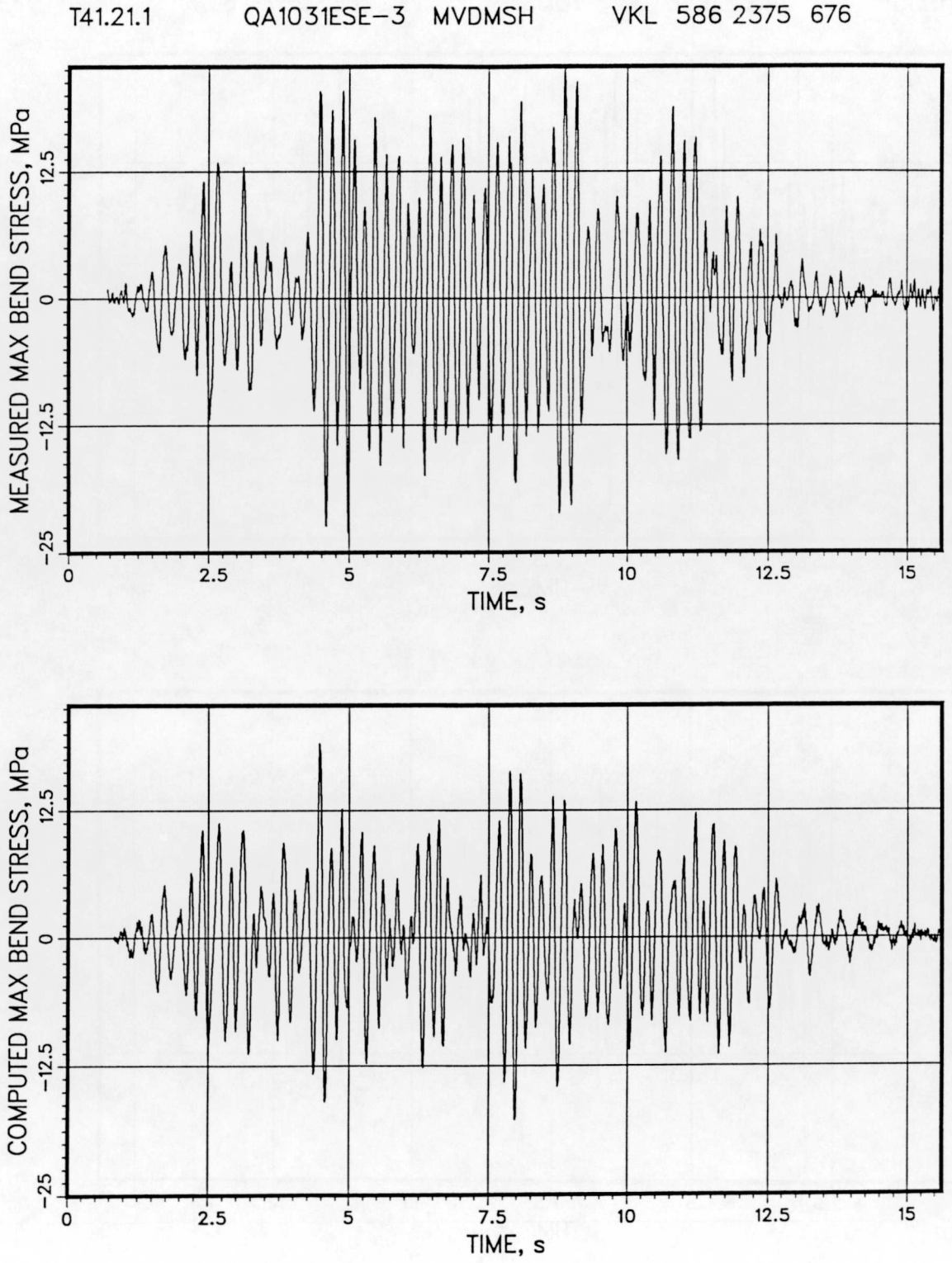
T41.21.1 QA1031ESE-3 MVDMSH VKL 586 2375 676
MEASURED MAX BEND STRESS, MPa
12.5
0
-12.5
-25
0
2.5
5
7.5
10
12.5
15
TIME, s
COMPUTED MAX BEND STRESS, MPa
12.5
0
-12.5
-25
0
2.5
5
7.5
10
12.5
15
TIME, s

T41.21.1 QA1032ESE–3 MVDMSH VKL 586 2375 676

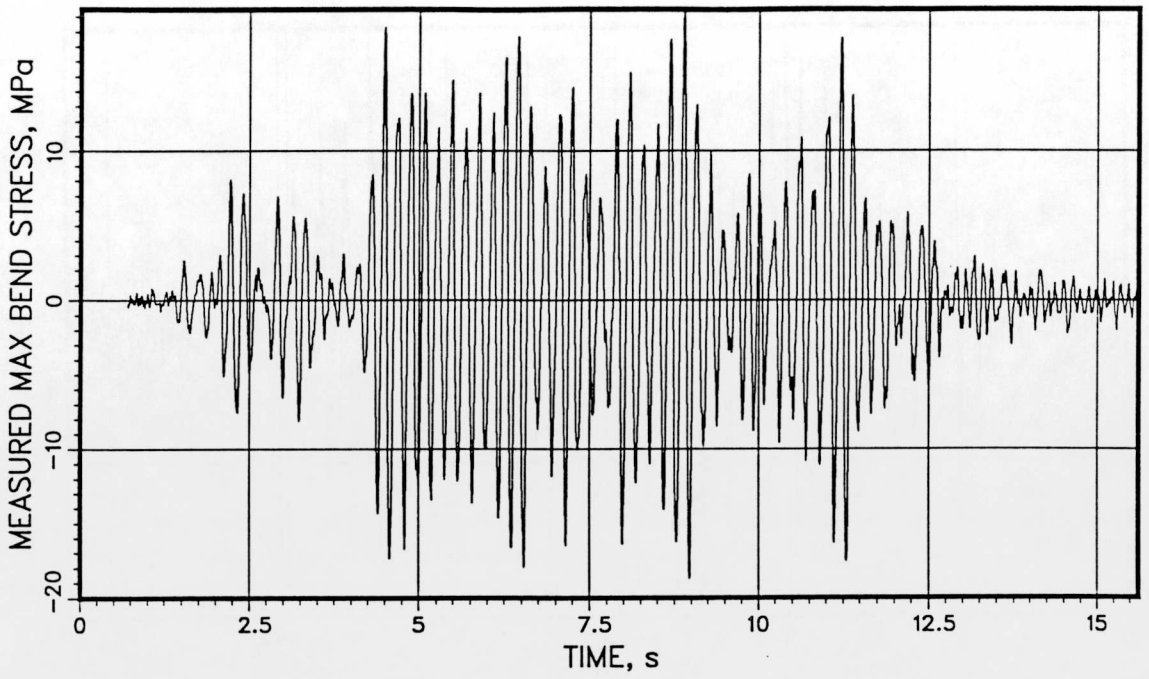

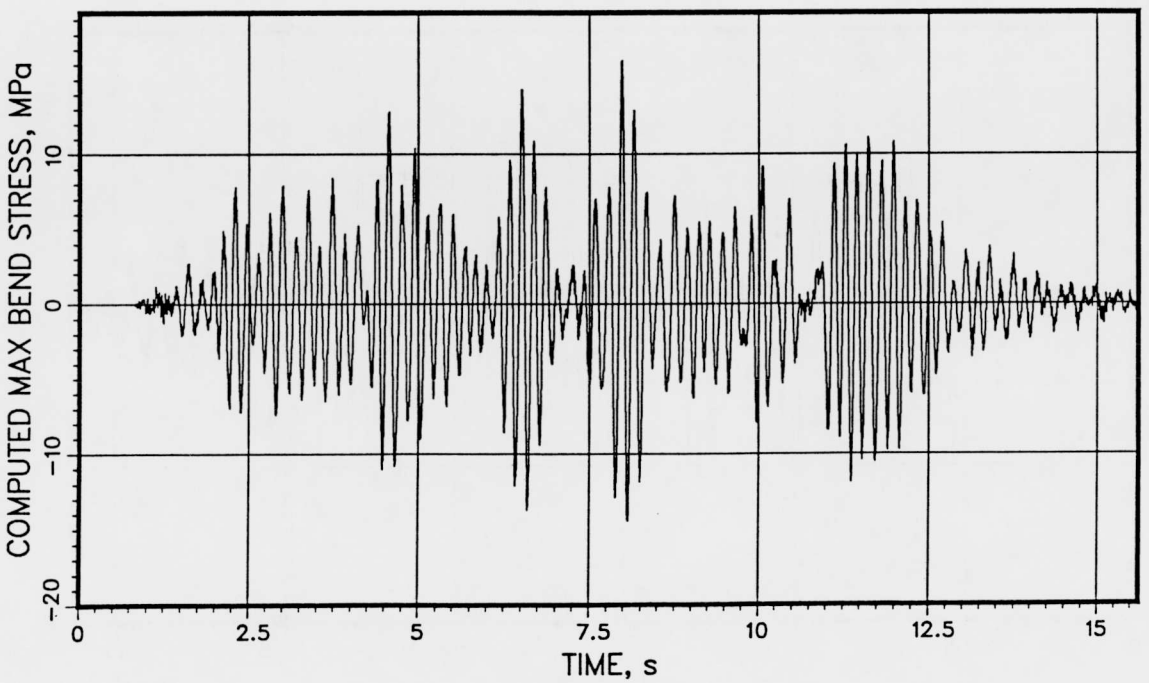

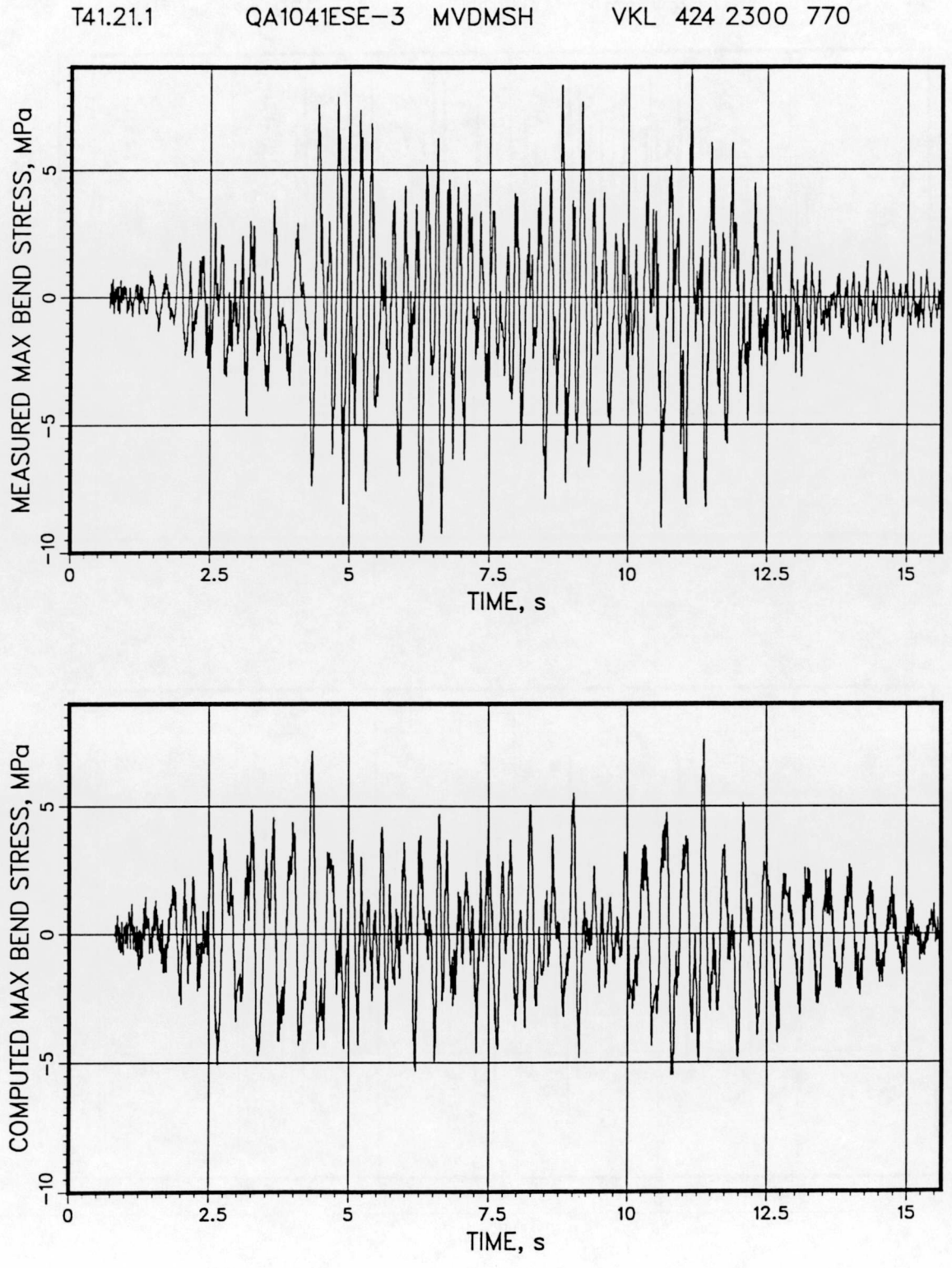
T41.21.1 QA1041ESE–3 MVDMSH VKL 424 2300 770
MEASURED MAX BEND STRESS, MPa
5
0
–5
–10
0
2.5
5
7.5
10
12.5
15
TIME, s
COMPUTED MAX BEND STRESS, MPa
5
0
–5
–10
0
2.5
5
7.5
10
12.5
15
TIME, s

T41.21.1 QA1042ESE–3 MVDMSH VKL 424 2300 770

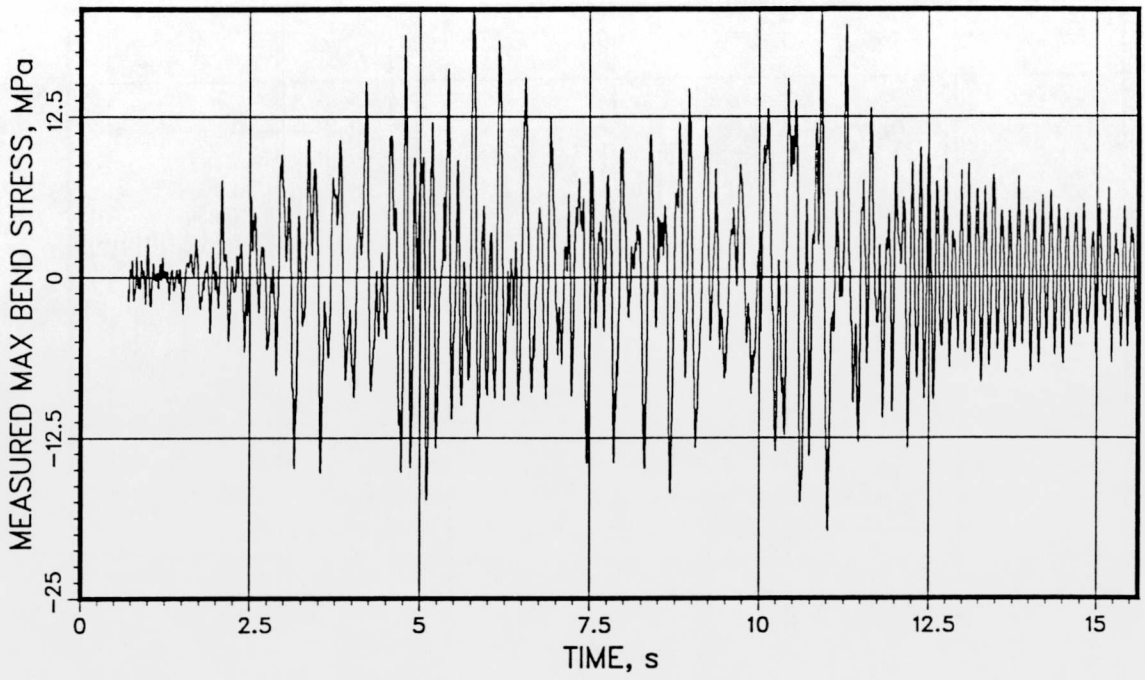

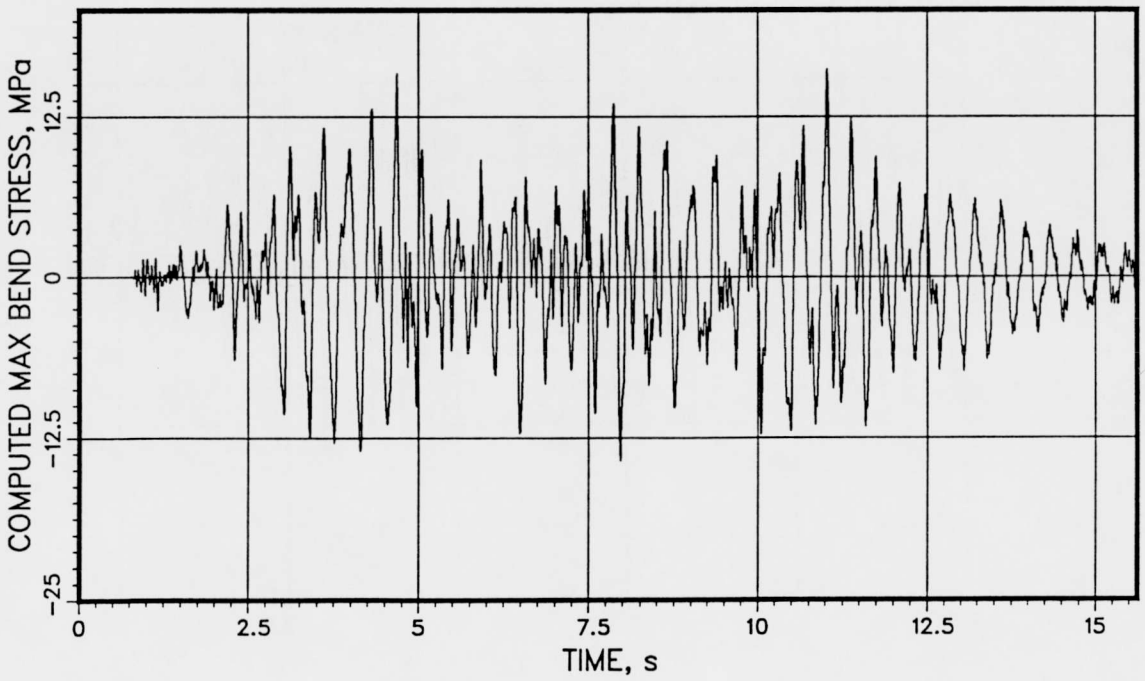

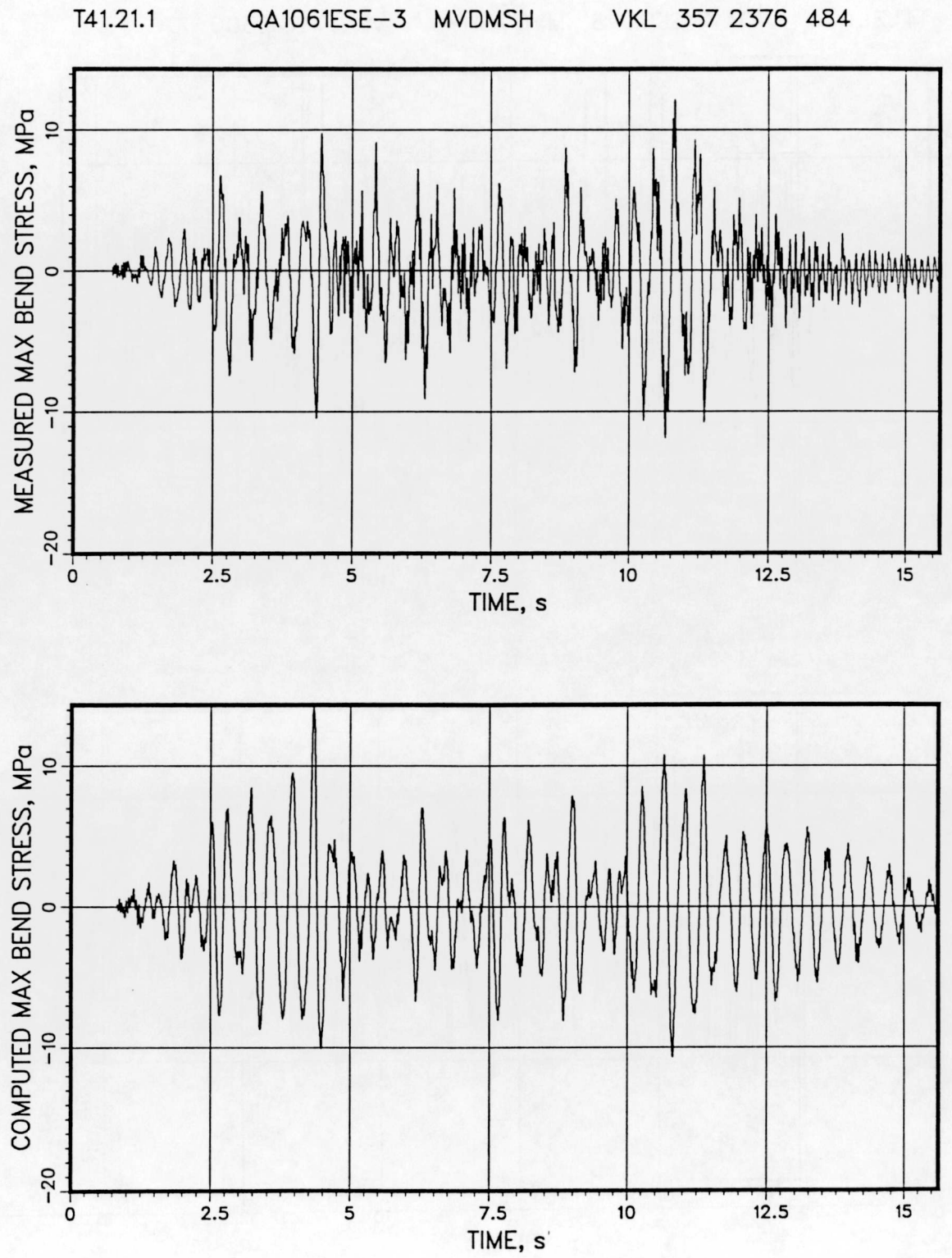
T41.21.1 QA1061ESE-3 MVDMSH VKL 357 2376 484
MEASURED MAX BEND STRESS, MPa
10
0
-10
-20
0
2.5
5
7.5
10
12.5
15
TIME, s
COMPUTED MAX BEND STRESS, MPa
10
0
-10
-20
0
2.5
5
7.5
10
12.5
15
TIME, s

T41.21.1 QA1062ESE–3 MVDMSH VKL 357 2376 484

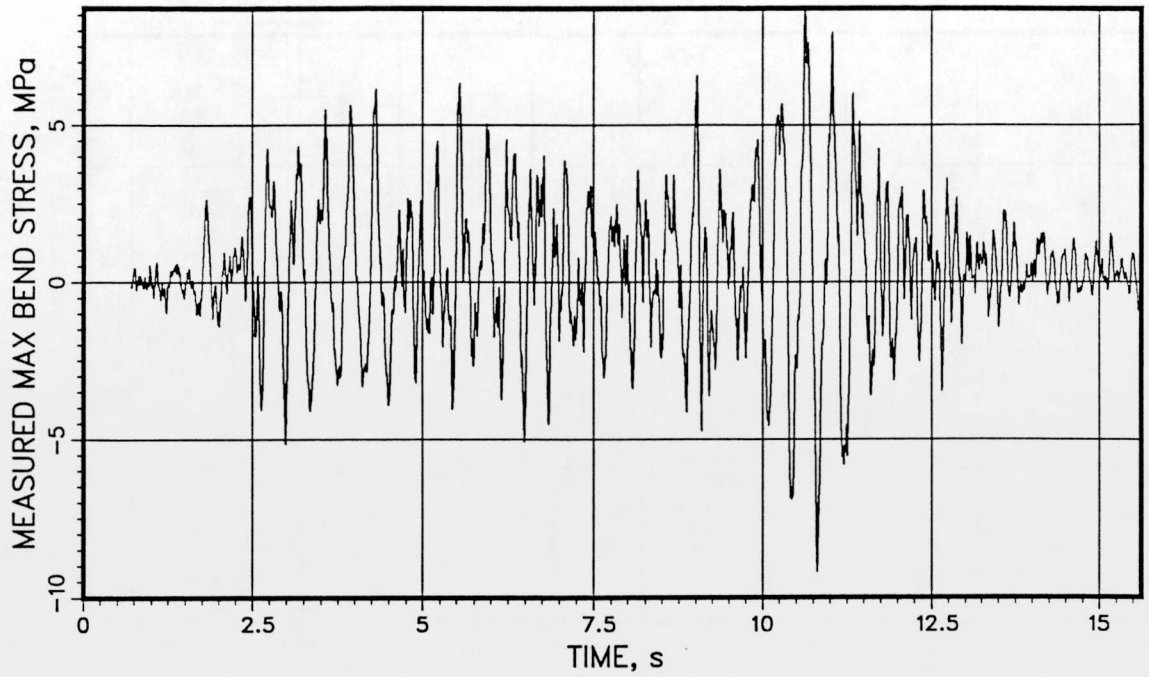

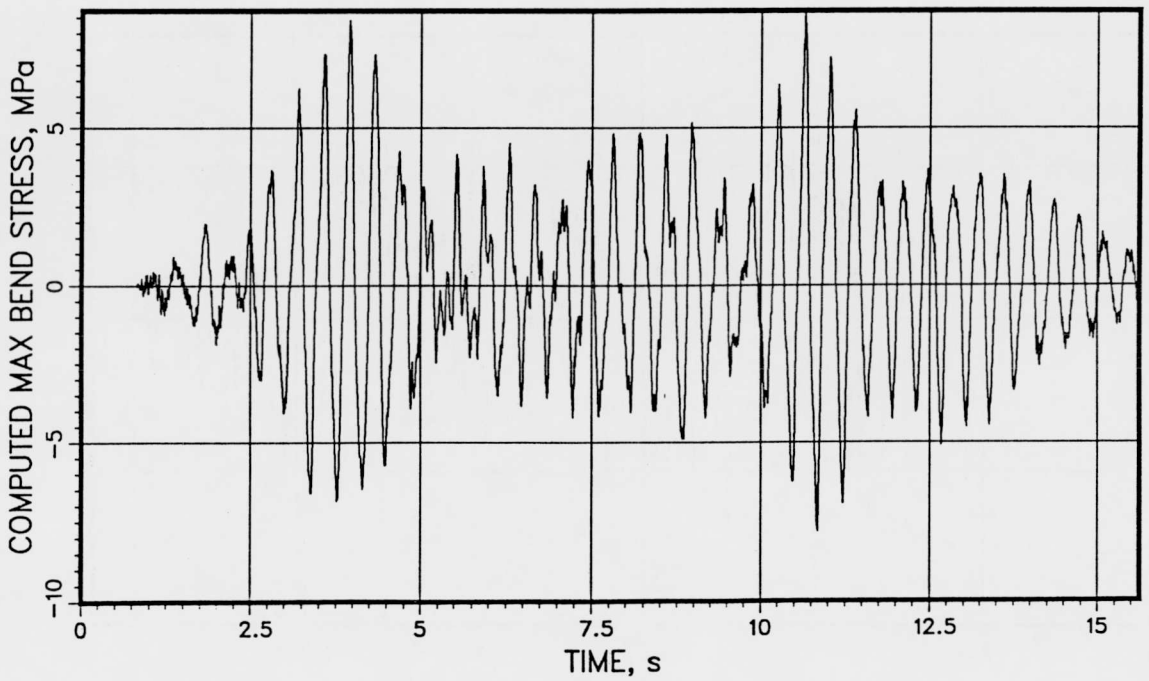

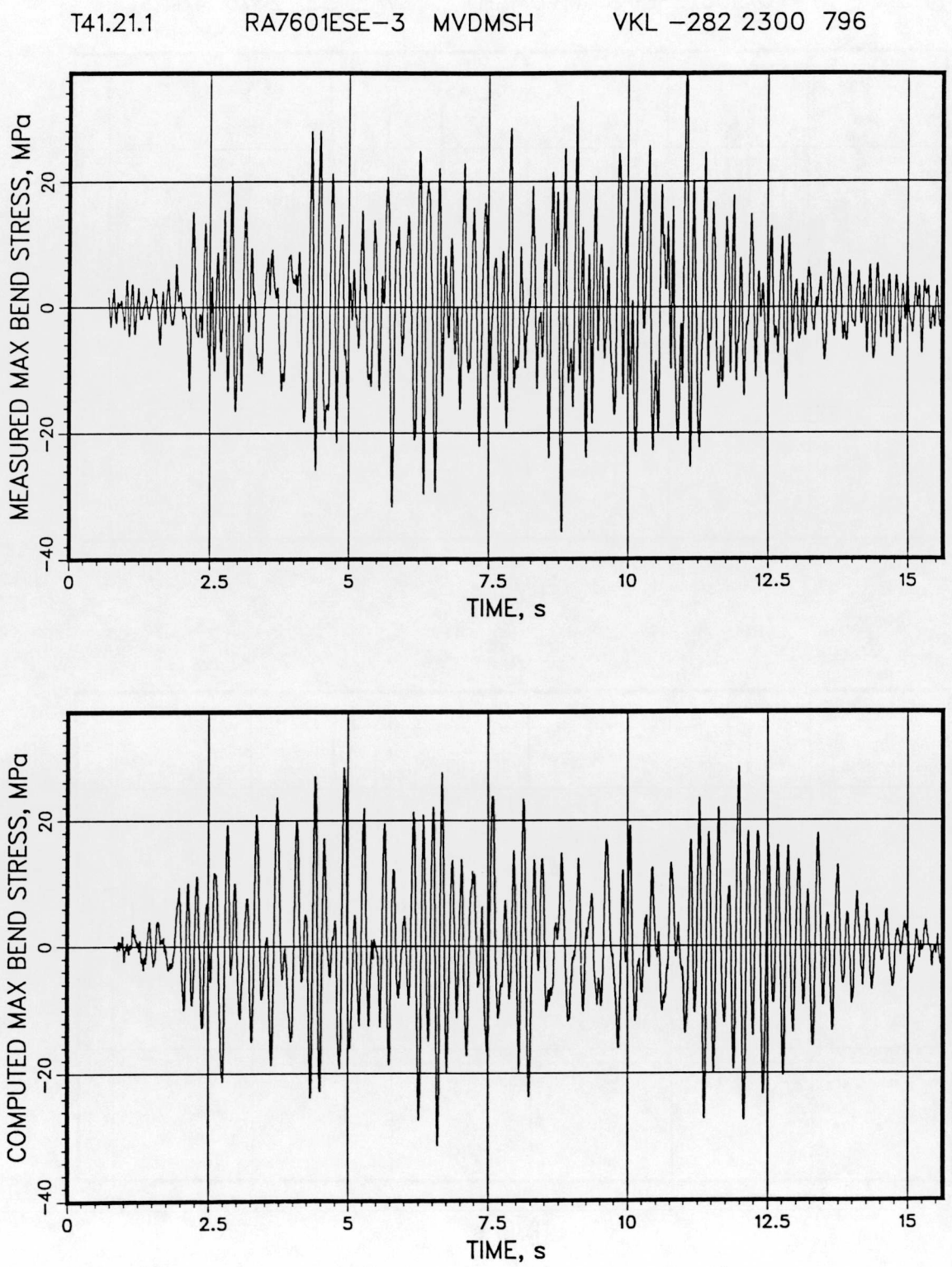
T41.21.1 RA7601ESE-3 MVDMSH VKL -282 2300 796
MEASURED MAX BEND STRESS, MPa
20
0
-20
-40
0
2.5
5
7.5
10
12.5
15
TIME, s
COMPUTED MAX BEND STRESS, MPa
20
0
-20
-40
0
2.5
5
7.5
10
12.5
15
TIME, s

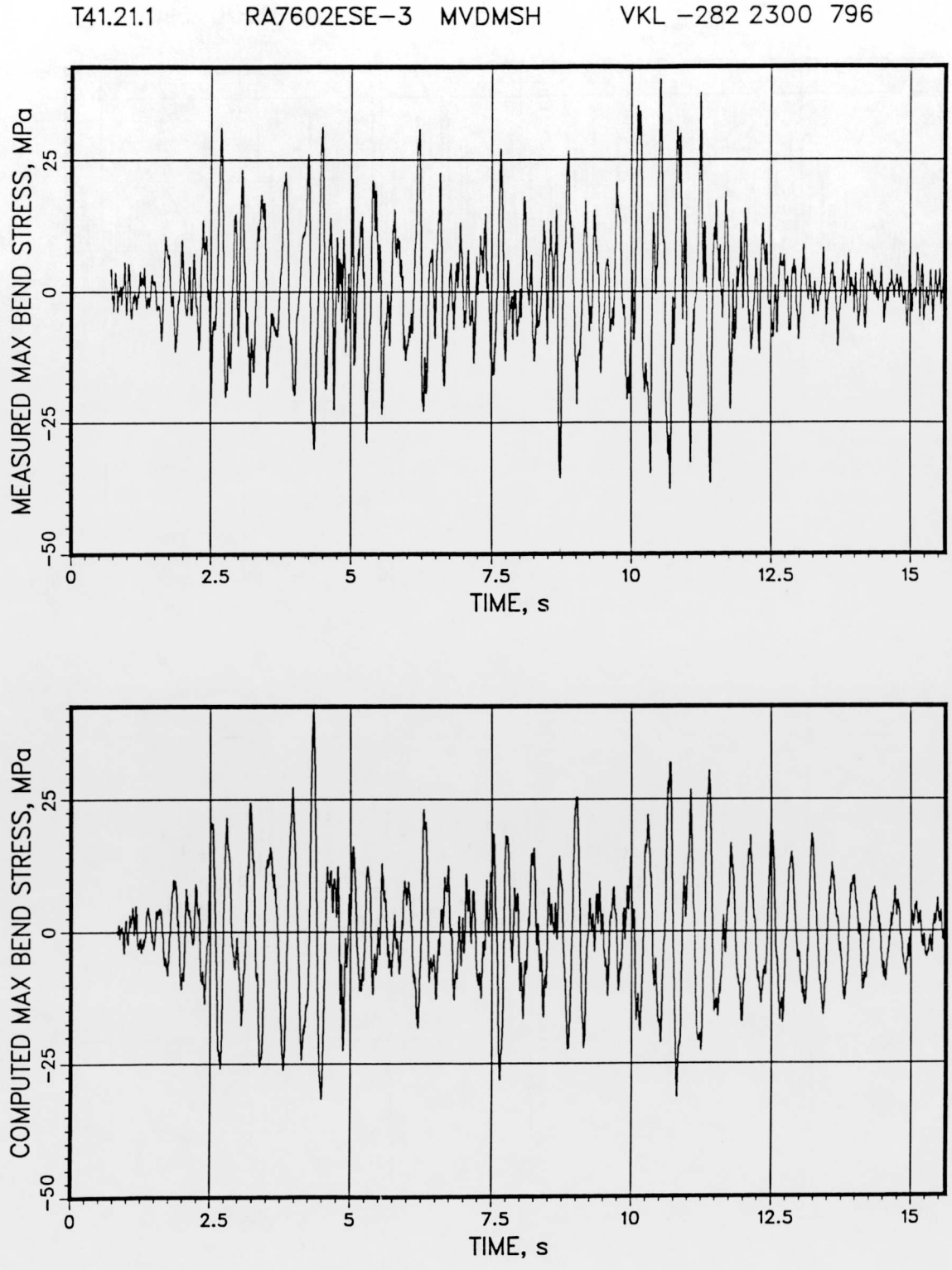
T41.21.1 RA7602ESE-3 MVDMSH VKL -282 2300 796
MEASURED MAX BEND STRESS, MPa
25
0
-25
-50
0
2.5
5
7.5
10
12.5
15
TIME, s
COMPUTED MAX BEND STRESS, MPa
25
0
-25
-50
0
2.5
5
7.5
10
12.5
15
TIME, s

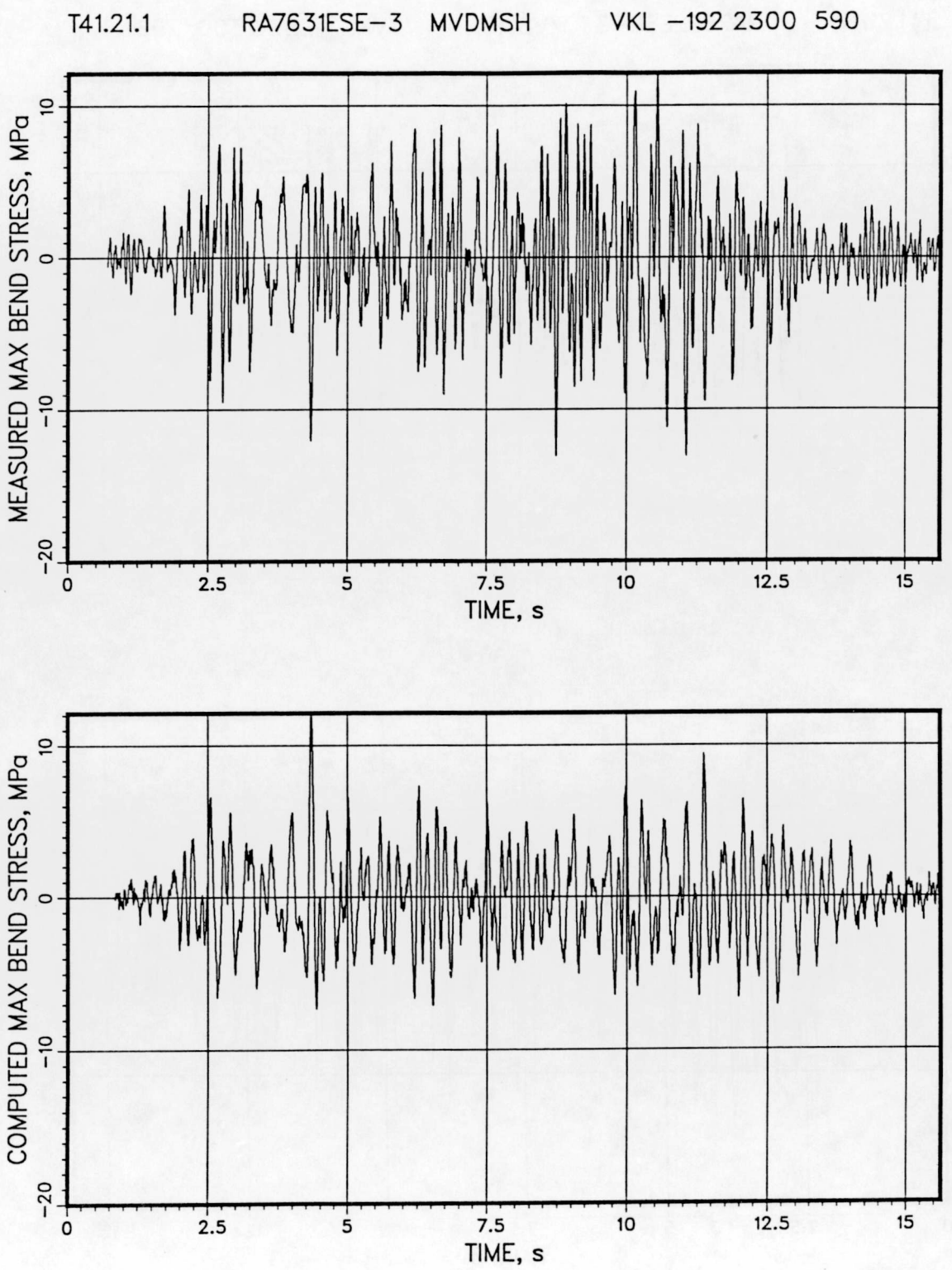
T41.21.1 RA7631ESE-3 MVDMSH VKL -192 2300 590
MEASURED MAX BEND STRESS, MPa
10
0
-10
-20
0
2.5
5
7.5
10
12.5
15
TIME, s
COMPUTED MAX BEND STRESS, MPa
10
0
-10
-20
0
2.5
5
7.5
10
12.5
15
TIME, s

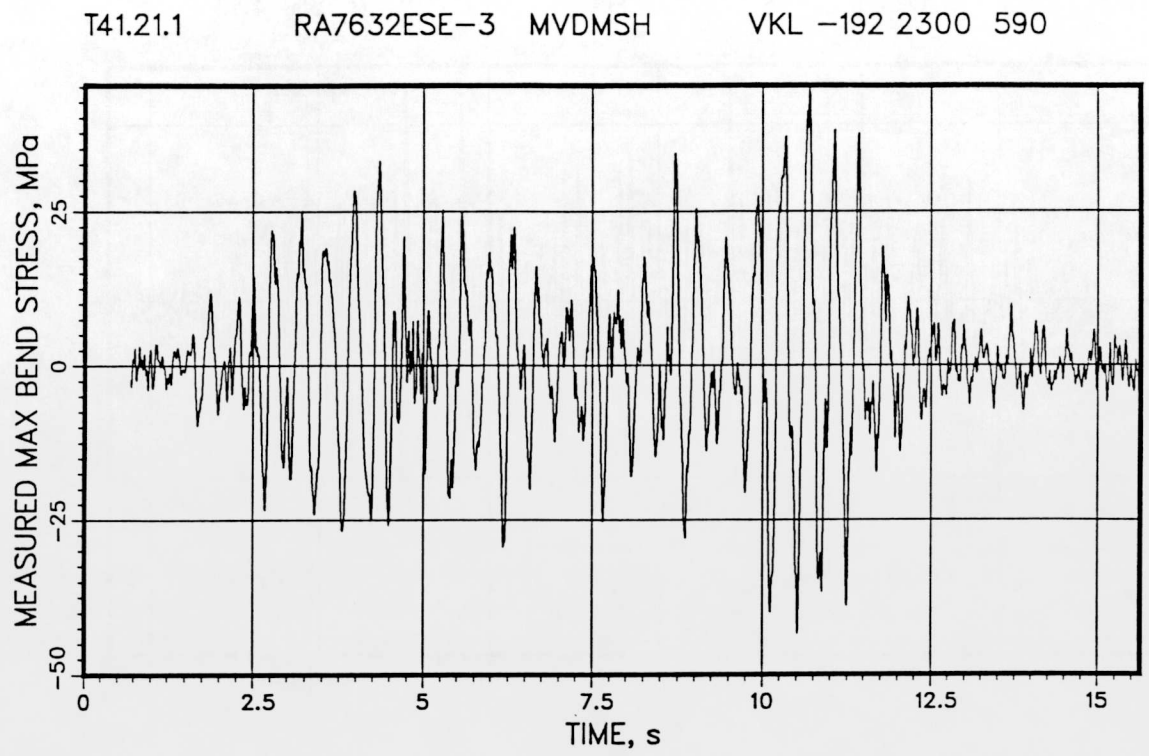
T41.21.1 RA7632ESE−3 MVDMSH VKL −192 2300 590
MEASURED MAX BEND STRESS, MPa
25
0
−25
−50
0
2.5
5
7.5
10
12.5
15
TIME, s

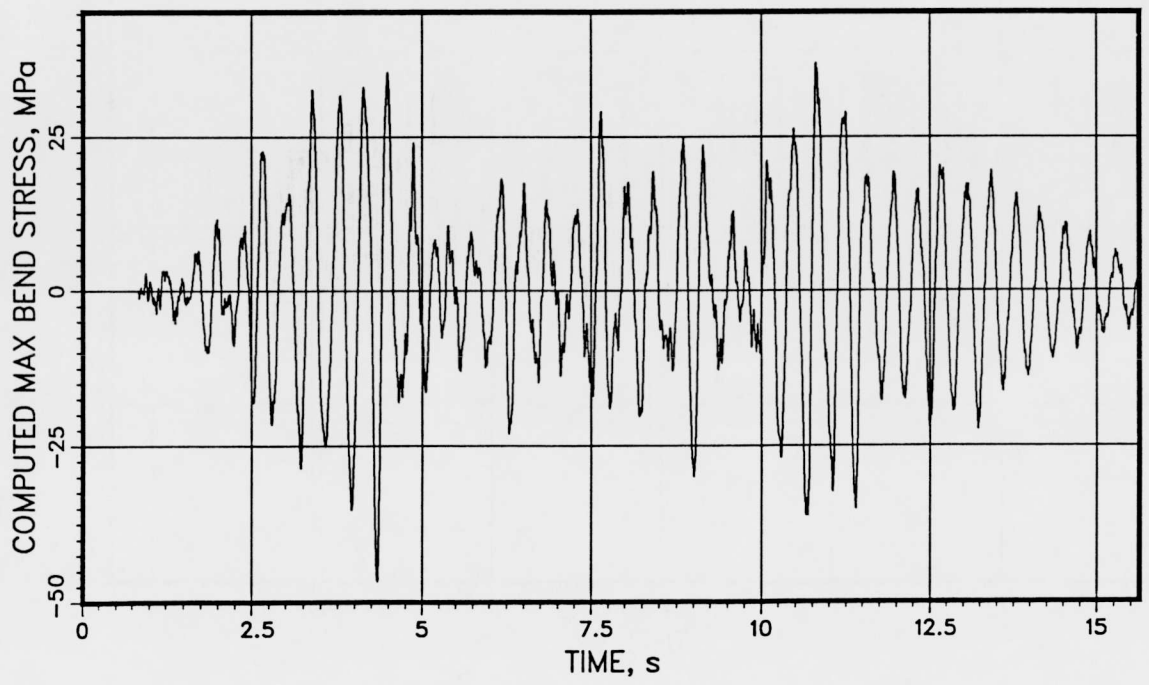
COMPUTED MAX BEND STRESS, MPa
25
0
−25
−50
0
2.5
5
7.5
10
12.5
15
TIME, s

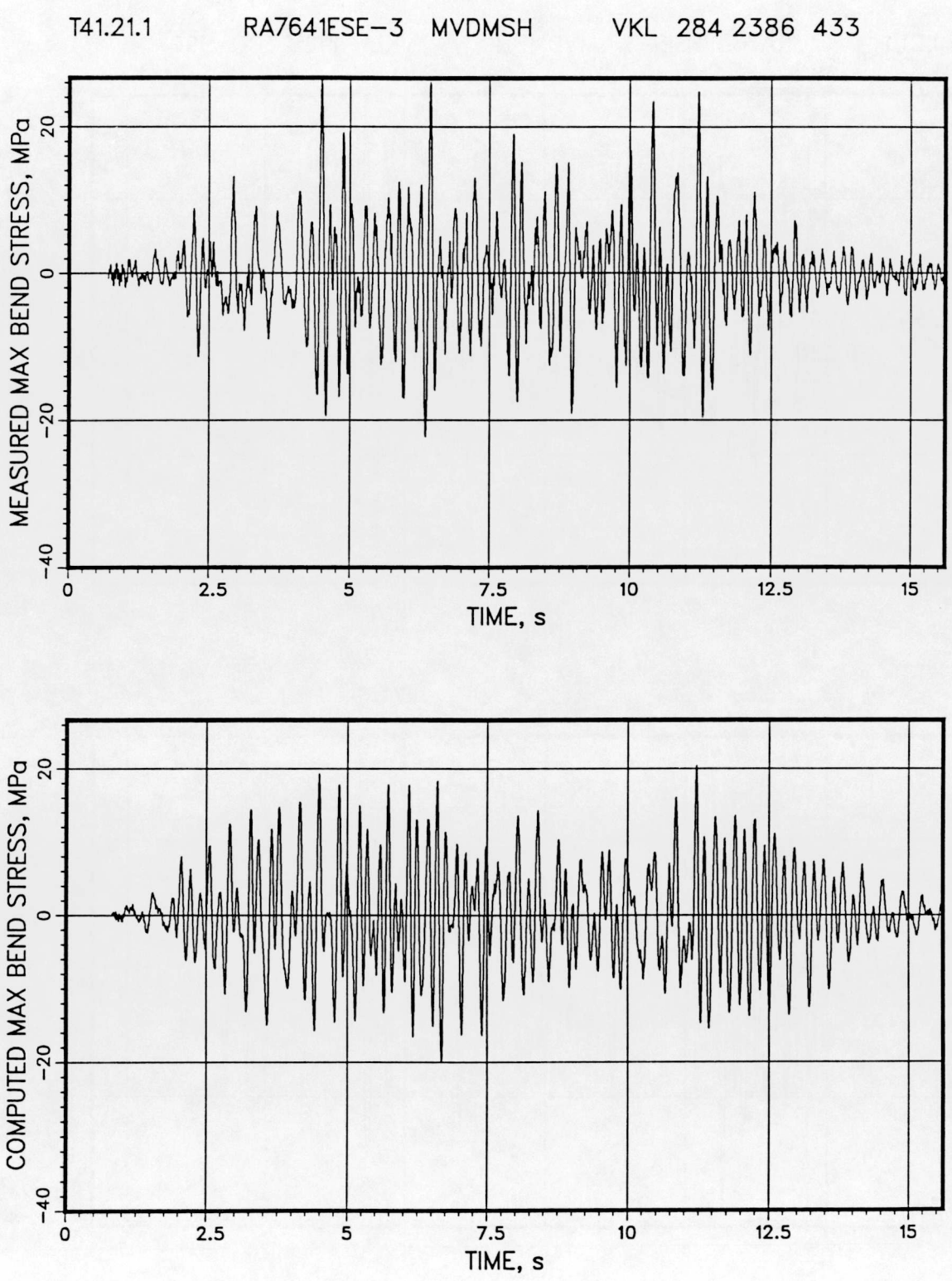
T41.21.1 RA7641ESE−3 MVDMSH VKL 284 2386 433
MEASURED MAX BEND STRESS, MPa
20
0
−20
−40
0
2.5
5
7.5
10
12.5
15
TIME, s
COMPUTED MAX BEND STRESS, MPa
20
0
−20
−40
0
2.5
5
7.5
10
12.5
15
TIME, s

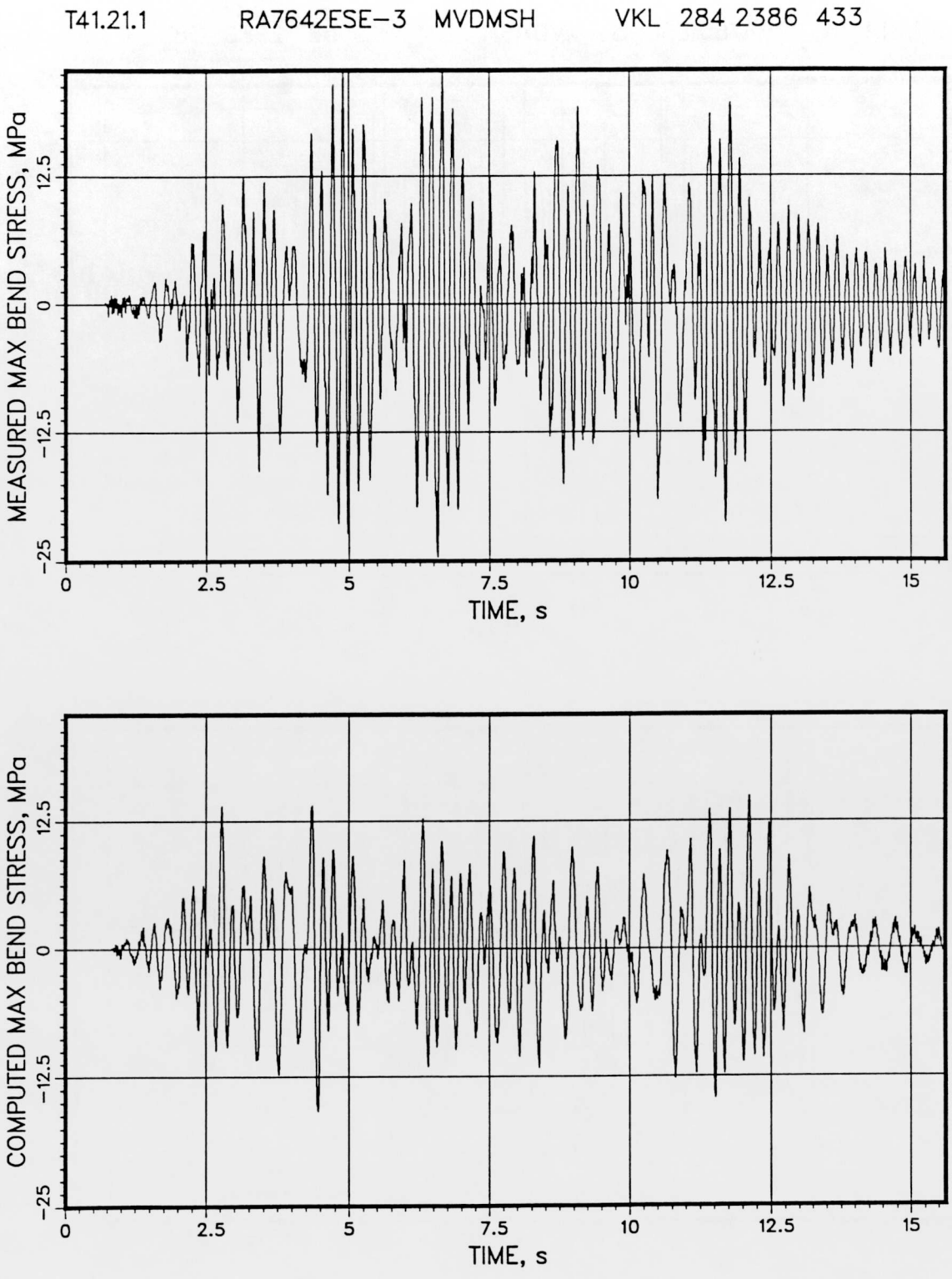
T41.21.1 RA7642ESE−3 MVDMSH VKL 284 2386 433
MEASURED MAX BEND STRESS, MPa
12.5
0
−12.5
−25
0
2.5
5
7.5
10
12.5
15
TIME, s
COMPUTED MAX BEND STRESS, MPa
12.5
0
−12.5
−25
0
2.5
5
7.5
10
12.5
15
TIME, s

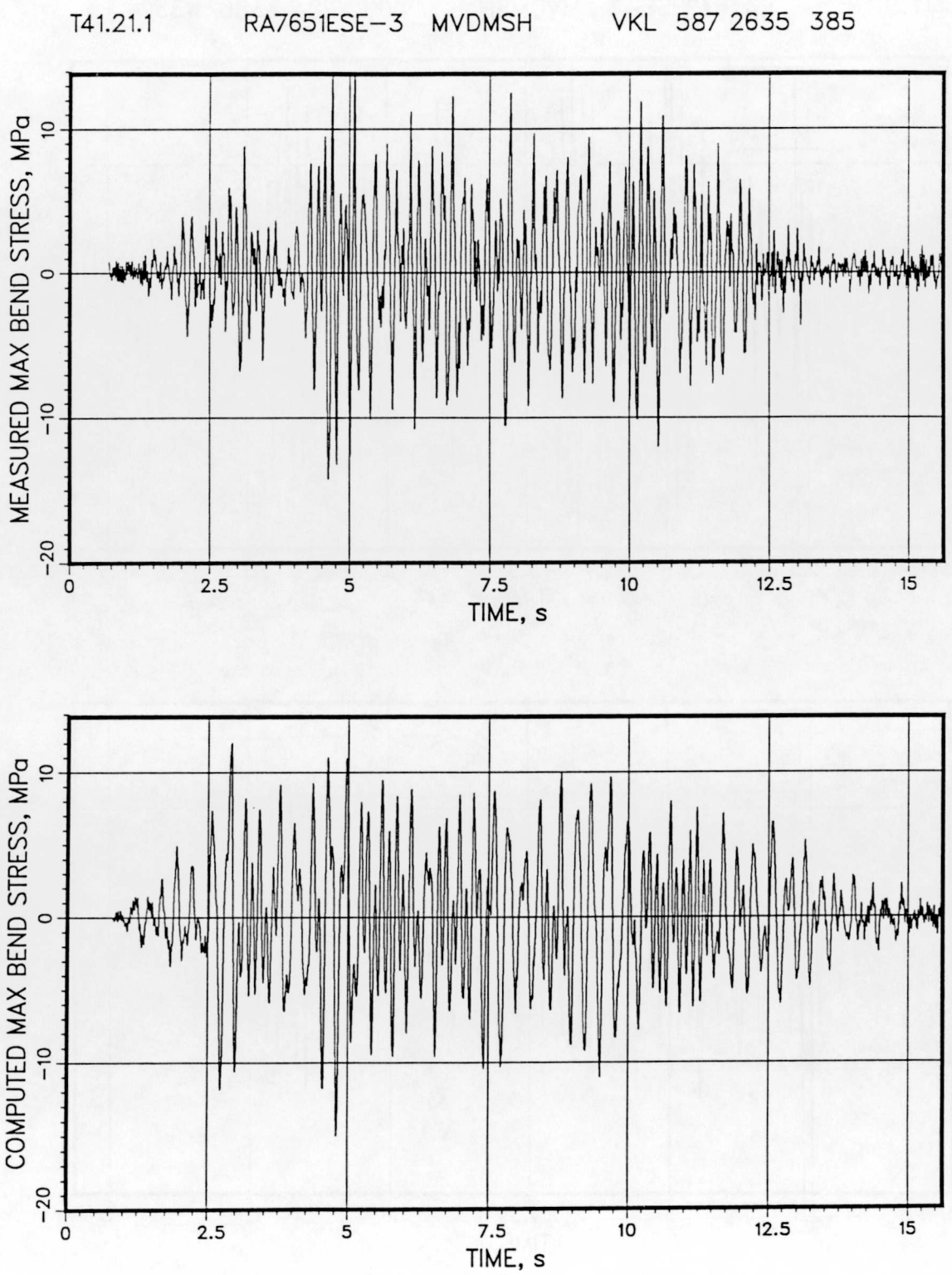
T41.21.1 RA7651ESE−3 MVDMSH VKL 587 2635 385
MEASURED MAX BEND STRESS, MPa
10
0
−10
−20
0
2.5
5
7.5
10
12.5
15
TIME, s
COMPUTED MAX BEND STRESS, MPa
10
0
−10
−20
0
2.5
5
7.5
10
12.5
15
TIME, s

T41.21.1 RA7652ESE–3 MVDMSH VKL 587 2635 385

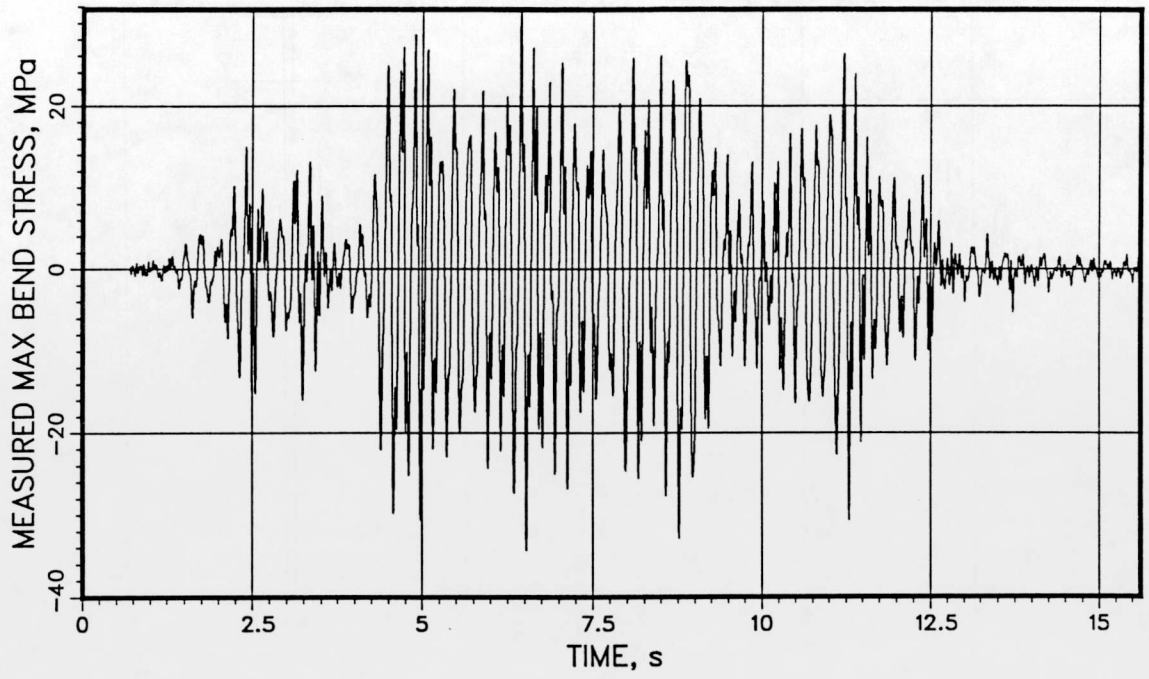

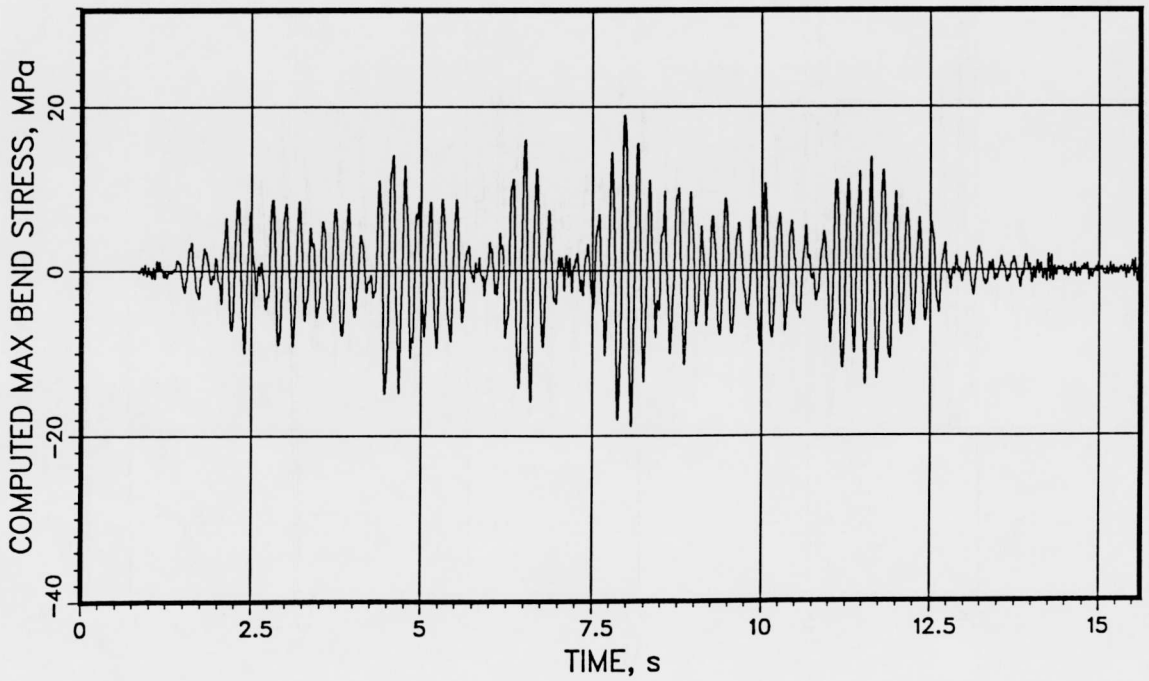

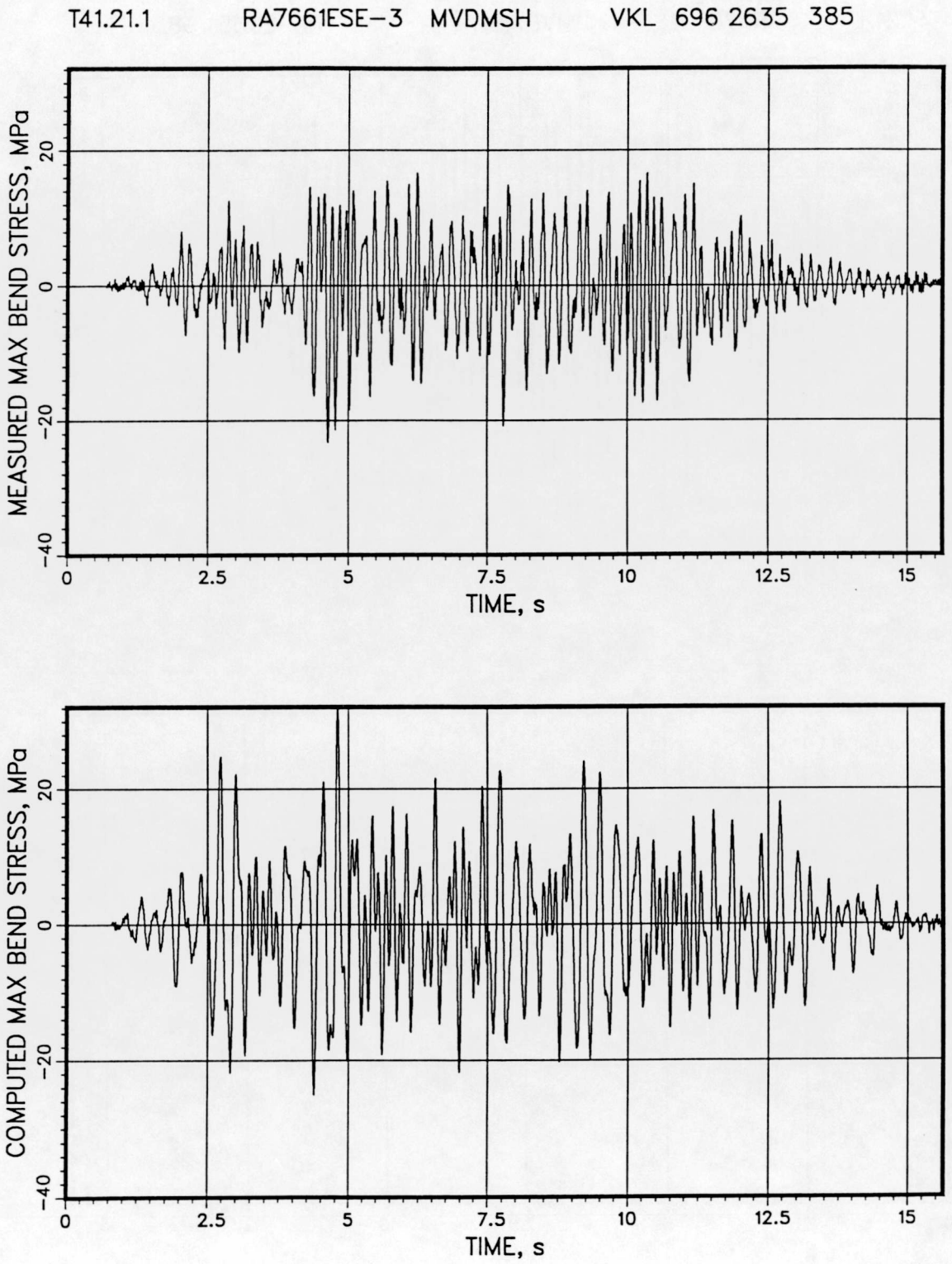
T41.21.1 RA7661ESE−3 MVDMSH VKL 696 2635 385
MEASURED MAX BEND STRESS, MPa
20
0
−20
−40
0
2.5
5
7.5
10
12.5
15
TIME, s
COMPUTED MAX BEND STRESS, MPa
20
0
−20
−40
0
2.5
5
7.5
10
12.5
15
TIME, s

T41.21.1 RA7662ESE−3 MVDMSH VKL 696 2635 385

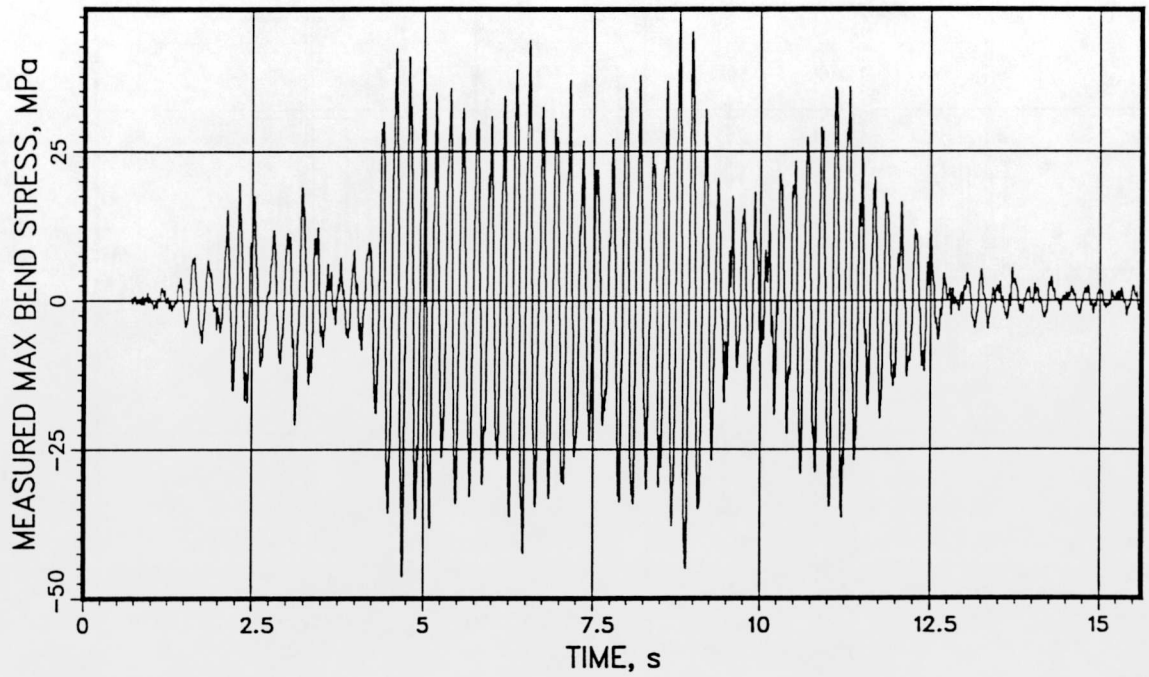

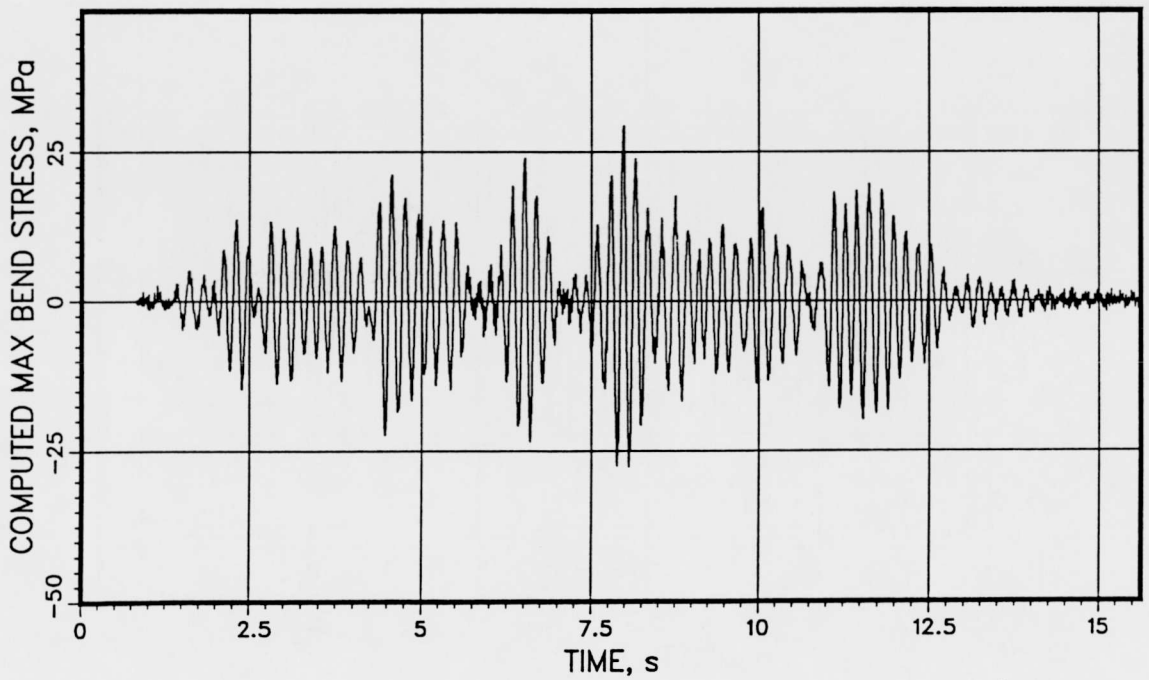

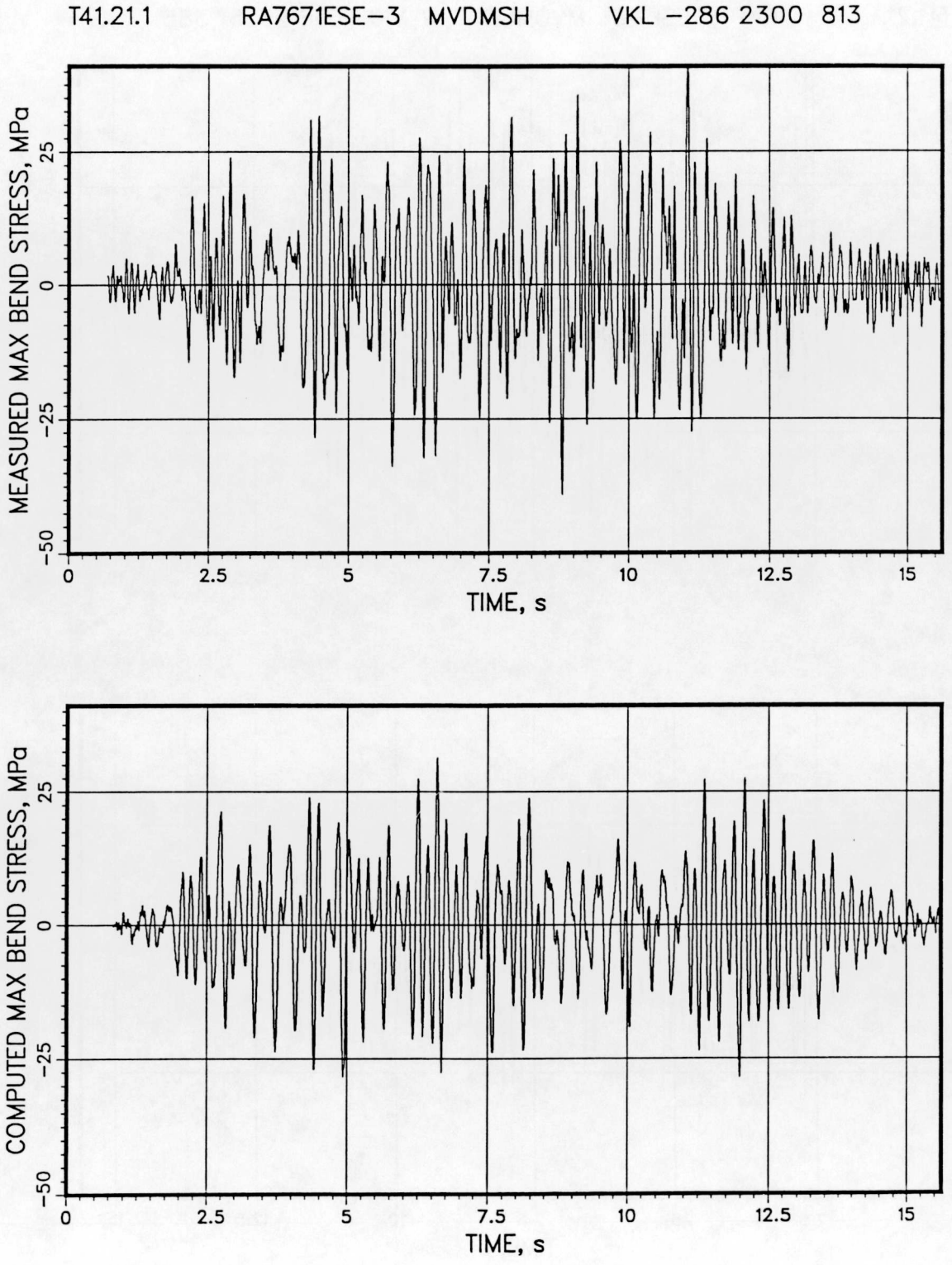
T41.21.1 RA7671ESE-3 MVDMSH VKL -286 2300 813
MEASURED MAX BEND STRESS, MPa
25
0
-25
-50
0
2.5
5
7.5
10
12.5
15
TIME, s
COMPUTED MAX BEND STRESS, MPa
25
0
-25
-50
0
2.5
5
7.5
10
12.5
15
TIME, s

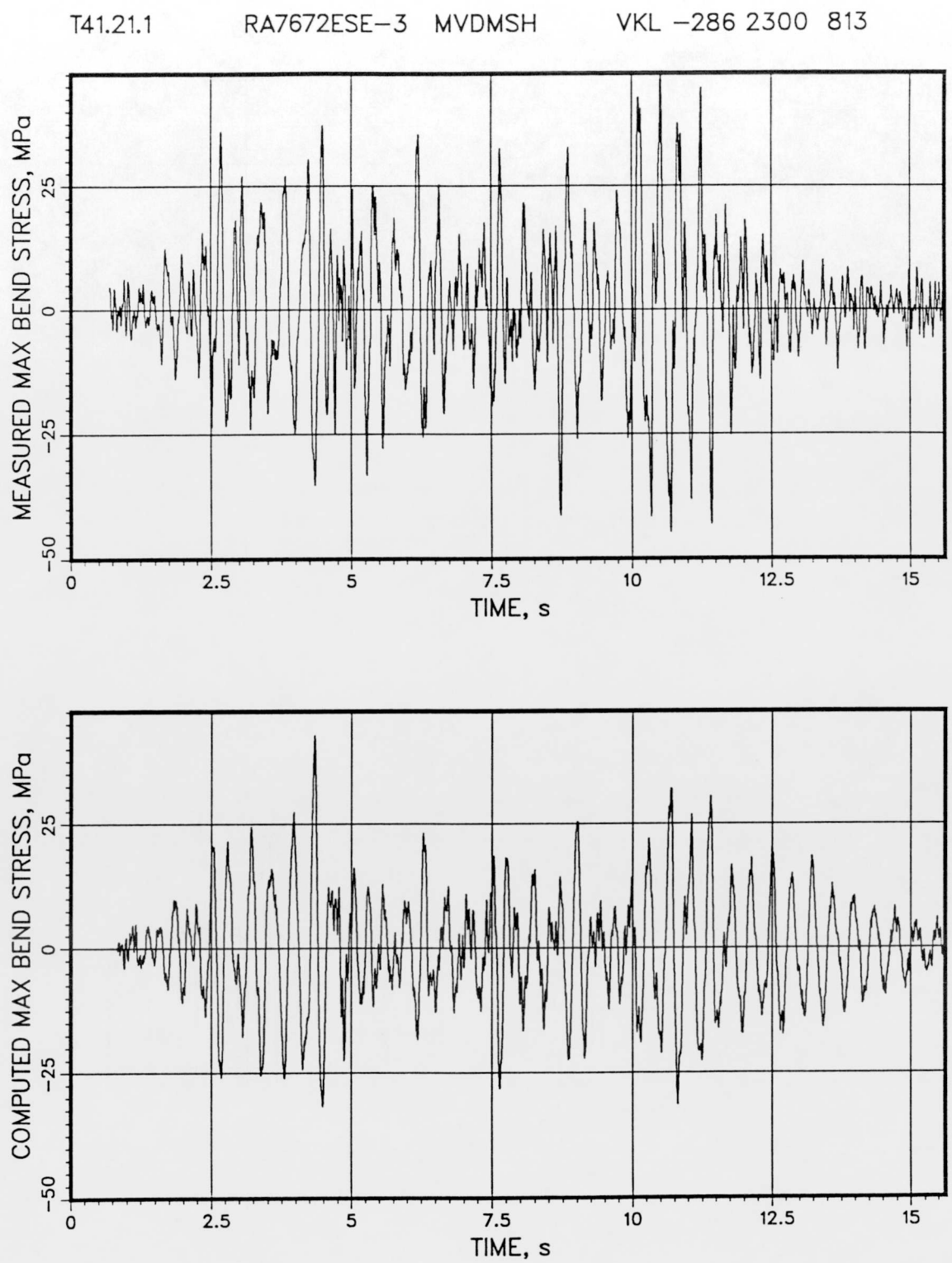
T41.21.1 RA7672ESE–3 MVDMSH VKL –286 2300 813
MEASURED MAX BEND STRESS, MPa
25
0
–25
–50
0
2.5
5
7.5
10
12.5
15
TIME, s
COMPUTED MAX BEND STRESS, MPa
25
0
–25
–50
0
2.5
5
7.5
10
12.5
15
TIME, s

Test: T41.31.2

T41.31.2 QA1001ESE-3 MVDMSH VKL 733 2561 502

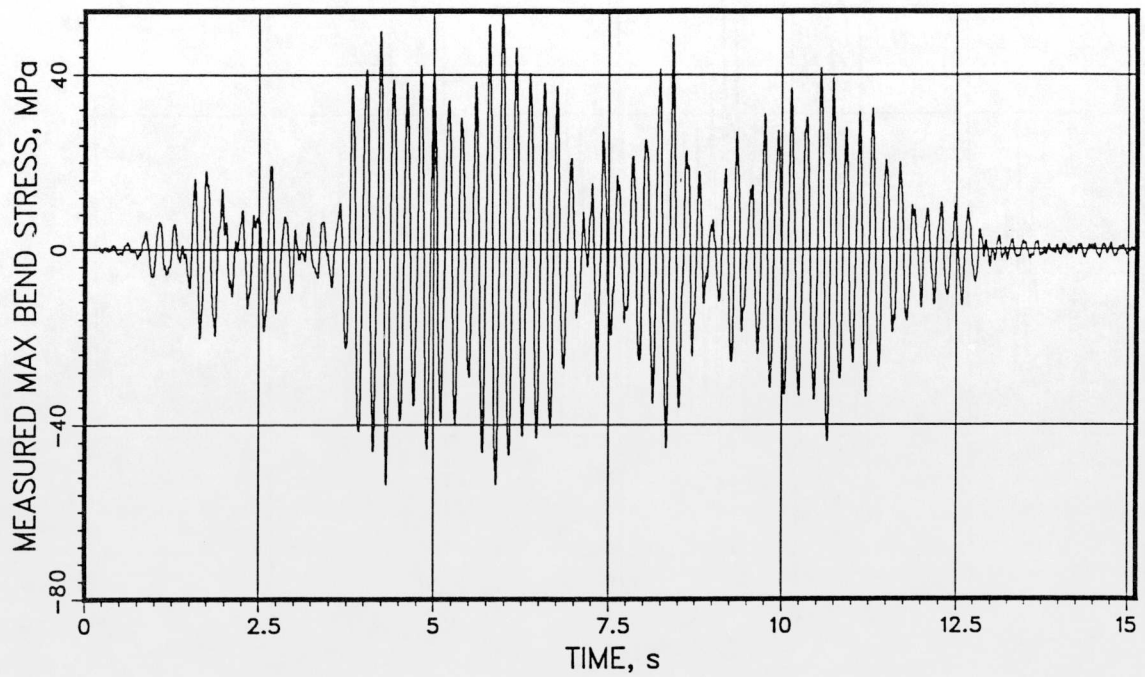

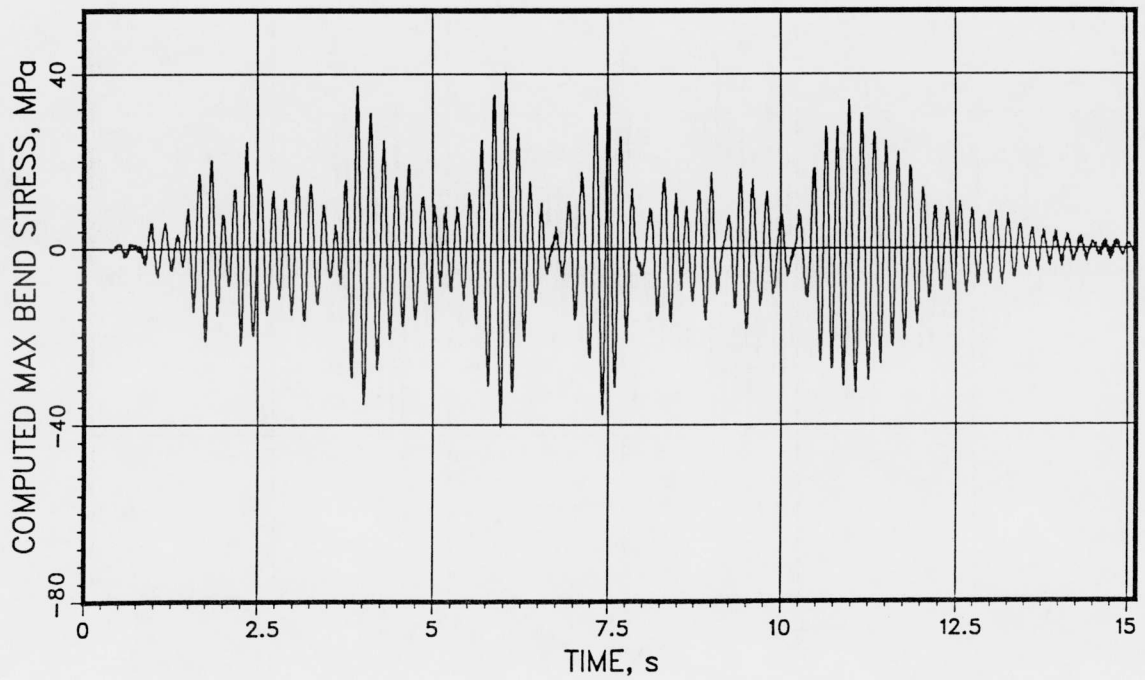

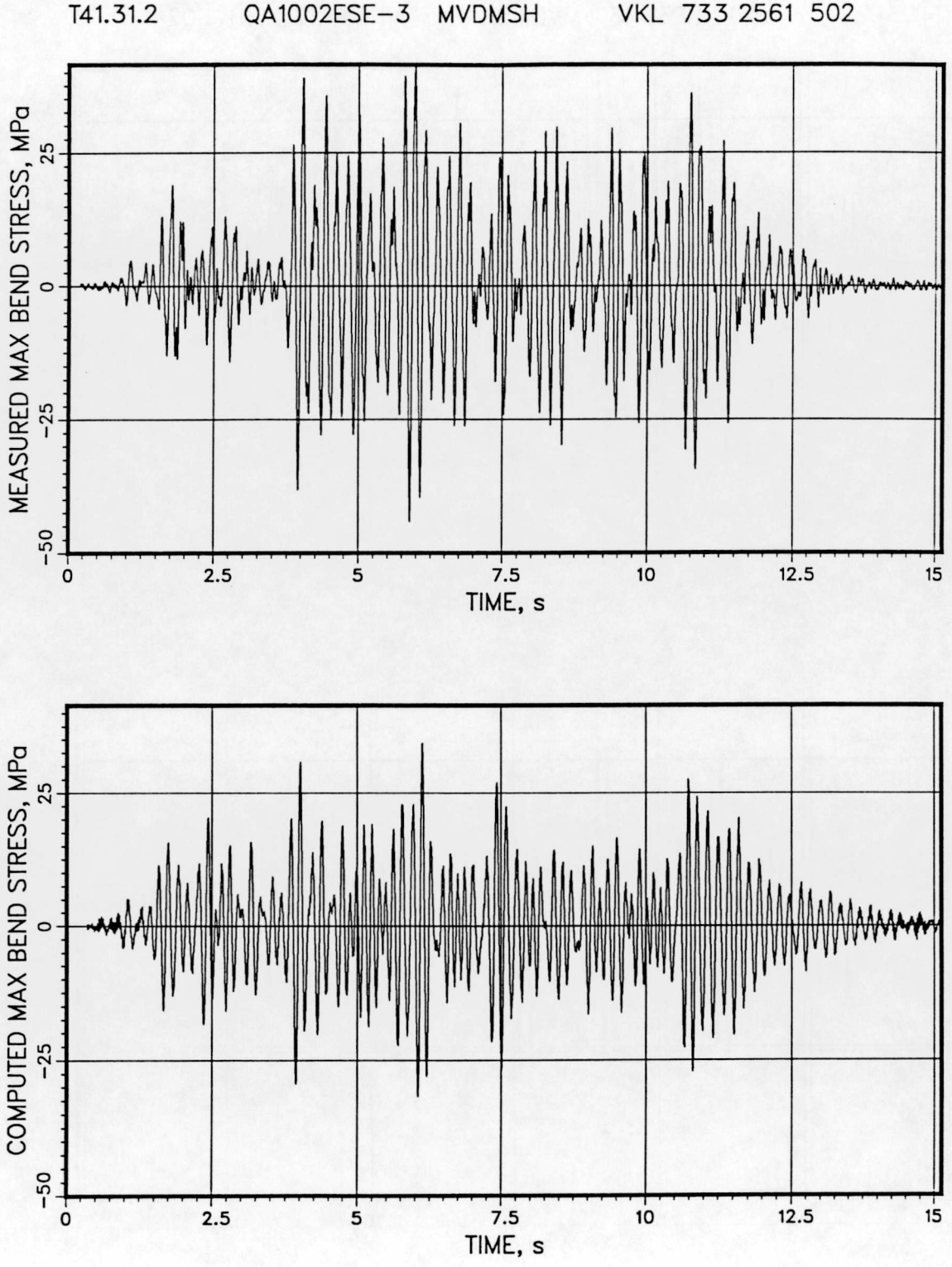
T41.31.2 QA1002ESE-3 MVDMSH VKL 733 2561 502
MEASURED MAX BEND STRESS, MPa
25
0
-25
-50
0
2.5
5
7.5
10
12.5
15
TIME, s
COMPUTED MAX BEND STRESS, MPa
25
0
-25
-50
0
2.5
5
7.5
10
12.5
15
TIME, s

T41.31.2 QA1021ESE-3 MVDMSH VKL 662 2371 604

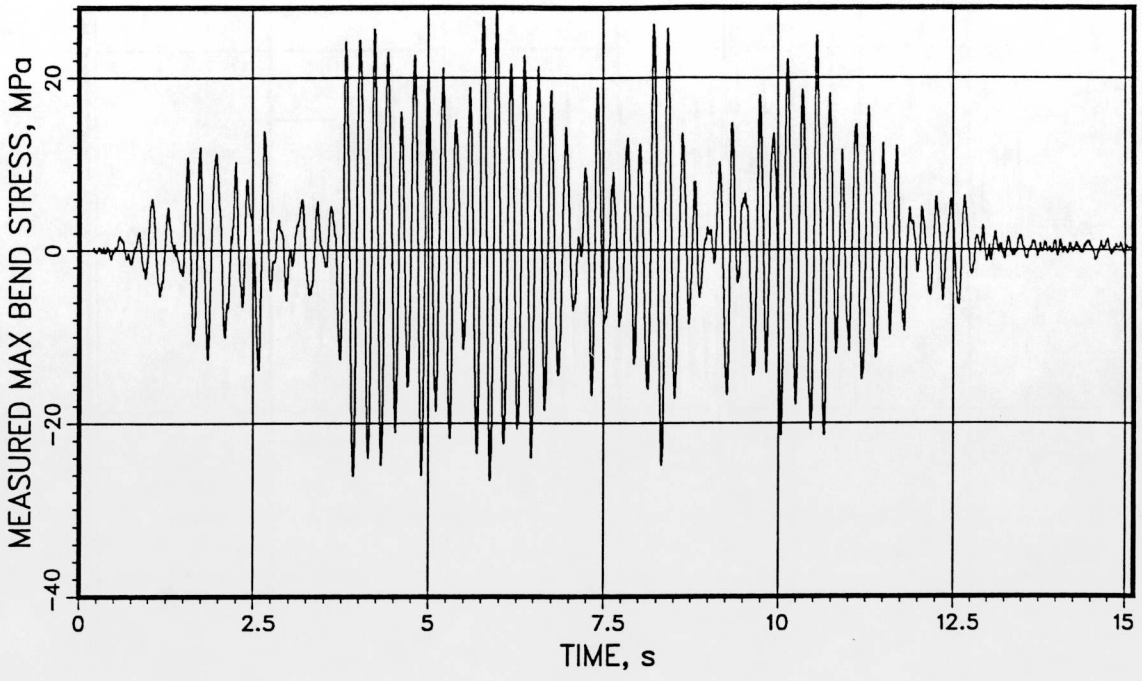

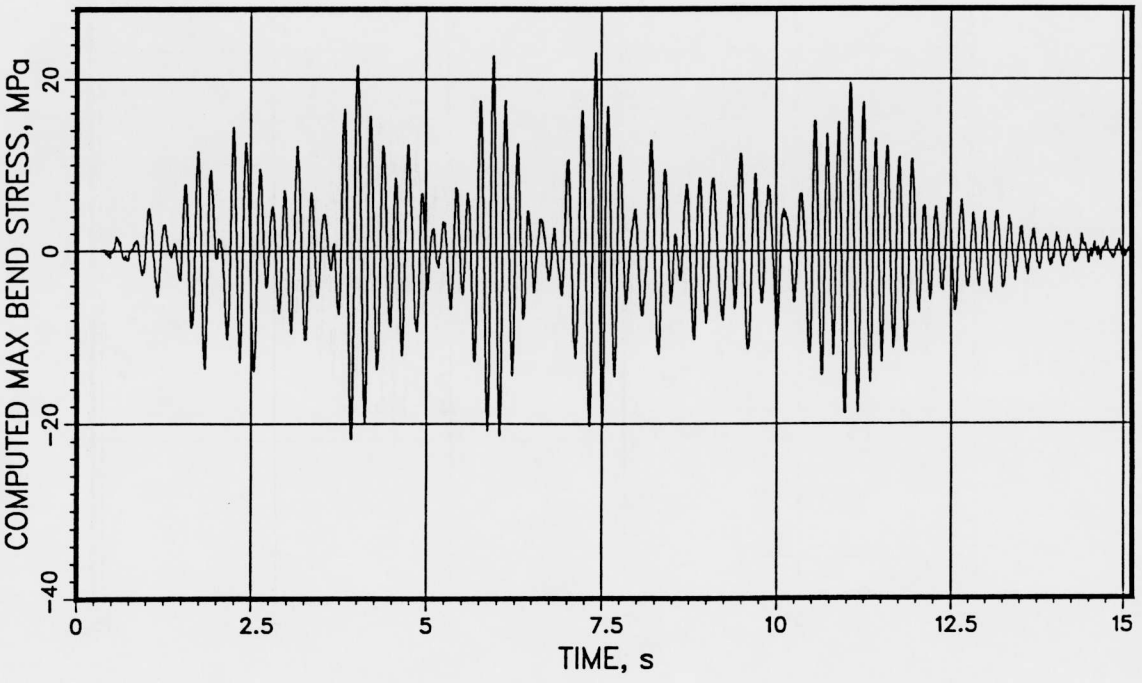

T41.31.2 QA1022ESE-3 MVDMSH VKL 662 2371 604

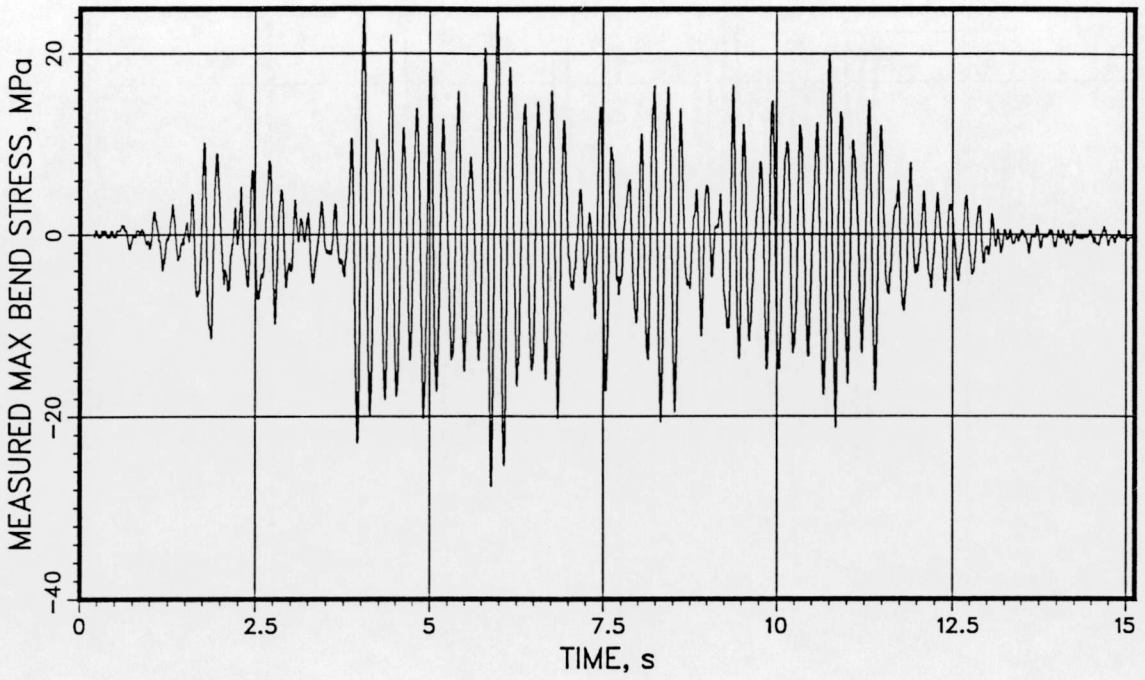

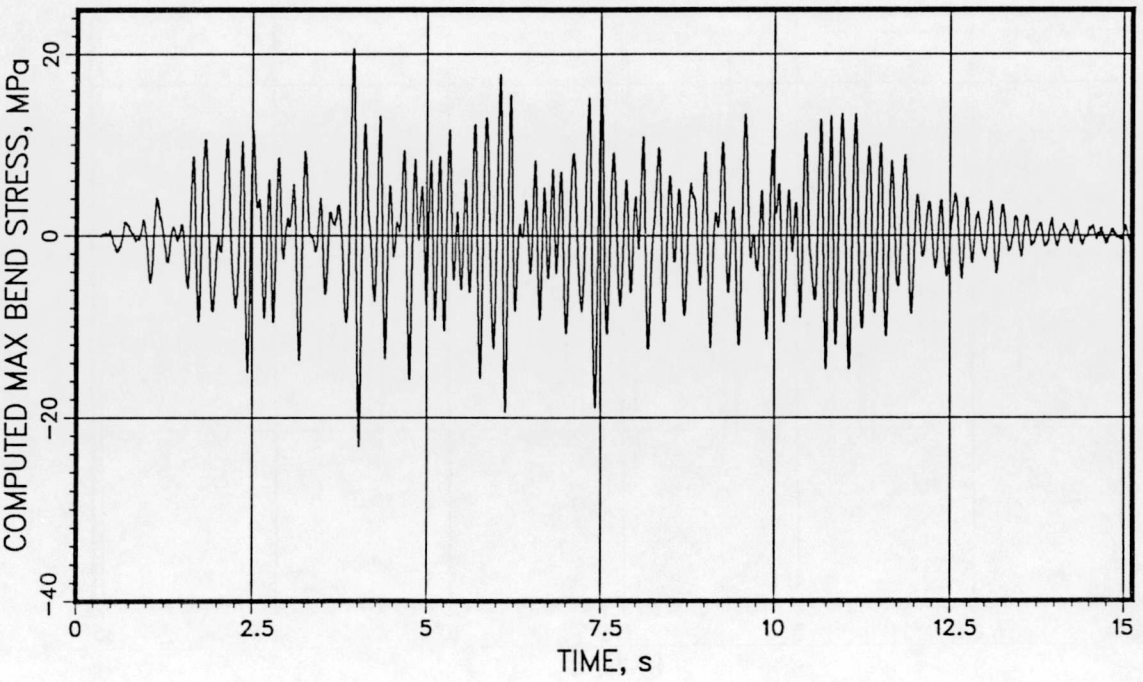

T41.31.2 QA1031ESE-3 MVDMSH VKL 586 2375 676

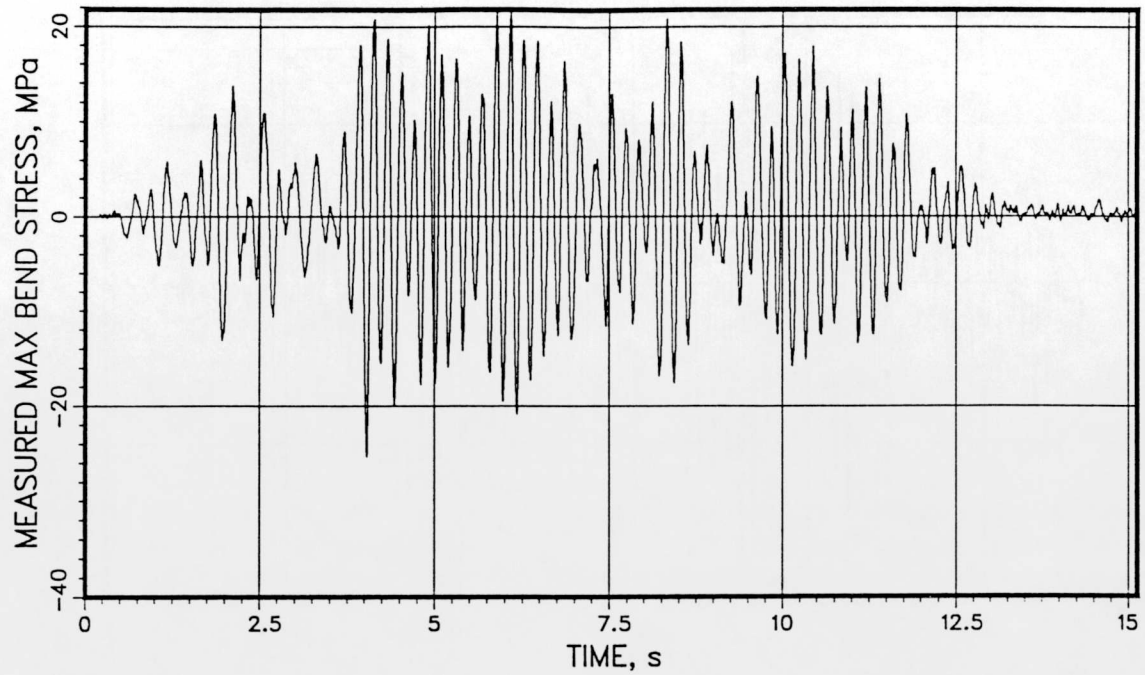

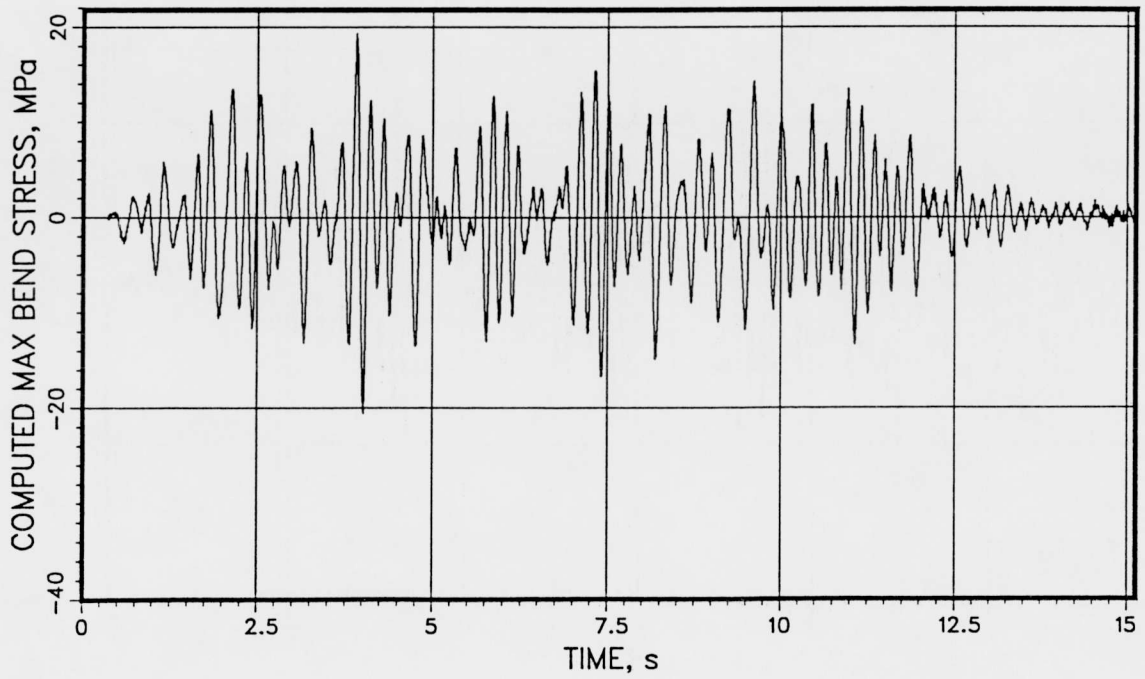

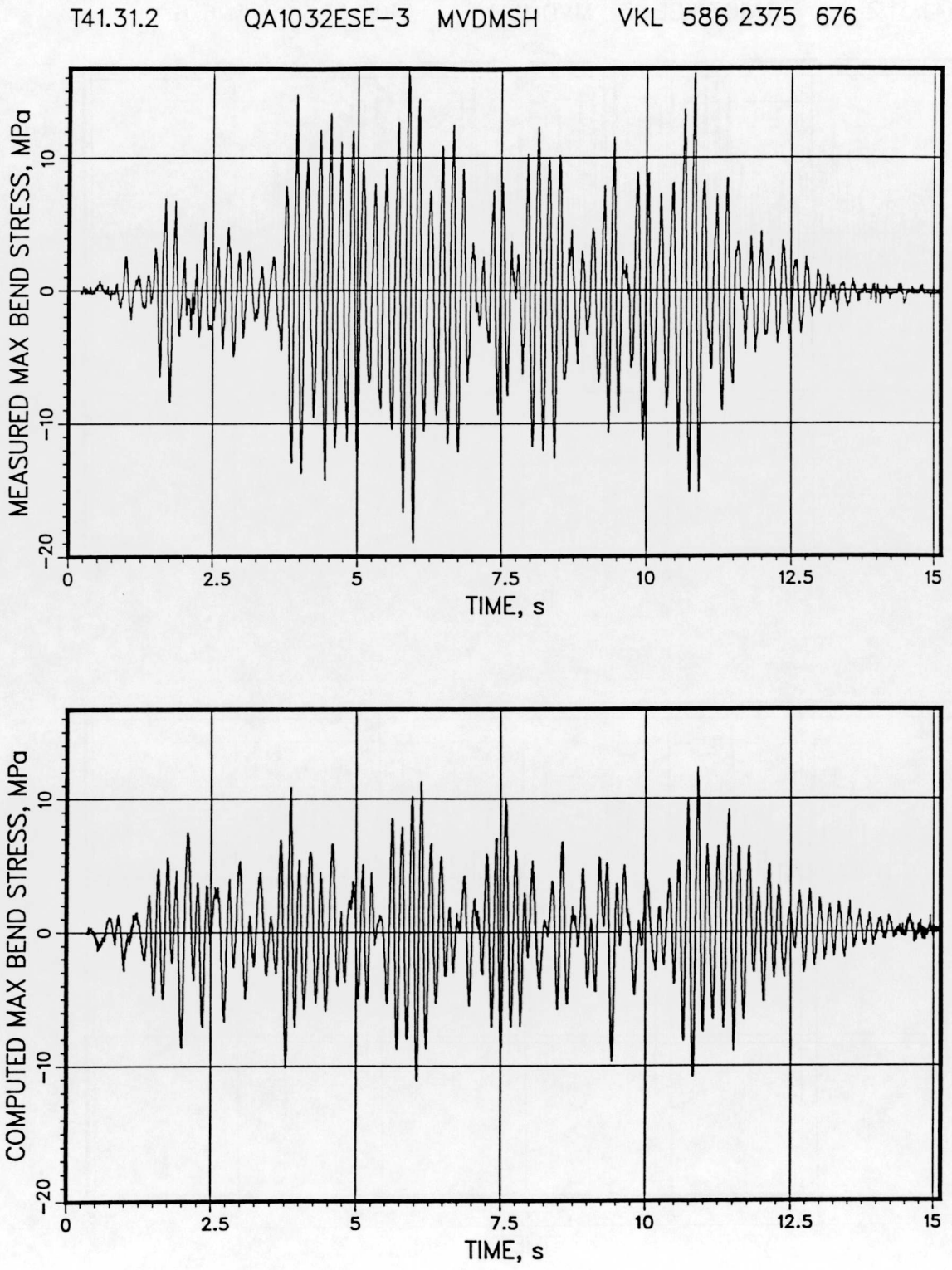
T41.31.2 QA1032ESE-3 MVDMSH VKL 586 2375 676
MEASURED MAX BEND STRESS, MPa
10
0
-10
-20
0
2.5
5
7.5
10
12.5
15
TIME, s
COMPUTED MAX BEND STRESS, MPa
10
0
-10
-20
0
2.5
5
7.5
10
12.5
15
TIME, s

T41.31.2 QA1041ESE−3 MVDMSH VKL 424 2300 770

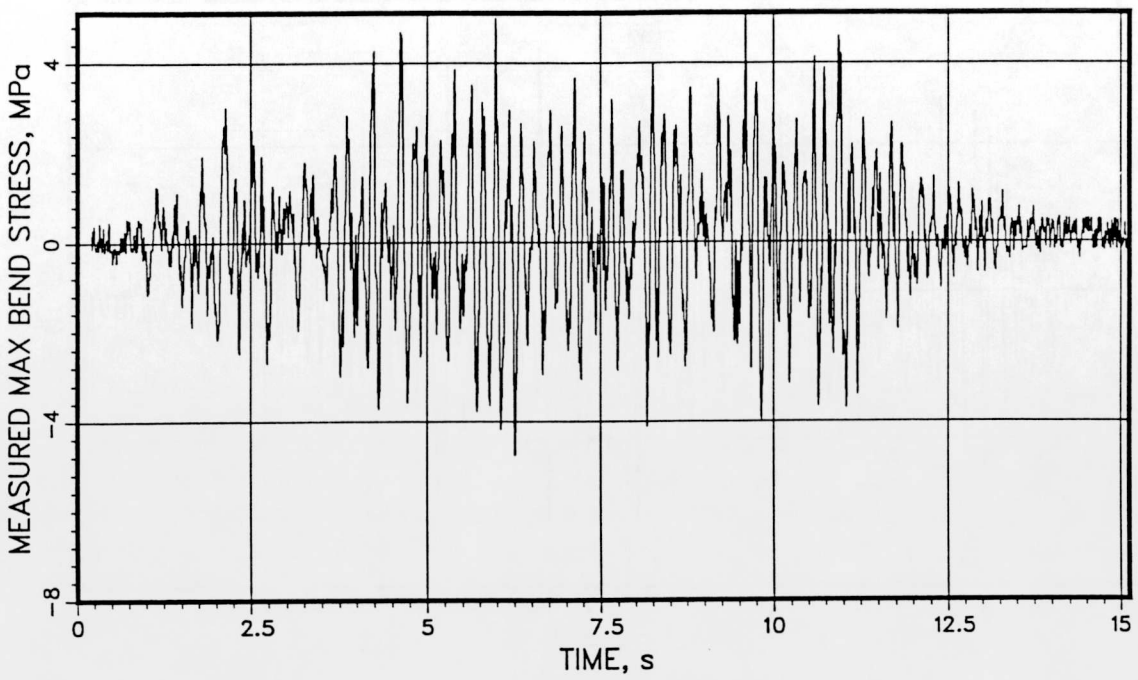

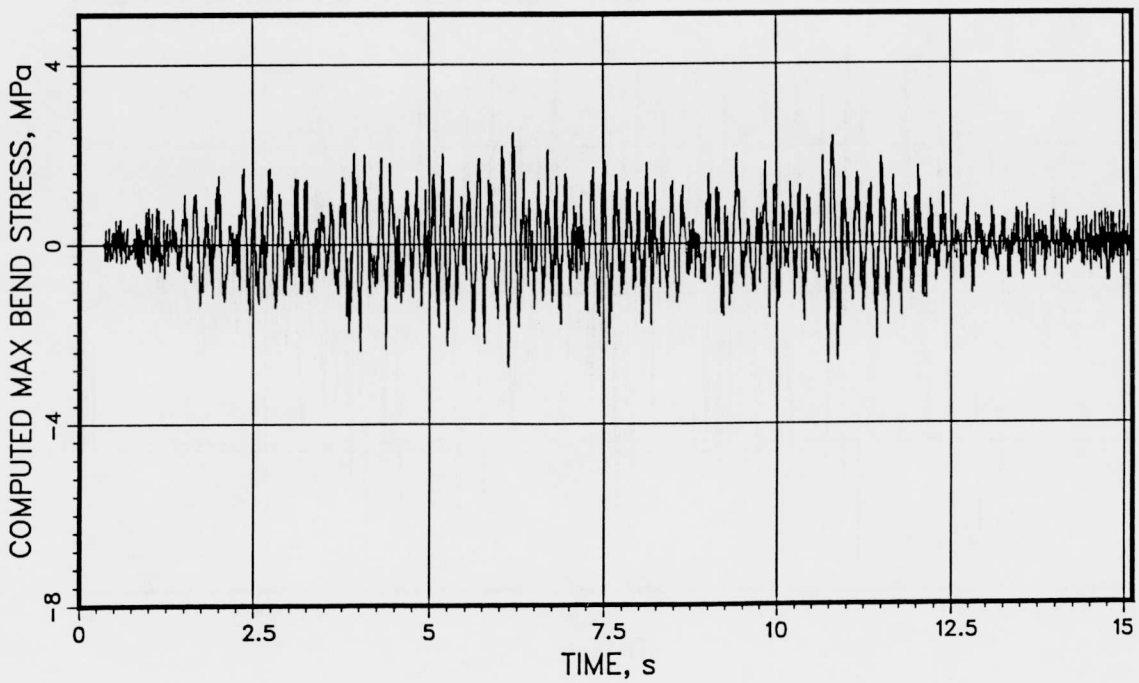

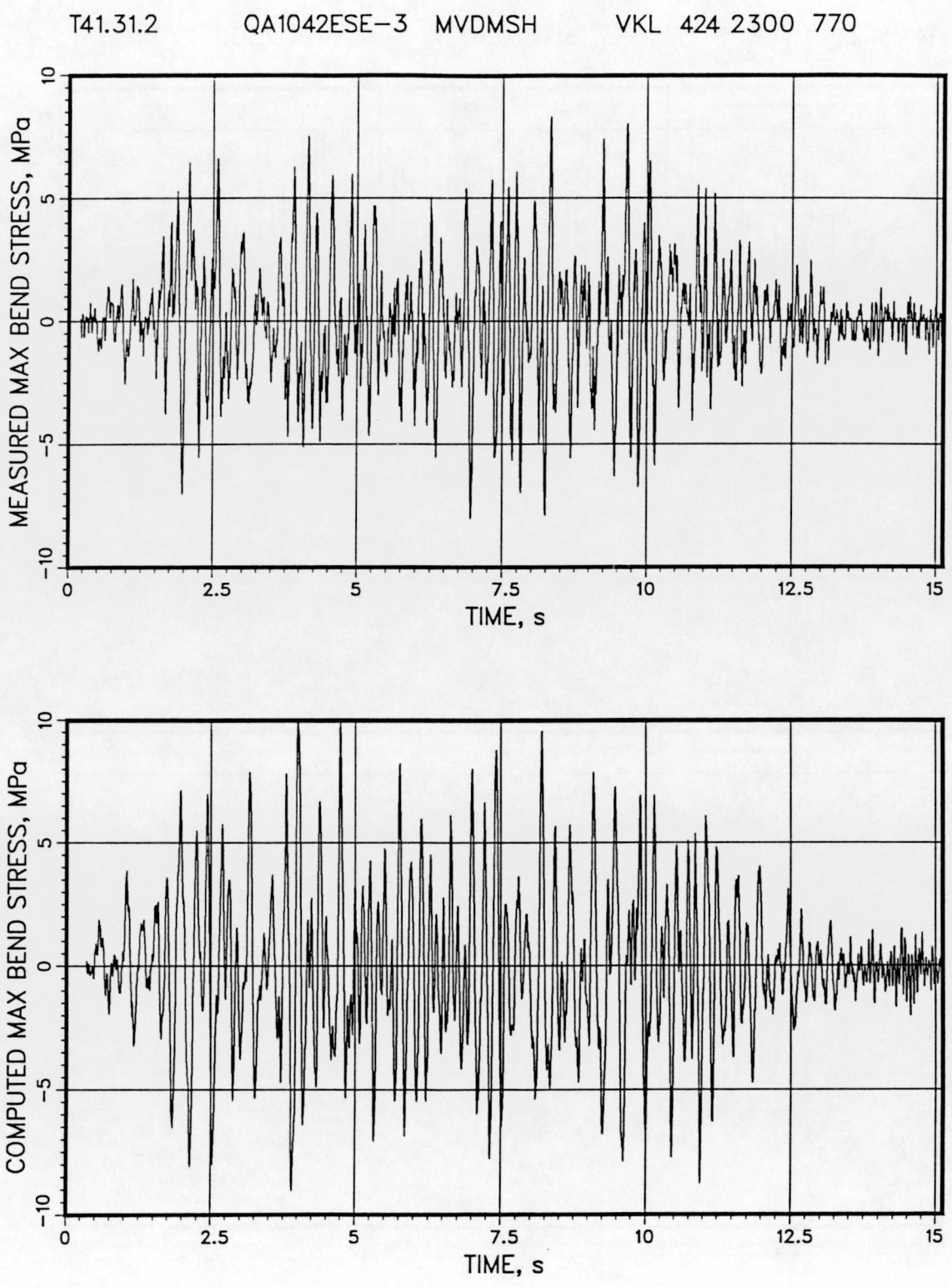
T41.31.2 QA1042ESE-3 MVDMSH VKL 424 2300 770
MEASURED MAX BEND STRESS, MPa
10
5
0
-5
-10
0
2.5
5
7.5
10
12.5
15
TIME, s
COMPUTED MAX BEND STRESS, MPa
10
5
0
-5
-10
0
2.5
5
7.5
10
12.5
15
TIME, s

T41.31.2 QA1061ESE−3 MVDMSH VKL 357 2376 484

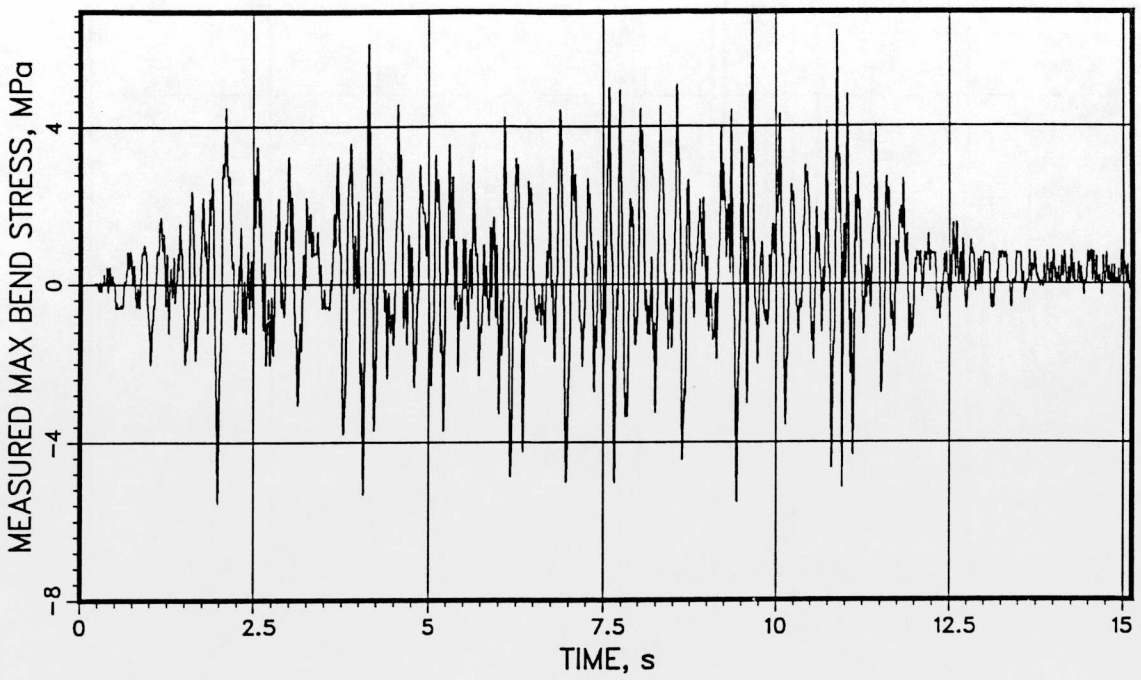

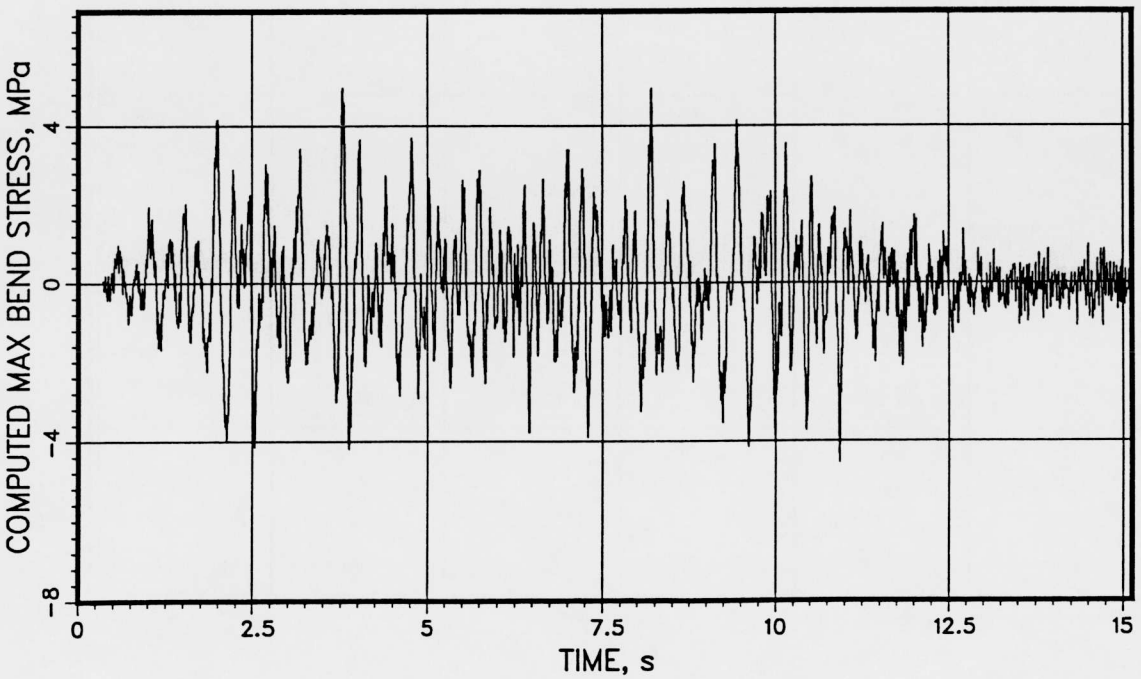

T41.31.2 QA1062ESE−3 MVDMSH VKL 357 2376 484

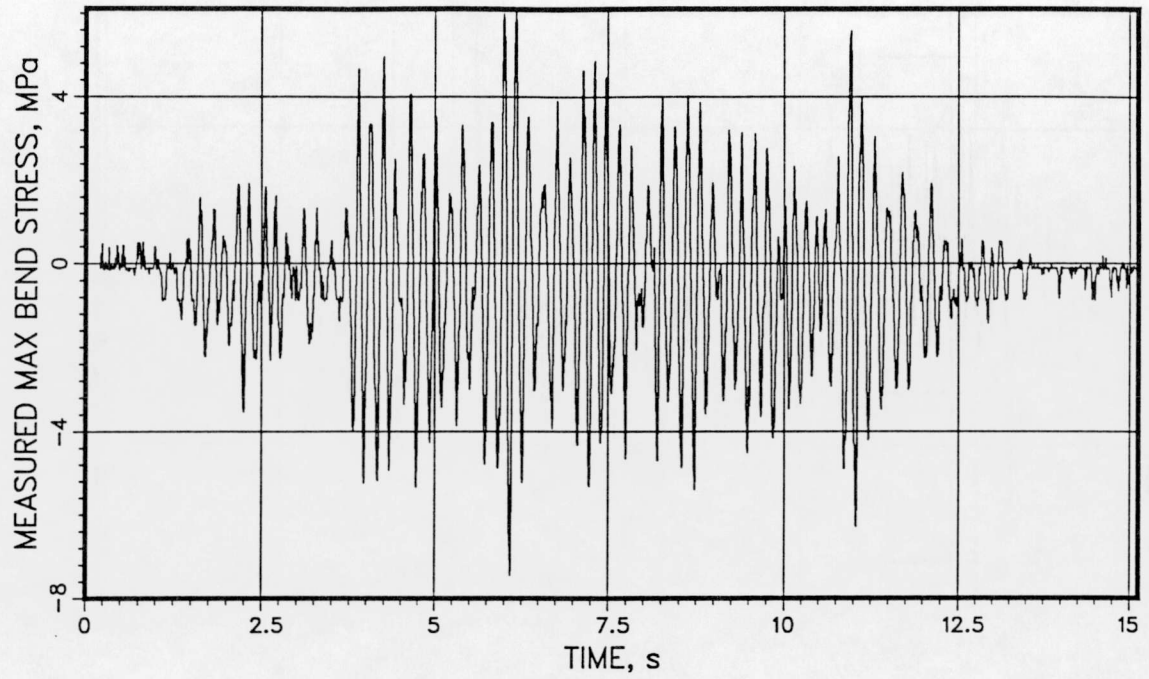

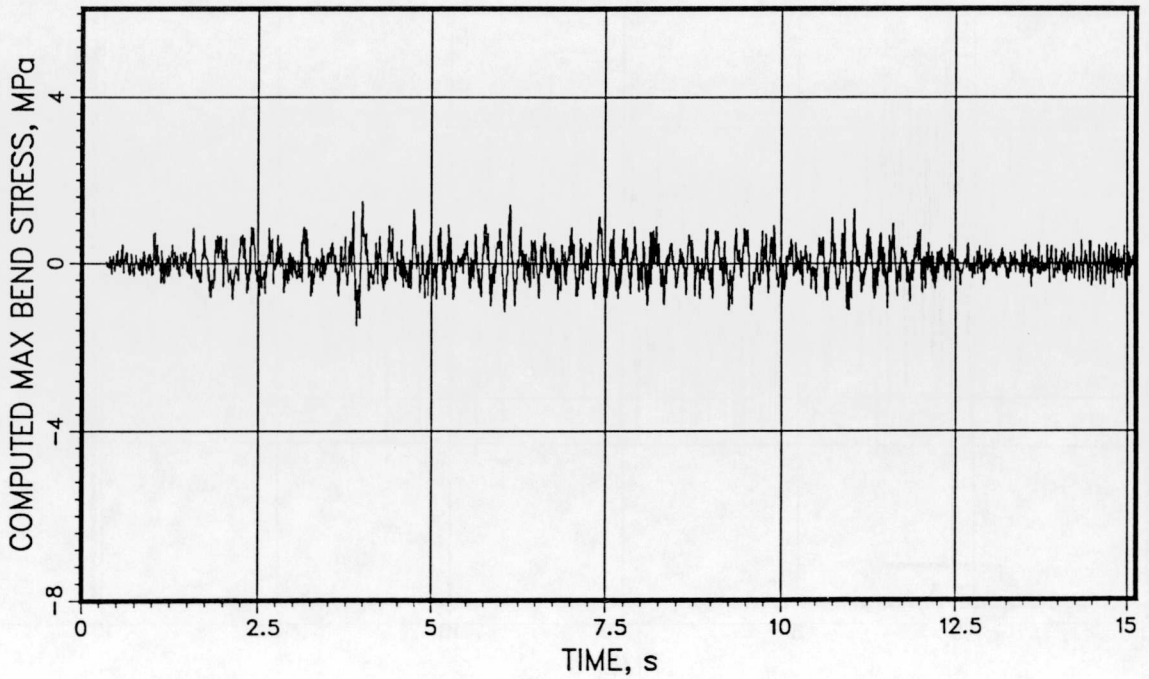

T41.31.2 RA7601ESE−3 MVDMSH VKL −282 2300 796

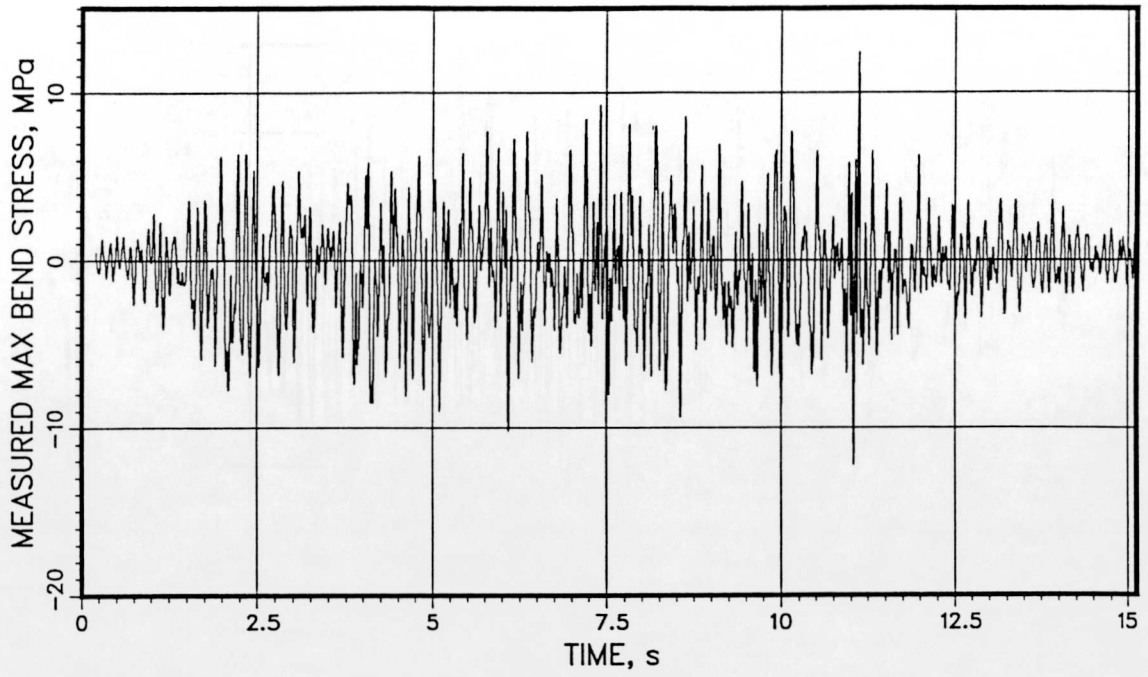

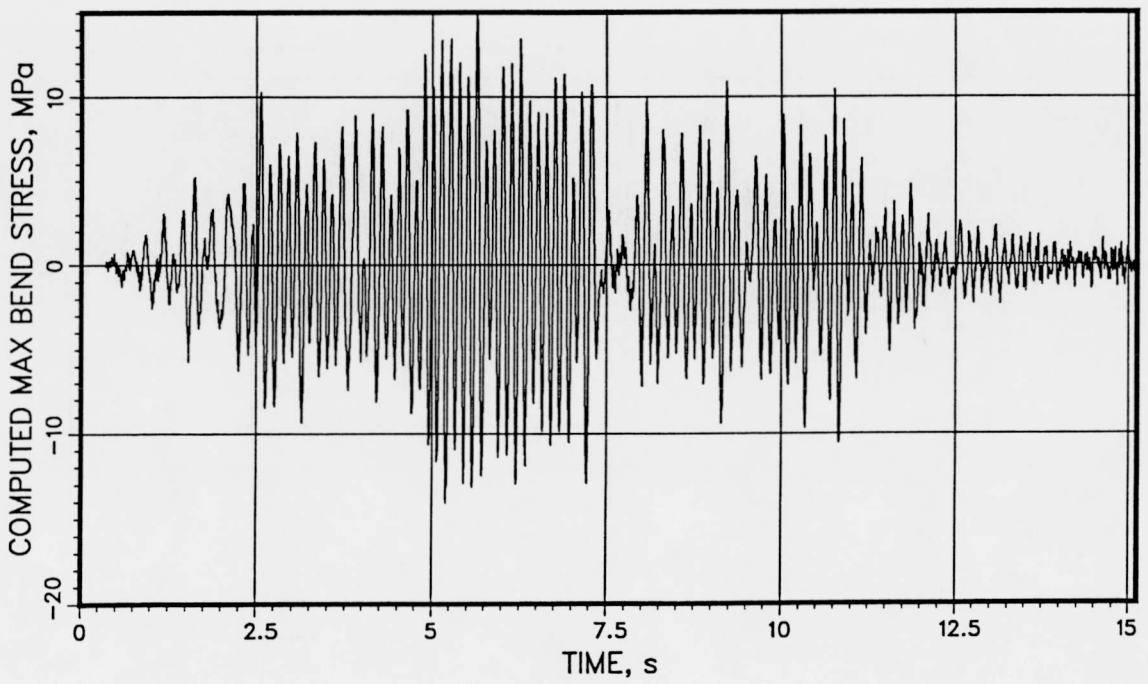

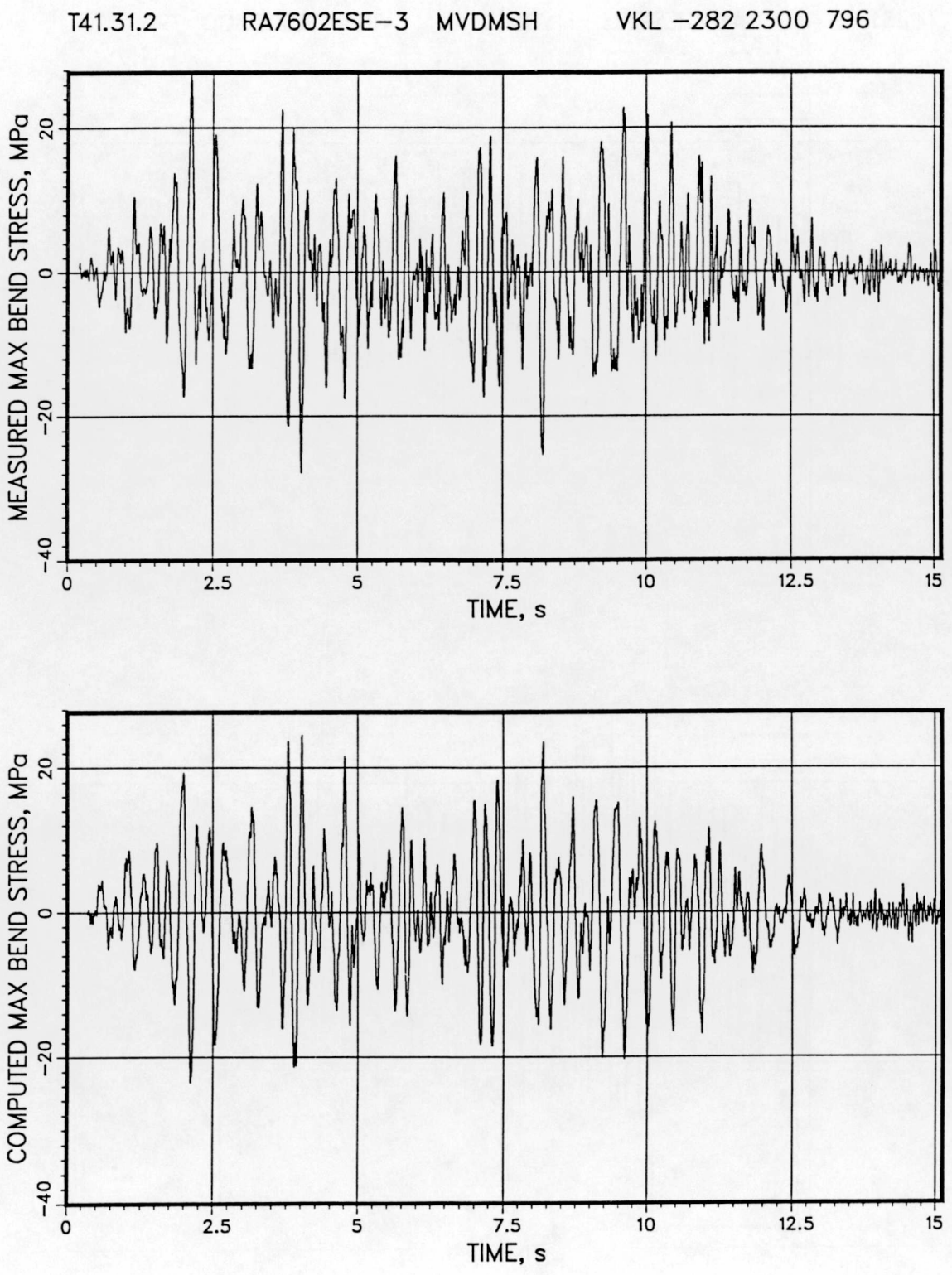
T41.31.2 RA7602ESE-3 MVDMSH VKL -282 2300 796
MEASURED MAX BEND STRESS, MPa
20
0
-20
-40
0
2.5
5
7.5
10
12.5
15
TIME, s
COMPUTED MAX BEND STRESS, MPa
20
0
-20
-40
0
2.5
5
7.5
10
12.5
15
TIME, s

T41.31.2 RA7631ESE−3 MVDMSH VKL −192 2300 590

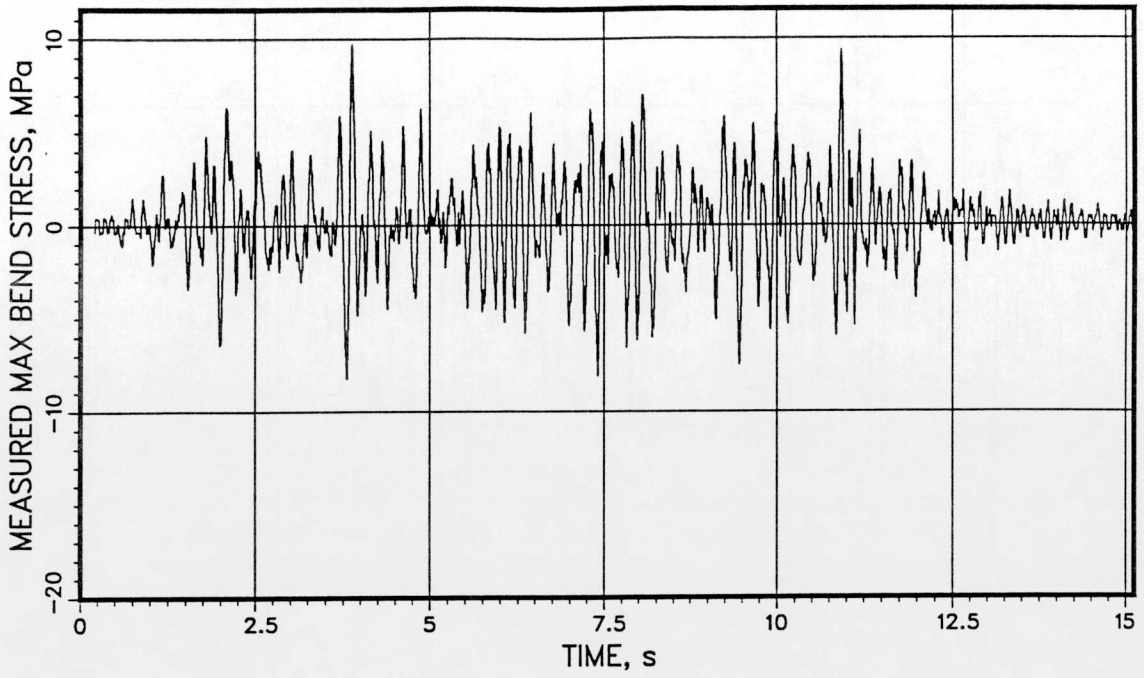

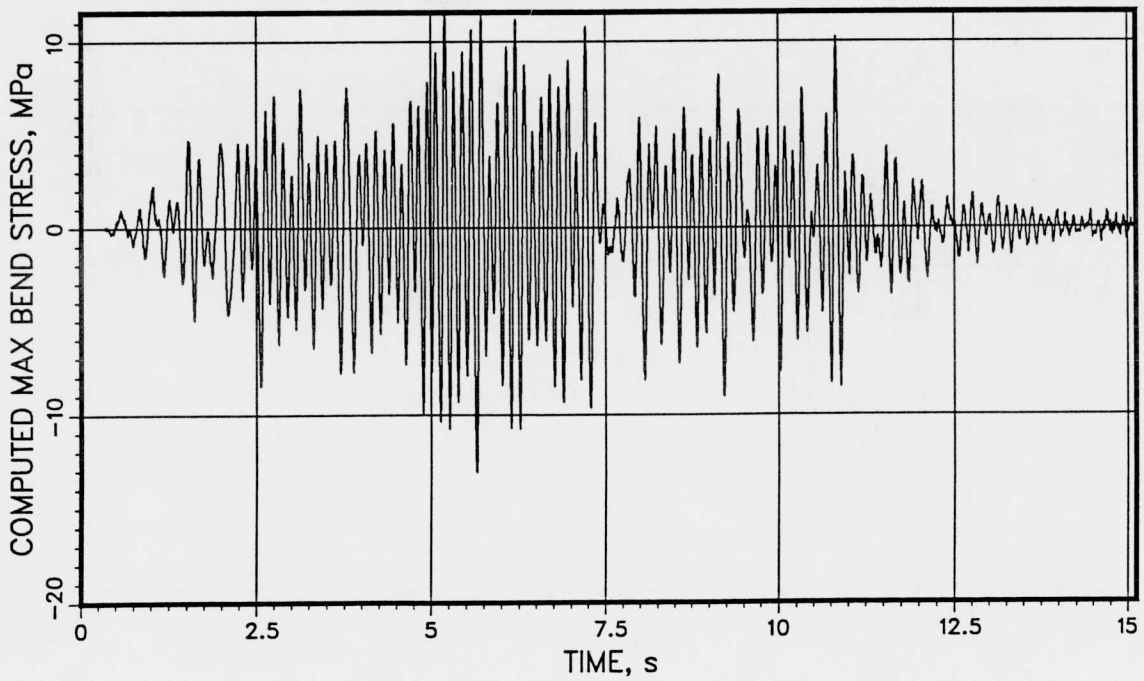

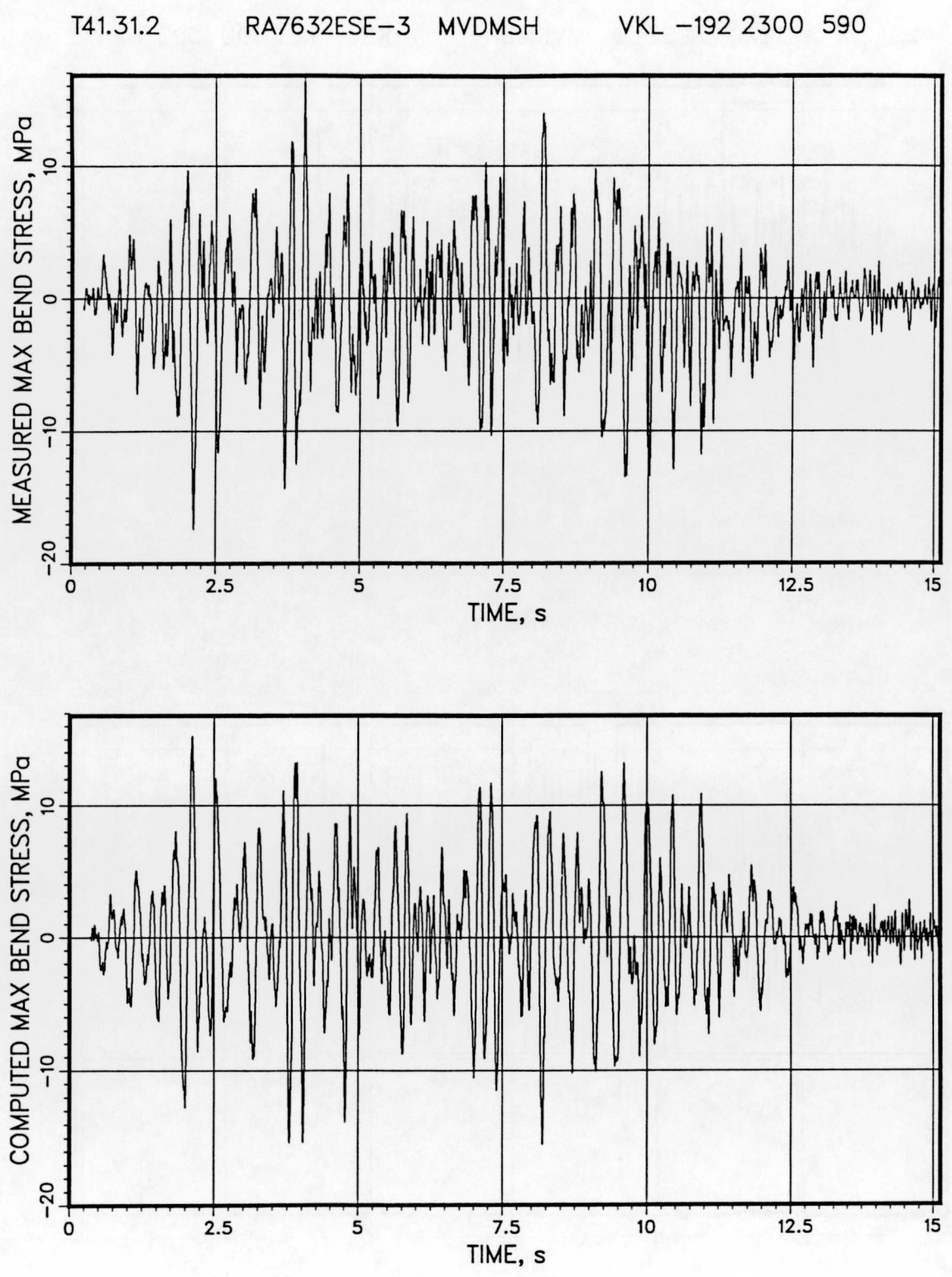
T41.31.2 RA7632ESE-3 MVDMSH VKL -192 2300 590
MEASURED MAX BEND STRESS, MPa
10
0
-10
-20
0
2.5
5
7.5
10
12.5
15
TIME, s
COMPUTED MAX BEND STRESS, MPa
10
0
-10
-20
0
2.5
5
7.5
10
12.5
15
TIME, s

T41.31.2 RA7641ESE-3 MVDMSH VKL 284 2386 433

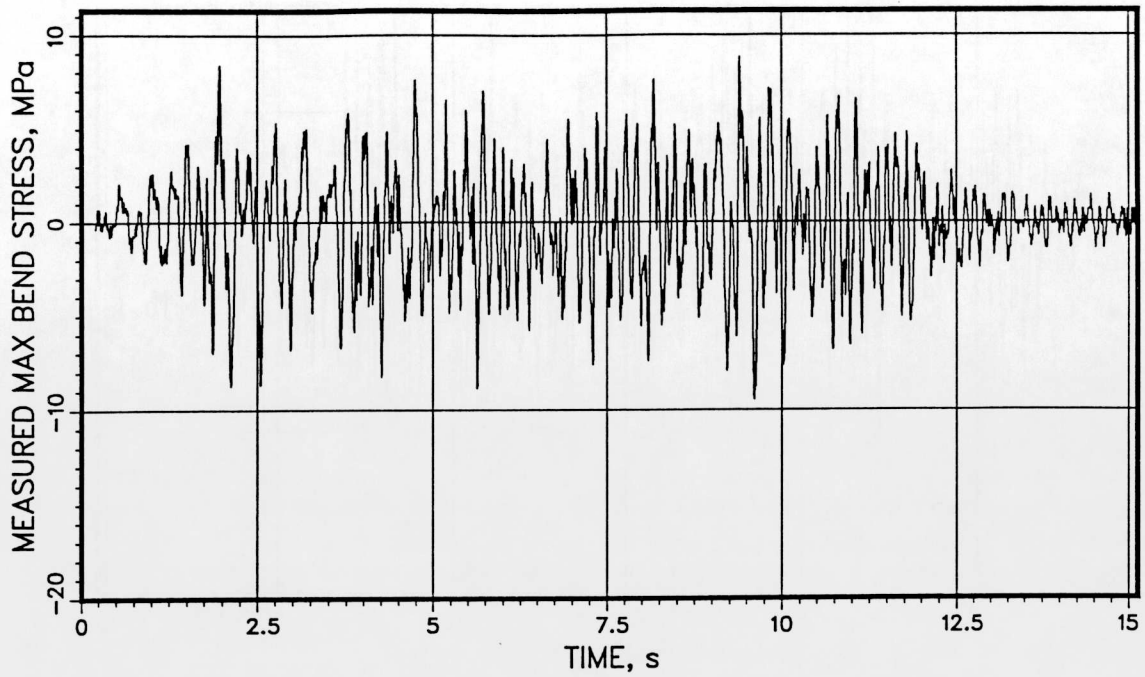

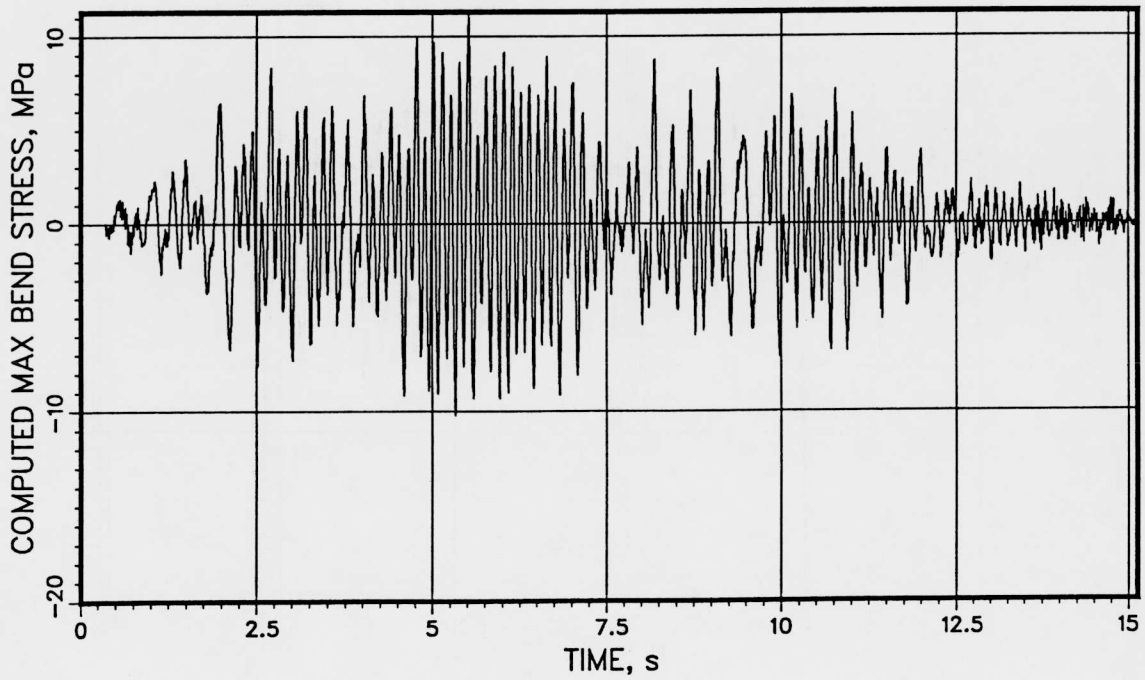

T41.31.2 RA7642ESE−3 MVDMSH VKL 284 2386 433

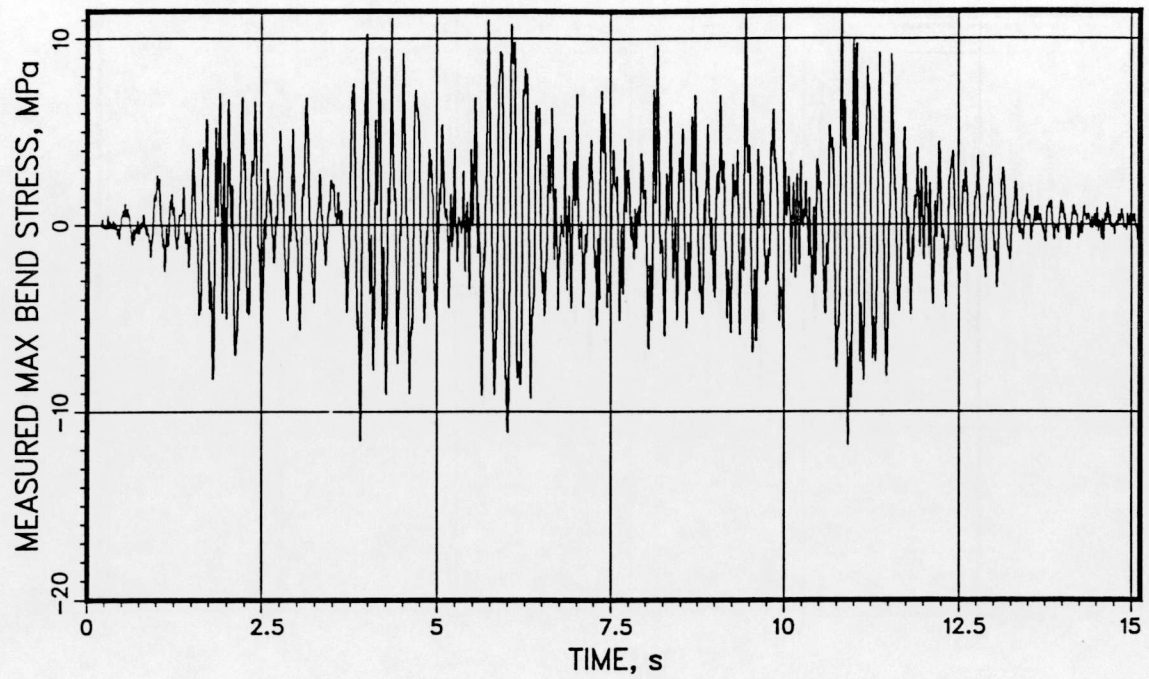

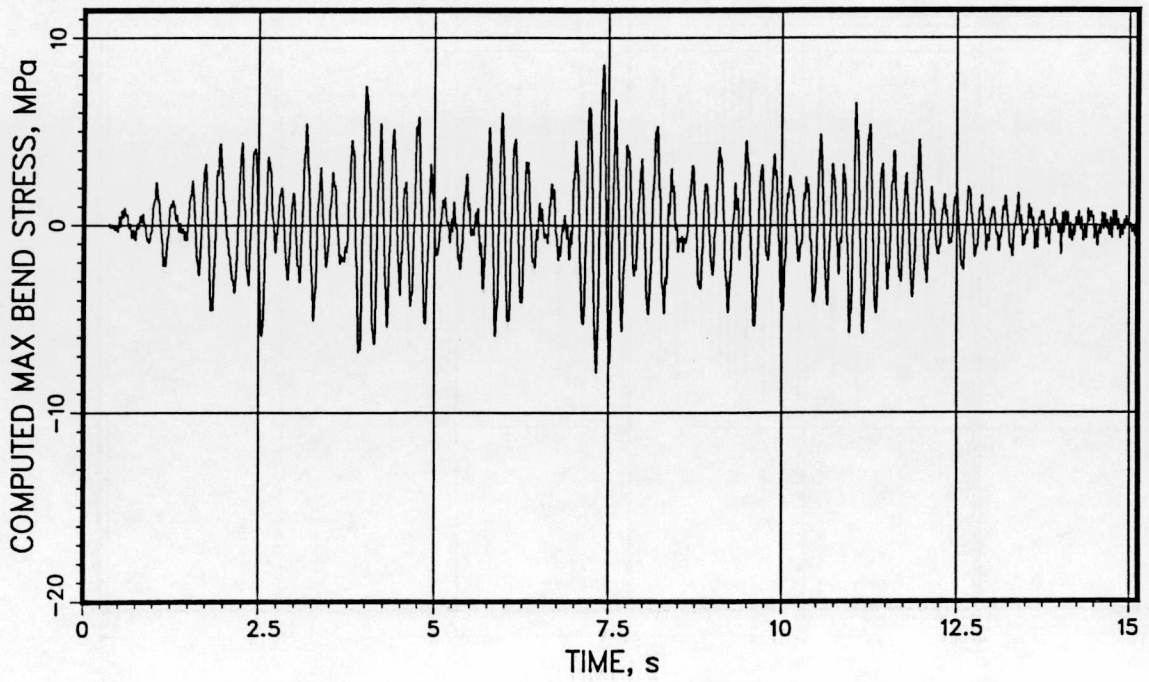

T41.31.2 RA7651ESE−3 MVDMSH VKL 587 2635 385

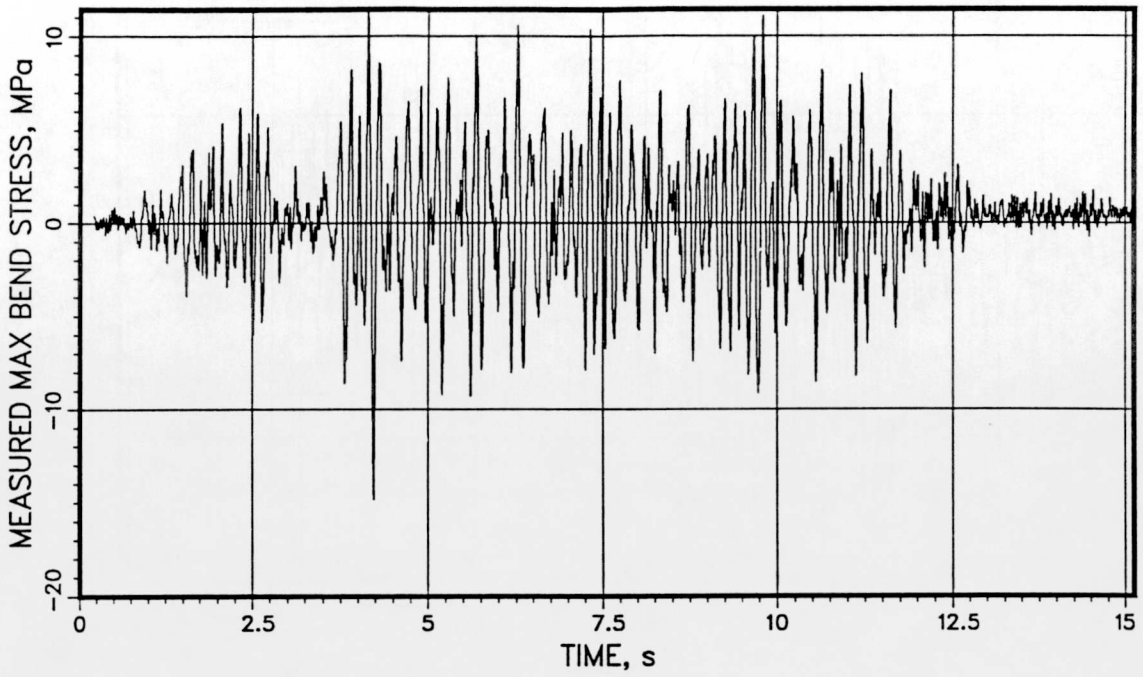

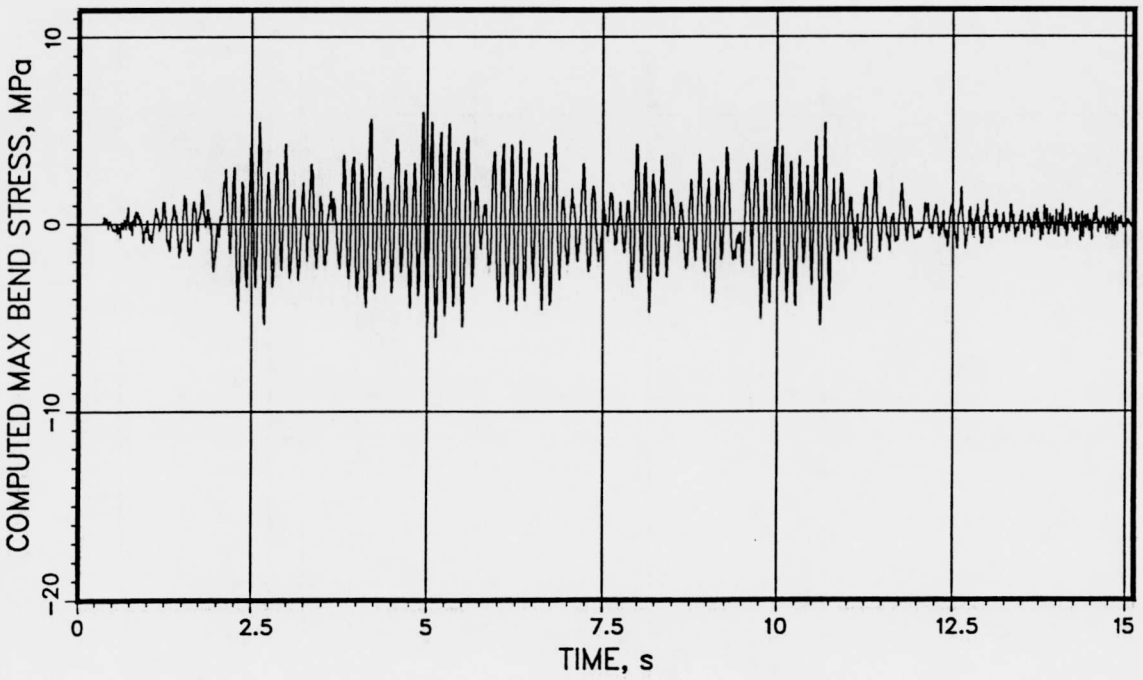

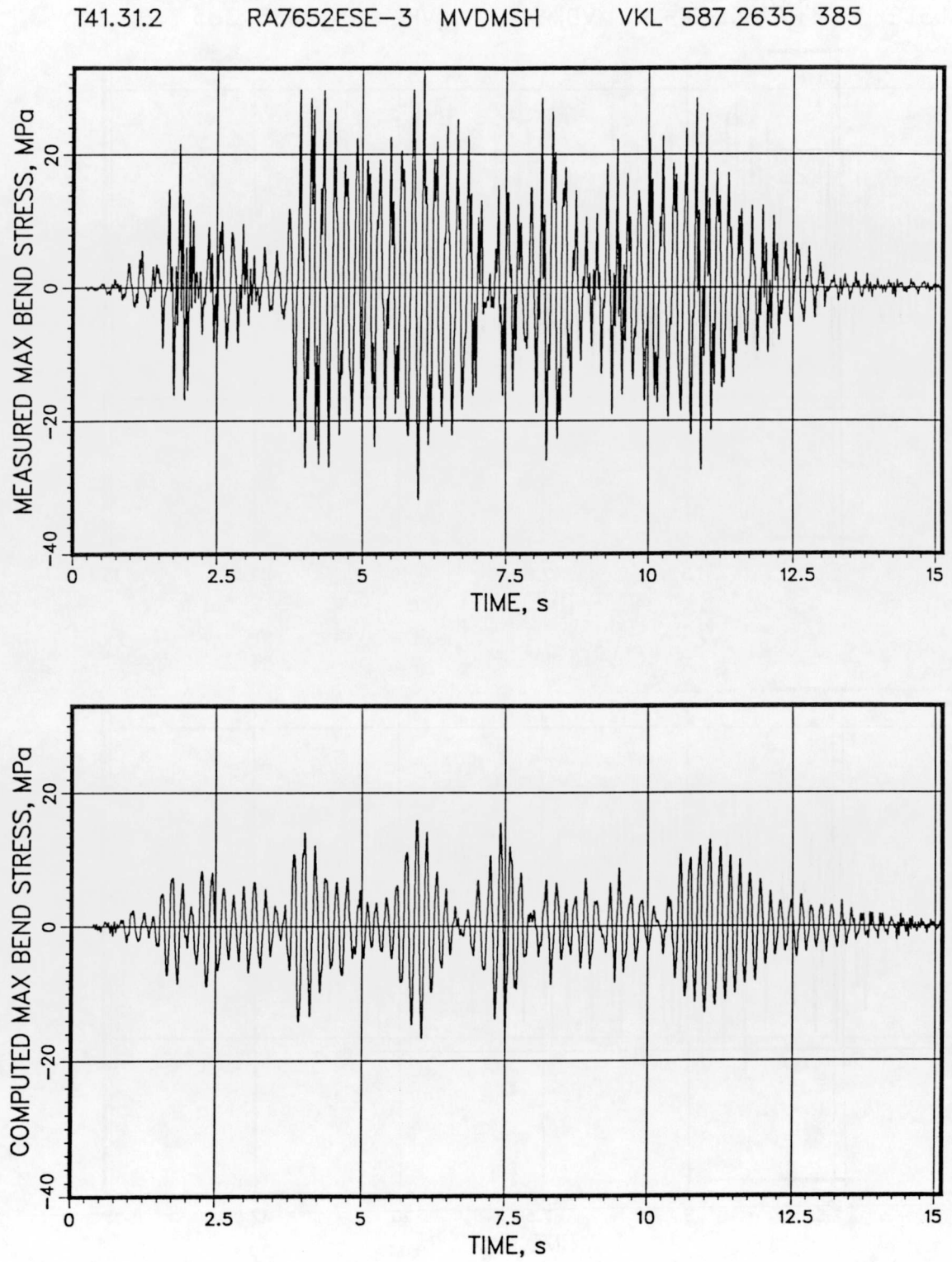
T41.31.2 RA7652ESE-3 MVDMSH VKL 587 2635 385
MEASURED MAX BEND STRESS, MPa
20
0
-20
-40
0
2.5
5
7.5
10
12.5
15
TIME, s
COMPUTED MAX BEND STRESS, MPa
20
0
-20
-40
0
2.5
5
7.5
10
12.5
15
TIME, s

T41.31.2 RA7661ESE-3 MVDMSH VKL 696 2635 385

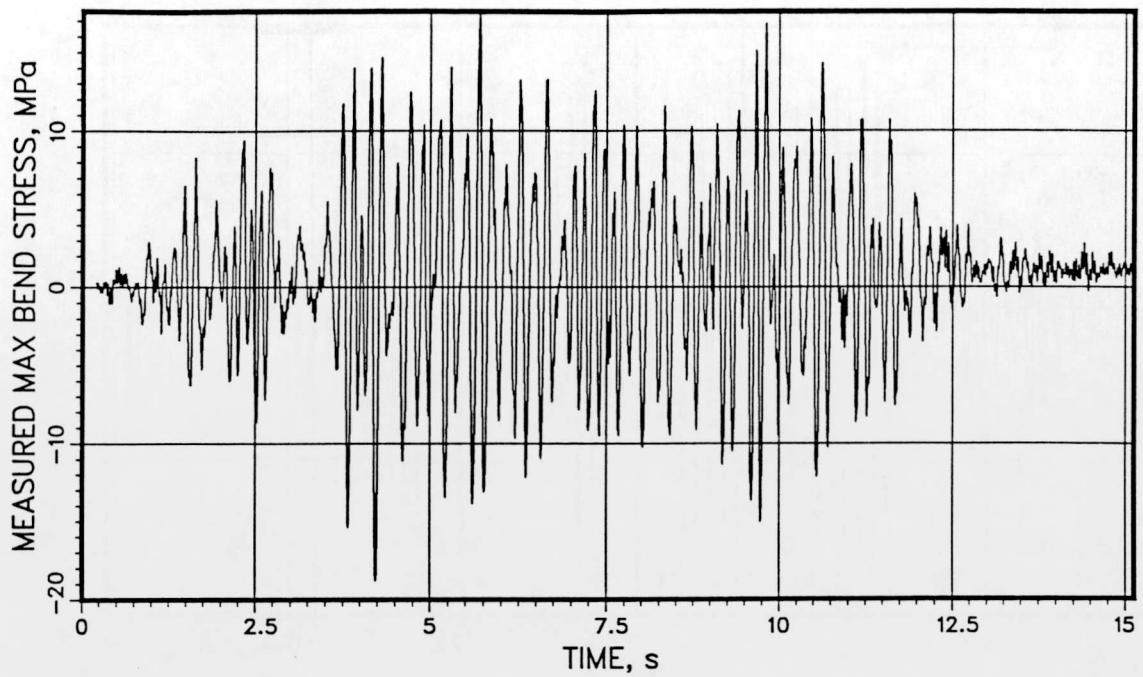

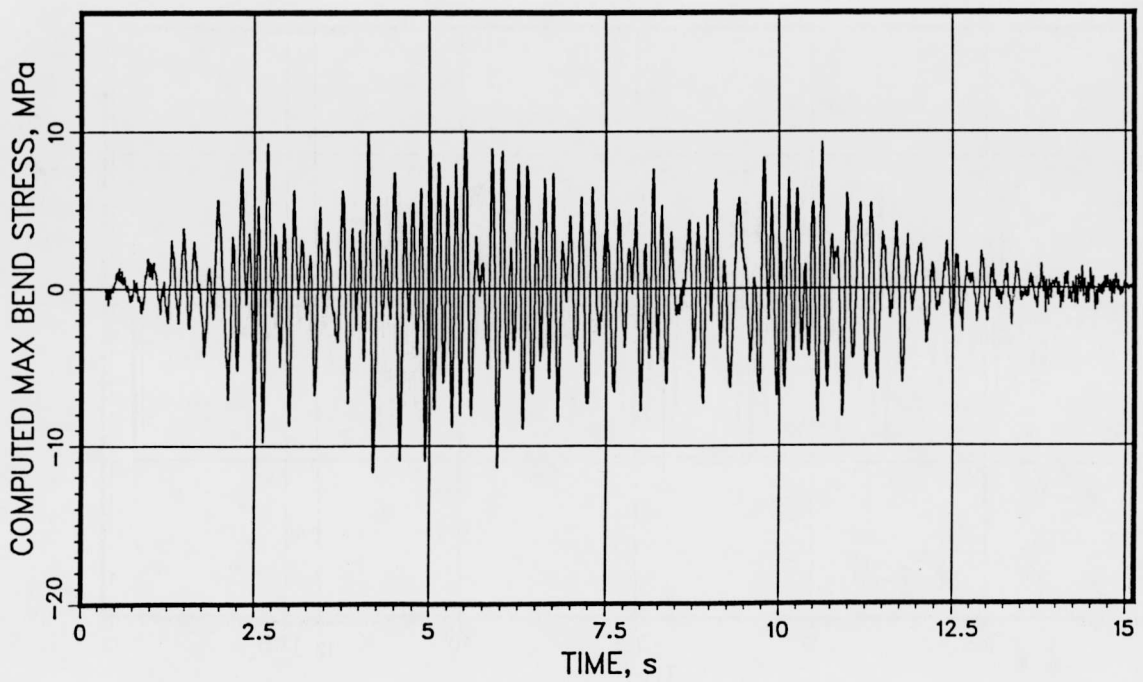

T41.31.2 RA7662ESE-3 MVDMSH VKL 696 2635 385

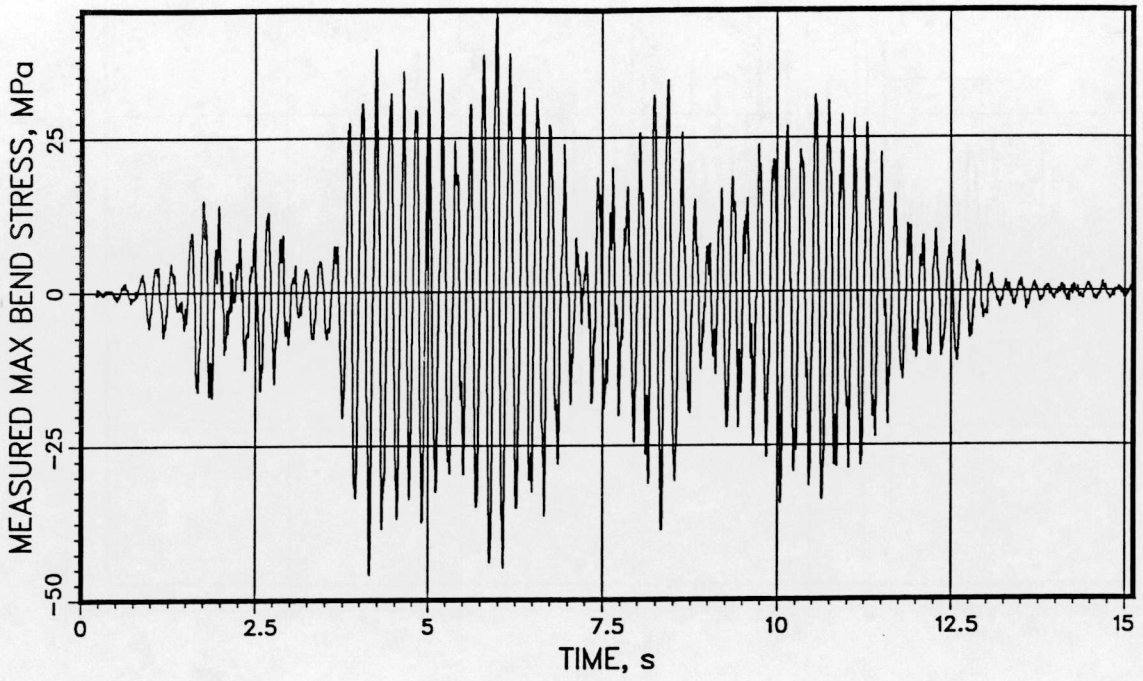

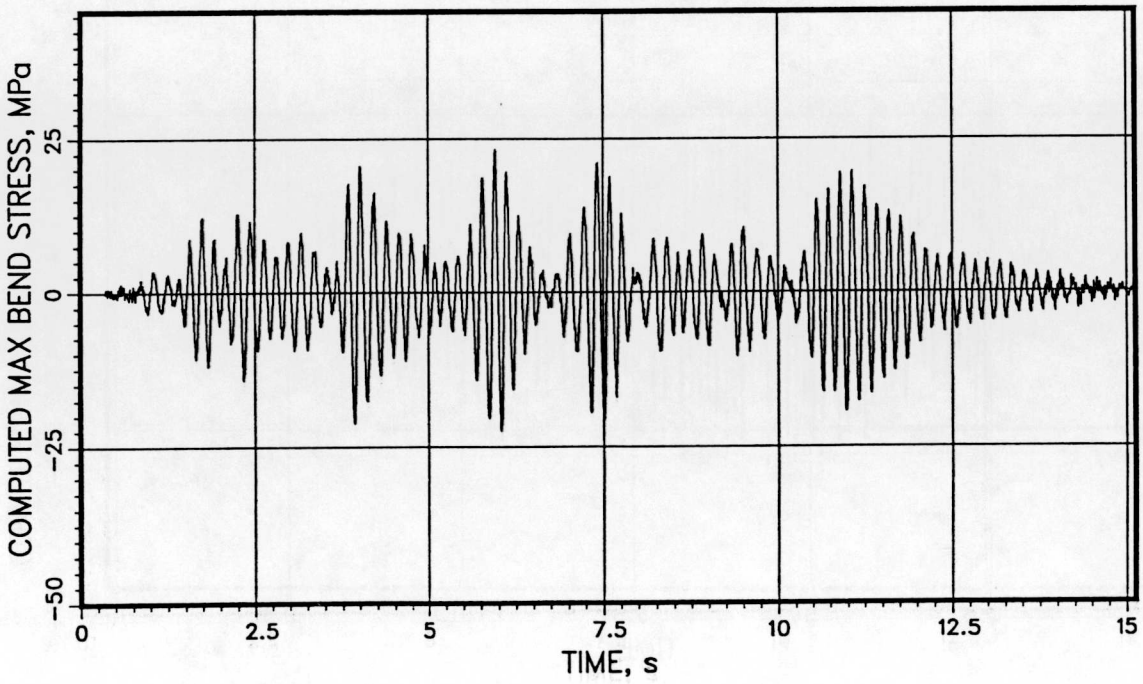

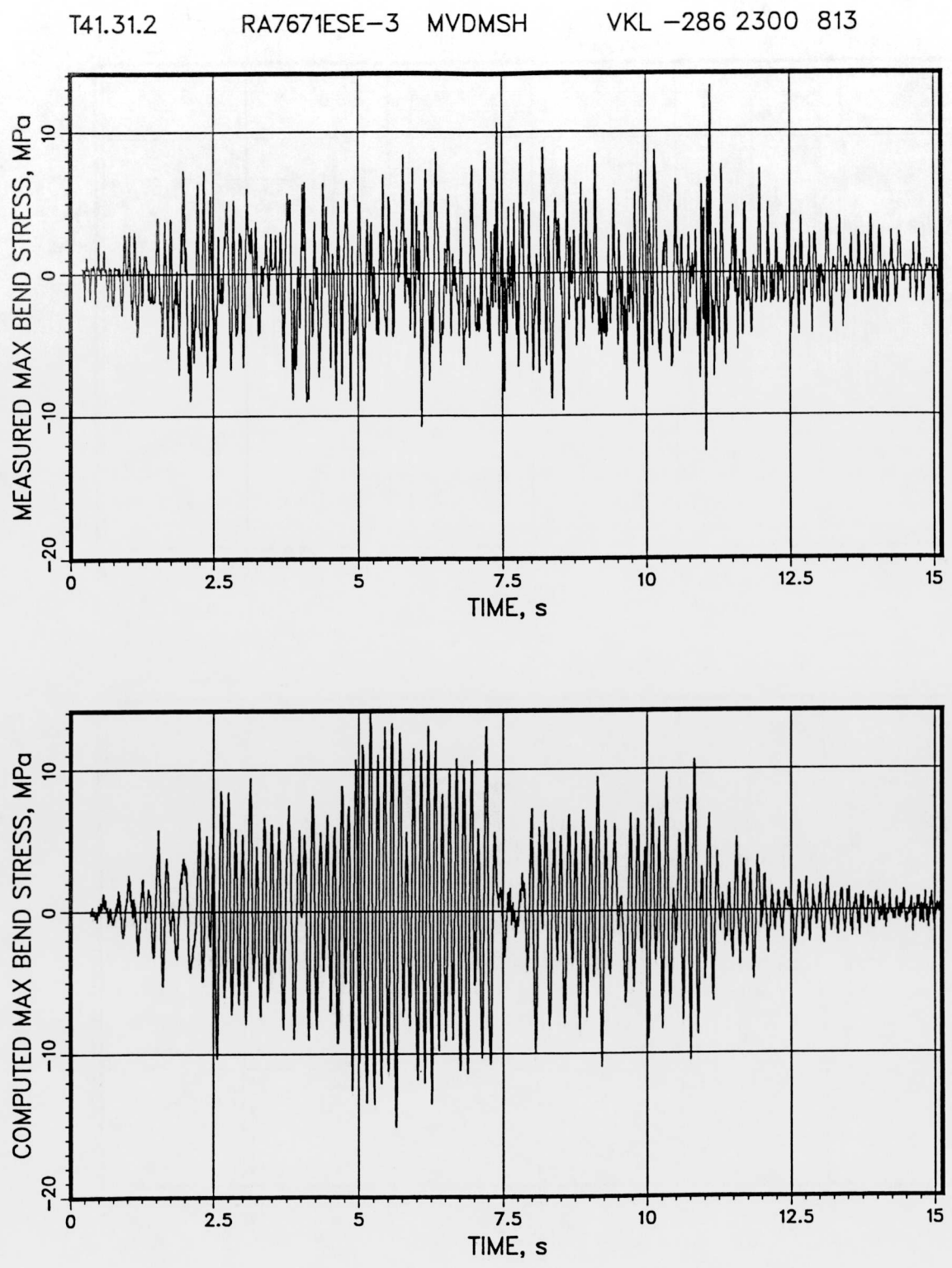
T41.31.2 RA7671ESE−3 MVDMSH VKL −286 2300 813
MEASURED MAX BEND STRESS, MPa
10
0
−10
−20
0
2.5
5
7.5
10
12.5
15
TIME, s
COMPUTED MAX BEND STRESS, MPa
10
0
−10
−20
0
2.5
5
7.5
10
12.5
15
TIME, s

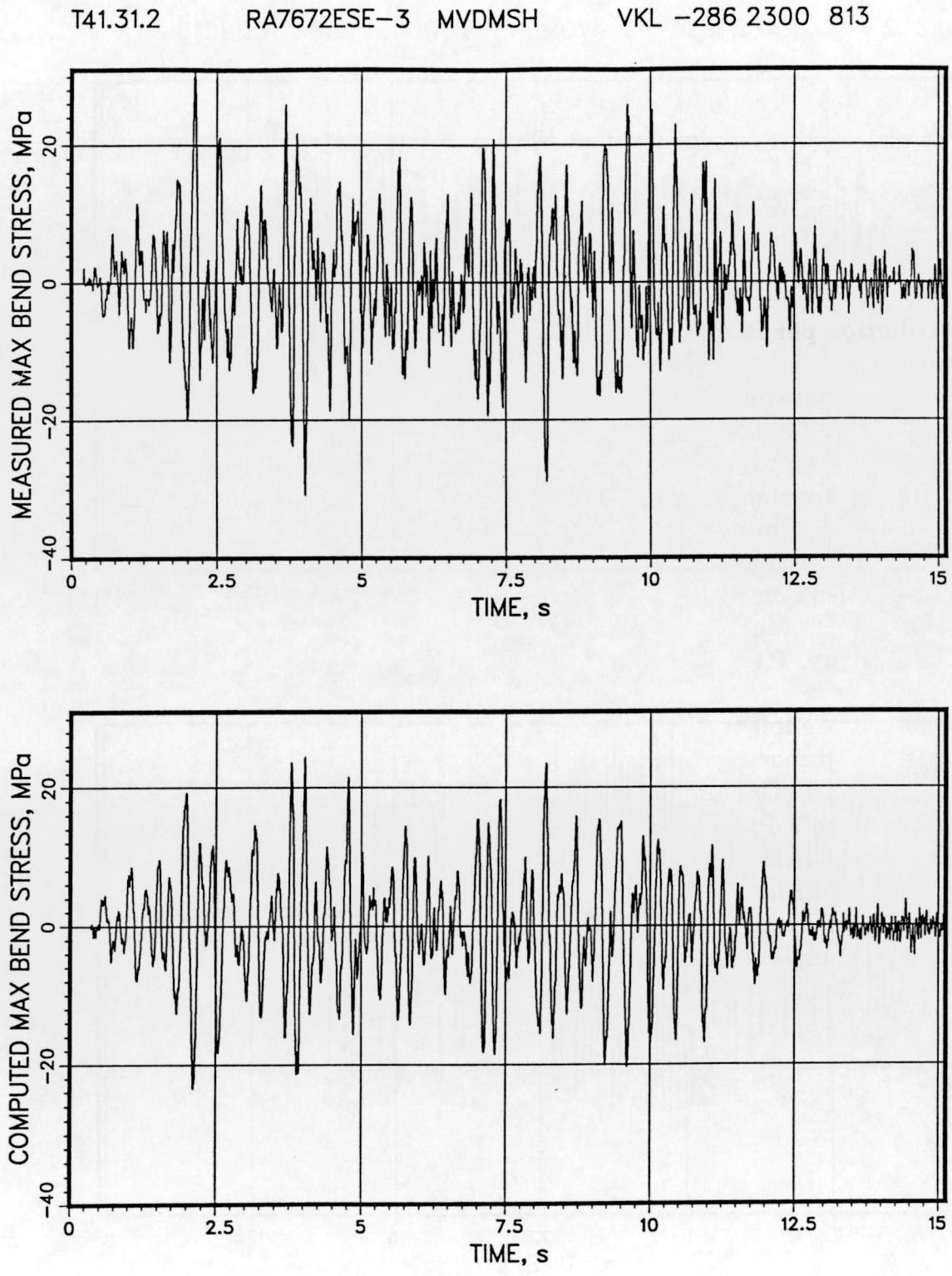
T41.31.2 RA7672ESE-3 MVDMSH VKL -286 2300 813
MEASURED MAX BEND STRESS, MPa
20
0
-20
-40
0
2.5
5
7.5
10
12.5
15
TIME, s
COMPUTED MAX BEND STRESS, MPa
20
0
-20
-40
0
2.5
5
7.5
10
12.5
15
TIME, s

Distribution for NUREG/CR–5757 (ANL–91/25)

Internal

M. G. Srinivasan (45)
TIS Files (3)
ANL Patent File
ANL Contract File

External

NRC, for distribution per RD
ANL Libraries
Manager, Chicago Operations Office, DOE
University of Chicago Review Committee for Reactor Engineering Division:

Dr. Joseph Sam Armijo, Program General Manager Space Power Programs, Astro–Space Division, General Electric Company, P.O. Box 8555, Building 21, Room 10Y05, Philadelphia, PA 19101

Dr. Paul W. Dickson, Jr., Technical Director, Reactor Restart, Westinghouse Savannah River Company, Building 703A, A0218, Aiken, SC 29802

Mr. Theodore C. McMeekin, Vice President, Design Engineering, Duke Power Company, P.O. Box 33189, 422 South Church Street, Charlotte, NC 28242

Dr. Daniel A. Meneley, Professor of Nuclear Engineering, Department of Chemical Engineering, University of New Brunswick, P.O. Box 4400, Fredericton, N.B., Canada 3B5A3

Dr. Roger E. Scholl, President, Counter Quake Corporation, 1901 Terry Lane, Redwood City, CA 94061

Dr. Neil E. Todreas, Professor, Department of Nuclear Engineering, Massachusetts Institute of Technology, 77 Massachusetts Avenue, Room 24–219, Cambridge, MA 02139

NRC FORM 335 (2-89) NRCM 1102, 3201, 3202

U.S. NUCLEAR REGULATORY COMMISSION

BIBLIOGRAPHIC DATA SHEET

(See instructions on the reverse)

1. REPORT NUMBER (Assigned by NRC, Add Vol., Supp., Rev., and Addendum Numbers, if any.)
NUREG/CR-5757
ANL-91/25

2. TITLE AND SUBTITLE

Verification of Piping Response Calculation of SMACS Code with Data from Seismic Testing of an In-Plant Piping System

3. DATE REPORT PUBLISHED
MONTH: September
YEAR: 1991

4. FIN OR GRANT NUMBER
A2251

5. AUTHOR(S)

M. G. Srinivasan, C. A. Kot, and B. J. Hsieh

6. TYPE OF REPORT
Technical

7. PERIOD COVERED *(Inclusive Dates)*

8. PERFORMING ORGANIZATION – NAME AND ADDRESS *(If NRC, provide Division, Office or Region, U.S. Nuclear Regulatory Commission, and mailing address; if contractor, provide name and mailing address.)*

Argonne National Laboratory
9700 South Cass Avenue
Argonne, IL 60439

9. SPONSORING ORGANIZATION – NAME AND ADDRESS *(If NRC, type "Same as above"; if contractor, provide NRC Division, Office or Region, U.S. Nuclear Regulatory Commission, and mailing address.)*

Division of Engineering
Office of Nuclear Regulatory Research
U.S. Nuclear Regulatory Commission
Washington, DC 20555

10. SUPPLEMENTARY NOTES

11. ABSTRACT *(200 words or less)*

The objective of this effort was to evaluate the piping analysis part of the SMACS code for estimating the response of realistic piping systems subjected to multiple independent support accelerations. Test data from the experiments on an in-plant piping system were used for this purpose. Two support configurations were selected for the evaluation: one a 'stiff' configuration containing both struts and snubbers, and the other, a more flexible configuration with no snubbers. Described are the analytical modeling, calculations, and results of the posttest simulation of two tests each for both support configurations. Almost all the calculated peak response quantities were smaller than the corresponding test measurements. However, pipe displacements and bending stresses were better estimated than the pipe accelerations and support forces. The discrepancies are mainly attributable to the inability of the linear analysis to model the nonlinear behavior of the piping system.

12. KEY WORDS/DESCRIPTORS *(List words or phrases that will assist researchers in locating the report.)*

Code Verification, SMACS Code, Linear Analysis, Simulation of Tests, Seismic Response, In-Plant Piping System, HDR, VKL, SHAM Tests, NRC, KWU, Support Configurations, Seismic Excitation, Pipe Accelerations and Displacements, Snubber and Strut Forces, Pipe Strains, Comparison of Test with Analysis

13. AVAILABILITY STATEMENT
Unlimited

14. SECURITY CLASSIFICATION
(This Page)
Unclassified
(This Report)
Unclassified

15. NUMBER OF PAGES

16. PRICE

THIS DOCUMENT WAS PRINTED USING RECYCLED PAPER

UNITED STATES
NUCLEAR REGULATORY COMMISSION
WASHINGTON, D.C. 20555

OFFICIAL BUSINESS
PENALTY FOR PRIVATE USE, $300

SPECIAL FOURTH-CLASS RATE
POSTAGE & FEES PAID
USNRC

PERMIT No. G-67